University of East Anglia

Synthesis and Properties of Redox-Switchable Non-Linear Optically Active Polyoxometalate Chromophores

A thesis submitted to the School of Chemistry at the University of East Anglia for the degree of Doctor of Philosophy

Bethany Rose Hood

April 2022

For Nanny and Grandad

xx

Abstract

This thesis discusses the synthesis and properties of a series of sterically protected redox-switchable non-linearly optically active polyoxometalate chromophores. A second series of compounds designed with the purpose of increasing non-linear optical activity over previously synthesised compounds is also discussed.

Chapter 1 gives an introduction into the background of Lindqvist polyoxometalates and their derivatives as well as non-linear optics and the NLO active chromophores synthesised over the years, while c*hapters 2* and *3* discuss the synthesis and analysis of nine sterically protective Lindqvist derivatives, five of which feature the amine electron donors needed for nonlinear optical activity. Two compounds featuring electron accepting nitro groups were also synthesised and investigated. The linear optical and electrochemical properties of the compounds are discussed in *chapter 2* while *chapter 3* explores the non-linear optical properties of the Lindqvist derivatives using DFT and Hyper-Rayleigh scattering, with the Hyper-Rayleigh experiments revealing redox-switchable responses observed for the first time in polyoxometalate chromophores.

The work discussed in *chapter 4* focuses on two series of novel multi-dimensional polyoxometalate chromophores, with the synthesis and properties of both one-donor-two-acceptor and two-donor-one-acceptor derivatives being discussed. These compounds are investigated by UV-vis absorption spectrometry, cyclic voltammetry, and Hyper Rayleigh Scattering. In *chapter 5*, the synthesis and properties of the first polyoxometalate chromophore featuring an alkene bridge between the amine donor and the POM acceptor is discussed, as well as the attempted synthesis of a similar but sterically protected analogue. The compound, like those in previous chapters, are investigated by UV-vis spectroscopy, DFT, electrochemistry, and Hyper-Rayleigh scattering, to reveal high NLO activity.

Acknowledgements

Table of Contents

List of Abbreviations

Å	Ångstrom
BE	Bulk Electrolysis
CV	Cyclic Voltammetry/Voltammogram
$\mathbf{I_{pc}}$	Cathodic peak current
$\mathbf{I_{pa}}$	Anodic peak current
$\mathbf{E_{pc}}$	Cathodic peak potential
$\mathbf{E_{pa}}$	Anodic peak potential
$\boldsymbol{\nu^{1/2}}$	Square root of scan rate
$\mathbf{\Delta E}$	Peak potential separation
$\mathbf{E_{1/2}}$	Half peak potential of a reversible CV
DAST	Dimethyl-Amino-Stilbazolium Tosylate
DCC	N,N'-dicyclohexylcarbodiimide
DCU	N,N'-dicyclohexylurea
DFT	Density Functional Theory
DMSO	Dimethylsulfoxide
DPV	Differential Pulse Voltammetry/Voltammogram
EFISH	Electric field induced second harmonic generation

ESD	Estimated Standard Deviation
Fc/Fc$^+$	Ferrocene/Ferrocenium
HOMO	Highest energy occupied molecular orbital
HRS	Hyper-Rayleigh Scattering
IHCT	Inter-hybrid charge transfer
IR	Infrared
LMCT	Ligand-to-metal charge transfer
LPCT	Ligand-to-POM charge transfer
LUMO	Lowest energy unoccupied molecular orbital
MLCT	Metal-to-ligand charge transfer
NLO	Non-linear Optics/Optical
POM	Polyoxometalate
PLCT	POM-to-ligand charge transfer
SHG	Second Harmonic Generation
TD-DFT	Time-Dependent Density Functional Theory
TMS	Tetramethylsilane
UV-vis	Ultraviolet-visible spectroscopy

Chapter 1

Introduction

1.1 Polyoxometalates

Polyoxometalates (POMs) are a widely variable class of anionic cluster compounds consisting mainly of transition metal cations, typically molybdenum, tungsten, or vanadium in their highest oxidation states, and bridging oxygen anions. These compounds can vary massively in terms of size, structure, elemental composition and properties, and as a result, are a family of compounds that have potential for use in a wide range of areas ranging from medicine[1] to catalysis[2] to non-linear optics.[3] Although due to these wide range of uses interest in POMs has recently surged, they are not a newly discovered class of compounds, with the first POM being reported back in 1826.[4] At the time of its synthesis, very little about the structure of the compound now known to be 12-phosphotungstic acid was understood, and this remained the case until in 1933 when with the help of X-ray diffraction, Keggin reported the structure of this first POM formed over 100 years before.[5]
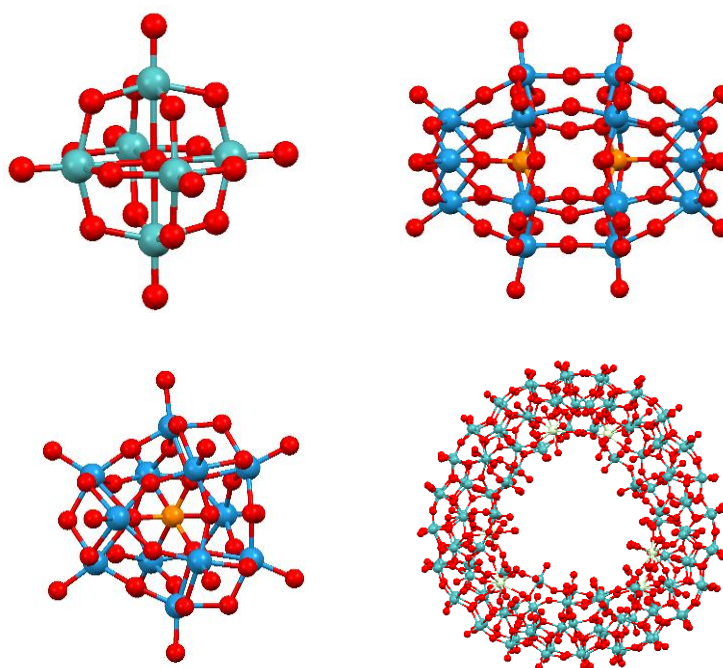
Figure 1.1a A selection of polyoxometalate structures; Lindqvist $[M_6O_{19}]^{2-}$ (top left),[6] Wells-Dawson $[P_2W_{18}O_{62}]^{6-}$ (top right),[7] Keggin $[PW_{12}O_{40}]^{3-}$ (bottom left),[8] and Molybdenum Blue $[Mo_{120}O_{366}(H_2O)_{48}H_{12}]^{24-}$ (bottom right).[9]

Since the first discovery of POMs, a huge number of complexes have been synthesised, with the compounds formed varying widely in terms of size, shape, charge, and elemental composition. For example, whilst the Lindqvist structure contains just six metal ions and 19 oxygen ions giving it an overall charge of 2-, the Mo-blue 'lemon' cluster contains 368 molybdenum cations,1032 oxygen anions, 240 water molecules, 16 hydrogen ions, and 28 sulfate ions, and has an overall charge of 48-.[10] There are a huge number and variety of polyoxometalate structures with sizes in between these two extremes, as well as examples containing heteroatoms seen in neither of the above compounds such as nitrogen and phosphorus. The large range of structures of polyoxometalate compounds can be increased even further once the possibility of functionalisation is considered. Overall, this variation results in a class of compounds with a wide variety of interesting properties, both physical and electronic, including but not limited to superacidity,[2] catalysis,[2] photochemical activity,[11] reversible redox behaviour,[12] host-guest chemistry,[13] anti-viral[14] and cytotoxic[15] properties, and as building blocks to produce larger molecules.

Polyoxometalates are usually formed in simple one-pot, one-step condensation reactions of monomeric oxometalate forms of the relevant metal under acidic conditions. Typically, the oxometalate is of the form $[MO_4]^{n-}$, where n depends on the transition metal cation and its oxidation state. The condensation reaction occurs by the protonation of the oxo groups on the oxometalate to give oxometalate-hydroxide intermediates of the form $[MO_3OH]^{(n-1)-}$, which can then react with a second oxometalate-hydroxide intermediate to produce a $[M_2O_7]^{(2n-2)}$ species with a metal-oxygen-metal bond and water. The condensation reactions can keep proceeding, resulting in larger and larger clusters, until no protons remain. This means that the average cluster size produced in the reaction is dependent on the ratio of moles of acid to oxometalate.[16]

$$p\text{H}^+ + q\text{MO}_4^{r-} \longrightarrow \text{H}_x\text{M}_q\text{O}_y^{z-} + (4q\text{-}y)\text{H}_2\text{O}$$

$$p\text{H}^+ + q\text{MO}_4^{r-} + \text{XO}_4^{n-} \longrightarrow (\text{H}_x\text{X}^{n+}\text{M}_q\text{O}_y)^{n-} + (4q\text{-}y)\text{H}_2\text{O}$$
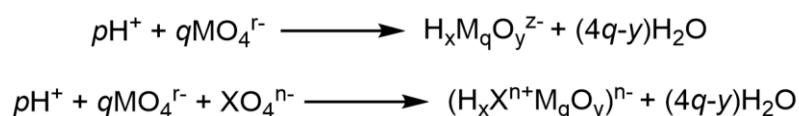
Figure 1.1b General formula for the synthesis of both isopolyanions (top) and heteropolyanions (bottom).

Although the ratio of oxometalate to acid used in the reactions is very important in determining the average size of the cluster produced, the product of a polyoxometalate reaction is not solely dependent on the ratio of protons to oxometalate anions; other factors such as type and concentration of the heteroatom, the presence of additional ligands, and the temperature of reaction can also have an effect especially when multiple isomers of certain POMs exist. For some POMs, the counterion can also play an important role in determining which isomer is predominantly formed. One example of the importance of other factors is $[Mo_8O_{26}]^{4-}$ which has been shown to exist as multiple isomers and for which the isomer produced during synthesis is dependent on both the pH of the solution and the cation present. The alpha isomer, which is the most commonly observed isomer, is the favoured product when the reaction is performed at a pH 2.7 whilst the beta is favoured when the reaction is performed at pH 2. The beta isomer is also favoured by the presence of smaller cations such as potassium or tetramethyl ammonium.[17]
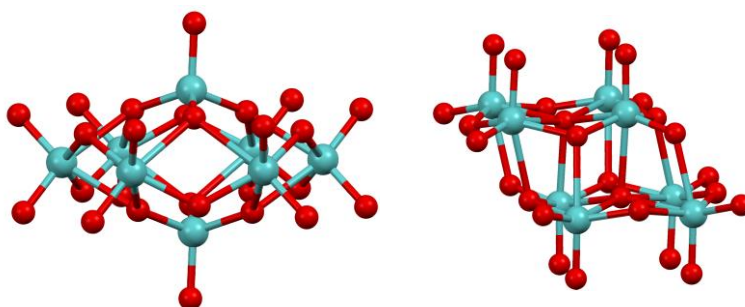
Figure 1.1c Crystal structures of α-octamolybdate (left) and β-octamolybdate (right).

1.2 Classes of Polyoxometalate

There are three main classes polyoxometalates; heteropolyanions, isopolyanions, and Mo-blue and Mo-brown reduced "giant" POM clusters.

Heteropolyanions, structures in which a heteroanion such as SO_4^{2-} or PO_4^{3-} is included within the main cluster, are the most explored of the three classes of polyoxometalate due to interest in their catalytic properties and their increased stability over the isopolyanions. The Keggin structure and the Wells-Dawson structure are both examples of heteropolyanions, the structures of which are shown in Figure 1.1a. In

contrast, isopolyanions are structures in which there is no internal heteroanion, meaning the main cluster consists only of the metal and oxygen ions. Isopolyanions are typically less stable than heteropolyanions and are therefore much less frequently used for purposes such as catalysis, however they still are of interest due to their interesting redox and nonlinear optical properties when functionalised, and their use as building blocks to synthesise nanoscale devises.[18]

Lindqvist-type polyoxometalates, with the general formula of $[M_6O_{19}]^{2-}$, are an example of isopolyanions and are typically produced with molybdenum, tungsten, and vanadium cations. The hexamolybdate Lindqvist POMs are the most easily functionalised of the three, however stability issues have led to attempts to produce derivatives of hexatungstate as well as compounds made using a mixture of the metals.

Functionalisation of the polyoxometalate is of interest for purposes such as polymer production, a result of coupling the inorganic POMs together using organic linking chains[19] as well as for the optical and electronic chemistry brought about by functionalisation with electron donor containing ligands.[3]

The third subgroup of polyoxometalates, the Mo-blue and Mo-brown structures, are typically much larger than the standard heteropolyanions and isopolyanions, having been produced with up to 368 transition metal centres. The Mo-blue and Mo-brown structures have properties making them suitable for uses such as as nanosensors,[20] and in catalysis. One interesting example is of {Mo_{368}},[10] the previously mentioned lemon cluster, which is the largest polyoxometalate compound of this type and is shown in figure 1.2a.
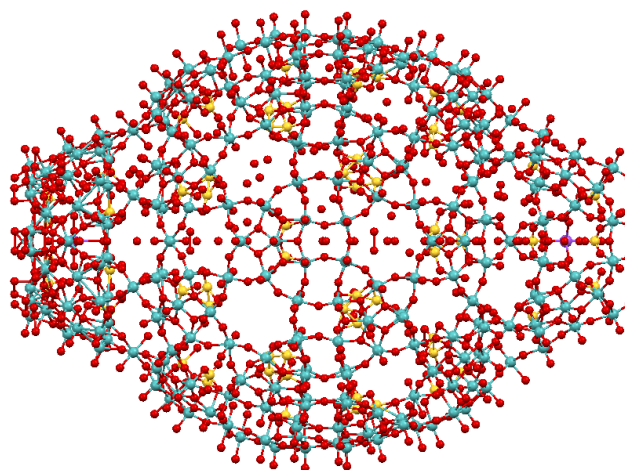
Figure 1.2a The {Mo_{368}} 'lemon cluster' first synthesised by Müller et al..[10]

1.3 Functionalisation of Lindqvist Polyoxometalates

Functionalisation of polyoxometalates can be achieved through the binding of an organic or organometallic group to the POM core, typically through a linking heteroatom or through the replacement of one of the transition metal centres by another atom such as phosphorus or silicon. Examples of functionalisation have been seen in Keggin, Wells Dawson, Anderson, and Lindqvist structures.[21] In particular, functionalisation of lacunary Keggin structures has resulted in a large variety of compounds, with transition metal substituted compounds being formed along with numerous organosilica derivatives.[22] In these compounds, the organic and POM fragments are typically linked by single oxygen bonds, limiting electron conjugation and communication between the two halves of the compounds and resulting in properties more similar to the parent species than seen for some other coupling methods. Similarly functionalised hexavanadate POMs have also been synthesised, with Petrovskii amongst others producing Lindqvist derivatives in which organic ligands were bound to the POM by the substitution of terminal oxo atoms with alkoxo groups.[23] This again resulted in only single bond connectivity.

In addition to the functionalisation of vanadium based Lindqvist POMs, multiple different types of functionalised molybdenum Lindqvist POMs have also been synthesised, with examples being the alkylimido,[24] arylimido,[25] nitrosyl,[26] and organodiazenido[27] derivatives. Multiple functionalisations of the same hexamolybdate core can also be performed, with literature reports of up to all six terminal oxygens being replaced.[28] Functionalisation of the bridging positions of hexamolybdate by replacement of the oxygen with an NR group has also been shown to be possible,[29] although this significantly less frequently reported. Attempts have also been made to functionalise the tungsten analogue of tetrabutylammonium hexamolybdate, however, due to the increased strength of the tungsten-oxygen bond, limited success has so far been achieved.[30]

Of the four types of terminally functionalised Lindqvist derivatives synthesised so far, the arylimido functionalised derivatives are of particular interest due to their relative ease of synthesis and, in the case of this work, the good conjugation between the π network of the aromatic ligand and the POM core which can allow electron donation from the organic ligand to the POM centre. This results in stronger electronic

communication between the POM core and the ligand and results in the emergence of properties not seen of either of the parent species.
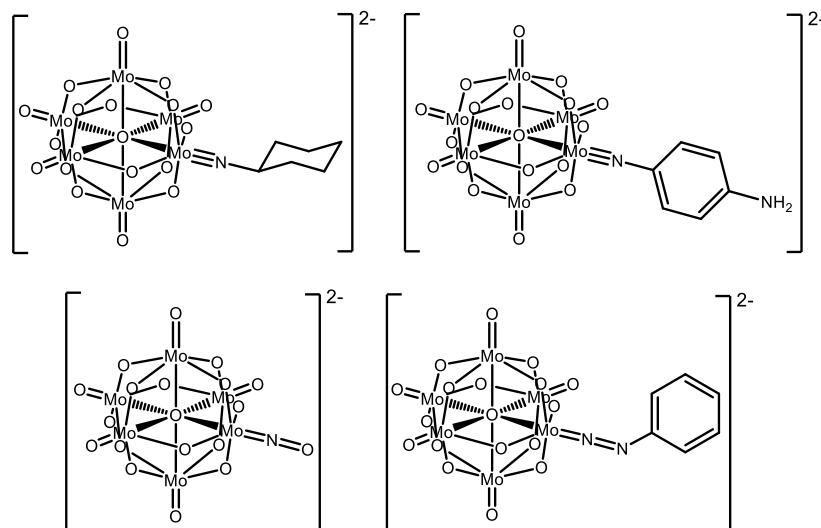
Figure 1.3a Examples of four types of hexamolybdate derivative; alkyimido (top left),[24] arylimido (top right),[25] nitrosyl (bottom left),[26] and organodiazenido (bottom right).[27]

The first method of functionalisation of tetrabutylammonium hexamolybdate(VI) was by reaction with phosphinimines and was reported by Maatta in 1992.[31] Since then it has been discovered that the imido functionalised POMs can also be synthesised by the reaction between the unfunctionalized tetrabutylammonium hexamolybdate and the relevant isocyanate[32] or aromatic amine.[25] From these reactions, the similarities between the behaviour of the molybdyl group and the carbonyl group was noticed as all three reactions are similar to reactions the reagents undergo with aldehydes and ketones.

Multiple methods of performing these reactions have been used involving a variety of solvents, temperatures, and reaction times in attempts to increase the purity and yield, but it wasn't until just over 10 years after the first POM functionalisation reaction that the benefit of the addition of carbodiimides such as DCC to the condensation reaction between the POM and the aromatic amines was discovered.[33] The addition of DCC both greatly improved the yield and purity and allowed the reaction to be performed under milder conditions and without the need for a nitrogen atmosphere. It also meant

the reaction could tolerate the addition of functional groups on the aromatic ring of the amine, something which until then had not been possible. This was at first thought to be due to the carbodiimide acting as a drying agent and reacting with the water produced in the condensation reaction, however, the same increase in reactivity was not seen with other dehydrating or drying agents such as magnesium sulfate, suggesting a second important role of the carbodiimide. It has since been suggested that the DCC activates the terminal molybdenum-oxygen bond just as it activates the carbonyl group in amide synthesis, and results in an increased electrophilicity of the molybdenum atom, increasing its affinity for the aniline coupling groups.

Despite the improvement in yield and milder reaction conditions needed when DCC is used as a coupling reagent, the ratio of DCC to reagents must be controlled as too much DCC reduces the yield of the desired product.[33] Investigation into this showed that addition of up to 1 molar equivalent of DCC to POM increased the yield of the reaction and decreased reaction time, but further addition of DCC resulted in a lower peak yield. It was also shown that allowing the reaction to continue after the peak yield has been reached in the presence of excess DCC resulted in a decrease of the yield. This is believed to be due to the excess DCC reacting with the functionalised product to form tetrabutylammonium octamolybdate, a major side product isolated from reactions probing this.

Interestingly, tetrabutylammonium octamolybdate has itself been readily used for the synthesis of hexamolybdate derivatives, with predominantly *bis*-functionalised derivatives being made from it and the hydrochloride salt of the relevant aniline.[34] Using similar reaction techniques, the formation of multi-functionalised POMs has been shown to be possible, with up to all six terminal oxygens being replaced by organic groups having been reported.[35] As a result, contamination of the sample with tetrabutylammonium octamolybdate, either through formation in situ due to reaction of functionalised hexamolybdate with DCC or through poor synthesis of the hexamolybdate, can significantly decrease both the yield and the purity of the product through accidental synthesis of unwanted multi-functionalised derivatives.

A second minor disadvantage of the DCC mediated coupling reaction used to synthesise these functionalised hexamolybdate derivatives is that although the coupling between hexamolybdate and electron rich anilines proceeds efficiently,

anilines with electron withdrawing groups, such as 4-nitroaniline do not couple quite as effectively due to the reduced nucleophilicity of the aniline. This can hinder the production of electron acceptor functionalised compounds, resulting in a lower crude yield and a decrease in purity through increased contamination of unreacted hexamolybdate. The decreased purity can reduce the yield further, with more extensive purification needed to remove the contaminating hexamolybdate.

Despite these few small drawbacks, the DCC mediated coupling reaction presents a hugely improved method over the older methods of functionalising hexamolybdate, methods requiring more vigorously dry conditions and harsh conditions, and has resulted in a wide range of interesting compounds over the years. Some examples include compounds such as the dumbbell shaped organoimido-bridged bis(hexamolybdate) complexes synthesised by Clegg et al.,[25] ferrocenylimido hexamolybdate complexes synthesised by Stark in 1995,[36] both shown in figure 1.3b, and porphyrin-POM hybrid materials synthesised by Araghi et al. in 2012.[37]
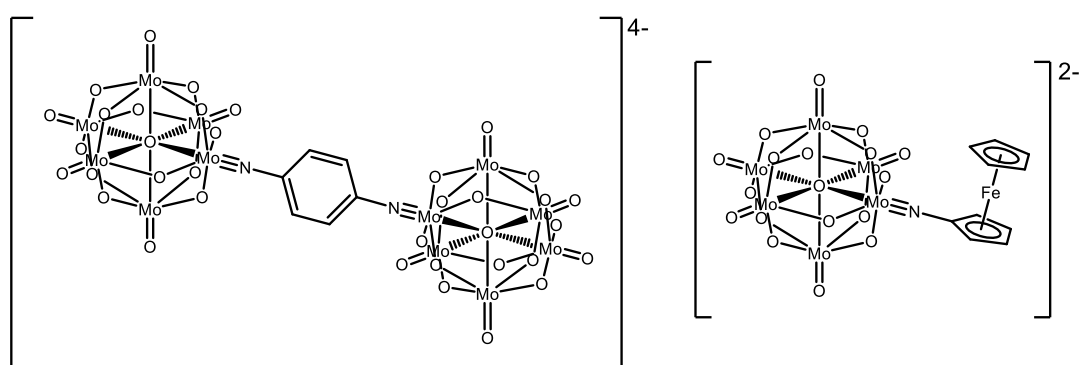
Figure 1.3b Functionalised molybdenum POMs synthesised by Clegg[33] (left) and Stark[72] (right).

Further reaction of the functionalised polyoxometalates to produce an even wider array of compounds is also possible, with both Sonogashira[38] and Heck[39] coupling reactions having been performed on iodo functionalised hexamolybdate derivatives in the past. This extension of the conjugated aromatic chain bonded to the hexamolybdate core allows for further integration of organic functional groups or metals, as well as incorporation of the derivatives into other materials such as polymers.[40,41]
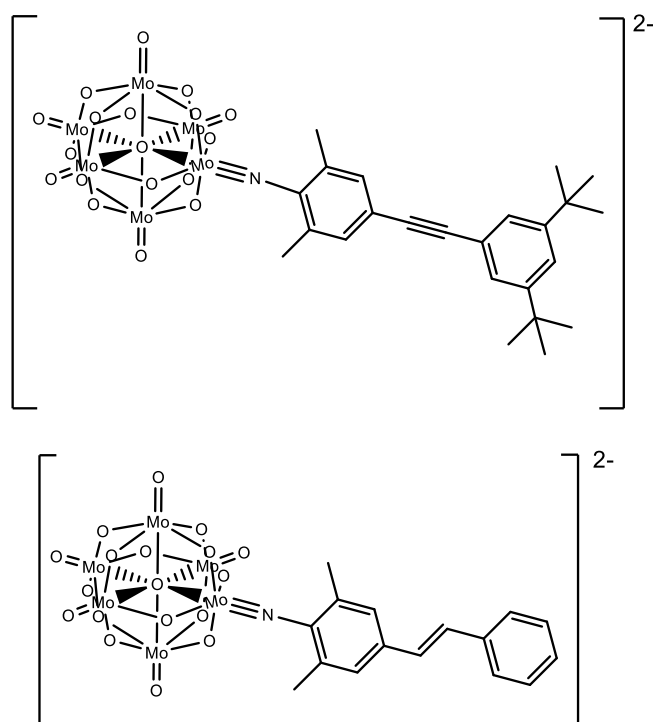
Figure 1.3c Functionalised molybdenum POMs synthesised by Xu[38] (top) and Zhu[39] (bottom).

The functionalisation of hexamolybdate and the ability to further react on from there has led to an extensive range of compounds which in turn have been investigated for use in a wide variety of fields. Examples include as dyes in dye sensitised solar cells,[42] as electropolymer poly-pyrrole films used for capacitance,[43] for reversible, proton-switchable fluorescence,[44] as anti-cancer agents,[15] and as nonlinear optically active chromophores with potentially switchable NLO responses.[3,45]

1.4 Basics of Non-Linear Optics

Non-linear optics has become an area of expanding scientific interest in recent decades as NLO materials have great potential in optical information processing, telecommunication, and integrated optics.[46] They are already of vital importance in the modern world, with uses ranging from the production of green laser beams in yttrium-aluminium-garnet lasers to the conversion of electrical signals into optical ones. This

is called electro-optical modulation and is crucial for the functionality of the fibre optic cabling used in modern day internet communication.[47]

Most NLO materials currently in use are inorganic crystals such as quartz, however, the usefulness of these is limited both by their activity, a restriction originating from the activity/transparency trade off, and slow response times, a result of the NLO activity of such crystals originating from slow lattice vibrations. More recently, conjugated organic chromophores have become a prominent area of research for use in such devices, as these present the significant advantage of the NLO responses resulting from electron polarization within the molecule which reduces response times to the tens of femtosecond timescale and broadens the potential uses of NLO compounds.[48] Another area of research is into compounds with switchable NLO responses for possible uses in optical information processing.

Non-linear optical effects were first seen as far back as 1870 when the DC Kerr effect, a phenomenon in which the application of a strong DC current to a material can alter the refractive index of the material, was first discovered, although they still remained relatively unexplored until after the invention of the ruby laser in 1960.[49] The first non-linear experiment was performed shortly afterwards in 1961 and demonstrated that shining laser light with the wavelength 694.3 nm through a quartz crystal could generate light with a wavelength of 347.15 nm, exactly half that of the incident laser light.

Despite the experiment demonstrating the interesting NLO properties of the quartz and the possibility of second harmonic generation, it also showed that the phenomenon was not at this stage useful as only 1 out of 10^8 photons detected had the doubled frequency.[50] Since then, the efficiency of second harmonic generation has been improved to tens of percent by phase matching, in which the phases of the laser light and higher energy emission are matched to reduce the conversion of the second harmonic light back to the fundamental light making second harmonic generation a useful phenomenon rather than just an interesting one.

Many other nonlinear optical effects were also discovered during the 1960s, with one example being optical rectification, a phenomenon in which the passing of laser light though a crystal connected to two capacitor plates produces a potential difference between the plates due to the laser causing displacement of the positive and negative

charges within the crystal. Another example is sum frequency generating in which two different energy photons are combined to generate a photon of a third frequency; second harmonic generation is a special case of this. A third example is difference frequency generating, in which a laser light can be split into two lower frequency waves by interaction with one of these lower wavelengths of light. There are many other interesting and useful non-linear optical effects that can be observed, however, for this work, only processes that result in the generation of the second harmonic are studied.

The generation of the second harmonic frequency in quartz, and many other NLO active crystals, is due to interaction of the electric field of light with matter inducing a polarization of the electron density in the atoms. This induced dipole moment, when multiple atoms are considered, results in polarization of areas of quartz. When the intensity of the light is relatively low, a linear relationship exists between the induced dipole (μ) and the energy of the incident beam (E), but at higher intensities, the linearity of this relationship fails and the polarisation, or optical susceptibility for bulk compounds, becomes dependant on the applied electric field.

$$\mu = \alpha E \qquad (1.4.1)$$

The polarisation induced by the electric field of the light can be expressed by a power series of the electric field (1.4.2) where α is the linear polarizability, β is the second-order polarizability, which is also known as the first hyperpolarizability, and γ is the third-order polarizability, which is also known as the second hyperpolarizability. It is these hyperpolarizabilities which, when the sample is irradiated, result in non-linear optical effects.

$$\mu = \alpha E + \beta E^2 + \gamma E^3 + \cdots \qquad (1.4.2)$$

The first hyperpolarizability, β, is a third rank tensor containing the 27 elements corresponding to the combinations of the three Cartesian components interacting with the two interacting electronic fields. Due to symmetry, the number of relevant components can often be reduced so that typically only a few elements are non-zero for any given compound. For example, all elements will be reduced to 0 for a centrosymmetric molecule. For much of this work, the symmetry of the compounds results in only one component out of the 27 being significantly large, reducing the number of relevant elements to one.

The magnitude of the first hyperpolarizability, β, determines the efficiency of the nonlinear optically active compound and can be described by the two-state model which was developed by Oudar and Chemla (1.4.3).[51] This model relates the first static hyperpolarizability to molecular parameters such as the energy of the optical transition between the relevant ground and excited states and the change in dipole this results in. It is valuable for understanding and designing molecular chromophores. Here, β_0 denotes the first static hyperpolarizability, μ_{12} denotes the electronic transition dipole moment, E_{max} denotes the energy of the optical transition between the ground and excited state, and $\varDelta\mu_{12}$ denotes the change in dipole moment between the ground and excited state. As can be seen from the equation, increased hyperpolarizability can be achieved by decreasing the energy of the relevant charge transfer peak, as well as increasing both the molecular dipole and the change in the molecular dipole between the ground and excited states.

$$\beta_0 = \frac{3\varDelta\mu_{12}(\mu_{12})^2}{2(E_{max})^2} \tag{1.4.3}$$

For the comparison and measuring of the NLO properties of a material, the static hyperpolarizability, β_0, is typically used rather than the hyperpolarizability, β. The first static hyperpolarizability represents the first hyperpolarizability extrapolated to zero frequency under non resonant conditions. The use of non-resonant conditions when determining the NLO properties of a material is vital, as resonance allows for the generated second harmonic to interact with higher level energy states of the material which can result in huge under or overestimates of β. The value of β_0 is also independent of the wavelength of the light whereas β varies depending on the frequency of the incident beam and use of β_0 therefore allows for a fairer comparison between materials. The first static hyperpolarizability can be calculated from the measured first hyperpolarizability under non-resonant conditions using the two state model (1.4.4). Here, λ_{max} is the wavelength of maximum absorption of the compound and λ is the wavelength of the incident laser light used during the experime (1.4.4) equation can also be written where the wavelength of the second harmonic is used as the denominator of the second term, removing the need for the doubling of the λ_{max} in the second nominator.

$$\beta_o = \beta \left[1 - \left(\frac{\lambda_{max}}{\lambda}\right)^2\right]\left[1 - \left(\frac{2\lambda_{max}}{\lambda}\right)^2\right] \tag{1.4.4}$$

There are currently four techniques available for the measurement of the second hyperpolarizability; Second Harmonic Generation, Electric Field Induced Second Harmonic Generation, Hyper-Rayleigh Scattering, and Stark spectroscopy. Second Harmonic Generation is a highly anisotropic, coherent, and phase matched process that results in the re-emission of photons of double the frequency of the incident beam from non-centrosymmetric crystals. It is by far the oldest technique used for measuring the hyperpolarizability of non-linearly active compounds, however, due to the necessity for an overall dipole for effects to be observed, its use is limited to non-centrosymmetric crystals and orientated thin films.

Electric Field Induced Second Harmonic Generation (EFISH) was a technique proposed shortly after the invention of SHG and presented a method suitable for the measurement of compounds in solution.[52] In the EFISH process, molecules in solution are aligned using an external electric field which when irradiated can initiate a strong NLO response. However, due to the electric field being used to align the compounds and create a net dipole, EFISH is not a technique suitable for solutions of ionic chromophores or centrosymmetric compounds.

In contrast to the two previous methods, Hyper-Rayleigh Scattering, which is the spontaneous, isotropic, and dephased re-emission of photons with double the energy of the incident beam, does not rely on the net dipole of the analyte, and instead occurs due to the presence of localised temporary dipoles.[53,54] This makes Hyper-Rayleigh Scattering suitable for measuring ionic solutions as well as solutions of centrosymmetric compounds, such as octupoles, which are either charged or do not have the diploe necessary to be aligned for measurement using EFISH. The $\beta_{0,zzz}$ calculatable from Hyper-Rayleigh Scattering experiments is also comparable with β_{EFISH} measured during EFISH¸ allowing for comparison of compounds measured using the two different techniques.

The fourth technique that can be used to determine Stark spectroscopy, although this method uses a more indirect technique than Second Harmonic Generation, EFISH, and Hyper-Rayleigh Scattering. Instead of directly measuring the intensity of the frequency doubled radiation emitted from the sample upon radiation, Stark Spectroscopy uses the electronic spectra to measure change in the dipole moment of a glass formed of the compound upon the application of a direct current.[55] These changes

in the dipole moment along with λ_{max} can be used to predict β using the two state model.[56] Stark spectroscopy has advantages over Second Harmonic Generation in that like EFISH and Hyper-Rayleigh Scattering, analysis can be carried out on solutions, and has further advantages over EFISH and Hyper-Rayleigh Scattering in that resonance effects do not result in underestimation of the results. However, Stark Spectroscopy has been shown to result in overestimation of β when compared to EFISH and Hyper-Rayleigh Scattering.[57] Stark spectroscopy also does not take into account the directionality of the dipoles, resulting in overestimation β values for multidimensional chromophores where dipoles would partially cancel.

1.5 Non-Linear Optically Active Materials

After the discovery of the nonlinear optical properties of quartz crystals in the 1960's, initial studies were focused mainly on inorganic crystals, such as $LiNbO_3$[58] and KH_2PO_4,[59] and was followed by research into the NLO properties of inorganic semiconductors such as GaAs[60]. While inorganic semiconductors rely on electronic transitions and therefore show significantly faster response times than inorganic crystals, semiconducting crystals are expensive to produce. More problematically, they also typically absorb in the visible region of the electromagnetic spectrum, resulting in reabsorption of the second harmonic and limiting the magnitude of NLO response.[61] In response, in recent decades research has been carried out into the use of organic or organometallic chromophores as cheaper, more transparent, and faster responding alternatives to purely inorganic materials. These NLO active organic and organometallic chromophores feature a permanent dipole through the inclusion of electron donor/acceptor pairs, while the conjugated bridge allows for charge transfer transitions to occur upon excitation. These result in the change in dipole moment within the molecule needed for NLO activity, as discussed in the form of the two state model mentioned previously.

The two state model can also be used to predict methods of increasing the activity of synthetic compounds. This can be achieved by increasing the charge separation between the ground and excited state which would increase the change in dipole moment, or by increasing coupling between the donor and acceptor which would increase the electronic transition dipole moment. The NLO activity of compounds can

also be improved by decreasing the energy of the transition between the ground and excited states through the use of strong donor/acceptor pairs and increasing the size of the conjugated π system in organic chromophores. Increasing the NLO properties of synthetic chromophores can be challenging, though, as it is difficult to simultaneously increase charge separation and increase coupling, meaning improvement in one sense often decreases performance in another. The two state model also shows how β can be increased by decreasing the energy of the maximum wavelength of the charge transfer peak, however, lowering the energy of this peak too much can result in reabsorption of the frequency doubled light, a problem often referred to as the transparency-efficiency trade-off.

The first molecular chromophores synthesised were neutral organic compounds, originally of interest due to their low cost, fast and large NLO response, and synthetic flexibility. Many of these earlier compounds were based on the derivatives of benzene, stilbene or styrene, with electron donating groups such as amines and methoxy groups featured at one end of the molecule and electron withdrawing groups such as nitro and cyano groups at the other. Separated by the conjugated π systems, these created the charge separation and net molecular dipole needed for NLO activity, with stilbene style compounds in particular showing good responses due to their longer conjugated π systems.[62]

Although not the most active or thermally stable of chromophores, these neutral organic chromophores allowed for investigation into the effects of the strength of the donor and acceptor groups as well as the length of the conjugated bridge on NLO activity. This provided valuable information and demonstrated that it is not just the three components as separate entities that effect the activity of the compound, but how they function together.[63] Investigation into this also showed that due to the importance of the interaction of the donor and acceptor orbitals with those of the bridge, it is not necessarily the compound with the strongest donor or acceptor that has the best NLO activity. Further investigation also showed that the most conjugated bridges did not lead to the highest responses, as increasing the coupling also decreases the charge separation, lowering the activity. These early organic chromophores also revealed that even compounds that have the bridge-separated donor and acceptor groups necessary for NLO activity may not be suitable for second harmonic generation in their solid state due to centrosymmetry of the crystal structure.[64]
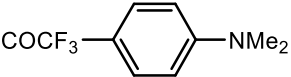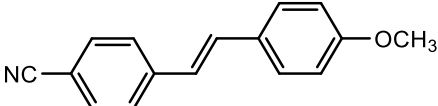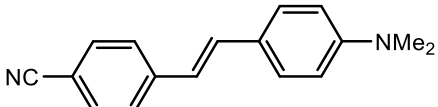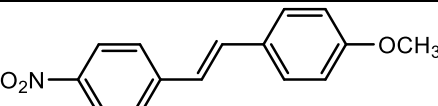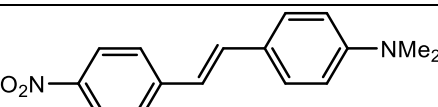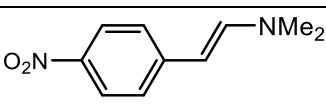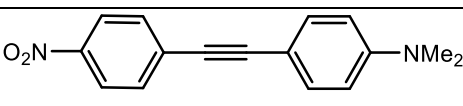
Compound	β (x 10^{-30} esu)
O$_2$N—⟨benzene⟩—NH$_2$	9.2
O$_2$N—⟨benzene⟩—NMe$_2$	12.0
COCF$_3$—⟨benzene⟩—NMe$_2$	10.0
NC—⟨benzene⟩—CH=CH—⟨benzene⟩—OCH$_3$	19.0
NC—⟨benzene⟩—CH=CH—⟨benzene⟩—NMe$_2$	36.0
O$_2$N—⟨benzene⟩—CH=CH—⟨benzene⟩—OCH$_3$	15.0
O$_2$N—⟨benzene⟩—CH=CH—⟨benzene⟩—NMe$_2$	73.0
O$_2$N—⟨benzene⟩—CH=CH—NMe$_2$	50.0[65]
O$_2$N—⟨benzene⟩—C≡C—⟨benzene⟩—NMe$_2$	46.0[66]

Table 1.5a A selection of NLO active organic chromophores.[64]

More innovative structures such as tricyanovinylthiophene derivatives,[67] substituted calixarenes,[68] zwitterions,[69] TICTOID (twisted intramolecular charge transfer) structures),[70] and polymers based on phenonitrobenzoxazole[71] have also been investigated for use as NLO chromophores over the years with the intention of improving SHG, encouraging the growth of noncentrosymmetric crystals, and increasing thermal and chemical stability.
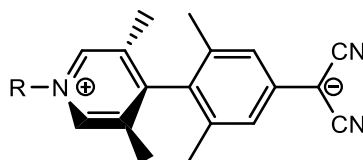
Figure 1.5a A TICTOID structure synthesised by Shi[70] for frequency doubling, reported to have a high NLO response due to the twist between the two phenyl rings increasing charge separation.

After the discovery of Hyper-Rayleigh Scattering enabling the measurement of charged compounds, investigation into the use of ionic organic molecules as NLO active chromophores was possible. These charged compounds tended to show higher thermal and photochemical stability than the original neutral organic chromophores. The counterion variability also leads to a wider range of possible structures for each chromophore, statistically increasing chances of producing a SHG active polar crystal structure.[72] Duan also demonstrated the increased hyperpolarizabilities of ionic compounds over similarly structured neutral compounds.[73] One notable example of charged organic material is Dimethyl-Amino-Stilbazolium Tosylate (DAST), which was first synthesised by Nakanishi et al. in 1989[74] and is the only commercially available nonlinear optically active organic chromophore to date. This has a β_0 value of 25×10^{-30} esu which is comparable to many other organic chromophores, however, DAST's increased stability allows for its use as a widely tuneable difference frequency generation source in the terahertz region.[75]
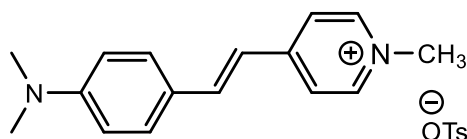
Figure 1.5b Dimethyl-amino-stillbazolium Tosylate (DAST).

In addition to purely inorganic and organic chromophores, studies have also been carried out on organometallic NLO chromophores, the first report of which with good SHG efficiency came in 1987 from Green et al., in the form of a (4-nitrophenyl)ethylene substituted ferrocene.[76] This compound was formed in both the

cis and *trans* isomer, however only the *cis* isomer demonstrated non-linear optical activity when investigated by second harmonic generation due to the *trans* isomer crystallising in a centrosymmetric space group.
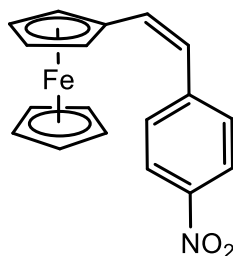
Figure 1.5c A nitrophenylethenyl substituted ferrocene synthesised by Green et al, the first organometallic chromophore to show good SHG efficiency.[76]

Since the first organometallic NLO active chromophore was synthesised by Green et al., chromium[77] and ruthenium[78] metallocene derivatives have also been investigated to show good nonlinear-optical activity. Transition metals, such as ruthenium,[79] nickel,[80] gold,[81] and iridium[82] have also been used as electron donors towards nitro or pyridinyl style acceptors in complexes such as the one synthesised by Coe et al. shown in figure 1.5d.[83,84]
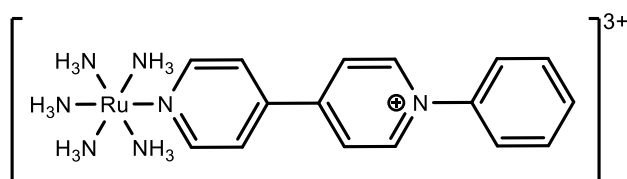
Figure 1.5d A push-pull chromophore with a ruthenium donor, synthesised by Coe et al, which gave a β_0 of 220×10^{-30} esu.

These such compounds typically show better NLO activity than their organic counterparts, a result of metal to ligand charge transfer (MLCT) transitions which result in large changes in dipole moment at relatively low energies. However, these low energy transitions result in decreased transparency. Changing the ligands bound to the metal ion can also be used to tune the properties of these organometallic

chromophores, with ligands of increasing electrophilicity increasing electron withdrawal from the metal and therefore increasing hyperpolarizability.

Although first used in the donor groups of NLO chromophores, as seen in the ferrocene derivatives synthesised by Green, transition metals have also since been used at the electron acceptor end of NLO chromophore. In some cases, transition metals have also been found in the bridge between the donor and acceptor ends. The range of uses for transition metals in chromophores arises ultimately from their variable oxidation states, resulting in hugely different properties and electron densities depending on environment. Ruthenium, previously shown in use as an electron donor, successfully demonstrates this flexibility of transition metals in NLO active chromophores, as in addition to being used as an electron donor in its +2 oxidation state, in its +3 oxidation state it finds use to as an electron acceptor.[85] As a result, some metal-metal NLO active chromophores feature ruthenium as both the electron donor and the acceptor. Tungsten,[86] iridium,[87] rhodium,[87] and osmium[87] have also all been employed as electron acceptors in NLO active chromophores with increased hyperpolarizabilities over the lone ligand due to ligand to metal charge transfer.[88,] Ligand to metal charge transfer (LMCT), like the metal to ligand charge transfer discussed previously, can have large transition dipole moments at relatively low energies, increasing hyperpolarizability through the two-state model presented earlier in the chapter.
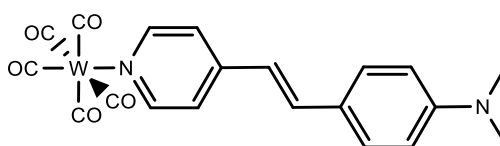
Figure 1.5e A push-pull chromophore with a tungsten acceptor, synthesised by Kanis et al, which gave a $\beta_{1.06}$ of 62×10^{-30} esu.[86]

Since their first use in organometallic chromophores as electron donors, metals have even been successfully used in the π conjugated bridges to result in increased non-linear optical activity, as was seen in the porphyrin-based push-pull chromophores studied by Karki[55] as well as in a series of platinum centred push-pull chromophores synthesised by Durand.[89] Nickel,[90] manganese,[91] and zinc[92] have also been used in

chromophores, this time featuring Schiff base style ligands, and although the metal centres in these compounds do contribute as electron donors, in systems with other strongly electron donating groups such as amines, their primary role in increasing the overall hyperpolarizability is much more similar to that played in the porphyrin-based chromophores. In these compounds the metal cations do not act as donors or acceptors, but rather sit in the π-conjugated core between the donor and acceptor groups and help to enhance the charge transfer through the π system.[93]

Compound	β_0 (x 10^{-30} esu)[a]	Role of Metal
	49[81]	Donor
	120[81]	Donor
	69[85]	Donor and acceptor
	150[94]	Donor and acceptor
	128 $(\beta_{1.34})$[87]	Acceptor
	235 $(\beta_{1.34})$[95]	Donor/bridge

Table 1.5b Hyperpolarizability of a selection of organometallic chromophores. Static hyperpolarizability is reported unless otherwise stated. [96]

1.6 Multidimensional Chromophores

In addition to improving the NLO activity/transparency trade off through the use of transition metals, the inclusion of different organic donors and acceptors, and alterations to the π conjugated bridge, research has proven that making alterations to the standard 1D donor-acceptor geometry of chromophores can lead to increased NLO activity for no additional loss in transparency.[97] Improving the efficiency-transparency trade off should also help to improve stability of the chromophores through reduced thermal decomposition due to reabsorption.

In a standard 1D donor-π-acceptor chromophore, the dominant tensor component of β, typically β_{zzz} lies directly along the dipolar axis, z. This often results in reabsorption of the second harmonic generated decreasing overall efficiency. In order to prevent this and improve the efficiency-transparency trade off, work has been carried out into the possibility of multidimensional chromophores such as 2D dipolar compounds with C_{2v} symmetry. In such compounds the dipoles displaying electronic transitions, μ_{12}, do not lie along the C_2 axis of the molecule, resulting in significant off-diagonal β components. The photons generated by the off-diagonal β components are polarized perpendicular to the dipoles of the electronic transitions that produced them and therefore cannot be reabsorbed in the same way as the β_{zzz} generated photons.[97]

Significant off-diagonal NLO responses have been observed from a variety of multidimensional chromophores. Octupoles, compounds with three donor/acceptor pairs arranged so the net dipole of the molecule is zero such as 1,3,5-triamino-2,4,6-trinitrobenzene, are seen to be promising NLO candidates due to their significant off-diagonal components increasing phase matching and improving the efficiency/transparency trade-off. Two dimensional V shaped compounds, where two donor/acceptor pairs intersect at a donor or acceptor group resulting in donor-acceptor-donor and acceptor-donor-acceptor compounds, have also been observed to show improved efficiency, transparency, and phase matching.[97]

Over the years, both organic and organometallic D-A-D and A-D-A chromophores have been synthesised and the effects of the V shape system on the NLO activity probed. In addition to synthesising ruthenium based NLO chromophores with a variety of donor and acceptor groups, Coe et al., also synthesised analogues of some of these structures featuring two amine acceptor groups as ligands to their ruthenium(II)

donor.[98] These typically featured the two donor groups in a *cis* geometry, giving the compounds the V shaped symmetry expected to increase the off-diagonal components of β. An example of one of these one-donor-to-acceptor chromophore gave a $\beta_{0,zzz}$ of 126×10^{-30} esu and a $\beta_{0,zyy}$ of -54×10^{-30} esu compared to a $\beta_{0,zzz}$ of 220 for the mono-substituted analogue, showing a slightly decreased $\beta_{0,zzz}$ but also a considerable off diagonal component.[99]
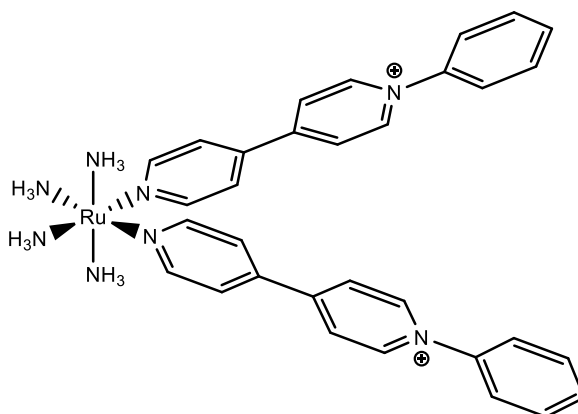
Figure 1.6a Two dimensional one-donor-two-acceptor complex synthesised by Coe et al., a chromophore which demonstrated increased β compared to its mono-substituted analogue.
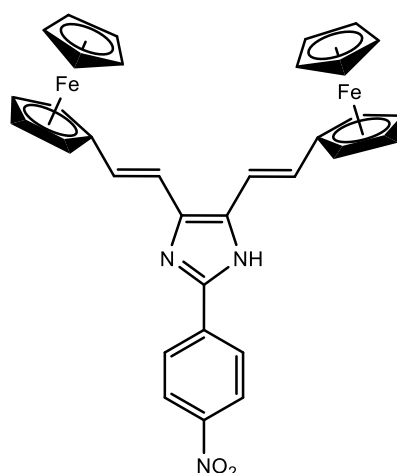
Figure 1.6b Two dimensional D-A-D NLO chromophore synthesised by Prabu et al.[100]

A recent example of organometallic two-donor-one-acceptor NLO active chromophores can be seen in work by Prabu et al[100] involving the synthesis and

23

analysis of push-pull imidazole chromophores, such as the one shown in figure 1.6b. These Y-shaped ferrocene conjugated imidazole chromophores show both a good hyperpolarizability, with a β_0 of -111×10^{-30} esu measured using EFISH and excellent thermal stability, a key advantage expected of C_{2v} chromophores over dipolar analogues due to the reduced reabsorption of the frequency doubled light.

Investigation into the ideal angle between the donor and acceptor branches of these Y-shaped systems has also been carried out, with calculations performed by a variety of groups over the years. In 2003, calculations by Yang and Champagne on a series of Λ-shaped organic chromophores showed that as the angle between the donor branches increases β_{zzz} will decrease, while the magnitude of the off diagonal component of β, β_{xxz}, will increase until the angle reaches 109.46° after which it will decrease. [101] The work also showed that if the angle between the two donor branches is below 120°, β_{zzz} will be the major component of β_{total}, whereas for compounds with a between branch angle of above 120°, the off diagonal components will likely be larger. Muhammed et al. also investigated the relationship between the angle between the donor or acceptor branches on a series of two-donor-one-acceptor and one-donor-two-acceptor borane cluster compounds and received similar results, with β_{zzz} decreasing as the angle between the donor or acceptor branches increased, and β_{zyy} increasing until a point at which it then too decreased.[102]

1.7 Switchable Chromophores

Molecular switches are defined as compounds that have multiple stable forms with differing properties which can be changed between by applying an external stimulus. These properties range from optical to electronic and magnetic, and a wide range of stimuli have been used to activate switching mechanisms, with examples including light, [103] electric field,[104] pH,[105] change of solvent,[106] and reduction/oxidation.[83,107]

In terms of nonlinear-optically active compounds, creating switchable chromophores is of interest for uses in telecommunications and optical computing, a technology that could vastly improve computer processing performance through increased speeds, higher parallelism, and lower energy consumption. This is of vital importance as we move into a more technology dependent world, with approximately 10% of the world's

energy usage already resulting from the computers and the internet, a figure 50% higher than aviation.[108]

Materials with switchable optical responses are already used in some aspects of modern technology, with fibreoptic internet routers using the electro-optical effect of inorganic crystals such as $LiNbO_3$ to change the electrical information into optical signals. These optical signals greatly increase bandwidth, speed and reliability over the electronic signals used in conventional copper wires. However, the electro-optical effects demonstrated by these inorganic crystals are very small, with application of the electrical field typically leading to a change in the refractive index of the crystal of less than 1%.[109] This limited response makes inorganic crystals unsuitable for purposes such as optical computing where a more complete on and off switching of activity is necessary. For such purposes, molecular chromophores are of interest.

Three main designs of switchable NLO active chromophores currently exist, with Coe having outlined the three switching mechanisms back in 1999.[110] Both organic and organometallic chromophores rely on three components for NLO activity; the donor, the acceptor, and the π bridge between, and Coe theorised that disruption to any one of these components would result in diminished hyperpolarizability.
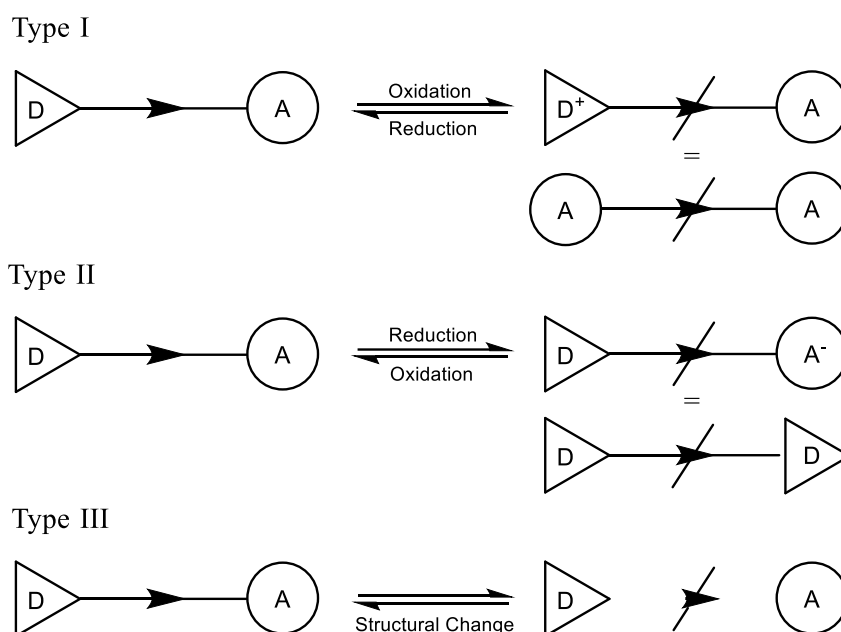
Figure 1.7a Scheme showing the three proposed switching mechanisms for turning off NLO responses in molecular chromophores.

In type I, disruption to the donor-π bridge-acceptor structure would occur through protonation or oxidation of the donor, therefore weakening electron donation, while in type II, the opposite would occur, with a second electron donor being formed through the reduction or deprotonation of the acceptor. In type III, the charge transfer between the donor and acceptor would be stopped not by removal of either the donor or acceptor, but by disruption of the conjugation in the π bridge through a structural change such as isomerisation.

Many of the first potentially switchable NLO chromophores were organic molecules or proteins such as the azo dye disperse red 1 or bacteriorhodopsin, with switchable responses originating primarily due to structural changes brough about through photoisomerisation. Irradiation of bacteriorhodopsin containing bacterium with 570 nm light resulted in up to a 90% reduction in the SHG intensity, with responses occurring in less than 1 μs.[103] As the protein completed its photocycle, complete reversibility of this weakening in NLO responses was seen. Shortly afterwards, retinal derivatives based on bacteriorhodopsin were also shown to demonstrate good reductions in HRS responses after photoisomerisation.[111]
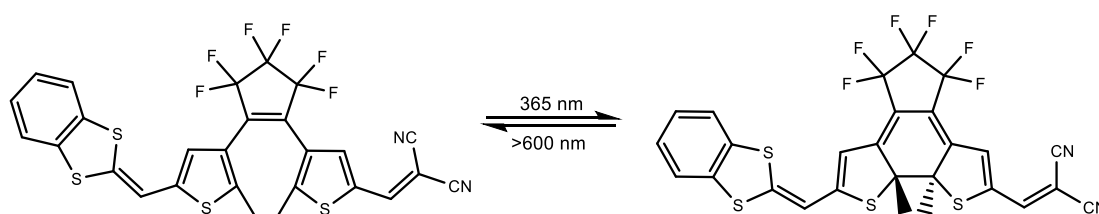
Figure 1.7b Thiophene derivatives of perfluorocyclopentene showed a reversible, repeatable increase in hyperpolarizability through increased conjugation due to photocyclization.

In 1995 it was discovered that thiophene derivatives of perfluorocyclopentene were photochromic due to photocyclization, resulting in a change from yellow to blue that were completely reversed upon exposure to lower energy light. The change in colour arises from increased conjugation in the cyclized isomer resulting in a near infra-red charge transfer from the 1,3-benzodithiole-2-ylideneyl donor group to the di-cyanomethylidenyl acceptor group. EFISH studies have since confirmed that the increased conjugation observed in the cyclized molecule initially demonstrated by the

charge transfer band did result in increased NLO activity, with a fully reversible four-fold increase in β response seen for the cyclised compound over the uncyclized.[112] Although these compounds showed good thermal and photochemical stability[113] as well as reversible NLO switchable responses, slow response times of around 30 seconds for complete cyclization and 5 minutes for complete regeneration of the original chromophore limit the usefulness of the compound in devises.

Since interest was first generated in molecular NLO chromophores, the inclusion of metals has helped to create compounds with much higher hyperpolarizabilities and stabilities than seen for conventionally bridged organics, but their changeable oxidation states also lead to the possibility of stable and fast switchable chromophores. One of the first examples of this was demonstrated by Coe at al.,[83] with the reversible and easily accessible chemical oxidation of his ruthenium(II) amine complexes of 4,4'-bipyridinium ligands to ruthenium(III) showing a 10- to 20-fold reversible and repeatable weakening in hyperpolarizability. Many similar systems with chemical redox initiated NLO switching, such as the octamethylferrocene donor, nitrothiophene acceptor systems synthesised by Malaun et al.[107] have since been synthesised.
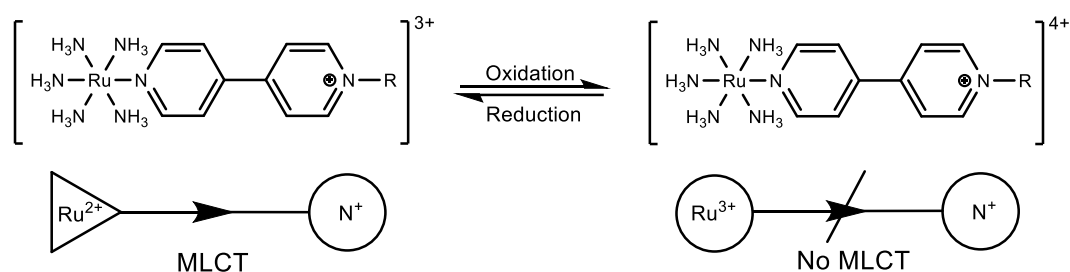
Figure 1.7c The ruthenium(II) amine complexes of 4,4'-bipyridinium ligands synthesised by Coe et al. demonstrated reversible and repeatable redox activated switching with a 10- to 20-fold reduction in hyperpolarizability.

Photoswitching of films made of platinum(III) compounds have also shown good responses, with Second Harmonic Generation experiments showing a considerable reduction in the hyperpolarizability of the films upon irradiation with UV light, an effect that could be repeatably reversed by irradiation with visible light.[114] Increased hyperpolarizability through protonation of cyclometalated platinum(II) chromophores

has also been observed, with further modulation of the NLO activity of the protonated compound possible through UV irradiation.[115]

Electrochemical redox activated switching of solutions was first performed on a ferrocene style compound with a nitrothiophene acceptor by Asselberghs et al.[116] using a specially developed cell. This cell allowed for simultaneous in situ oxidation and re-reduction of the ferrocene donor and measurement of the Hyper-Rayleigh scattering and ultimately revealed reversable and repeatable NLO switching with a reduction in activity similar to the 92% previously seen during chemical switching.[116] Although the timescale of the oxidations and re-reductions achieved using this cell were not as fast as had been seen during chemical reduction, the cell still provided a means to simultaneous achieving electrochemical switching and Hyper-Rayleigh scattering measurements. Achieving NLO switching through electrochemical redox processes is advantageous as unlike methods such as chemical reduction and protonation, switching can be achieved without altering the composition of the sample through the addition of redox agents, enabling theoretically infinitely repeatable switching. If immobilisation of chromophores on an electrode could be achieved, this could also lead to very fast response times.

In addition to compounds showing on/off switching of the NLO properties, compounds calculated to show the reverse effect of this have also been reported, where oxidation or reduction leads to an increase in hyperpolarizability. Calculations by Guan et al performed in 2008 suggest Keggin-type polyoxometalate derivatives with the form $[PW_{11}O_{39}\{Sn(p\text{-}C_6H_4I)\}]^{4-}$ would show off/on redox activated NLO responses, with a 72 fold increase in β_0 predicted upon a multi-electron reduction.[117]

Off/on switching of organometallic chromophores has also been experimentally observed, with the bis(salicylaldiminato)zinc(II) Schiff-base complexes synthesised by Bella et al., demonstrating hugely increased NLO activities after the formation of the pyridine adduct.[118] These compounds demonstrated impressive switching abilities, with β_0 increasing to 330×10^{-30} esu upon addition of pyridine, however due to the nature of the switching mechanism, easy reversal of the modulation was not possible. Switching through protonation has also been observed in a platinum complex synthesised by Attar et al., with a 12 fold increase in β from 60 to 735×10^{-30} esu upon protonation of the ligand.[119] In this case, hyperpolarizability measurements taken after

addition of NH_3 suggested regeneration of the original chromophore had occurred. Electrochemical redox activated switching on of non-linear optically active compounds has also been recorded, with measurement of a series of mono- and bi-ruthenium complexes synthesised by Karthika et al revealing substantially increased hyperpolarizabilities when oxidised due to increased ligand to metal charge transfer in the oxidised species.[120] These were performed using the same technique as the on/off switching of the ferrocene derivatives published by Asselberghs et al, with oxidation achieved in between 30 and 70 minutes depending on the sample.

Since the concept of redox switchable chromophores was first suggested, redox switchable NLO active polymers and thin films have also become area of interest due to the increased potential of solid state chromophores over those in solution state for technological applications such as optical computing. To produce NLO active films, significant numbers of chromophores need to be incorporated into polar materials with their dipoles aligned, while for switching, these compounds still need to be electrochemically accessible. Multiple techniques can result in this, such as through the formation of thin films on conductive glass by ionic surface interactions, as seen in the work by Boubekeur-Lecaque[121] who reported the first redox switchable NLO active film, synthesised by the deposition of ruthenium(II) chromophores synthesised by Coe et al.[122] on ITO-coated hydrophilic glass, as well as through covalent means in the form of polymerisation of NLO active monomers,[123] although these have yet to be seen to be switchable. The benefit of a solid state, redox-switchable NLO active chromophore, a system much more suitable for use in real-world applications than a chromophore dissolved in an electrolytic solution, means research into the formation of such systems is ongoing.

1.8 Polyoxometalate Based chromophores

Over the years, a great many types of NLO chromophore have been investigated, ranging from inorganic to organic to organometallic. These systems all have their pros and cons, with inorganic crystals showing good thermal stability but slow response times, organic systems showing quicker responses and being relatively cheap to make yet lacking potential for redox activated switching, and organometallic compounds overcoming this hurdle to provide switchable responses but often at the cost of low

transparency and the use of precious metals such as ruthenium. In recent years, the use of polyoxometalates as NLO chromophores has been discussed, with some focus on the imido functionalised hexamolybdate derivative.
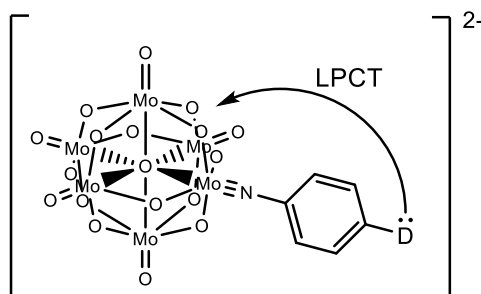
Figure 1.8a Scheme showing donor-π-acceptor structure of a generic imido functionalised hexamolybdate derivative, with the donor represented by D and the POM core acting as the acceptor.

The non-linear optical behaviour of these compounds originates from the strong electronic coupling between the organic ligand and the POM centre through the conjugated imido bond. The POM core, despite being anionic, is a strong electron acceptor due to its unoccupied d orbitals, and as a result, can accept electrons from the delocalised π system of the organic ligand. The strength of this ligand to POM charge transfer (LPCT) can be increased by addition of an electron donor, such as an amine, to the organic ligand. This results in a donor-π-acceptor system similar to previously shown of the organic and organoimido NLO active chromophores.

In 2005, density functional theory calculations performed on predicting the nonlinear optical properties of organo-imido functionalised POMs were published by Yan[124] in a response to previously synthesised hexamolybdate salts showing promising charge transfer abilities between the cations and the anionic hexamolybdate core.[125] These compounds had already demonstrated the ability of hexamolybdate to act as an excellent electron acceptor, however, the charge transfer between the donor, situated on the counter cations, and the POM was relatively weak, a result of the limited coupling between the two ions in the solid state. In an effort to generate stronger responses, increasing electronic communication between the donor and the hexamolybdate core through covalently bonding the donor to the hexamolybdate core

was investigated,[126] and it was some of these conjugated systems synthesised by Wei in the early 2000's[127,38] that Yan used for his calculations. These organoimido hexamolybdate derivatives featured unfunctionalised ligands, however even without a donor group, the calculations still predicted strong charge transfer transitions from the HOMO, formed primarily of the aromatic π system of the ligand, to the LUMO, comprising primarily of the unoccupied d orbitals in the delocalised POM core, a promising result for NLO activity.

In 2016, nine years after these first promising calculations, the nonlinear optical properties of functionalised polyoxometalates was investigated experimentally for the first time by Al-Yasari et al.[3] Some of the compounds probed featured amine or pyrrole donor groups *para* to the POM-imido bond on their aromatic ring, resulting in strong ligand to POM charge transfer transitions in their electronic spectra. Hyper-Rayleigh Scattering experiments of these compounds demonstrated NLO activity at both 1064 and 800 nm, with β_0 values of up to 133×10^{-30} esu being calculated from the raw β_{HRS} obtained in the experiments.[3] These compounds also showed good transparency when compared to organic chromophores with similar β_0 values. Despite the DFT calculations predicting high NLO activity of compounds without a resonance donor, significant β_0 values were only observed for polyoxometalate chromophores featuring an electron donor.[128]
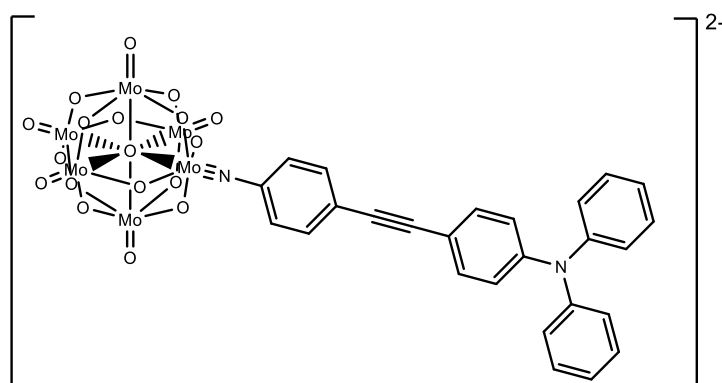
Figure 1.8b. A nonlinear optically active organoimido polyoxometalate chromophore synthesised by Al-Yasari et al. in 2018 with a β_0 of 196×10^{-30} esu.

The β_0 values for functionalised POMs has since been increased further by using weaker but more conjugating electron donors, with compounds reported by Al-Yasari in 2018 having activities of up to 196×10^{-30} esu. These compounds also had the best transparency/non-linearity seen for similar materials.[45] This was thought to be due to the charge transfer transition responsible for λ_{max} extending into the POM core, resulting in an unusually large change in dipole moment ($\Delta\mu$) for the size of the π system whilst not decreasing the donor/acceptor coupling.

In addition to the dipolar chromophores already reported, further work by Al-Yasari et al.[129] has led the possibility of Y-shaped one-donor-two-acceptor POM chromophores, with both 1,4- and 1,3-bishexamolybdate compounds having been synthesised in recent years. The 1,4- substituted compounds do not demonstrate the C_2v symmetry needed to result in off-diagonal components of hyperpolarizability, but the 1,3- systems, if a donor could be introduced at the 5 position, have potential for use as Y-shaped multi-acceptor chromophores. Two-POM lindqvist derivatives have also been synthesised by Sun et al., with the two POMs featured on separate extended arms of a central triarylamine.[130] Alternately, the reports of the cis-geometry *bis*-substituted POM complexes[131,127] also lead to the possibility of synthesising two-donor-one-acceptor systems if a donor group could be introduced to the ligands. Calculations with such *bis*-substituted compounds have already been performed by Janjua et al.[132] and show good diagonal and off-diagonal NLO responses, however, no experimental HRS work has yet been performed on *bis*-functionalised derivatives.
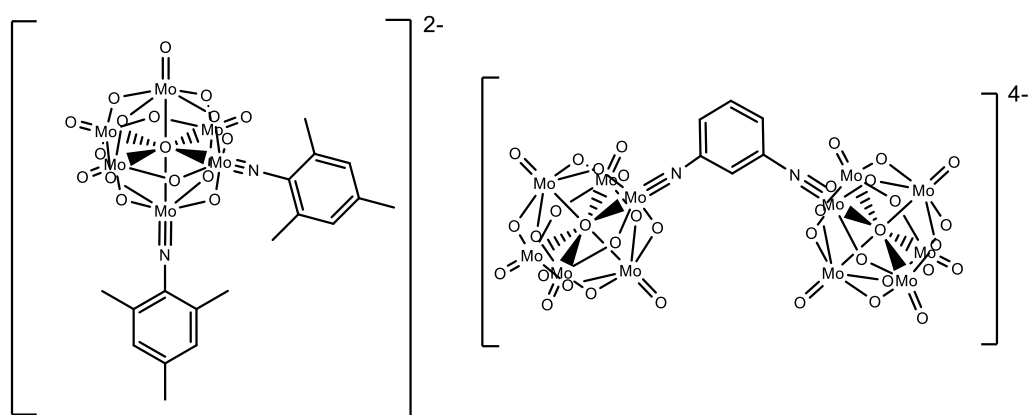
Figure 1.8c Hexamolybdate derivatives demonstrating C_2v symmetry by Xu et al. (left) and Al-Yasari (right).

In addition to the good NLO activity of the organoimido polyoxometalate chromophores synthesised by Al-Yasari, the compounds also demonstrated good redox chemistry,[3] with the POM reduction peak remaining as reversible as seen for unfunctionalised hexamolybdate. This stable redox behaviour combined with the good NLO activity led to the compounds being investigated for NLO switching with the hope that reduction of the POM core would reduce the acceptor behaviour of the POM and weaken the ligand to POM charge transfer transitions responsible for the NLO activity of the compounds. Unfortunately, when investigating this, it was discovered that reduction of the compounds left the imido bond attaching the donor containing ligand to the POM susceptible to hydrolysis, resulting in decomposition of the chromophores.[133] Overall, though, the results for these compounds were promising, as although not suitable for switching due to the susceptibility of their imido bond, the organoimido hexamolybdate derivatives demonstrated high NLO high β_0 values for the size of their π systems as well as good transparency.

1.9 Increasing Stability of the Imido Bond

So far, most of the work into functionalised derivatives of Lindqvist polyoxometalates has focused on the molybdenum structure, with a small number of vanadium based derivatives also having been synthesised. Despite the advantages of functionalised hexatungstates, one being improved stability over their molybdenum cousins, very limited numbers of functionalised hexatungstate derivative have so far been reported. This significant lack of investigation when compared to the functionalised molybdenum Lindqvist POMs is due mostly to the difficulty of synthesising functionalised tungsten derivatives, as the DCC mediated coupling reaction that works so well for the molybdenum polyoxometalate anions has yet to be successful for the tungsten alternatives. This is likely due to the stronger tungsten-oxygen bond, the factor that makes the idea of these functionalised tungsten Lindqvist POMs so interesting, impeding the exchange of the terminal oxygen with the nitrogen of the amine.

Over the years, there has only been one example of the successful formation of a tungsten imido POM; a compound synthesised by Mohs[134] in 1995 by the reaction of $[WO_4]^{2-}$ with an excess of a phenyl isocyanate in pyridine for 5 days. Unfortunately,

this method also produced a lot of unfunctionalised polyoxometalate, resulting in only a 10% yield of the desired product along with a considerable amount of unfunctionalised POM as the side product. Upon investigation, the stability of this hexatungstate derivative proved promising; heating with 1 equivalent of water for 26 days and then with a further 10 equivalents for 5 days resulted in no evidence of decomposition by ^{1}H-NMR. This demonstrated that although the functionalised tungsten polyoxometalates were harder to functionalise than their molybdenum counterparts due to the stronger tungsten-oxygen bond, there was indeed an increase of stability of the derivative. If an improved method for their synthesis could be found, they could be interesting compounds for further investigation for use in and may provide the answer to stable redox switchable NLO active polyoxometalate chromophores.

In an attempt to combine the potential stability of the imido tungsten polyoxometalates and the easier synthesis of the imido molybdenum polyoxometalates due to the weaker molybdenum-oxygen bond, tungsten/molybdenum hybrids have previously been investigated previously by Wei,[135] Sanchez, [136] and Clegg.[30] Sanchez attempted the synthesis of the tetrabutylammonium salt of $[VW_5O_{19}]^{2-}$ by the acid catalysed reaction of Na_2MoO_4 and activated WO_3 whilst Clegg attempted a method involving the reaction of $[WO(OMe)_4]$ and $[MoO_4]^{2-}$, however neither reaction produced a clean product in reasonable yield due to the self-assembly mechanism of both reactions resulting in a lack of control and a variety of side products. Wei, however, reportedly synthesised $[W_5MoO_{19}]^{2-}$ using a block assembly approach, a method that had previously been used to synthesise other hybrid POMs such as $[VW_5O_{19}]^{2-}$.[137] For this method, he used $[MoO_4]^{2-}$ and $[W_5O_{18}]^{6-}$ as reagents which were formed in situ by the dissociation of $[Mo_2O_7]^{2-}$ and $[W_{10}O_{32}]^{4-}$ respectively. After purification, this method gave the intended product with a 50% yield, which was a large improvement over previous synthesis attempts. The mixed metal POM was then functionalised using the DCC mediated coupling to produce two functionalised tungsten/molybdenum POMs with the amine group bonded to the molybdenum in both cases.

Although not previously used for the stabilisation of hexamolybdate derivatives, other methods of stabilising compounds do exist, with two examples being encapsulation in macromolecules such as cyclodextrins and steric protection. It has previously been shown that encapsulation of hexamolybdate is possible, with Falaise et al.[138] reporting

the encapsulation of sodium hexamolybdate in γ-cyclodextrin in aqueous media, interesting due to the difficulties normally associated with isolating sodium hexamolybdate from aqueous solution. Hexamolybdate derivatives with steric bulk included at the ortho positions of the imido ring have also been previously synthesised, with an early example synthesised by Strong et al.[24] shown in figure 1.9a, however no reason for the inclusion of the alkyl groups had been explicitly stated prior to 2021 when Al-Yasari reported two C_{2V} organoimido polyoxometalates with methyl steric protection.[129] These compounds showed significantly decreased hydrolysis compared to unprotected analogues, showing increased stability of hexamolybdate derivatives could be achieved at least in their natural states through steric protection of the imido bond.
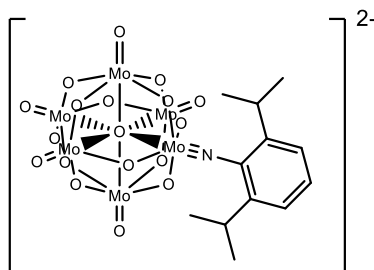
Figure 1.9a A hexamolybdate derivative synthesised by Strong et al. demonstrating the inclusion of alkyl groups at the 2 and 6 positions of the aromatic ring.

1.10 Aims for this Research

In this work, nine sterically protected monofunctionalised hexamolybdate derivatives were designed, synthesised and their properties investigated using cyclic voltammetry, bulk electrolysis, spectroelectrochemistry, X-ray crystallography, and Hyper-Rayleigh Scattering. The intention of producing these sterically protected compounds was to increase stability to the extent that investigation of the linear and nonlinear optical properties in their reduced states could be studied to determine if such polyoxometalate chromophores could be used for redox activated non-linear optical switching.

To determine the potential of multidimensional polyoxometalate chromophores, investigation was also carried out into two families of novel two-donor-one-acceptor

and one-donor-two-acceptor hexamolybdate derivatives. Five novel chromophores were synthesised and their properties studied using cyclic voltammetry, differential pulse voltammetry and Hyper-Rayleigh Scattering. Due to previous work on NLO active chromophores having shown the benefits of alkene over alkyne bridges between the donor and acceptor components, synthesis of a compound featuring an alkene π bridge between the amine donor and the POM was also carried out. The resulting compound was studied by DFT and Hyper-Rayleigh scattering to determine the effect of using an alkene bridge novel for such systems on the non-linear optical activity.

Overall, this work has four main aims:

1. Synthesise monofunctionalised hexamolybdate derivatives with steric protection at the 2 and 6 positions of their aromatic rings with the aim of achieving stability enough in their reduced state to allow for linear and non-linear optical analysis.

2. Investigate the linear and non-linear optical properties of these compounds in both their natural and reduced states to determine both the NLO activity and the investigate the potential of these compounds for molecular switching.

3. Explore the possibility of further increasing the hyperpolarizability of the hexamolybdate derivatives through multidimensional V shaped two-donor-one-acceptor and one-donor-two-acceptor systems.

4. Explore the effect of changing the linker bridge between the amine donor and POM acceptor of the extended compounds, with the expectation that increased conjugation through the alkene bridge will increase hyperpolarizability.

Chapter 2

Synthesis and Stability Studies of Sterically Protected

Monofunctionalised Hexamolybdate Derivatives

2.1 Introduction

The non-linear optical properties of functionalised Lindqvist polyoxometalates were first investigated computationally in 2005,[124] with the first experimental work being performed by Al-Yasari in 2016.[3] The promising non-linear optical activities of these compounds were then improved upon in 2017[128] and 2018[45] to result in compounds with better β_{zzz} to λ_{max} relationships than previously synthesised purely organic compounds with comparable π bridges. One such compound is shown in figure **2.1a**.
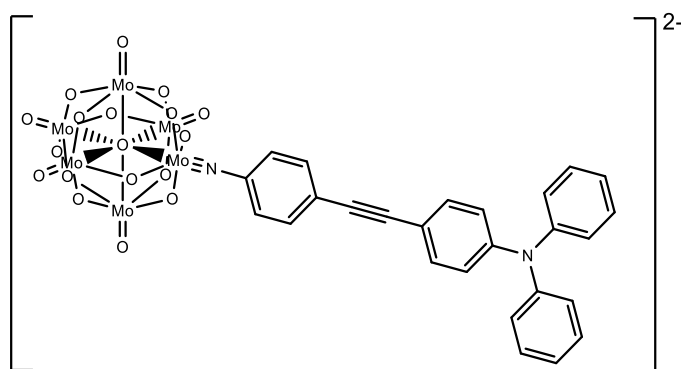
Figure 2.1a A hexamolybdate derivative with a high β_{zzz} value previously synthesised by Al-Yasari et al..[3]

Due to their impressive NLO activity resulting from ligand to POM charge transfer transitions and highly reversible electrochemical reduction of their hexamolybdate cores, the possibility of redox switching the NLO activity was investigated. Unfortunately, bulk electrolysis demonstrated that reduction of the hexamolybdate derivatives resulted in destabilisation of the imido bond, leading to decomposition at rate too quick for investigation into the optical and non-linear optical properties of the compounds to be performed.[133] An example of this can be seen in figure **2.1b**, which displays the bulk electrolysis result of compound **I**, a compound previously synthesised by Al-Yasari[3] which will be used for comparison purposes in this work. The cyclic voltammogram taken before bulk electrolysis is displayed in blue, with the major wave being assigned to compound **I**, while the CV taken after 23 minutes of reduction is shown in red. Here, the substantial decrease in the concentration of analyte can be seen along with an increased current of a peak resulting from the reduction of

tetrabutylammonium hexamolybdate, seen at -0.815 V. As it was thought that the observed breakdown of the functionalised POM derivatives into hexamolybdate was occurring through hydrolysis of the imido bond, the possibility of preventing this attack by sterically shielding the amine bond from the attack of water was investigated.
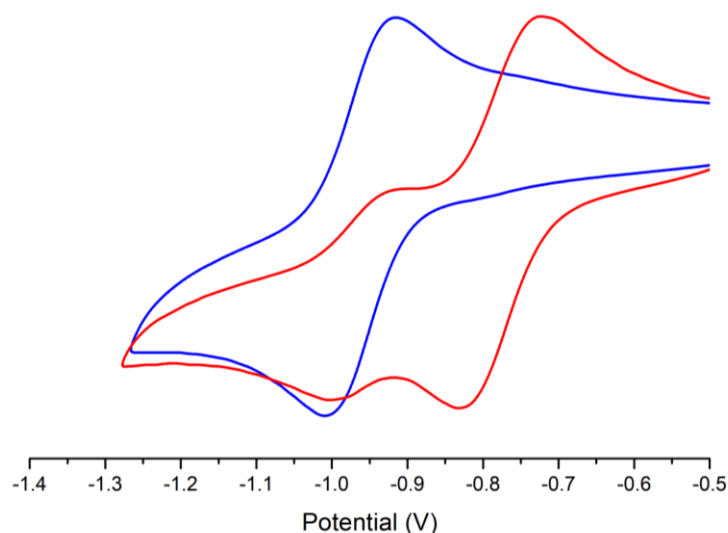
Figure 2.1b The bulk electrolysis experiment of compound **I**, with the CV taken before reduction being shown in blue, and the one taken after reduction being shown in red. Both cyclic voltammograms are referenced to Fc/Fc$^+$ and the starting currents normalised.

Two different methods of shielding the imido bond from the attack of water were researched within the group, with one method focused on stabilisation by encapsulation of the functionalised POM in cyclodextrins and calixarenes, while the other, the method this work is based upon, focused on stabilisation by the addition of alkyl groups at the 2 and 6 positions of the aromatic ring bonded to the POM. Upon finding this method to be successful at preventing decomposition of the compounds by hydrolysis when in their reduced states, a series of diisopropyl protected, donor containing functionalised hexamolybdate derivatives hopefully suitable for switched nonlinear optics was synthesised. This chapter therefore describes the synthesis, analysis, and initial stability studies of a series of novel sterically protected functionalised Lindqvist POMs, the structure and purity of which were all confirmed by ^{1}H-NMR and ^{13}C-NMR spectroscopy, mass spectrometry, elemental analysis, UV-vis spectroscopy, IR spectroscopy, and X-ray crystallography.
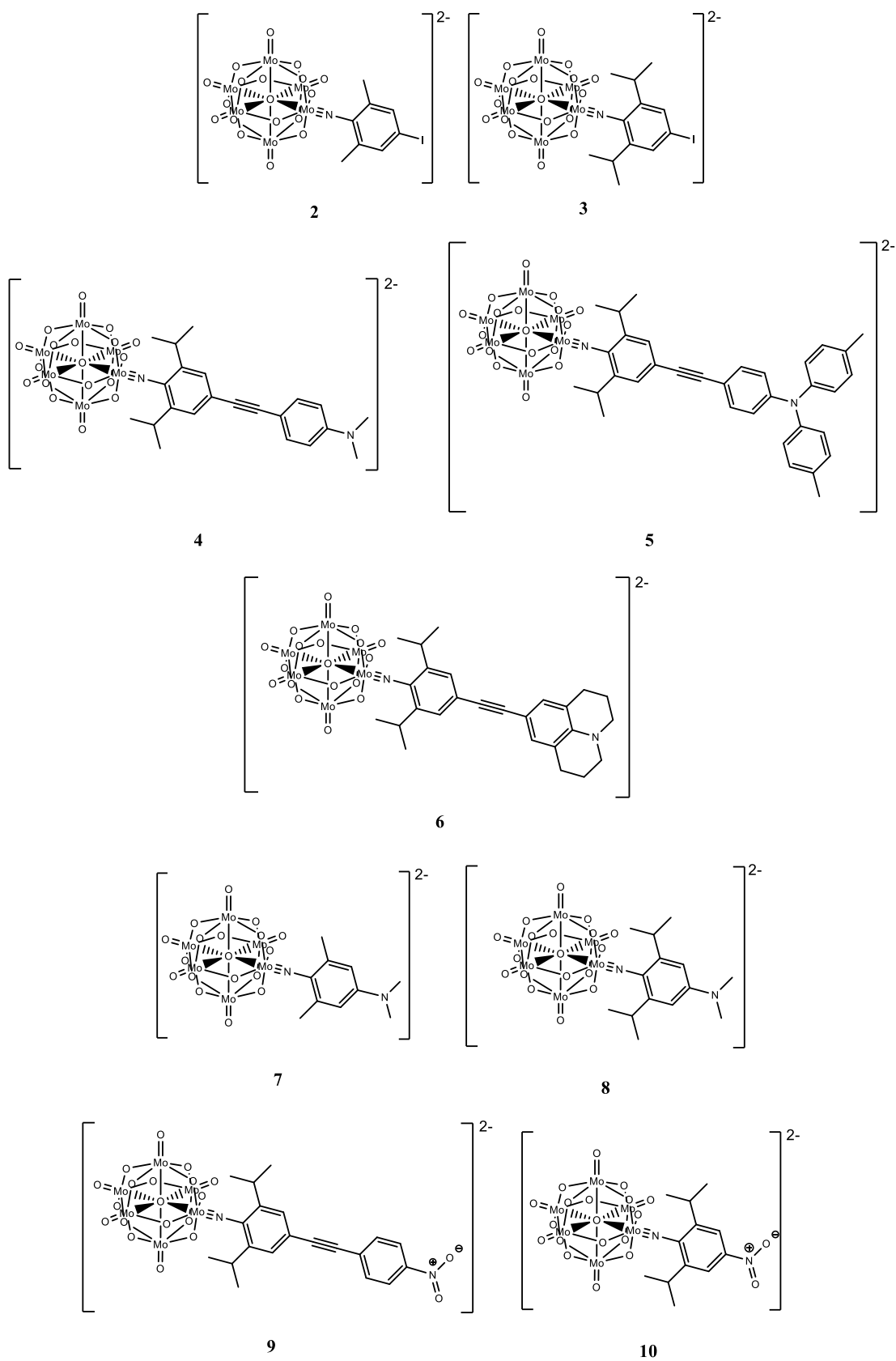
Figure 2.1c Structures of sterically protected derivatives of tetrabutylammonium hexamolybdate **2** to **10**.

2.2 Synthesis of Iodo Functionalised Derivatives

To investigate whether introducing steric bulk at the 2 and 6 positions of the aromatic ring would effectively stabilise the imido bond holding the organic ligand to the POM core, two hexamolybdate derivatives, **2** and **3** were designed. These compounds, both shown in figure 2.2a, featured alkyl groups in the 2 and 6 positions of the aromatic ring as well as iodine at the 4 position to allow for further functionalisation of the compounds through Sonogashira coupling reactions. Compound **2** had been synthesised previously by Xu but never used for reduced state stability studies.[38]
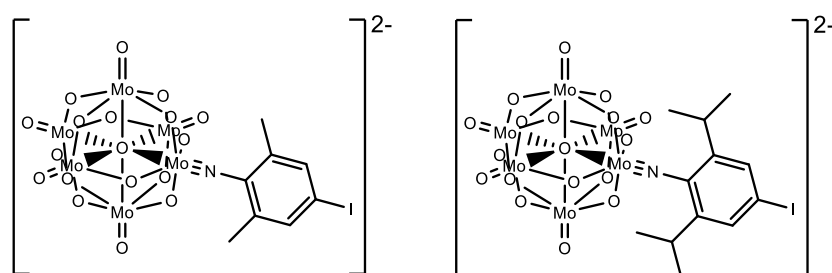
Figure 2.2a Hexamolybdate derivatives **2** (left) and **3** (right). Tetrabutylammonium was used as the counter cation for both compounds.

Synthesis of compounds **2** and **3** was performed using a DCC mediated coupling reaction between tetrabutylammonium hexamolybdate and 2,6-dimethyl-4-iodoaniline or 2,6-diisopropyl-4-iodoaniline respectively using a modified version of the method reported by Wei in 2001.[33] In this work, dry DMSO was used as the solvent in place of dry acetonitrile as previous research within the Fielden group[3] had shown it gave a better yield and resulted in a purer product. The products were obtained from the reaction by precipitation from the filtered DMSO solution using a mixture of diethyl ether, ethyl acetate, and ethanol as the antisolvents.

The red solids isolated as the product from both reactions contained impurities of unreacted tetrabutylammonium hexamolybdate as well as very small amounts of the *bis*-functionalised compound, a result of two equivalents of DCC and the aniline attacking one hexamolybdate core. Purification of both products was achieved through multiple recrystallisations from hot acetonitrile cooled to room temperature. Purity of the compounds was confirmed by ^{1}H-NMR and ^{13}C-NMR spectroscopy, mass

spectrometry, elemental analysis, UV-vis spectroscopy, IR spectroscopy, and X-ray crystallography.
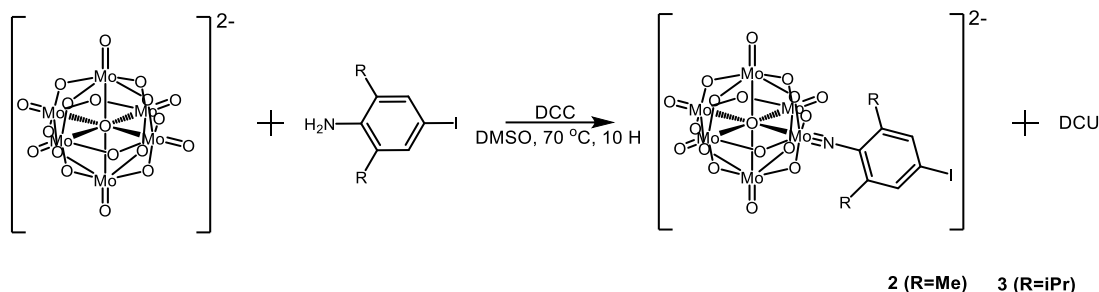
Figure 2.2b Reaction scheme for the synthesis of compounds **2** and **3**.

Formation of the desired compounds was confirmed initially using ^{1}H-NMR spectroscopy, a technique which also provided crucial in determining the ratio of product to the impurities mentioned above. The percentage impurity of hexamolybdate could be calculated by estimating all excess integration of the tetrabutylammonium peaks seen at 0.97, 1.36, 1.60, and 3.70 ppm resulted from the tetrabutylammonium hexamolybdate impurity. For example, the crude ^{1}H-NMR of compound **2** gave an integration of 1.64 for the *meta* protons on the aniline ring out of the expected two, implying that around 82% of the anions for the tetrabutylammonium cations were the desired product. The *bis*-functionalised POM impurity gave a peak with an integration of 0.05, indicating around 1.25 % of the anions in the sample were *bis*-functionalised.

The ^{1}H-NMR of compound **3** and its precursor, seen in figure 2.2b, shows a significant downfield shift of the peak caused by the protons *meta* to the C-N bond when compared to 2,6-diisopropyl-4-iodoaniline, from 7.23 ppm to 7.51 ppm, suggesting deshielding as a result of conjugation to the electron withdrawing POM core. Downfield shifts were also observed for both peaks relating to the protons in isopropyl groups from 2.89 ppm to 3.78 ppm for the CH protons and 1.18 ppm to 1.27 ppm for the CH_3 protons, with a larger shift seen for the CH septet due to the proton's proximity to the electron withdrawing POM core. Although not present in the spectrum shown in figure 2.2c, a slightly reduced downfield shift was observed for all three peaks of the *bis*-functionalised impurity due the electron withdrawing effect of the POM core being weakened by the inclusion of two ligands rather than one. The ^{1}H-NMR of

compound **2** showed similar downfield shifts of the ligand peaks when compared to that of its precursor.
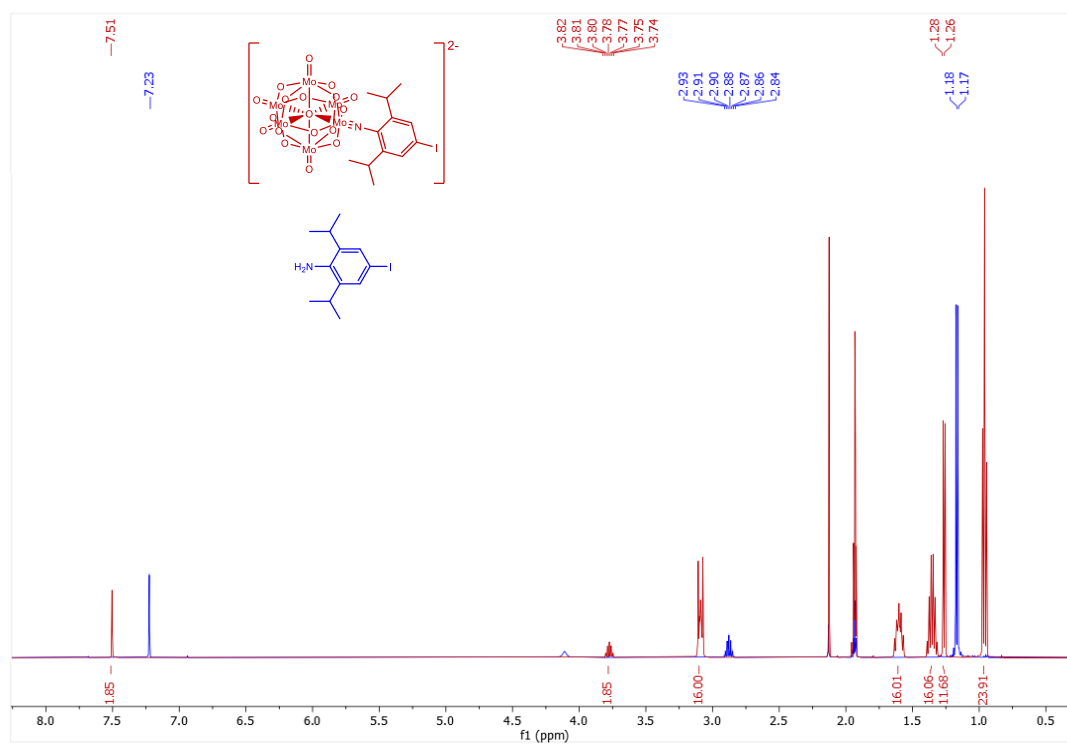
Figure 2.2c ¹H-NMR of compound **3** (red) and 2,6-diisopropyl-4-iodoaniline (blue). Both spectra were obtained in d-acetonitrile and referenced to TMSA using the solvent peak as an internal reference.

UV-vis absorption spectroscopy was also useful in confirming the successful coupling of the tetrabutylammonium hexamolybdate and the anilines, as after coupling, a new peak with a wavelength of 364 nm grew in for both compounds **2** and **3**. This peak cannot be attributed to either starting material, and previous investigation of similar compounds suggest it results mainly from electron donation from the π system of the ligand to empty d orbitals within the POM core. Some of this peak can also be accredited to π - π* transitions within the ligand, lowered in energy by interaction with the POM core, as well as O to d transitions within the POM core.[128] Very little difference between the electronic spectra of compound **2** and compound **3** were observed, with the ligand to POM charge transfer (LPCT) peak being observed at 364 nm in both compounds, with similar extinction coefficients of 27.5×10^3 M^{-1}cm^{-1} and 23.5×10^3 M^{-1}cm^{-1} respectively. The shift of this IVCT peak occurs at a slightly longer

wavelength than was seen for non-sterically protected compound **I**, observed at 355 with an extinction coefficient of 27.0×10^3 M^{-1}cm^{-1}, due to alkyl groups on compounds **2** and **3** resulting in more electron rich ligands.
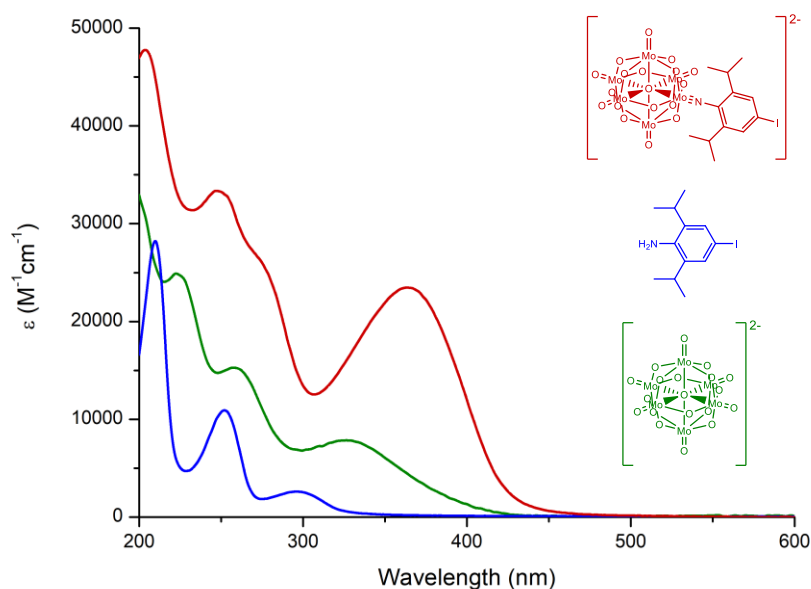
Figure 2.2d Electronic spectra of compound **3** (red), 2,6-diisopropyl-4-iodoaniline (blue), and tetrabutylammonium hexamolybdate (green). All spectra were obtained in acetonitrile.

Single crystals suitable for X-ray diffraction were grown of both compounds **2** and **3**, with the crystals for compound **2** being grown from hot acetonitrile and the crystals of compound **3** being grown from the vapour diffusion of diethyl ether into acetone. The crystals of compound **2** yielded a high quality structure with an R_1 of 4.52% in the *P-1* space group with two molecules of compound **2** and one of acetonitrile in the asymmetric unit, while the crystals for compound **3** yielded a high quality structure with an R_1 of 3.49% in the space group *P2$_1$/C*, also with two molecules of compound **3** and two molecules of acetone in the asymmetric unit. Disorder of the tetrabutylammonium counter cations was resolved for the structures of both compounds.

As previously seen on similar compounds, the Mo-N-C bond angle was closer to 180º than 120º for both compounds **2** and **3**, suggesting the formally double Mo-N bonds have significant triple bond character in both cases. Donation of the lone pair on the nitrogen to form this triple bond would result in a formal positive charge on the

nitrogen. Also, as was observed for similar compounds,[24] a displacement of the central oxygen atom resulted in the Mo-O^c bond lengths being on average longer than the Mo^{im}-O^c bond by about 0.15 Å, lengthening from around 2.20 Å to 2.34 Å.
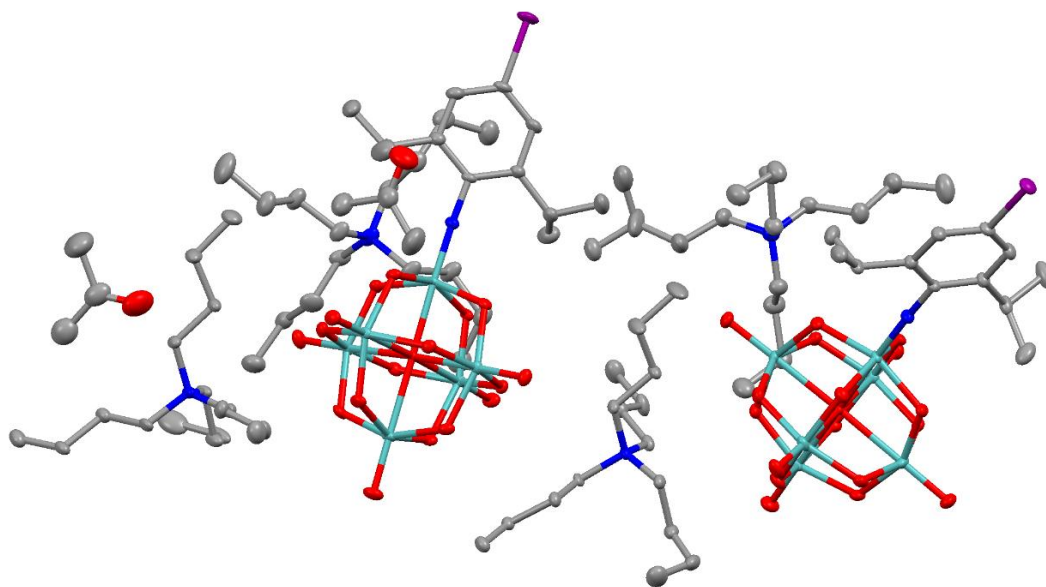
Figure 2.2e Unit cell of compound **3**. Thermal ellipsoids are at 30% probability level. The colour scheme shows Mo in green, O in red, N in blue, C in grey, and I in purple. Hydrogen atoms are omitted for clarity. Only part one is shown for clarity.

Comparison of the structures obtained for compounds **2**, **3** and the published data for compound **I** suggested the inclusion of alkyl groups at the *ortho* positions of the imido ring did not have a significant impact on the Mo^{im}-N bond lengths or the Mo^{im}-O bond lengths. However, a significant change in the O-Mo^{im}-N and Mo^{im}-N-C bond angles was observed, both of which increased in linearity with increasing steric bulk, suggesting more triple bong character and therefore a stronger bond. The O-Mo^{im}-N bond showed a straightening from 174.72° for compound **I** to 176.69° for compound **2** to 178.03° for compound **3**, while the Mo^{im}-N-C bond straightened from 164.8° for compound **I** to 170.8° for compound **2** to 176.85° for compound **3**. A shortening of the N-C bond with increased steric bulk at the *ortho* positions was also observed agreeing with the previous suggestion that a stronger N-C bond is observed for the compounds with bulkier *ortho* substituents, however, this pattern was not significant when compared to the estimated standard deviation values.
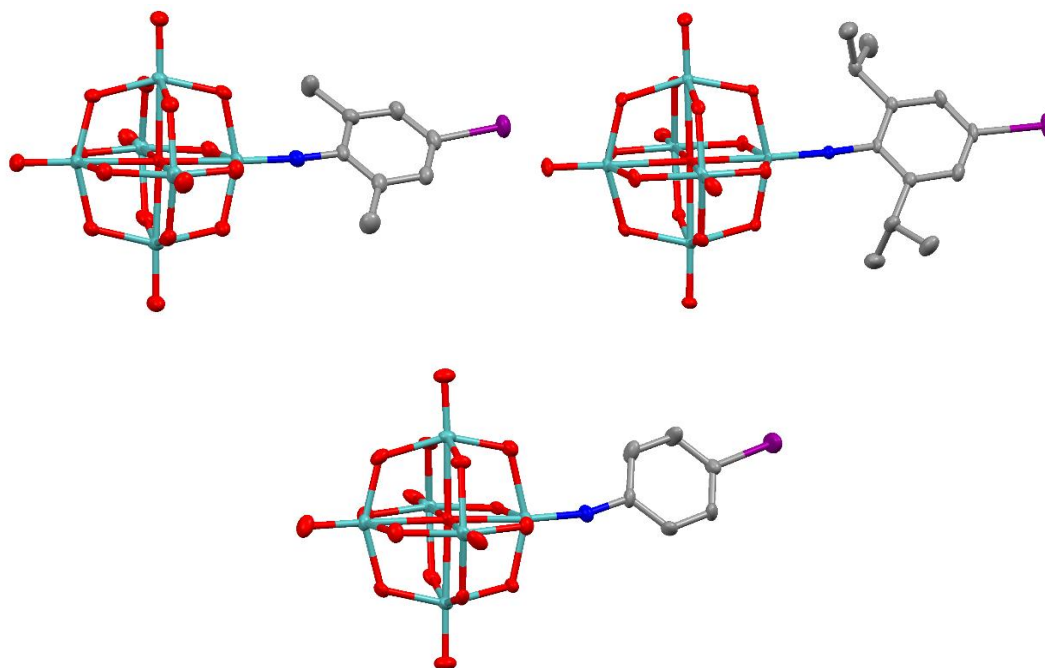
Figure 2.2f Crystal structure images of compounds **2**, **3** and **I**. Thermal ellipsoids are at 30% probability level. The colour scheme shows Mo in green, O in red, N in blue, C in grey, and I in purple. Tetrabutylammonium counter cations and hydrogen atoms are omitted for clarity.

It is likely this trend of increasing linearity arises due to the *ortho* substituents not only protecting the bond as intended, but also reducing the flexibility of the imido bonds due to steric repulsion. A more linear bond typically arises from increased triple bond character,[139] implying increased both strength and conjugation. For these functionalised hexamolybdate derivatives, the increased triple bond character of the imido bond could also lead to increased coupling between the inorganic cluster and the organic ligand. Although analysing the electronic spectra of compounds **2** and **3** provided no evidence of this, with both compounds showing peaks at identical wavelengths with very similar extinction coefficients, compound **I** did appear significantly different, with the LPCT peak appearing at 355 nm rather than the 364 seen for compounds **2** and **3**. It is possible this increase in energy of the ligand to POM charge transfer peak suggests a weaker coupling between the aromatic ring and the POM core, but it could also result from increased electron donation from the alkyl groups of compounds **2** and **3** increasing the energy of their HOMOs and lowering the energy of the overall transition.

	Mo-N	Mo^{im}-O^c	Mo-O^c (av)	Mo-O^t (av)	N-C	O-Mo^{im}-N	Mo^{im}-N-C
I	1.743(4)	2.199(3)	2.343(3)	1.684(3)	1.391(5)	174.7(1)	164.8(3)
2	1.737(4)	2.213(3)	2.338(3)	1.686(4)	1.387(6)	176.7(2)	170.8(4)
3	1.741(2)	2.198(2)	2.343(2)	1.690(2)	1.382(3)	178.0(1)	176.9(6)

Table 2.2a Comparison of the bond lengths for compounds **I**, **2**, and **3**. Here Mo^{im} refers to the imido coupled molybdenum, O^t refers to the terminal oxygen atoms on the other five molybdenum atoms, and O^c refers to the central oxygen atom.

2.3 Synthesis of Derivatives with Electron Donors

Synthesis of the five hexamolybdate derivatives with the electron donor functional groups needed for NLO activity was achieved using two different methods, with the synthetic pathway used depending on the type of bridge between the amine donor and the POM core.
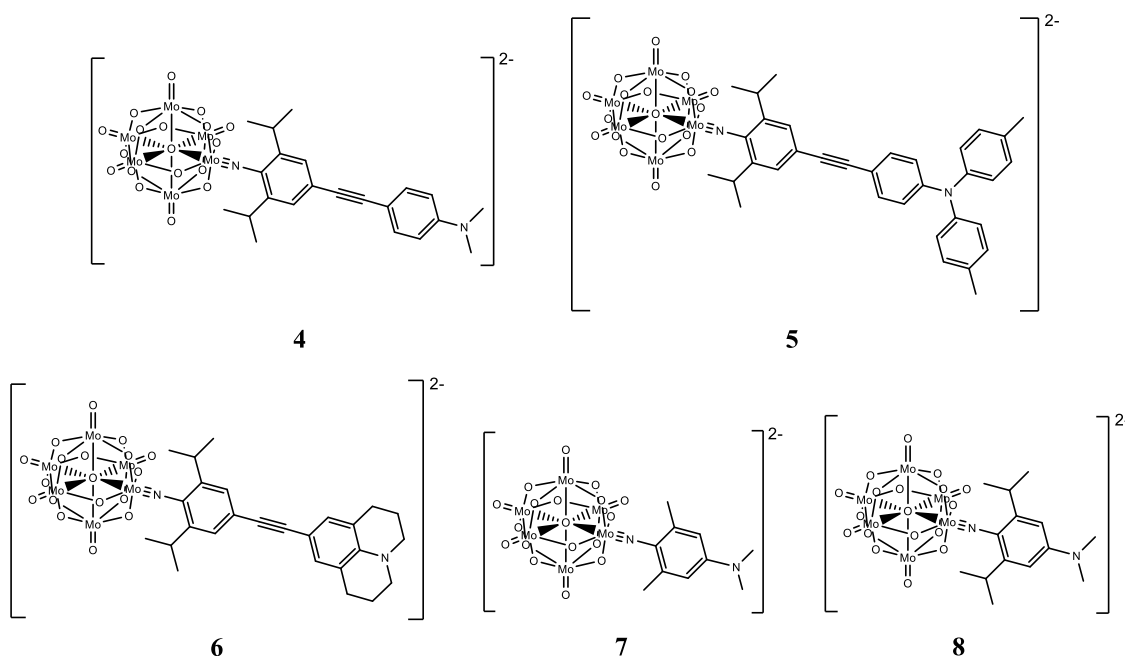
Figure 2.3a The five sterically stabilised hexamolybdate derivatives with electron donor ligands synthesised in this chapter.

The diphenylethyne bridged compounds, compounds **4**, **5**, and **6** were synthesised using compound **3** as a precursor, with the 1-alkyne-4-amino donor containing fragment attached using a Sonogashira reaction,[38] while the phenyl bridged compounds, compounds **7** and **8**, were synthesised directly from tetrabuylammonium hexamolybdate and either 4-dimethylamino-2,6-dimethylaniline or 4-dimethylamino-2,6-diisopropylaniline using the same DCC mediated coupling used to form compounds **2** and **3**. This will be discussed in more detail later in the chapter.

The electron donor unit used to synthesise compound **4**, 1-ethynyl-N,N-dimethylbenzenamine, was commercially available, and so purchased and used as received, however, for the synthesis of compounds **5** and **6**, both alkynyl donors were synthesised and purified prior to use. The synthesis of the electron donor unit for compound **5** involved two different palladium catalysed carbon coupling reactions; a Buchwald reaction, which was used to form 4-bromophenyl-4,4'-ditolylamine from 4-iodobromobenzene and ditolylamine and was previously reported by Man,[140] followed by a Sonogashira reaction with trimethylsilylacetylene, which enabled the alkynylation of the triarylamine. The alkyne was then deprotected under basic conditions to give the completed ligand.
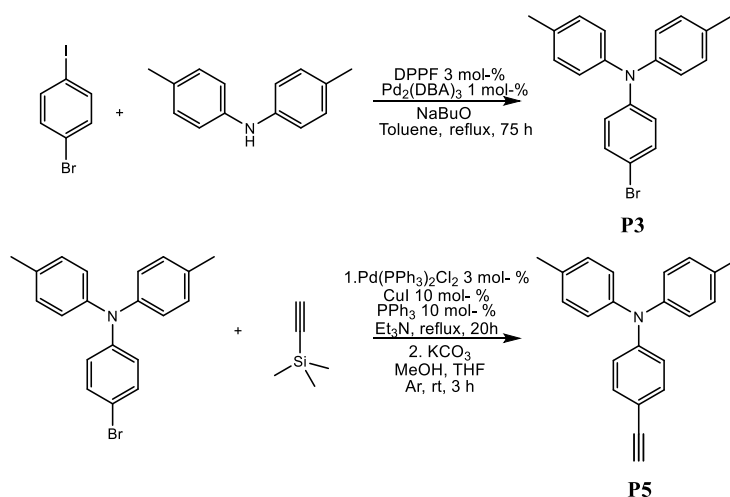
Figure 2.3b The synthetic scheme for the formation of compound **P5**, the ligand used in the synthesis of compound **5**.

The synthesis of compound **6** was performed by first iodinating julolidine using iodine to produce 4-iodojulolidine before coupling the alkyne using a Sonogashira reaction and deprotecting under basic conditions. Iodination of the julolidine initially proved troublesome as reaction with both n-iodosuccinimide and iodine monochloride failed to produce the desired product and instead resulting in the decomposition of the julolidine. After research into the iodination of N,N-dimethylaniline, another compound with a strong donor group *para* to the position of intended iodination and for which the iodination of is also difficult, the desired produced was achieved using iodine as the iodinating agents as seen in a method previously reported by Scarpaci[141] for the iodination of N,N-dimethylaniline. The Sonogashira reaction was performed as reported by Breiten[142] and the completed donor unit achieved by desilylation under basic conditions.
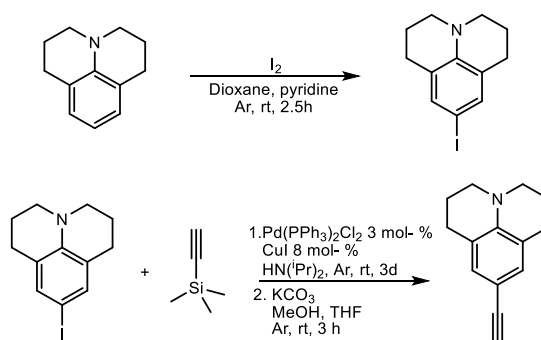
Figure 2.3c The synthetic scheme for the formation of compound **P13**.

The coupling of the donor units discussed to compound **3** in order to achieve the successful preparation of compounds **4**, **5**, and **6** was achieved using a Sonogashira reaction, the general mechanism of which is shown in figure **2.3d**. These reactions involve the oxidative addition of the aromatic halide to the palladium catalyst followed by transmetalation to exchange the halide with the alkynyl, calculated to be the rate limiting step of Sonogashira reactions.[143] After cis-trans isomerisation, the product can be eliminated, and the catalyst regenerated, by reductive elimination. The mechanism also shows the use of copper iodide in catalytic amounts and triethylamine as a sacrificial reductant to activate the alkyne for transmetalation. In some cases, the reaction is performed using an amine base as the solvent, seen previously during the synthesis of compounds **P5** and **P13**.
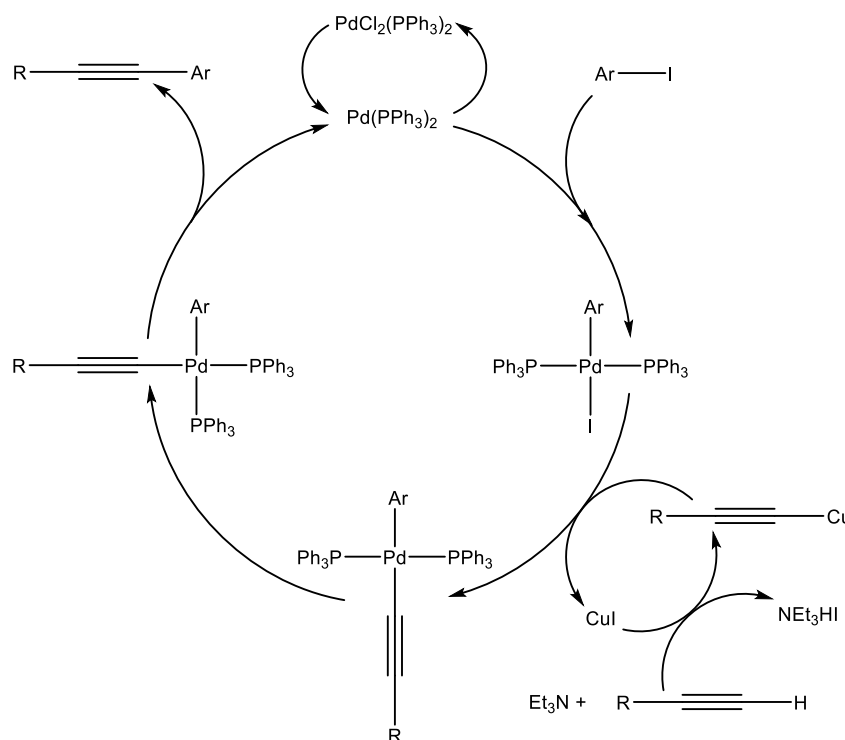
Figure 2.3d The general catalytic cycle of a Sonogashira coupling, featuring bis(triphenylphosphine) palladium(II) dichloride as a catalyst, copper iodide as a co-catalyst, and triethylamine as a sacrificial reductant.

As with many previous Sonogashira reactions, the formation of compounds **4**, **5**, and **6** were carried out under an inert atmosphere, [144] to prevent homo-coupling of the alkynes and decomposition of the POMs, and at room temperature, due to the increased facility of the transmetalation step. Despite having been shown to increase reaction rate, an amine solvent was not used due to the insolubility of the polyoxometalate salts. As had been reported previously for similar compounds, the reactions took significantly less time than the 16 to 24 hours usually taken for Sonogashira reactions to go to completion,[145] with clean products being isolated after only 45 minutes in all cases. This frequently observed increased activity is likely due to the electron withdrawing properties of the POM increasing both the affinity of the aryl halide for oxidative addition through stabilising the carbanion needed to form the Ar-Pd bond as well as the electrophilicity of the palladium species during the rate limiting transmetalation step.[146] The scheme for the formation of compound **5** from compound **3** shown in figure **2.3e**.
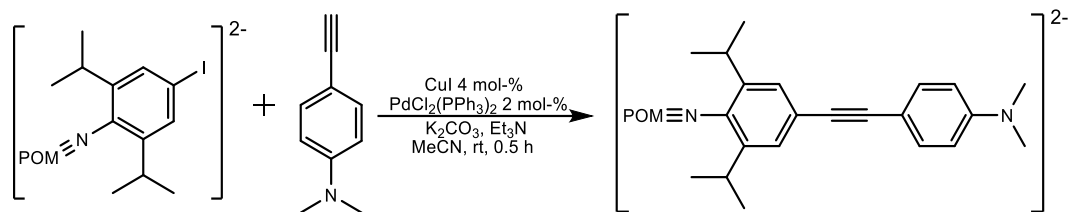
Figure 2.3e The synthetic scheme for the formation of compound **4** from compound **3** and 1-ethynyl-N,N-dimethylbenzenamine.

The reactions to synthesise compounds **4**, **5**, and **6**, all produced the expected products in yields of 47 to 56% upon precipitation from the reaction using diethyl ether as the anti-solvent. Purification of these compounds was achieved through recrystallisation from acetone/diethyl ether vapour diffusion and confirmed by ^{1}H-NMR and ^{13}C-NMR spectroscopy, mass spectrometry, elemental analysis, UV-vis spectroscopy, IR spectroscopy, and X-ray crystallography.

	Ar-**H**	**CH**(CH$_3$)$_2$	CH(**CH$_3$**)$_2$
3	7.51	3.78	1.27
4	7.25	3.83	1.31
5	7.28	3.83	1.31
6	7.20	3.83	1.30

Table 2.3a Comparison of ^{1}H-NMR shifts for compounds **3**, **4**, **5**, and **6** shows correlation with donor group. All ^{1}H-NMR were taken in acetonitrile-d3 and referenced to TMS.

Synthesis of compounds **4**, **5**, and **6** was initially confirmed by ^{1}H-NMR spectroscopy with further analysis showed an upfield shift of the protons *meta* to the nitrogen on the imido ring of all three compounds when compared to compound **3**. As can be seen from table 2.3a, increasing shift was observed with increasing strength of the amine donor groups.

This upfield shift, a result of increased shielding through electron donation, and the increase in shift observed for the more donating compounds, demonstrated the significant communication between the amine donor and the POM core through the

conjugated alkynyl bridge. A small downfield shift was observed for the diisopropyl protons of all three compounds, suggesting they have been slightly deshielded by the coupling. This change in shift did not vary significantly with the strength of the donor group, suggesting some isolation from the conjugated π system.
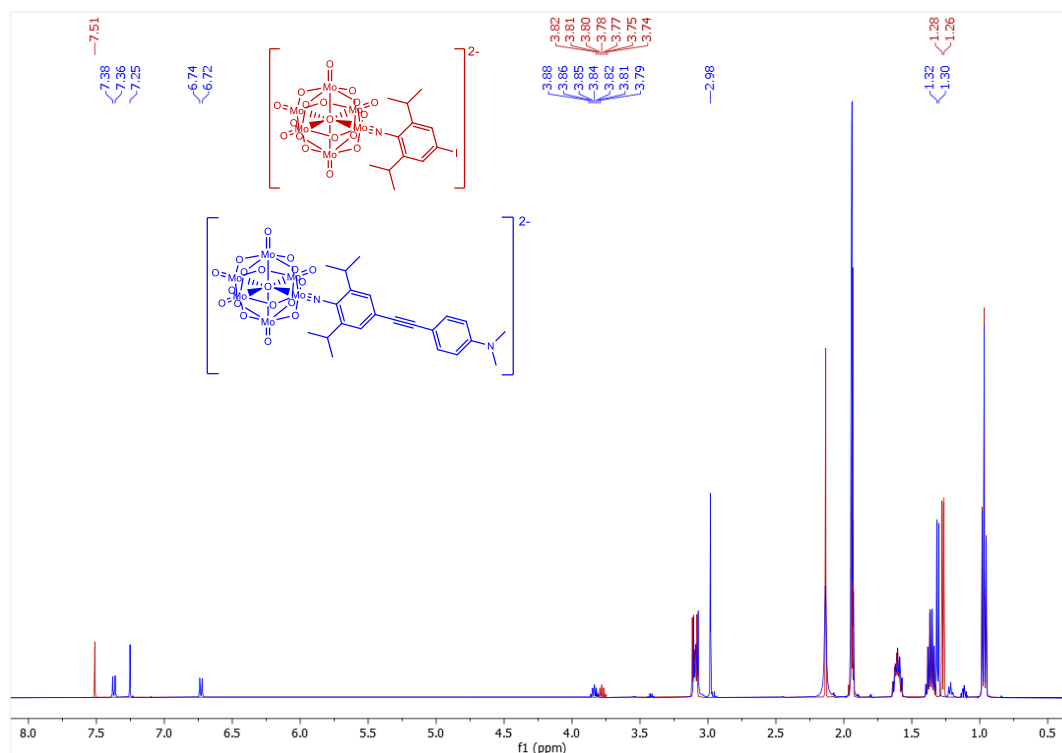
Figure 2.3f ^{1}H-NMR of compounds **3** (blue) and **4** (red). Both ^{1}H-NMR were taken in acetonitrile-d3 and referenced to TMS.

While the aniline precursor for compound **7**, 4-dimethylamino-2,6-dimethyl aniline, was provided for use by another group member and used as received, the synthesis of the ligand used to synthesise compound **8**, compound **P11**, was carried out using a five-step scheme based on one previously reported in the literature.[147] This involved the protection of the aniline on 2,6-diisopropylaniline using toluene sulfonyl chloride followed by nitration at the 4 position of the aromatic ring, reduction, methylation of the amine, and then finally deprotection of the amine. All steps were carried out as previously reported with the exception of the methylation of the amine for which tetrahydrofuran was used as the solvent as one had not being stated in the literature.

Overall, the synthesis proceeded as expected, producing **P11** pure by ^{1}H-NMR analysis with an overall yield of 29% *vs* 21% seen in the literature. The overall scheme for the synthesis of compounds **P11** is shown in figure 2.3e.
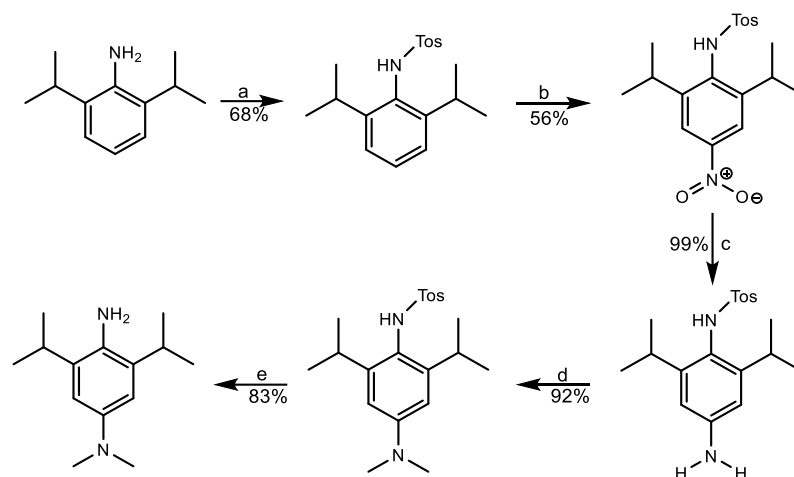
Figure 2.3g The scheme used to synthesise ligand **P11**. **a**. Toluene sulfonyl chloride, pyridine, reflux, 4 H. **b**. Nitric acid, sodium nitrite, glacial acetic acid, water, reflux, 12 H. **c**. Tin chloride dihydrate, ethanol, reflux, 23 H. **d**. Formaldehyde, 3M HCl, NaBH$_4$, THF/water, 15°C, 2 mins. **e**. 95% H$_2$SO$_4$, 40°C, 16 H.

Synthesis of compounds **7** and **8** by the coupling of 4-dimethylamino-2,6-dimethyl aniline and precursor **P11** respectively was achieved using the same DCC catalysed coupling reaction used to produce compounds **2** and **3**. Purification was again achieved by recrystallisation from hot acetonitrile to give pure compounds **7** and **8** confirmed by ^{1}H-NMR and ^{13}C-NMR spectroscopy, mass spectrometry, elemental analysis, UV-vis spectroscopy, IR spectroscopy, and X-ray crystallography. The ^{1}H-NMR of compound **8** when compared to that of the aniline shows an upfield shift of the *meta* aromatic protons, 6.39 ppm vs 6.53 ppm of the aniline precursor, as well as a significant downfield shift of the isopropyl septet, 3.82 ppm vs 2.99 ppm, and a smaller downfield shift of the isopropyl doublet, 1.30 ppm vs 1.20 ppm. The upfield shift is a result of increased shielding due to electron donation from the dimethylamine through conjugation improved by the coupling to the electron withdrawing POM. The downfield shift of the diisopropyl protons suggests deshielding, as is expected from the coupling of the strongly electron withdrawing POM core. The ^{1}H-NMR of compound **7** showed a similar upfield *meta* aromatic shift to compound **8**, 6.34 ppm

compared to 6.45 ppm of its aniline precursor, as well as a similar downfield shift of the *ortho* methyl protons, 2.57 ppm vs 2.09 ppm.
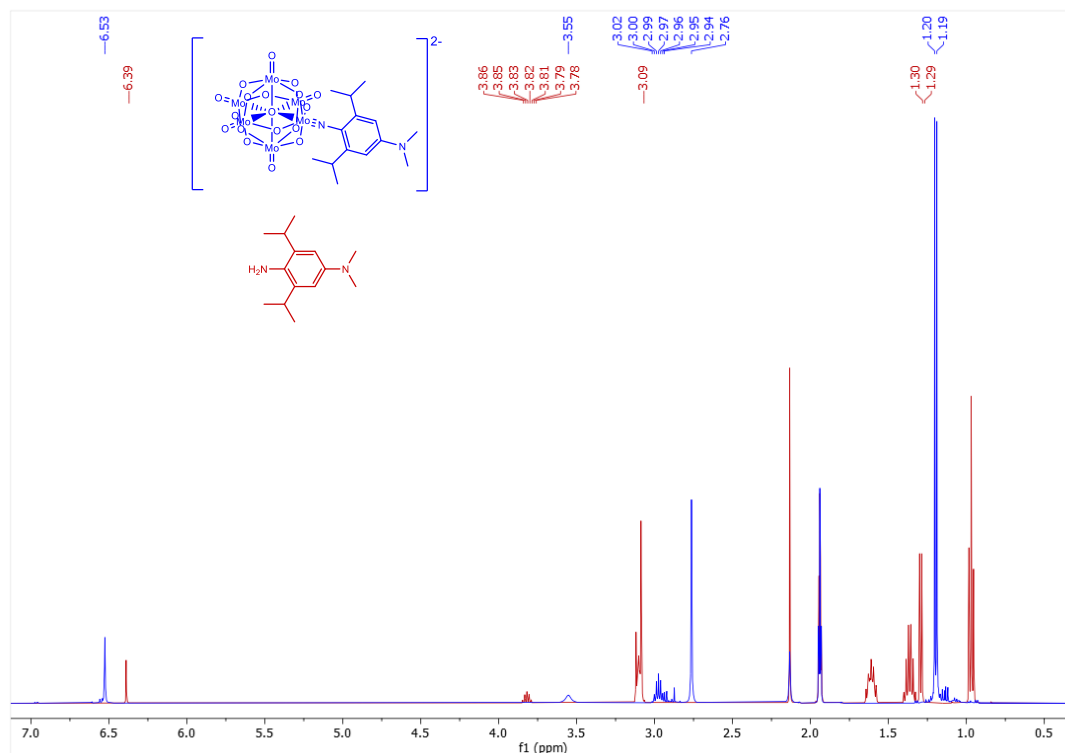
Figure 2.3h ^{1}H-NMR of compound **8** (red) and precursor **P11** (turquoise). Both ^{1}H-NMR were taken in acetonitrile-d3 and referenced to TMS.

Comparison of the ^{1}H-NMR of dimethylamino derivative **4** to its extended analogue, compound **8**, shows a significant upfield shift of the *meta* aromatic protons on the imido ring (6.39 vs 7.25 ppm), a result of increased shielding due to the increased proximity to the electron donating dimethylamino groups. This demonstrates the increased coupling through the shorter conjugated π system.

	Ar-**H**	C**H**(CH$_3$)$_2$	CH(C**H**$_3$)$_2$
4	7.25	3.83	1.31
8	6.39	3.82	1.30

Table 2.3b Comparison of ^{1}H-NMR shifts for compounds **4**, **5**, **6**, and **8**. All ^{1}H-NMR were taken in acetonitrile-d3 and referenced to TMS.

The UV-vis absorption spectra of compounds **4**, **5**, **6**, **7**, and **8** all showed a significant decrease in the energy of the lowest energy peak compared to that of their precursors, tetrabutylammonium hexamolybdate and the aniline ligands for compounds **7** and **8** and compound **3** for compounds **4**, **5**, and **6**. Although some of the redshift observed of compounds **7** and **8** resulted from the same lowering in energy of the π to π^* and O to d transitions seen for compound **3**, much of the shift can be accredited to the newly formed charge transfer between the donor group on the ligand and the electron accepting POM core. This ligand to POM charge transfer is also responsible for the significant redshift of the lowest energy peak when compounds **4**, **5**, and **6** are compared to compound **3**.
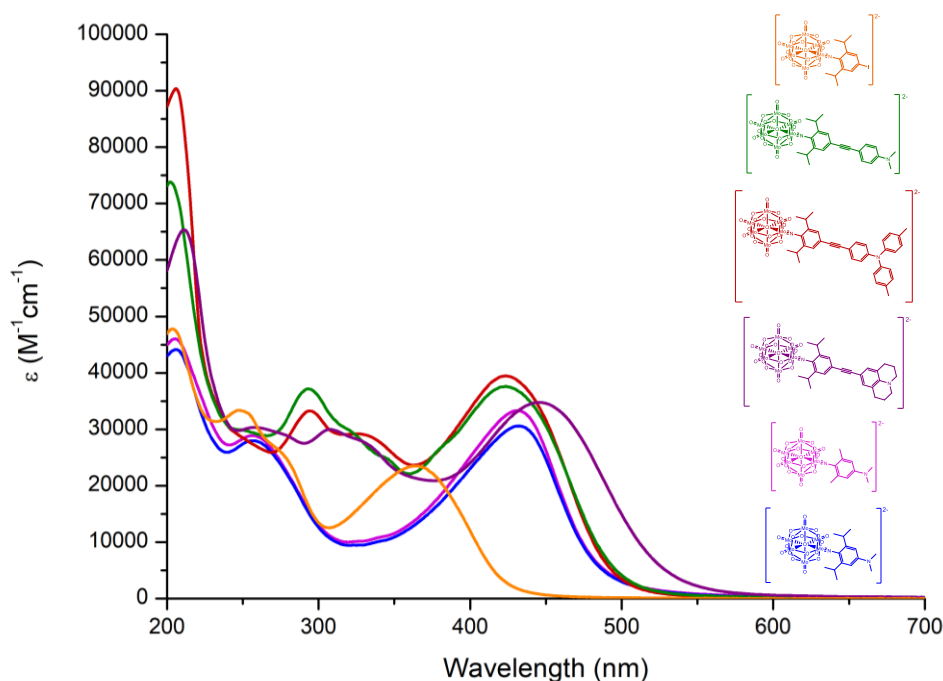
Figure 2.3i Electronic spectra of compounds **3** (orange), **4** (green), **5** (red), **6** (purple), **7** (pink), and **8** (blue). Spectra were taken in dry acetonitrile.

Overall, there is very little difference between the electronic spectra of compounds **4** and **5** despite the dimethylamine on compound **4** being a slightly stronger donor, with the LPCT peak being seen at almost identical wavelengths of 423 nm and 424 nm respectively. This similarity may be due to the reasonably small difference in donor strengths, but could also be a result of electronic isolation between the electron donor

and the POM core over the alkyne bridge. Compound **6**, however, a compound with a much stronger electron donor did show a significantly lower energy LPCT peak (445 nm) compared to that of either of the two weaker donors. The three compounds also show slightly different spectral shapes at higher energies due to differences in their ligand structure resulting in differing π to π^* transitions.

Compounds **7** and **8** gave very similar spectra with LPCT peaks at 430 nm and 431 nm respectively, a small decrease in energy when compared to the peak of compound **4** (424 nm). The decrease in the energy of this peak despite the identical donor groups is likely a result increased electronic coupling through the shorter bridge increasing electron donation to the POM core. It is, however, in contrast to many organic compounds, where a longer bridge between the donor and accepter outweighs increased coupling through proximity and results in a lower energy peak.[148,149] Despite their increased donor-POM coupling, compound **6**, with its stronger donor group, still shows a lower energy LPCT peak.

	Wavelength (nm)	ε (M^{-1}cm^{-1})
4	424	37.6×10^3
5	423	39.4×10^3
6	445	34.7×10^3
7	430	33.3×10^3
8	431	30.7×10^3

Table 2.3c Comparison of the LPCT peak of compounds **4**, **5**, **6**, **7**, and **10**. All spectra were taken in dry acetonitrile.

Single crystals suitable for X-ray diffractometry were grown of compounds **4**, **5**, **6**, **7**, and **8**, with the crystals for compound **4**, **5**, and **6** being grown from the vapour diffusion of diethyl ether into acetonitrile and compounds **7** and **8** being grown from the slow evaporation of acetonitrile. The crystals of compound **5** yielded a high quality structure with an R_1 of 6.06% in the space group $P2_1/c$, with two molecules of compound **5**, one molecule of diethyl ether, and one molecule of acetonitrile being displayed in the asymmetric unit. The crystals of compounds **6** and **7** yielded high quality structures with R$_1$ values of 6.28 and 5.23% respectively, both in the space

group *P*-1 with just one molecule of each in the asymmetric units, while the crystals of compound **8** yielded a high quality structure with an R_1 of 5.18% in the space group *C*2/c, with one molecule of compound **8** and one molecule of dimethyl sulfoxide being displayed in the asymmetric unit.
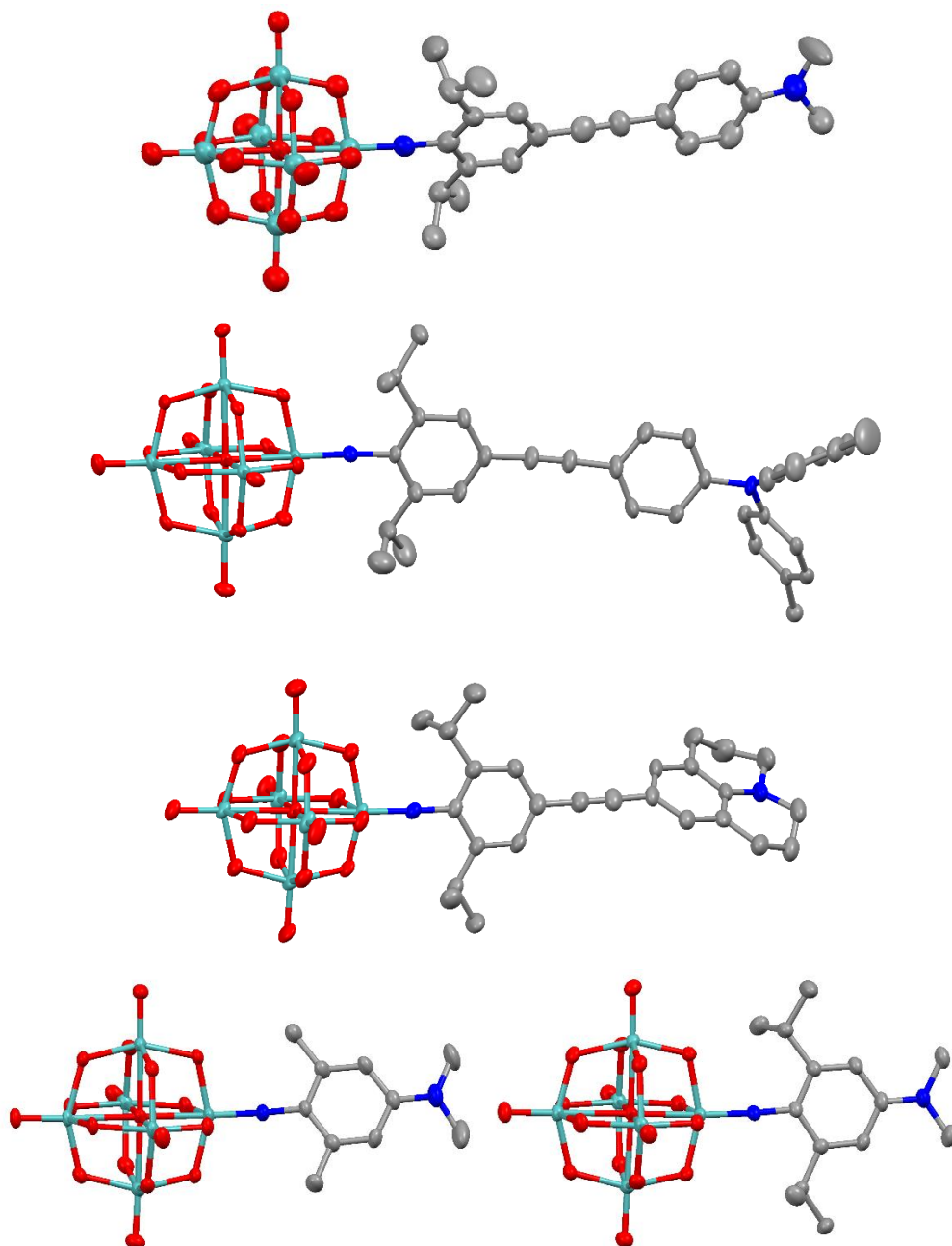
Figure 2.3j Crystal structure images of compounds **4**, **5**, **6**, **7**, and **8**. Thermal ellipsoids are at 30% probability level. The colour scheme shows Mo in green, O in red, N in blue, and C in grey. Tetrabutylammonium counter cations and hydrogen atoms are omitted for clarity.

The crystals of compound **4** yielded a structure in the *I-4* space group with an R_1 of 5.73%, however, due to the compounds not being identified as non-centrosymmetric prior to running, completeness for the data set was only 94%. Further runs were attempted after the reason for the lower than anticipated completeness was identified, however these failed to produce high quality data suitable for refining.

Comparison of the Mo-O bond lengths of compounds **4**, **6**¸ and the average of the two molecules of compound **5** in the unit cell did not show any significant variation, suggesting the strength of the donor did not have an effect on the structure of the POM core. This matches with the results of similar previous work.[133] A small variation in the N-C bond length was seen, with compound **6**, the compound featuring the strongest donor, having the shortest bond and compound **5**, the compound featuring the weakest donor having the longest bond, however this variation was not significant compared to the errors associated with the bond lengths. A significant variation was seen in both the Mo-N-C bond angles, with compound **6** having the most linear bond at 177.7° and compound **5** having the least linear bond length at 174.2, suggesting slightly increased triple bond character with increasing donor strength. This suggestion of slightly increased bond strength with increased donor strength matches with decreasing N-C bond length for increasing donor strength despite the variation not being significant compared to the error margins.

Investigation of the twist around the alkyne unit showed significant variation between the three alkynyl bridged compounds, with considerably more twist being observed for compound **6** (44.5°) than for compounds **4** or **5** (17.6° and 11.8° respectively). This increase in twist around the alkyne with increasing donor strength agrees with what has been previously observed in similar but unprotected compounds.

	Mo-N	Mo-O	$Mo^{im}-O^b$ (av)	$Mo-O^t$ (Av)	N-C	O-Mo-N	Mo-N-C
4	1.737(11)	2.205(8)	1.973(10)	1.682(10)	1.385(18)	178.1(5)	175.5(11)
5	1.738(3)	2.201(3)	1.953(3)	1.687(3)	1.390(5)	176.5(1)	174.2 (3)
6	1.736(4)	2.203(3)	1.949(4)	1.686(4)	1.382(6)	178.1(2)	177.7 (4)

Table 2.3d Comparison of the bond lengths for compounds **4**, **5**, and **6**.

	Mo-N	Mo-O	Mo^{im}-O^{b} (av)	Mo-O^{t} (Av)	N-C	O-Mo-N	Mo-N-C
II	1.737(3)	2.211(2)	1.959(3)	1.687(3)	1.383(5)	173.7(1)	162.6(3)
7	1.741(4)	2.215(3)	1.954(4)	1.689(4)	1.378(6)	177.7(2)	174.8(4)
8	1.748(3)	2.198(3)	1.962(3)	1.690(3)	1.367(5)	177.0(1)	175.3(3)

Table 2.3e Comparison of the bond lengths for compounds **II**, **7**, and **8**.

Comparison of compounds **7** and **8** did not show the same increase in linearity or shortening of the imido bond with increased steric bulk as was seen for compounds **2** or **3**. However, both did have significantly more linear O-Mo-N and Mo-N-C bonds than the previously reported non-sterically protected analogue, compound **II**,[133] suggesting that the increase in linearity of the imido bond was not a phenomenon observed of only the iodine functionalised compounds.

2.4 Synthesis of Derivatives with Electron Acceptors

In addition to synthesis of the amine donor functionalised Lindqvist derivatives, two nitro acceptor containing compounds were also synthesised. Synthesis of these acceptor containing compounds was achieved using similar methods to those used to synthesise the amine donor containing compounds, with compound **10** being produced from tetrabutylammonium hexamolybdate and 4-nitro-2,6-diisopropylaniline in a DCC mediated coupling reaction, and compound **9** being synthesised from compound **3** and 1-alkynyl-4-nitrobenzene in a Sonogashira reaction. Purification of these compounds was achieved through recrystallisation from hot acetonitrile and confirmed by ^{1}H-NMR and ^{13}C-NMR spectroscopy, mass spectrometry, elemental analysis, UV-vis spectroscopy, IR spectroscopy, and X-ray crystallography.

The Sonogashira reaction proceeded as expected and produced the desired product in a 53% yield. However, at 30%, the yield of the DCC mediated coupling reaction to produce compound **10** was considerably lower than seen for previous reactions. A considerable amount of unreacted tetrabutylammonium hexamolybdate left in solution and this, along with the significant amount of the *bis*-substituted compound produced

in the reaction, lowered the yield even further due to the number of recrystallisations needed to achieve purification.
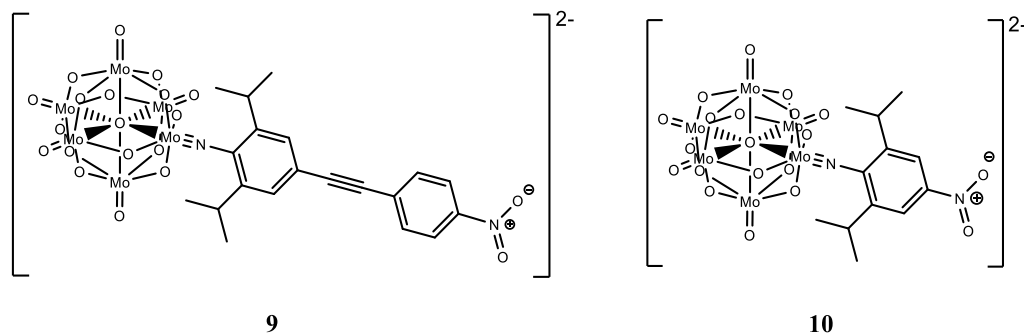
Figure 2.4a Compounds **9** and **10**. Tetrabutylammonium was used as the counter cation for both compounds.

^{1}H-NMR analysis of compound **9** showed a small upfield shift of the *meta* aromatic protons on the imido ring compared to that of compound **3** (7.40 vs 7.51) in contrast to the downfield shift that had been expected due to the conjugation to the electron withdrawing nitro group. This shows a significant amount of isolation despite the conjugated the alkyne bridge and suggests that the electron rich alkyne has more of an effect on the shielding of the *meta*-protons than the nitro group at the end of the ligand. It is also possible that the nitro group is pulling electron density back form the hexamolybdate core, increasing shielding of the protons in the bridge in between.

Comparison of nitro derivative **10** with iodo derivative **3** did however show a significant downfield shift, 7.99 ppm vs 7.51 ppm for compound **3**, a result of decreased shielding by the electron withdrawing nitro group compared to the iodo on compound **3**. This again demonstrated the increased electronic communication within the phenyl-bridged compounds. As discussed previously, compound **8**, with the dimethylamino donor in the *ortho* position, showed increased shielding over iodo containing compound **3**. For direct comparison, an ^{1}H-NMR of the three short-bridged, diisopropyl protected compounds is shown in figure 2.4b. The difference in shift between compound **8** with the strong donor group, compound **3** with the weak acceptor group, and compound **10** with the strong acceptor group can be clearly seen.
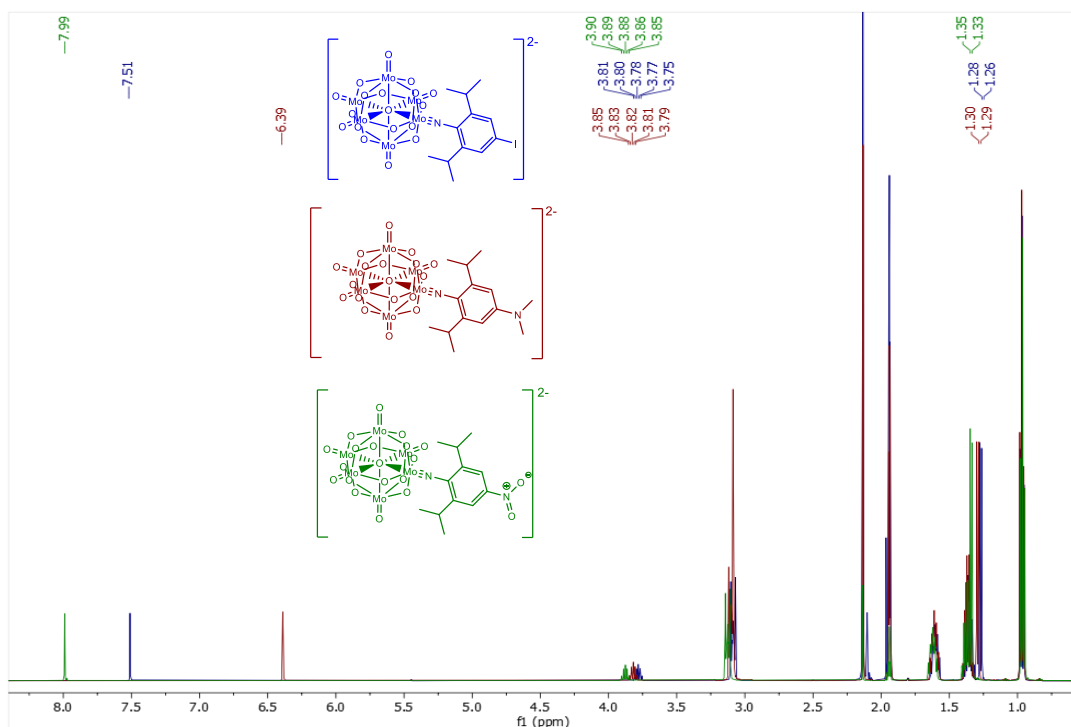
Figure 2.4b ^{1}H-NMR of compound **10** (green), compound **3** (blue), and compound **8** (red). All ^{1}H-NMR were taken in acetonitrile-d3 and referenced to TMS.

Analysis of the electronic spectra of compounds **9** and **10**, shown in figure 2.4c, showed low energy peaks at 399 and 382 nm respectively, LPCT transitions which despite featuring stronger acceptors, are both lower in energy than that observed for compound **3**. The likely reason for this observation is due to transitions not only occurring from the π system of the ligand to the POM core, but from the π system to the nitro acceptor group too. This significant aromatic to nitro component makes referring to these peaks as LPCT peaks somewhat unfitting, with the term intra-hybrid charge transfer peaks (IHCT) being more suitable for these compounds. These additional ligand to nitro transitions would also explain both the slight redshift of the peak of compound **9** with its larger π system compared to compound **10** as well as the increase in the extinction coefficient from 24.7×10^{-3} to 53.7×10^{-3} M^{-1} cm^{-1}.

Comparison of the electronic spectra of the three short bridged, diisopropyl protected compounds, compounds **3**, **8**, and **10**, can be seen in figure 2.4d, clearly demonstrating the increased red shift seen for the dimethylamino derivative over the iodo and the nitro derivatives. The increased red shift of the nitro derivative compared to the iodo derivative despite being a strong acceptor is likely a result of the π to ligand transitions.
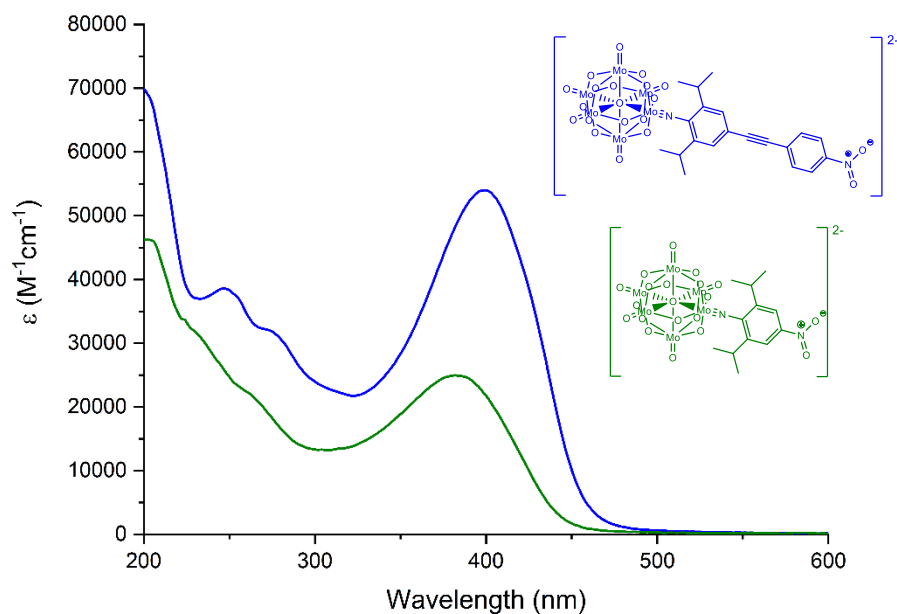
Figure 2.4c UV-vis absorption spectra of compounds **9** (blue) and **10** (green). Spectra were all taken in dry acetonitrile.
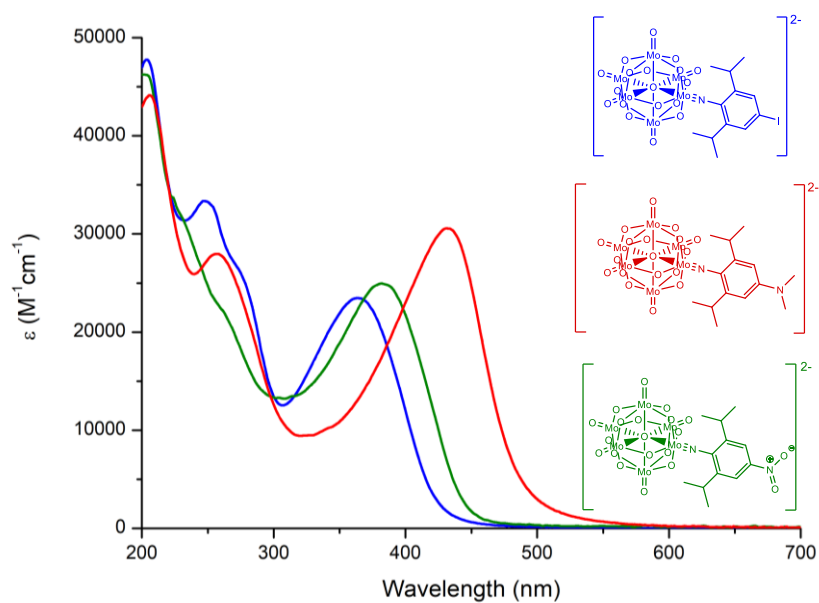
Figure 2.4d Electronic spectra of compounds **10** (green), **3** (blue), and **8** (red). Spectra were all taken in dry acetonitrile.

X-ray diffraction yielded high quality crystal data for compounds **9** and **10**, with crystals grown from diethyl ether vapour diffusion into acetone solution for compound **9** and from hot acetonitrile for compound **10**. The crystals of compound **9** yielded a

high quality structure with an R_1 of 3.59% in the P -1 space group with one molecule of compound **9** in the asymmetric unit while the crystal of **10** yielded a high quality structure with an R_1 of 5.86% in the P 1 $2_1/c$ 1 space group, also with one complete molecule in the asymmetric unit. The structures of both compounds followed the general expectations for the class of compounds, with reasonably linear imido bonds suggesting triple bond character and the frequently observed shortened $Mo^{im}-O^c$ bond. Comparison of the amide bond angle to that of an unprotected analogue of compound **9** revealed the steric protection had again resulted in a more linear imido bond, 173.9° vs 163.5°.[133]
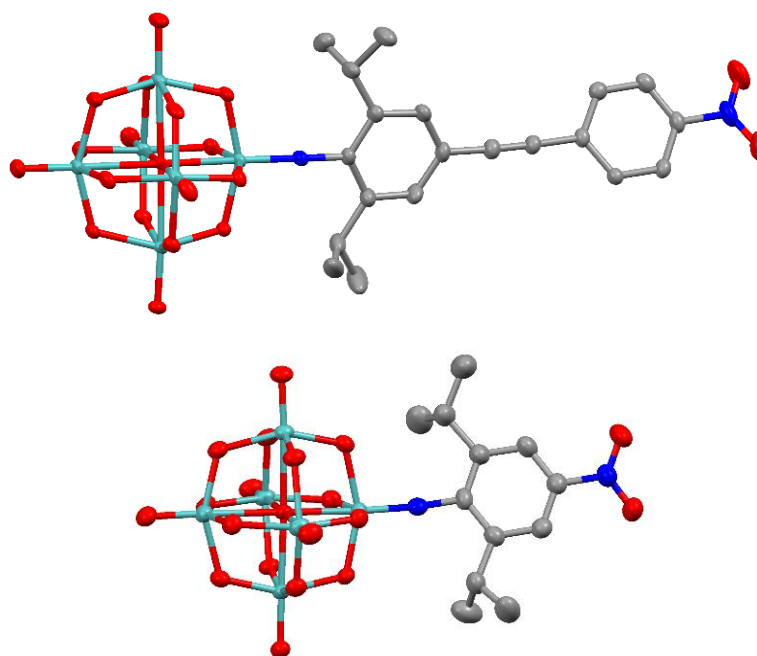
Figure 2.4e Crystal structure images of compounds **9** and **10**. Thermal ellipsoids are at 30% probability level. The colour scheme shows Mo in green, O in red, N in blue, and C in grey. Tetrabutylammonium counter cations and hydrogen atoms are omitted for clarity.

	$Mo^{im}-N$	$Mo^{im}-O^c$	$Mo^{im}-O^b$ (Av)	$Mo-O^t$ (Av)	N-C	O-Mo-N	Mo-N-C
9	1.742(2)	2.202(2)	1.952(2)	1.690(2)	1.385(3)	177.7(2)	176.0(2)
10	1.740(5)	2.214(3)	1.977(4)	1.690(4)	1.377(7)	176.6(2)	173.9(4)

Table 2.4a Comparison of the bond lengths for compounds **4**, **5**, and **6**.

Comparison of the structures obtained for iodo derivative **3**, dimethylamino derivative **8**, and nitro derivative **10** gave no significant variation or trend in the bond lengths when increasing or decreasing the donor strength over that of compound **3**. Compounds **8** and **10** both presented marginally less linear O-Mo-N and Mo-N-C bonds, showing the linearity of the imido bond was also not influenced by the donor strength. This is a similar result to as was seen for comparison of compounds **4**, **5**, and **6**.

	Mo^{im}-N	Mo^{im}-O^c	Mo^{im}-O^b (Av)	Mo-O^t (Av)	N-C	O-Mo-N	Mo-N-C
3	1.741(2)	2.198(2)	1.952(2)	1.690(2)	1.382(3)	178.0(1)	176.9(1)
8	1.748(3)	2.198(3)	1.962(3)	1.690(3)	1.367(5)	177.0(2)	175.3(3)
10	1.740(5)	2.214(3)	1.977(4)	1.690(4)	1.377(7)	176.6(2)	173.9(4)

Table 2.4b Comparison of the bond lengths and angles for compounds **3**, **8**, and **10.**

2.5 Electrochemical and Stability Studies

Electrochemistry is a branch of chemistry focused on probing the relationship between applied electrical potential and chemical changes in compounds. Many different electrochemical techniques exist, with a few examples being cyclic voltammetry, potential step experiments, bulk electrolysis, differential pulse voltammetry, and rotating disk experiments, resulting in a wide variety of applications, such as measuring redox potentials,[150,151] determining diffusion coefficients,[152] and monitoring isomerization reactions.[153] In this work, cyclic voltammetry was the technique used predominantly, along with bulk electrolysis.

During electrochemical analyses such as cyclic voltammetry, an applied charge is transferred between electrodes and the analyte dissolved in a conductive solution, resulting in either oxidation or reduction of the species at the working electrode depending on both the compound and whether an anodic or cationic potential is being applied. In this work, cathodic scans were typically performed, with compounds

initially being reduced at the working electrode before reoxidation occurred during the reverse scan.

Reduction of the analyte at the working electrode results in a localised depletion of the initial analyte, *Ox*, and a localised increase of the reduced species, *Red*. The relationship between the equilibrium of the concentration of these two species and the potential of the cell can be represented by the Nernst equation (2.5.1). Here [*Ox*] and [*Red*] are the concentrations of the two compounds at the working electrode, E_0 is the standard potential of a species F is Faraday's constant, R is the universal gas constant, n is the number of electrons, and T is the temperature.

$$E = E^0 + \frac{RT}{nF} \ln \frac{[Ox]}{[Red]} \tag{2.5.1}$$

Cyclic voltammetry uses a three electrode set up, with an inert working electrode, typically made of glassy carbon or platinum, a counter electrode, typically platinum, and a reference electrode, usually silver wire for non-aqueous procedures, and involves performing a triangular sweep from one potential, E_1, to another, E_2, and then back again. The potential is varied linearly at a constant rate, v, typically100 mVs^{-1} for standard cyclic voltammetry.
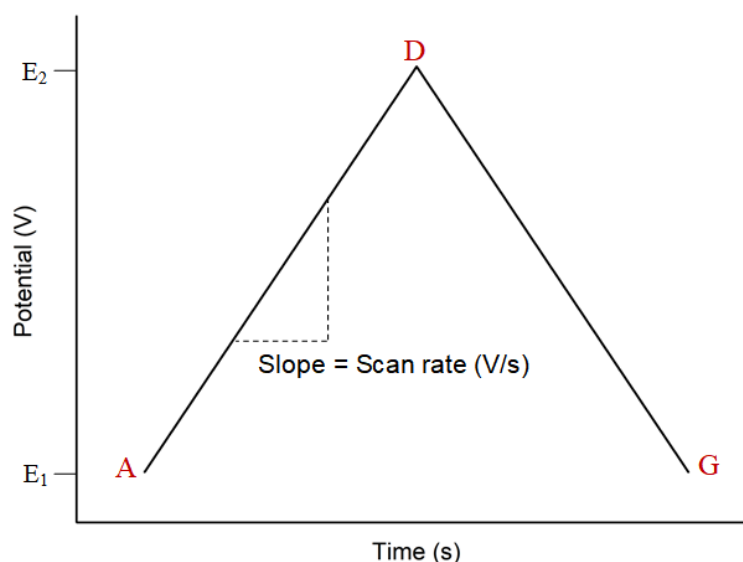
Figure 2.5a Plot of potential applied as a function of time for a standard cyclic voltammogram.

As a change in potential is applied to the system, the current passed varies, relaying information on any reduction or oxidation of the analyte. Typically, an increase in current is seen once the potential to allow the redox process to occur is reached, seen at B in figure 2.5b. The magnitude of this current relates to the amount of analyte being reduced or oxidised at the working electrode, which in turn relates to both the concentration of the bulk solution and the thickness of the diffusion layer.

The diffusion layer is the volume of solution around the surface of the electrode containing the newly reduced/oxidised analyte, and as the sample continues to be reduced/oxidised at the electrode, the size of this grows. This growth slows down the rate at which analyte is delivered to the electrode, and so over time, after all the sample initially at the electrode is oxidised/reduced, the current at the working electrode will decrease.
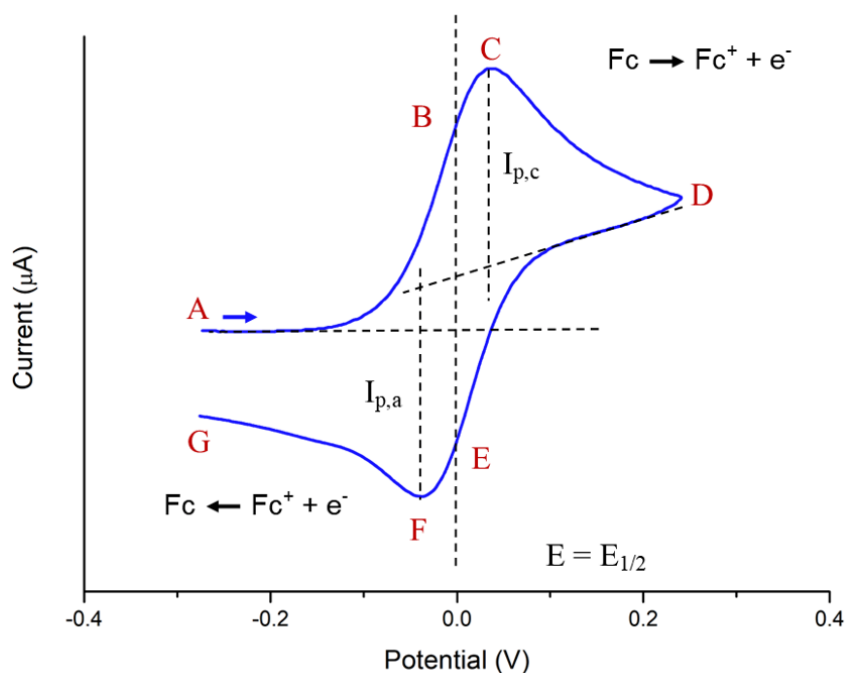
Figure 2.5b A cyclic voltammogram taken of Ferrocene, with key points being A, start potential; B, current increase as potential for oxidation reached; C, oxidation peak potential, after which current is limited by mass transfer; D, reversal point; E, increase in magnitude of current as potential for reduction of Fc^+ is reached; F, reduction peak potential, after which current is limited by mass transfer; G, stop potential.

If the redox process is reversible, a return peak with a similarly increased magnitude of current will be observed upon reversal of the scan, giving rise to the so-called duck-shaped cyclic voltammogram often referred to in electrochemistry. An example of this is shown in figure 2.5b, with the key points of the reversible oxidation of ferrocene indicated. For a reductive process, the opposite wave would be seen, with the initial peak occurring with a negative current and reoxidation being observed with a positive current.

If the reduction/oxidation of a compound is both chemically and electrochemically reversible, the difference between the potential of the forward and reverse scan peaks (ΔE_p) will be 57 mV at 25°C. Chemical reversibility relates to the stability of a compound in its reduced/oxidised state, whereas electrochemical reversibility refers to the electron transfer kinetics between the analyte and the electrode. If transfer kinetics are slow or decomposition of the compound in its reduced/oxidised state occurs, an increased ΔE_p will be observed.

The reversibility of a reduction/oxidation can also be monitored by changing the scan rate. For a completely reversible reaction, no increase in ΔE_p will be observed with changing scan rate and there will be a linear relationship between the peak current (i_p) of the forward scan and the square root of the scan rate (v). This increase in peak current as scan rate increases results from the increased gradient of the diffusion layer at higher scan rates and can be defined by the Randles-Sevcik equation (2.5.2).[154] Here, n is the number of electrons transferred in the reduction/oxidation, A (cm^2) is the surface area of the electrode, D_o (cm^2 s^{-1}) is the diffusion coefficient of the analyte, and C^0 (mol cm^{-3}) is the bulk concentration of the analyte.

$$i_p = 0.446nFAC^0 \left(\frac{nFvD_0}{RT}\right)^{\frac{1}{2}} \qquad (2.5.2)$$

Plotting peak current against the square root of the scan rate in mV produces a straight-line graph with a 0,0 intersect for completely reversible processes. For a quasi-reversible process, decreased peak currents will be observed, resulting in a non-linear plot.

The second technique used in this work was bulk electrolysis, a process that involves reducing or oxidising the entirety of a sample of analyte using a high surface area electrode combined with vigorous stirring. Usually, this process is paired with analysis

by cyclic voltammetry, with a scan being taken before and after bulk electrolysis to monitor for any changes in the sample generated by the oxidation and reduction. This can be used as a stability test to monitor for decomposition of a compound in its reduced/oxidised state on a timescale longer than is usually monitored for in a cyclic voltammogram.

Electrochemical studies were performed on compounds **2** to **10**, with the compounds being investigated by both cyclic voltammetry and bulk electrolysis. The cyclic voltammetry was carried out in acetonitrile under inert conditions using tetrabutylammonium tetrafluoroborate as the electrolyte. Glassy carbon was used as the working electrode, platinum as the counter electrode, and silver wire as the pseudo-reference. Ferrocene was later added as a reference to all samples unless otherwise stated. Bulk electrolysis was carried out in a three compartment cell with glassy carbon as the working electrode for the cyclic voltammogram scans, platinum gauze as the working electrode during bulk electrolysis, platinum as the counter electrode, and silver wire as the internal reference.

The electrochemical properties of tetrabutylammonium hexamolybdate have been well documented through the years, with two reductions being reported in the literature. [155,31] The first, at a potential of -0.815 vs Fc/Fc^+ in acetonitrile, is reversible, whereas the second, at a more negative potential, is not. These peaks result from two reductions of molybdenum cations to produce the stable $Mo(V)Mo(VI)_5$ species and the less chemically stable $Mo(V)_2Mo(VI)_4$ species respectively. In both cases the electron is delocalised over the cluster at room temperature.

After functionalisation, the hexamolybdate derivatives still typically exhibit most of the electrochemical properties seen for hexamolybdate, with the first reduction peak retaining its reversibility on the electrochemical time scale and the second remaining irreversible. However, due electron donation from the ligand into the POM core through the conjugated imido bond, the first reduction of the hexamolybdate derivatives is typically observed at a more negative potential than hexamolybdate itself.

Cyclic voltammogram show compounds **2** through **10** all demonstrate the two reductions typically seen for hexamolybdate derivatives, with the less negative peak being fully reversible in all cases, a key feature necessary for potential non-linear

optical switching. For all compounds ΔE_p was a little larger than the expected 57 mV, however, a similar value was seen for the Fc/Fc$^+$ oxidation couple (78 mV), a process well known to show ideal behaviour, suggesting the slightly slower than expected reductions may be due to increased resistivity in the set up rather than slow response times of the compounds themselves. The linear fitting of the peak current vs square root of scan rate plot of compound **3** in figure 2.5c demonstrates the reversibility of the less negative POM reduction peak.
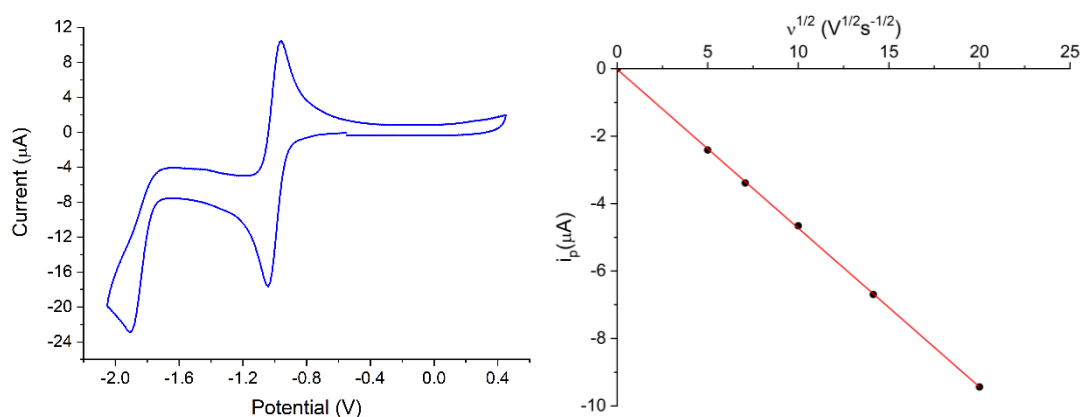
Figure 2.5c Cyclic voltammogram of 0.8 mM compound **3** vs Fc/Fc$^+$ in 0.1 M [Bu4N][BF4] in MeCN (left) and plot of peak current vs square root of scan rate for the first reduction (right).

Previously, it has been shown that functionalisation with a ligand containing a more electron donating functional group resulted in a larger negative shift, particularly for compounds without the alkyne spacer between the functional group and the hexamolybdate core.[133] This was a trend also seen for compounds **4** to **6**, with compound **6**, the compound with the strongest electron donor, having the most negative peak of the three diphenylethyne bridged compounds. As expected, the peak of both compounds **7** and **8** was observed at a more negative potential than seen for any of the diphenylethyne bridged compounds due to the proximity to the amine donor group to the hexamolybdate core. Similarly, the first reduction peak of compound **10** is at a less negative potential than that of compound **9** due to the increased influence of the electron withdrawing nitro group.

	E_{pc} $[ArMo_6O_{18}]^{4-/3-}$	$E_{1/2}$ $[ArMo_6O_{18}]^{3-/2-}$	ΔE_p (mV)
2	-1.925	-0.964	78
3	-1.910	-1.002	85
4	-1.837	-1.013	73
5	-1.905	-1.009	83
6	-1.831	-1.020	85
7	-1.878	-1.071	73
8	-1.926	-1.101	73
9	-1.901	-1.001	76
10	-1.834	-0.936	73

Table 2.5a Table summarising the molybdenum reduction peaks of compounds **1** to **10**. Fc/Fc⁺ was used as the internal reference in all cases.

In the cases of compounds **4** to **10**, additional peaks relating to the functional groups on the ligands were also observed, with amine oxidations being seen for compounds **4**, **5**, **6**¸ **7**, and **8**, and quasi-reversible nitro reduction peaks being seen in between the two POM reduction peaks for compounds **9** and **10**. In some cases, small amounts of hexamolybdate was also observed in the sample, indicated by a peak at -0.815 V.
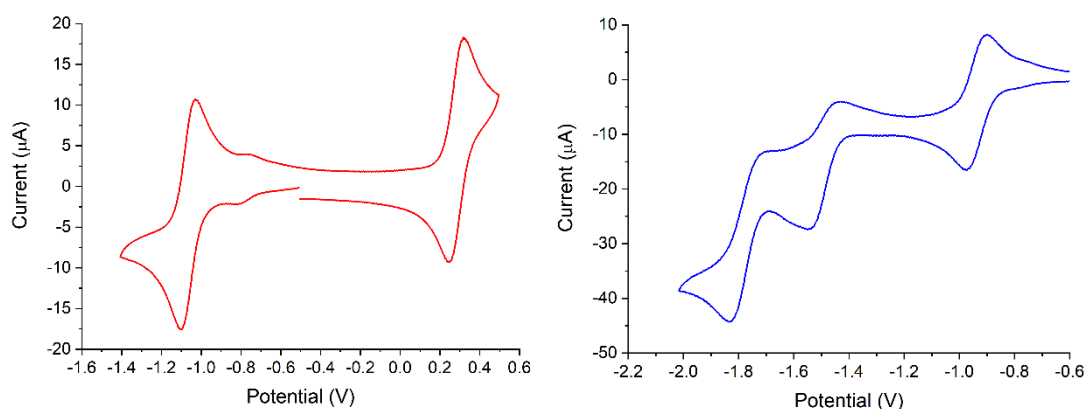
Figure 2.5d Cyclic voltammograms of 0.8 mM solutions of compound **7** (left) and compound **10** (right) in 0.1 M [Bu₄N][BF₄] in MeCN. Fc/Fc⁺ was used as the internal reference.

While these amine oxidation peaks were irreversible in the cases of compounds **4** and **6** and quasi reversible in the case of compound **5**, in the cases of compounds **7** and **8**,

reversible oxidation peaks were observed suggesting some stability of the oxidised amine on the CV timescale. This reversibility of the amine oxidation for compounds **7** and **8** led to the investigation of switchable responses not just using reduction but oxidation too for these compounds.

	$E_{1/2}$ [ArMo$_6$O$_{18}$]$^{4-/3-}$	E_{pc} NO$_2$	E_{pc} [ArMo$_6$O$_{18}$]$^{3-/2-}$	E_{pa} NR$_2$
2	-1.925	-	-0.964	-
3	-1.910	-	-1.002	-
4	-1.837	-	-1.013	0.338 irr
5	-1.905	-	-1.009	0.493 quas
6	-1.831	-	-1.020	0.119 irr
7	-1.878	-	-1.071	0.323 rev
8	-1.885	-	-1.101	0.303 rev
9	-1.901	-1.411 quas	-1.001	-
10	-1.834	-1.491 quas	-0.936	-

Table 2.5b Table summarising the cyclic voltammetry peaks of compounds **2** through **10**. All peaks are reported in V. Fc/Fc$^+$ was used as the internal reference in all cases. A 0.1 V/s scan rate was used for all measurements.

Determination of the reduced state stability of compounds **2** through **10** was caried out using bulk electrolysis, with initial studies being carried out on compound **2** and **3** prior to synthesis of the succeeding compounds. Bulk electrolysis was carried out in a three compartment cell using 0.8 mM solutions of analyte and 0.1 M solutions of [Bu$_4$N][BF$_4$] in dry acetonitrile. A platinum gauze working electrode was used during the bulk electrolysis runs, with reduction always being performed with vigorous stirring under an argon atmosphere for 22 minutes. Cyclic voltammograms were taken before and after bulk electrolysis and recorded as in previous experiments.

Previous reduced state stability studies of hexamolybdate derivatives demonstrated considerable hydrolysis of the imido bond during the 22-minute reduction period even when using dry solvent and inert conditions, resulting in large amounts of hexamolybdate being formed during the experiments as a result. This resulted in not only a significant decrease in the current of the reduction peak of the hexamolybdate

derivative, but the growth of a hexamolybdate reduction peak at -0.815 V. This can be seen in the cyclic voltammogram of compound **I** displayed in figure 2.5e.
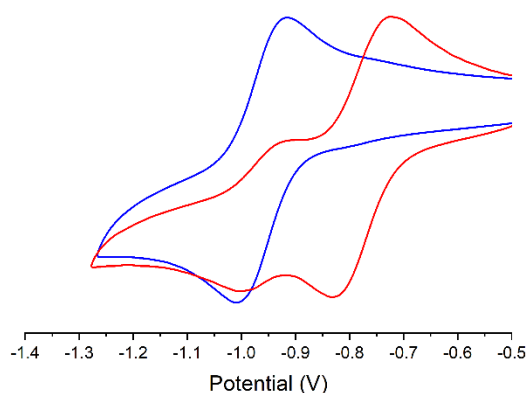
Figure 2.5e Cyclic voltammograms of compound **I**, with scans taken before bulk electrolysis being shown in blue and scans taken after bulk electrolysis shown in red. Currents of the before and after bulk electrolysis cyclic voltammograms have been normalised for clarity.
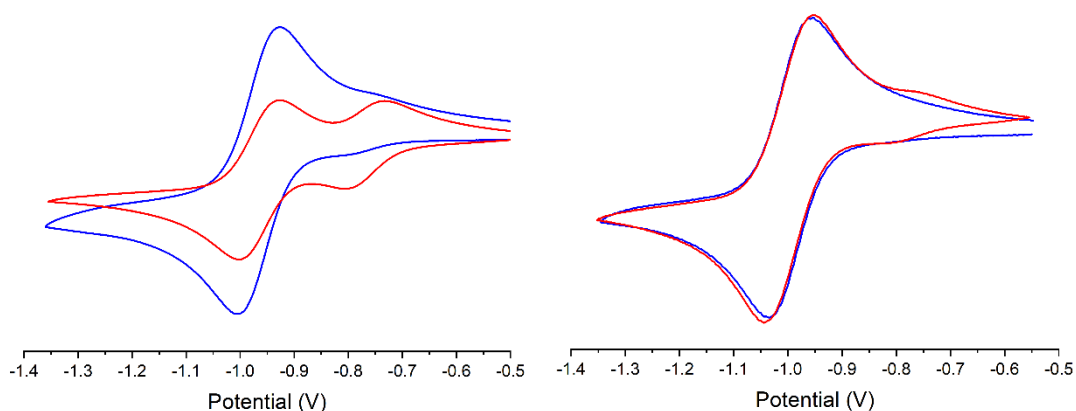
Figure 2.5f Cyclic voltammograms of compounds **2** and **3**, with scans taken before bulk electrolysis being shown in blue and scans taken after 22 minutes of bulk electrolysis shown in red. Fc/Fc$^+$ was used as the internal reference in all three cases. Currents of the before and after bulk electrolysis cyclic voltammograms have been normalised for clarity.

Reduced state stability studies of compounds **2** and **3** showed significant improvement over that of compound **I**, with approximately 2/3 of compound **2** remaining in solution after bulk electrolysis, and considerably less decomposition being observed for compound **3**. This improvement in stability with increasing size of the alkyl substituent

showed that stability of these compounds in the reduced state could be achieved by steric protection of the imido bond by alkyl groups. It was here that the further derivatives were synthesised, with isopropyl groups being included at the 2 and 6 positions of the amido ring in most compounds to hopefully afford maximum steric protection of the imido bond.

Bulk electrolysis experiments of compounds **4** through **10** demonstrated the effectiveness of the use of steric protection to improve stability in the reduced state even with the inclusion of electron donors or acceptors on the ligand. In the cases of compounds **7** and **8**, very little decomposition of the hexamolybdate derivatives was seen, with the stability of compound **8** appearing almost identical to its iodo analogue and compound **7** surpassing its own. In both cases, a very small increase in the amount of hexamolybdate could be seen in the solutions.
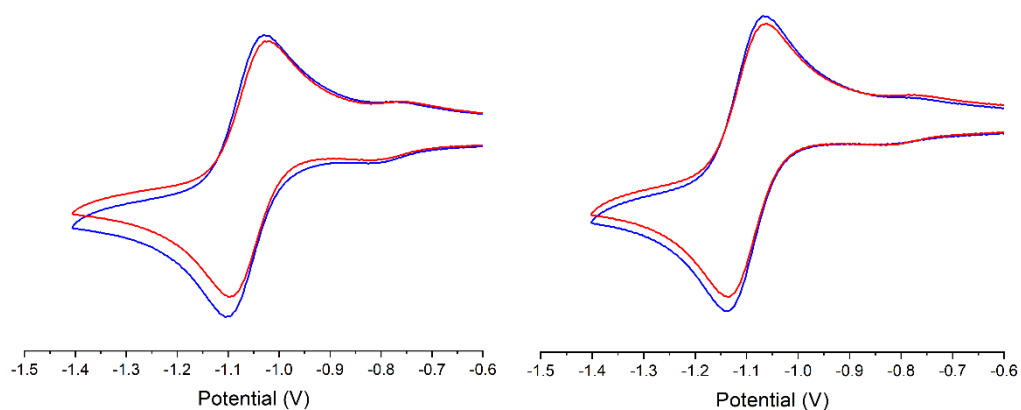
Figure 2.5g Cyclic voltammograms of compounds **7** (left) and **8** (right), with scans taken before bulk electrolysis being shown in blue and scans taken after bulk electrolysis shown in red. Fc/Fc$^+$ was used as the internal reference in both cases. Currents of the before and after bulk electrolysis cyclic voltammograms have been normalised for clarity.

Following on, compounds **4**, **5**, and **6** also showed good stability in the reduced states, with considerable amounts of the hexamolybdate derivative still being present in the samples after the bulk electrolysis. Compound **5** appeared marginally more stable than both compounds **4** and **6**, suggesting the stronger donors slightly decreased stability. Also, more decomposition was observed for compound **4** than for compounds **7** and **8** despite the identical the donor group and the increase in steric protection over

compound **7** suggesting the extension of the ligand reduces the stability of the derivative.
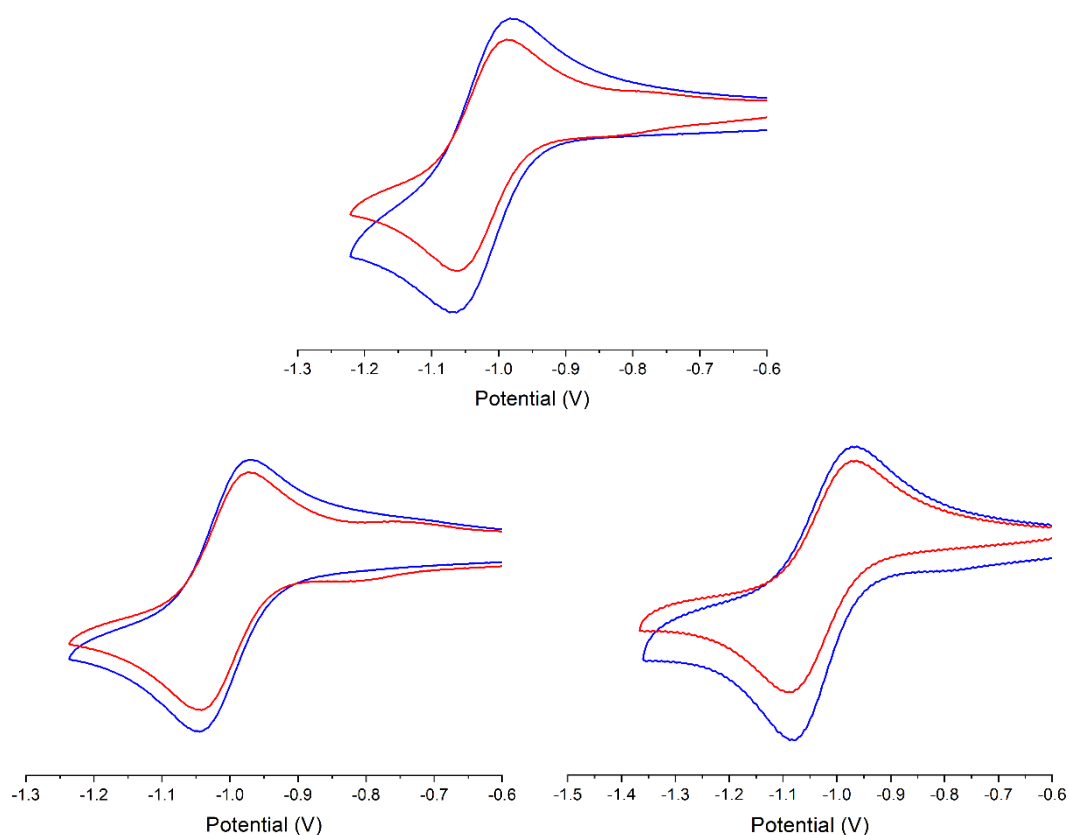
Figure 2.5h Cyclic voltammograms of compounds **4** (top), **5** (left), and **6** (right), with scans taken before the 23 minute bulk electrolysis being shown in blue and scans taken after bulk electrolysis shown in red. Fc/Fc$^+$ was used as the internal reference in all three cases. Currents of the before and after bulk electrolysis cyclic voltammograms have been normalised for clarity.

Interestingly, very little growth of the hexamolybdate reduction peak was seen for any of compounds **4**, **5**, or **6** despite the noticable decrease of the concentration of the derivatives in the samples, suggesting decomposition of these compounds was not occuring through the hydrolysis pathway previously observed for similar hexamolybdate derivatives and instead resulted in fragmentation of the hexamolybdate core itself.

One possible route for this decomposition is by the the loss of both the ligand and the imido molybdenum from the hexamolybdate core after reduction, resulting in a

destabilised five molybdenum cluster which could then fragment into smaller, redox inactive polyoxometalate fragments such as $[MoO_4]^{2-}$ and $[Mo_2O_7]^{2-}$. For similar previously synthesised compounds without the steric protection, this breakdown pathway may not have been observed during bulk electrolysis due to the succeptability of the imido bond to hydrolysis, resulting in decomposition to hexamolybdate before this second fragmentation pathway could take place.

$$O_{18}Mo_6{\equiv}NAr^{3-} \longrightarrow 2Mo_2O_7{}^{2-} + MoO_4{}^{2-} + Mo{\equiv}NAr^{3+}$$

Figure 2.5i A scheme showing one possible fragmentation pathway of the decomposition of compounds **4**, **5**, and **6**.

Fragmentation of the hexamolybdate core of functionalised deriatives has been reported previously, once through purposeful breakdown in a collision-induced dissociation experiment in which the fragments were monitored using mass spectrometry[156] and once through chemical reaction inside cells.[15] While the work involving fragmentation through chemical breakdown of the ligand poduced only MoO_4, the products of collision-induced dissociation resulted in a much larger range of fragments. Cao's work[31] into the gas-phase fragmentiation of hexamolybdate derivatives also demonstrated the possibility of MoNAr units becoming detatched from the main POM core, resulting in further destabilisation of the remaining cluster. This work also observed increased fragmentation of compounds functionalised with OMe donor groups, posibly due to the electron donation resulting in a more polar imido bond and a more electron rich POM core. The increased decomposition for compounds with stronger donor groups was an observation also made in this work.

Interestingly, decomposition by this pathway was not obseved to significantly occur for neither compounds **7** or **8** in their reduced states despite the increased elecron donation from the more proximal amino group suggesting the decomposition was somehow facilitated by the alkyne bridge. This may be due to solubility, with the larger organic component of the diphenylethyne bridged compounds increasing solubility of the imido fragments and facilitating the decomposition.

Although not included in the decomposition scheme, it was thought stabilisation of the MoNAr entity by coordination of solvent molecules would likely occur, producing a compound similar in shape to previously reported WNArCl$_4$. As it was thought the coordination of the solvent may stabilising the breakdown product, investigation into whether increased stability could be achieved by performing the reduction in a less cooridinating solvent was performed. Repeating the bulk electrolysis experiment using less coordinating DCM as the solvent did indeed result in reduced amounts of decomposition, although did not prevent its occurrence entirely.
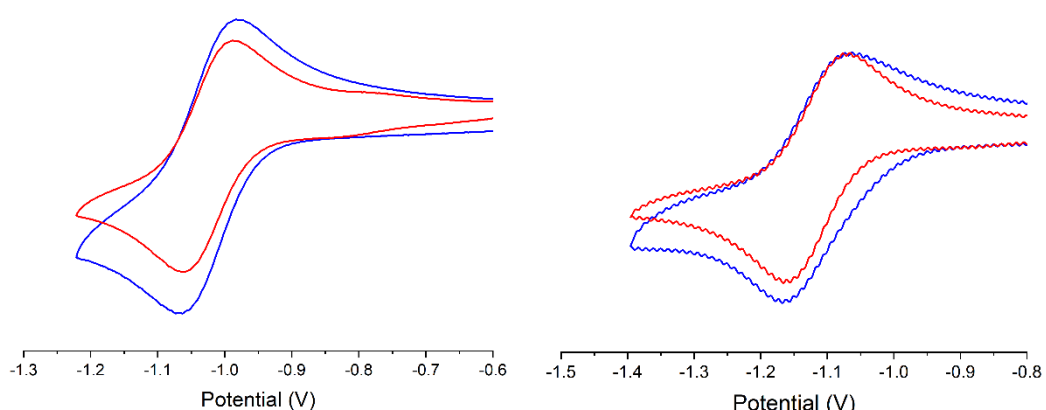
Figure 2.5j Cyclic voltammograms of compound **4** in acetonitrile (left) and dichloromethane (right), with scans taken before the 23 minute bulk electrolysis being shown in blue and scans taken after bulk electrolysis shown in red. Fc/Fc+ was used as the internal reference in all three cases. Currents of the before and after bulk electrolysis cyclic voltammograms have been normalised for clarity.

To identify the fragments produced in the second decomposition route, IR spectroscopy was employed. This was used to monitor for any changes in the Mo-O vibrational peaks of a sample over the course of a prolonged bulk electrolysis experiment. Here, electrolyte solution was used as a background, and solutions of Mo$_6$O$_{19}$$^{2-}$, Mo$_2O_7$$^{2-}$ and MoO$_4$$^{2-}$ were prepared and scanned to provide comparison. Due to the absorption peaks of acetonitrile, some wavelengths in the relevant area of the spectrum were obscured, but the key peaks were visible and unobstructed enough to demonstrate a clear difference between the samples. The acetonitrile peak at about

960 cm^{-1} necessitated the addition of a break in the axis of the printed spectra for clarity.

Scans performed early on during the reduction process did not display much resemblance to that of compound **4**, $Mo_6O_{19}^{2-}$, $Mo_2O_7^{2-}$, or MoO_4^{2-}, likely due to the formation of an intermediate such as Mo_5 species, but comparison of the final scan to one of $Mo_2O_7^{2-}$ confirmed the presence of Mo_2O_7 amongst other components in the sample. This formation of $Mo_2O_7^{2-}$ confirmed the decomposition of compounds **4**, **5**, and **6** was occurring through fragmentation of the hexamolybdate core rather than the hydrolysis mechanism previously seen, likely after the reduction mediated removal of one $MoNAr^{3+}$ unit. Possible causes of the peak at 940 cm^{-1} in the final scan, the only peak not caused by the $Mo_2O_7^{2-}$, were investigated without success. However, due to its proximity to the Mo=N peak of compound **4**, it is currently assumed this peak results from either the molybdenum-imido fragment or a decomposition product of the fragment.
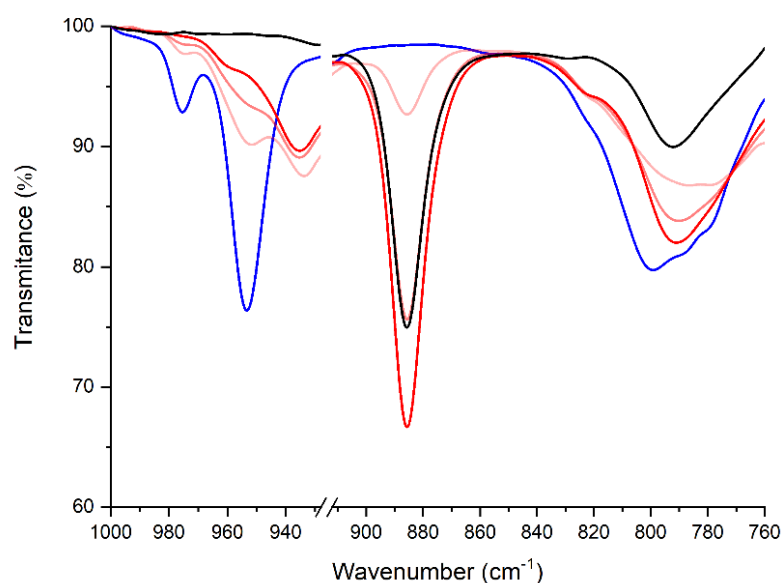
Figure 2.5k Vibrational spectra of compound **4** taken before extended bulk electrolysis (blue) and throughout (darkening red) with the spectra of $[Mo_2O_7]^{2-}$ included (black) for comparison. All spectra were taken in acetonitrile solution and included 0.1M NBu$_4$BF$_4$.

Despite the decomposition of compounds **4**, **5**, and **6** observed during their bulk electrolysis experiments, peak currents of the cyclic voltammetry runs suggested approximately 75% of compounds **4** and **6** and 83% of compound **5** remained in solution after the 23 minutes of reduction. This meant that despite the newfound stability issues involving the unexpected fragmentation of the hexamolybdate core, investigation on the reduced states of the compounds would still be possible.

Bulk electrolysis of compounds **9** and **10** also showed reasonable stability of the acceptor containing compounds, with a small amount of decomposition being seen in both cases. These compounds were not as stable as the iodo or amino analogues, with more decomposition being seen for compound **10** than for either compounds **3** or **8**, likely due to the nitro acceptor group reducing electron donation from the ligand to the hexamolybdate core. The less electron dense imido bond would then be more susceptible to nucleophilic attack of water, increasing the amount of hydrolysis seen compared to the weaker acceptor and donor containing compounds. However, as with compounds **2** through **8**, despite some breakdown being observed, enough functionalised hexamolybdate still remained after the 23 minutes of reduction that investigation of the reduced state of the compounds would still be possible.
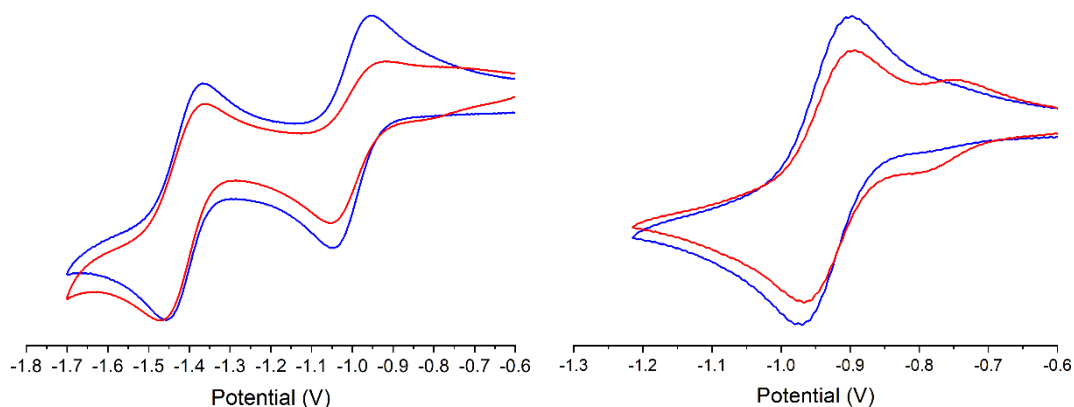
Figure 2.5l Cyclic voltammograms of compounds **9** (left), and **10** (right), with scans taken before bulk electrolysis being shown in blue and scans taken after a 23 minute bulk electrolysis shown in red.

2.6 Conclusion

In conclusion, this chapter has discussed the synthesis and characterisation of nine sterically protected hexamolybdate derivatives, all of which have been characterised by ^{1}H-NMR, ^{13}C-NMR, IR, UV-vis, elemental analysis, mass spectrometry, and X-ray crystallography. Analysis of the electronic spectra of compounds **2** to **10** showed IHCT peaks lowered in energy by ligand to POM coupling through the conjugated imido bond. Donor containing compounds showed additional red-shifting of this peak, with more shifting observed for compounds containing stronger donors and shorter bridges. This suggests increased NLO activity for derivatives featuring stronger electron donors.

Cyclic voltammetry of these compounds revealed the $Mo(VI)_6$ to $Mo(VI)_5Mo(V)$ reduction typically observed for hexamolybdate derivatives was still reversible on the cyclic voltammetry timescale. The cyclic voltammetry also revealed additional peaks for many of the compounds, with amine oxidation peaks being observed for compounds **4** through **8** and quasi reversible nitro reduction peaks being observed for compounds **9** and **10**. Of the amine reductions observed, those of compounds **7** and **8** demonstrated good reversibility on the cyclic voltammetry timescale, leading to the possibility of oxidatively switchable NLO properties for these compounds.

Longer scale stability studies of these compounds, performed using bulk electrolysis, demonstrated the increased stability of the sterically protected containing compounds, with enough stability achieved for most compounds that investigation of the optical properties in the reduced state should be a possibility.

Chapter 3

Optical Analysis of Monofunctionalised Hexamolybdate Derivatives in their Oxidised and Reduced States

3.1 Introduction

In chapter two, the successful synthesis and analysis of a series of nine sterically protected hexamolybdate derivatives was discussed. UV-vis absorption spectroscopy showed strong ligand to POM charge transfer transitions of the amine donor functionalised derivatives, transitions shown to result in good non-linear optical activity in a set of similar but unprotected compounds synthesised by Al-Yasari.[3,45,128] In his previous work, Al-Yasari had investigated the potential to use these chromophores for redox activated NLO switching due to the reversible and quick reduction of the electron accepting POM core, however instability of the compounds in their reduced state caused difficulties and meant no reduced state measurements could be collected.[133] This lead to the synthesis of sterically protected compounds investigated for NLO switching in this work.

In chapter two, the bulk electrolysis experiments of the sterically protected derivatives were discussed, with the results demonstrating the increased stability of these compounds in the reduced state over previously synthesised unprotected analogues. In all cases the sterically protected compounds were stable enough for switching to be investigated using spectroelectrochemistry, with some compounds showing almost no decomposition of the imido bond was observed even after 23 minutes of continued reduction. It was hoped this increased stability would allow these compounds to act as redox activated type II switchable NLO chromophores, as outlined by Coe in 1999.[110] Previously, only a small number of electrochemically switched NLO chromophores have been reported, with switching of other compounds occurring through less easily reversible mechanisms such as chemical reduction or change of solvent.

In this chapter, the compounds synthesised in chapter two were investigated further by UV-vis spectroelectrochemistry and TD-DFT before Hyper-Rayleigh scattering was used to probe the NLO activity of the chromophores in both their oxidised and reduced states. The aim of this investigation was to determine the NLO activity of the compounds, particularly compound **6**, a compound with a stronger donor than had previously been tested, and to explore the switchable optical and non-linear optical properties of the compounds to better understand their potential for use as redox switchable non-linear optically active chromophores.

3.2 Spectroelectrochemistry

Ultraviolet-visible spectroelectrochemistry is a method of analysis involving the study of the electronic transitions of an analyte simultaneously undergoing reduction or oxidation initiated by an external potential. Spectroelectrochemistry can be used as a more reversible alternative to chemical reduction or oxidation, or to monitor real time changes in transitions as compounds are switched between their natural and reduced or oxidised states.

In this work, an OTTLE cell, standing for optically transparent thin layer electrochemical cell,[157] was used to perform the spectroelectochemical analysis. Shown in figure 3.2a, the OTTLE cell is an adapted Specac omni cell, featuring a specially made between-window spacer housing the electrodes. The working electrode, positioned directly over the window to aid complete electrochemical conversion at the optical measurement site, and the counter electrode are both made of highly conductive platinum gauze, while referencing is performed using a small silver wire positioned at the bottom of the cell. The cell used in this work had CaF_2 windows for full optical transparency from 180 nm to 8 µm, making it more than suitable for studying the region of interest of these compounds.
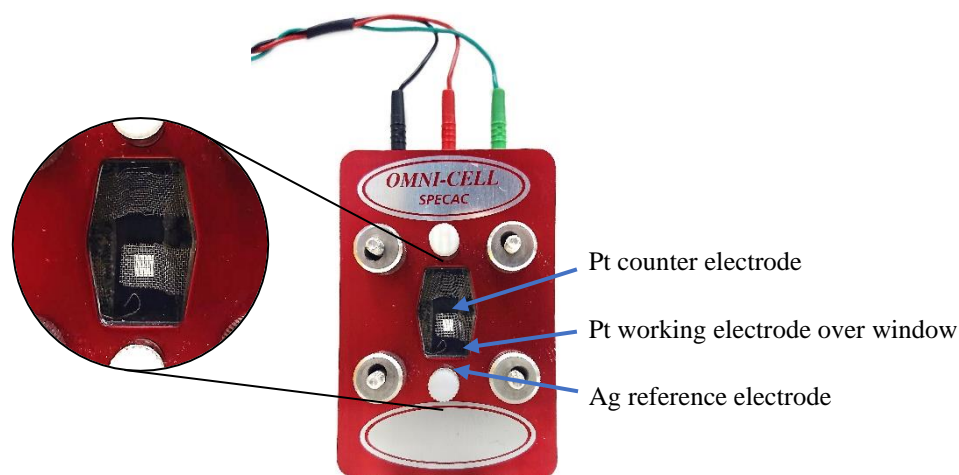
Figure 3.2a The OTTLE cell used to perform the ultraviolet-visible spectroelectrochemistry of compounds **2-10**.

In order to reduce the diffusion or current induced mixing of the reduced compound at the working electrode and the unreduced sample in the rest of the cell, the path length

of the OTTLE cell is considerably shorter than seen in both a standard Specac omni cell and in UV-vis spectroscopy, at just 0.2 mm. This was a key feature of the cell, as previous work performed using a setup more akin to holding electrodes in a narrow cuvette led to confusion, as what originally looked to be re-oxidation of the reduced sample was later discovered to be diffusion of fresh compound into the optical window of the cell.[133] The short path length also allowed for increased concentration of the compound, bringing the concentration used in the spectroelectrochemistry roughly into line with what had been used during the bulk electrolysis experiments, a concentration at which the stability of the compounds had already been probed to reveal good results.

Spectroelectrochemistry was carried out on compounds **2** to **10** at concentrations in the range of 0.36 to 0.72 mM in 0.3 M solutions of electrolyte. The concentration of the compounds varied due to differences in the extinction coefficients requiring different concentrations to get a satisfactory absorption spectrum. The potentials at which reduction and reoxidation were performed at were also varied as needed, with reduction being performed at between -0.5 V and -1.2 V and oxidation between -0.3 V and 0.75 V due to potential drift and variations in the conductance of the cell. Absorption spectra were recorded every 15 seconds throughout the reduction and reoxidation processes, leading to a near-continuous monitoring of the samples.
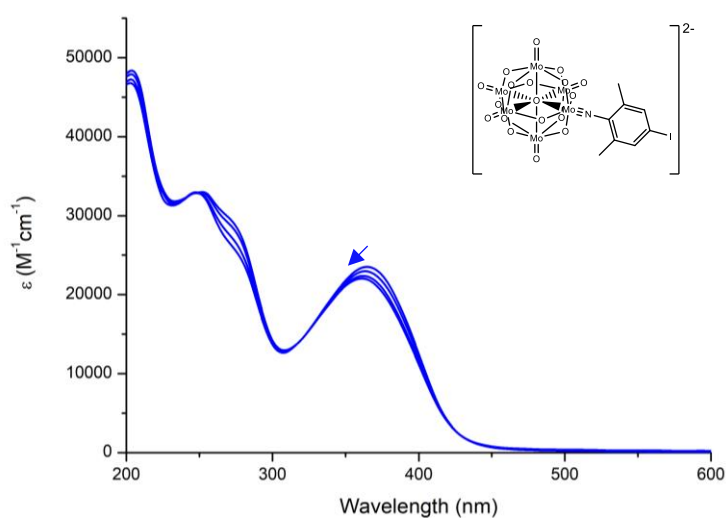
Figure 3.2b Spectroelectrochemical analysis of the reduction of compound **3**. A -0.55 V potential was used to reduce the sample and scans are shown at 30 s intervals.

Reduction of compounds **2** and **3**, the two iodo functionalised derivatives, resulted in almost identical results, with a 4 nm blueshift of the IHCT peak being observed for both compounds upon reduction. The extinction coefficient of the new peaks were also both slightly lower than for the IHCT peaks of the compounds in their oxidised states. In both cases this decrease in peak wavelength was perceived to be a result of the increased energy of the LUMOs after reduction due to the reduced POMs core acting as poorer acceptors of the electrons donated from the aromatic rings of the ligands.

After no further changes of the electronic spectra were observed and reduction was perceived to be complete, reoxidation of the compounds was then performed. In both cases the reoxidation resulted in a reversal of the changes observed during reduction over a similar timescale to with which they occurred during the reduction process. This was much faster than the recovery observed in previous styles of spectroelectrochemistry cell, which later was shown to be due to diffusion of fresh sample into the analysis window.
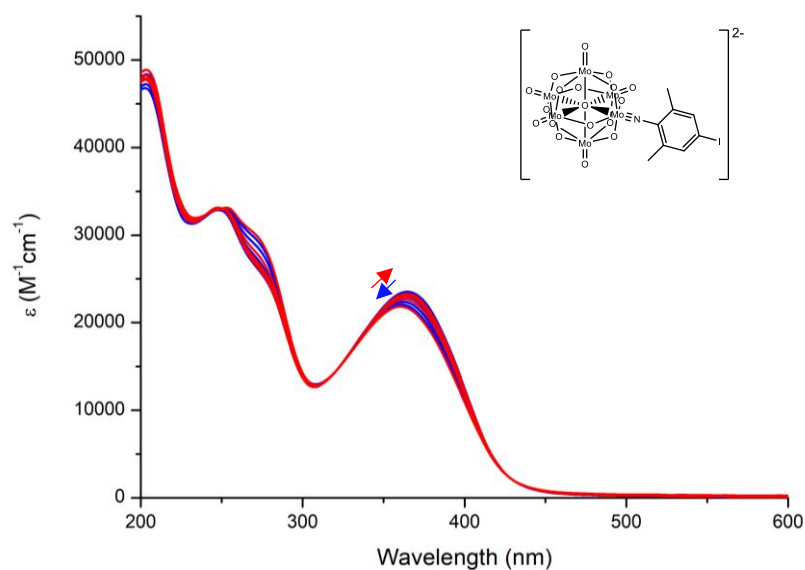
Figure 3.2c Spectroelectrochemical analysis of the reduction (blue) and re-oxidation(red) of compound **3**. A -0.55 V potential was used to reduce the sample and a -0.15 V potential was used for the re-oxidation. Scans are shown at 30 s intervals.

As had been seen during the bulk electrolysis, very little decomposition of compound **3** occurred during the reduction, with a full recovery of the original spectrum during re-oxidation demonstrating the redox activated switching of the LPCT enabled by the compounds increased stability. Although full reversal of the shift of the IHCT peak was also seen for compound **2**, returning from 160 nm to 164, a small reduction in the intensity of the IHCT peak was seen after re-oxidation was complete, suggesting some decomposition took place. This was not unexpected as some decomposition of compound **2** had occurred during the bulk electrolysis experiments, a likely result of the smaller methyl groups less effectively preventing hydrolysis than the isopropyl groups featured at the 2 and 6 positions of the aromatic ring in compound **3**.
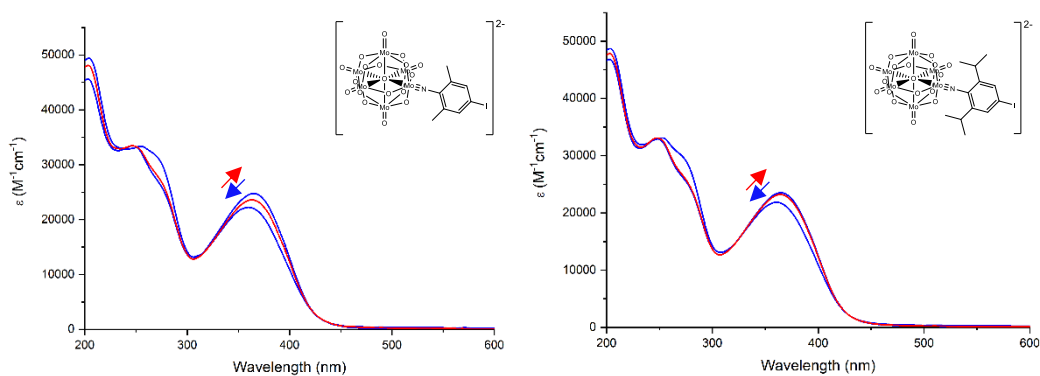
Figure 3.2d Electronic spectra of compounds **2** (left) and **3** (right), with scans taken before and after spectroelectrochemical reduction in blue and after re-oxidation in red.

The changes in energy and intensity of the IHCT peaks observed upon reduction of compounds **2** and **3** were small, however this was consistent with the lack of a strong donor group and the relatively weak charge transfer character previously described for similar compounds.[128] In particular, the run of compound **3** functioned well in demonstrating the increased stability of the sterically protected compounds could enable the monitoring of changes in the electronic spectra brought about by reduction and reoxidation of the compounds. These scans also acted as a standard to compare future runs to, enabling the confirmation that any additional changes observed during the spectroelectrochemical analysis of compounds **4** to **10** would be due to their donor or acceptor groups rather than a response of the functionalised POM itself.

Spectroelectrochemical analysis of compound **4** revealed a much more significant change upon reduction than compounds **2** or **3**, with a complete loss of the original LPCT peak at 424 nm and the appearance of a new peak at 406 nm. This increase in energy of the LPCT peak by a wavelength of 16 nm suggests a significantly less favourable ligand to POM charge transfer transition when the electron acceptor is reduced which in turn suggests a significant weakening of the donor-acceptor pair. As this donor-acceptor transition is the source of the NLO properties of the compound, this is a good indication that reduction of the compounds may result in a decrease in the NLO responses. The increased extinction coefficient of this higher energy peak is likely a result of contributions by other transitions such as amine to aryl transitions not previously observed to any great extent due to the strongly electron accepting POM core.
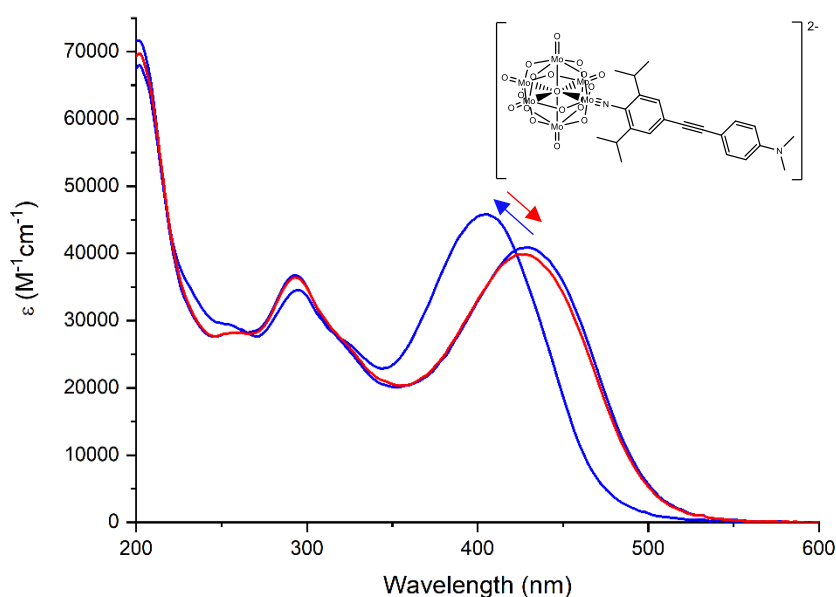
Figure 3.2e Spectroelectrochemical analysis of the reduction of compound **4**, with scans taken before and after spectroelectrochemical reduction in blue and after re-oxidation in red. A -0.55 V potential was used to reduce the sample and a -0.3 V potential was applied to re-oxidise the sample.

As was observed for both compounds **2** and **3**, the LPCT of compound **4** shifted back to its original lower energy upon reoxidation, showing almost full recovery of the original species in a similar timescale for what was observed of the reduction. While

a small decrease in the extinction coefficient of the LPCT peak suggested a small amount of decomposition of the chromophore, a good majority of the compound remained in solution, again showing the benefit of the inclusion of the sterically bulky groups to protect the imido bonds. What this spectroelectrochemistry run revealed was redox switchable electronic transitions of a sterically protected donor containing hexamolybdate derivative, a phenomenon which had not been seen before and would hopefully lead to redox switchable NLO activity when measured.

Upon investigation, similarly successful reversible redox inducible switching of the compound's LPCT peak was discovered for both compounds **5**, the ditolylamino and **6**, the julolidinyl derivative, with reduction causing a loss of the original peaks of both compounds and revealing a new higher energy ligand to reduced POM peak. This again suggested less favourable ligand to POM transitions. A similar shift of 17 nm, from 423 to 406 nm, was observed for both compounds **5** and **4** despite the increase in the strength of the donor group, a result of the electronic isolation between the donor group and the POM cores as discussed in chapter 2, but compound **6**, which featured a donor considerably stronger than those seen in compounds **4** and **5**, did show a larger shift of 31 nm. In both cases, like had been seen for compound **4**, a more intense, higher energy IHCT peak was observed for the compounds in their reduced state, possibly resulting from contributions from amine to aryl transitions.
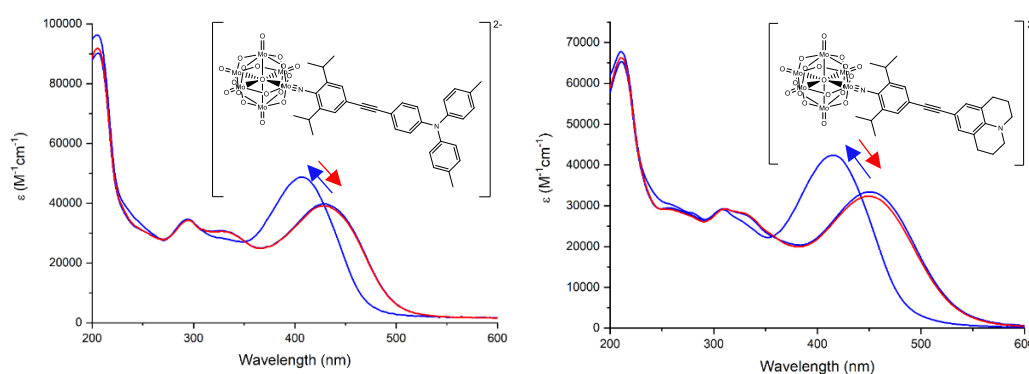
Figure 3.2f Electronic spectra of compounds **5** (left) and **6** (right), with scans taken before and after spectroelectrochemical reduction in blue and after re-oxidation in red.

Slightly more recovery of the original spectrum was seen for compound **5** than for compounds **4** and **6** upon reoxidation, 98% as opposed to 97% for both compounds **4** and **6**, resulting in almost fully reversible changes to the spectrum and matching well with the increased stability of compound **5** observed during the bulk electrolysis experiments, 83% as opposed to 75% for compounds **4** and **6**. The improved stability observed in the spectroelectrochemistry compared to the bulk electrolysis experiments is likely due to the shorter timescale, as reduction took place over only a few minutes in each case during the spectroelectrochemistry while was the samples were held at a reductive potential for 22 minutes in the bulk electrolysis.

As had been observed for compounds **4**, **5**, and **6**, compounds **7** and **8** also both demonstrated reversible shifting of their LPCT peaks, with complete loss of the original peaks, at 430 and 431 nm respectively, and the growth of higher energy peaks at 399 and 398 nm respectively occurring during reduction in both cases. The shifts of the LPCT peaks for compounds **7** and **8**, 31 and 33 nm respectively, were larger than those seen for compounds **4**, **5**, and **6**, again likely a result of the increased coupling between the POM and the donor group of compounds with the shorter bridging π systems. Reoxidation resulted in near full recovery of compound **7** and full recovery of compound **8**, again showing the reversibility of the redox switching of the LPCT peak and demonstrating the potential of these compounds for use as redox switchable NLO active chromophores.
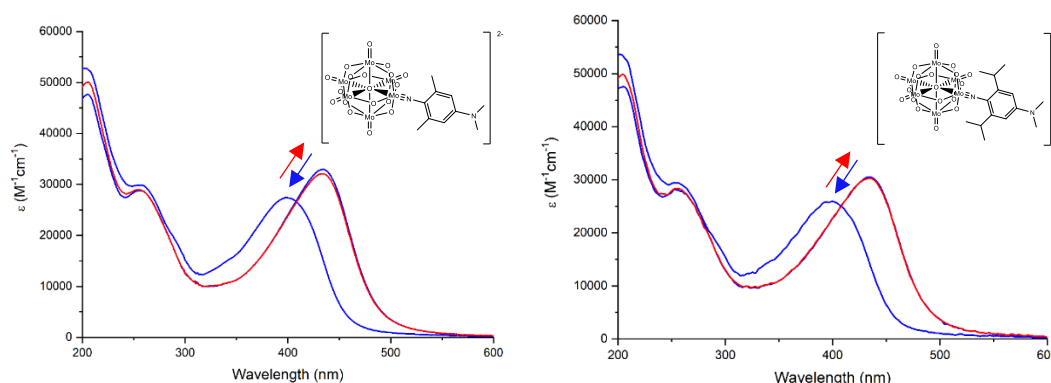
Figure 3.2g Electronic spectra of compounds **7** (left) and **8** (right), with scans taken before and after spectroelectrochemical reduction in blue and after re-oxidation in red.

Spectroelectrochemical analysis of compounds **9** and **10** also revealed switchable transitions of the IHCT peaks, of +11 nm from 399 to 410 in the case of compound **9** and of +26 nm from 382 to 406 nm for compound **10**. Interestingly, these shifts contrasted those seen for the IHCT peaks of both the iodo functionalised and amine donor functionalised compounds, all of which revealed higher energy IHCT peaks in the reduced state as opposed to the lower energy peaks seen for compounds **9** and **10** upon reduction.

The electronic absorption spectra of both compounds **9** and **10** were discussed in chapter two, where the decreased energy of the IHCT peak of compound **10** compared to compound **3** despite the even weaker donor ability was noted. This was decided to be a result of contributions from aryl to nitro transitions overlaying with the aryl to POM transitions in the IHCT peak. This analysis has since led to the suggestion that these new lower energy transitions of compounds **9** and **10** seen upon reduction arise not from weakened ligand to POM charge transfer as is usually seen when the POM core is reduced, but from POM to ligand charge transfer with the electron rich reduced state POM acting as the donor group for the nitro acceptor. Upon reoxidation, a near complete recovery of compound **9** was observed along with a complete recovery of compound **10**, again showing the compounds' increased stability in their reduced state due to the steric protecting groups on the aniline ring.
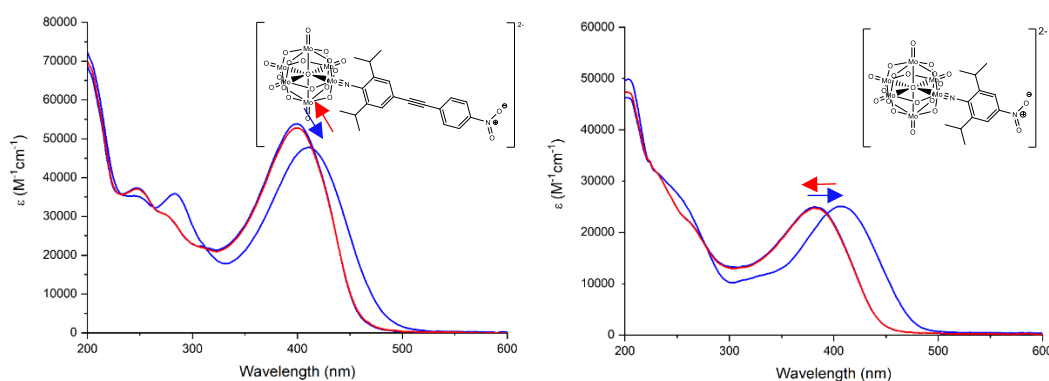
Figure 3.2h Electronic spectra of compounds **9** (left) and **10** (right), with scans taken before and after spectroelectrochemical reduction in blue and after re-oxidation in red.

These new, lower energy transfer transitions observed in the reduced state as a result of new POM to ligand charge transfer led to the suggestion that although the nitro functionalised hexamolybdate derivatives have previously been shown to be HRS inactive in their oxidised states, they may in fact be HRS active while reduced. This possibility of polyoxometalate chromophores with increased NLO activity after electrochemical switching has been investigated computationally for Keggin type POMs[117] but so far no experimental work has been carried out.

	IHCT peak (natural) (nm)	IHCT peak (reduced) (nm)	Shift observed (nm)
2	364	360	-4
3	364	360	-4
4	424	406	-18
5	423	406	-17
6	445	414	-31
7	430	399	-31
8	431	398	-33
9	399	410	+11
10	382	406	+24

Table 3.2a Comparison of the IHCT peak of compounds **2** to **10** in their natural and reduced states.

In addition to investigating the potential redox activated switching of compounds **4** to **8** by reduction of their POM cores, for a selection of the compounds, investigation of the possibility of switching by oxidation of the amine was also carried out. Electrochemical analysis, discussed in chapter 2, had already demonstrated the reversibility of the amine oxidation peaks of compounds **7** and **8** as well as the quasi-reversibility of the amine oxidation peak of compound **5**, and therefore spectroelectrochemical analysis of two of these compounds was performed.

Upon oxidation of the amine of compound **8**, a reversible decrease in the LPCT peak at 430 nm was observed along with the reversible growth of two new lower energy peaks at 495 nm and 640 nm. Ammonium radical localised transitions have previously

been reported in the range of 600 to1000 nm,[158] suggesting this is the origin for the peak at 640 nm. The peak at 495 nm is in a similar region to a peak observed of oxidised dimethyl aniline[159] and is likely due to transitions from the organic π system to the ammonium cation. Although unlike in previous spectroelectrochemistry experiments of the donor containing compounds, no clear, blue-shifted LPCT transition could be seen upon switching, a new high-energy shoulder peak at 303 nm did grow in during the oxidation and it is possible that this results from the LPCT transitions being weakened more than observed during any previous experiments by the presence of the strongly withdrawing ammonium radical.
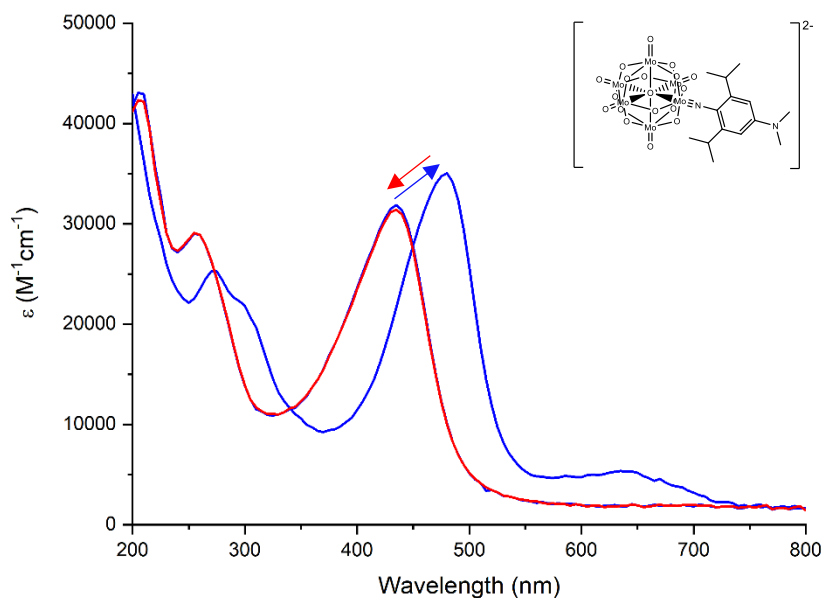
Figure 3.2i Spectroelectrochemical analysis of the oxidation (blue) and re-reduction (red) of compound **8**. A 0.9 V potential was used to oxidise the sample and a 0.8 V potential was used for the re-reduction.

Upon re-reduction, a full return to the original spectrum of compound **8** occurred, demonstrating the reversibility of this oxidative switching mechanism on a longer timescale than had previously been investigated since no oxidative bulk electrolysis experiments had been performed. This opened the possibility of these compounds not only acting as on/off switchable NLO chromophores reductively, but oxidatively too.

Oxidative spectroelectrochemical analysis was also carried out on compound **5** and revealed the same decrease in the LPCT peak and the growth of the ammonium radical cation peak at 636 nm as had been seen for compound **8**. However, in contrast to what was observed during the spectroelectrochemical analysis of compound **8**, no new peak at around 495 nm grew in, potentially due to the alkyne bridge resulting in electronic insulation between the ammonium cation and the rest of the molecule. In addition, whereas once fully oxidised the spectrum of compound **8** stabilised, the spectrum of compound **5** never did, suggesting decomposition of the oxidised compound, a theory quickly confirmed by incomplete regrowth of the LPCT peak during re-reduction.
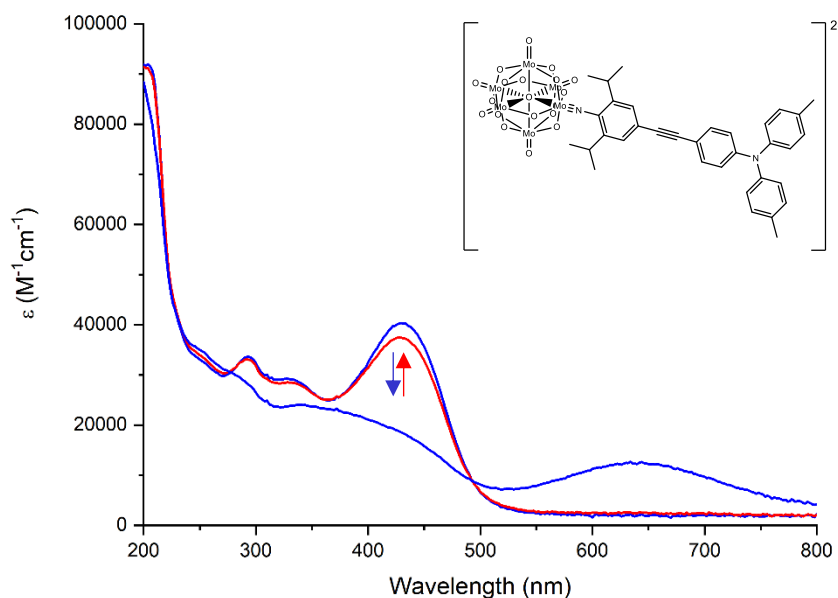
Figure 3.2j Spectroelectrochemical analysis of the oxidation (blue) and re-reduction (red) of compound **5**. A 2.2 V potential was used to oxidise the sample and a 0 V potential was used for the re-reduction.

In order to test the completeness of the reductions achieved through electrochemical means, chemical reduction was also explored, with an excess of cobaltocene being used to chemically reduce a sample of compound **8** under inert conditions. Despite its sensitivity to air, cobaltocene was chosen as the chemical reductant due to its transparency below 350 nm allowing easy observation of the LPCT peaks and its reduction potential of -1.33 V vs Fc/Fc$^+$ [160] making is suitable for initiating a single reduction of the doubly reducible POM even in excess.

The UV-vis absorption spectra taken before and after the addition of the cobaltocene revealed a near identical transformation to what had been observed for compound **8** using electrochemical reduction, with the complete loss of the peak at 431 and the growth in of a peak at 398 suggesting full reduction of the compound had been achieved during spectroelectrochemistry. The additional peak observable at 328 nm in the spectrum taken after reduction as well as the increase in the baseline at lower energies can be attributed to the excess cobaltocene that remained in solution after full reduction of compound **8** had occurred.[161]

This shift of the LPCT peak could be partially reversed by shaking the contents of the flask with air, suggesting the reduced compound was stable enough to be at least partially re-oxidised by the air rather than decomposed. A more complete recovery of compound **8** may have been achieved through more thorough means of mixing with oxygen or another oxidant, but as the main goal of the chemical reduction was to record the spectrum of a fully reduced sample of compound **8**, this was deemed unnecessary.
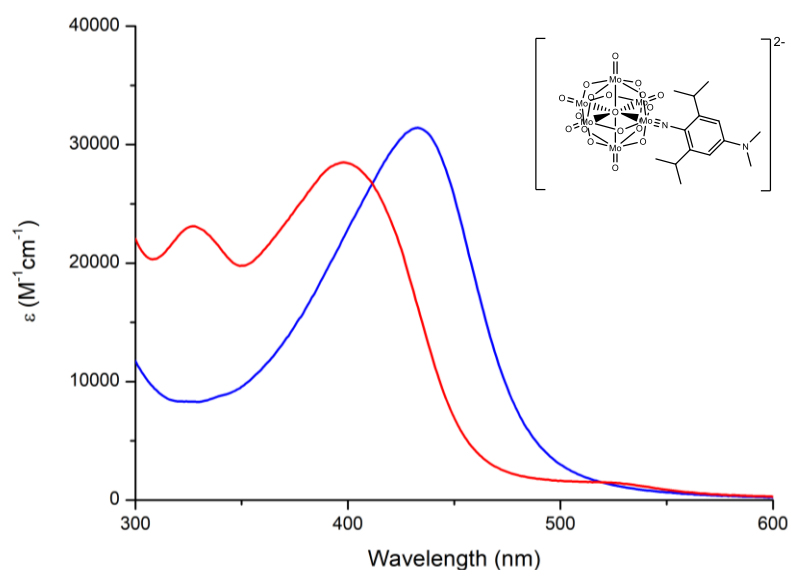
Figure 3.2k Chemical reduction of compound **8** was performed using cobaltocene revealing an identical shift in the IHCT peak as seen during electrochemical reductions. The spectrum taken before reduction is shown in blue, and after is shown in red.

Overall, the spectroelectrochemical analysis performed on compounds **2** to **10** proved successful and revealed repeatable and reversible redox activated switching of the IHCT peak in the linear absorbance spectra, changes which would hopefully bring

corresponding weakening or strengthening of the NLO activity of the compounds when measured.

3.3 DFT and TD-DFT Calculations

In order to better understand the electronic spectra of both the oxidised and reduced states of compounds **2** to **10** as well as predict the NLO properties of the compounds, DFT calculations were performed using Gaussian. The calculations were achieved using Gaussian 16, with the CAM-B3LYP functional being used for the geometry optimisations, the TD-DFT calculations, and calculations to predict both the static and dynamic hyperpolarizabilities. CAM-B3LYP is a range separated hybrid functional, meaning the percentage of Hartree-Fock and DFT exchange vary for longer and shorter range interactions.[162] These type of functionals are more computationally intense than examples which model electron density more locally, but can produce better results for compounds where longer distance exchanges such as the charge transfer between the ligand and the POM are important. For all calculations, the 6-31++G(d,p) basis set was used for carbon, nitrogen, oxygen, and hydrogen atoms while LANL2DZ was used for the molybdenum and iodine atoms. The W06 fitting set was used to produce the UV-vis trace as an output of the TD-DFT calculations. For all calculations, the solvent effects of acetonitrile were modelled using SCRF, and in all cases, the geometry optimisation was performed using the geometry from crystal structures of the compounds as a basis.

Initially, a range of basis sets and functionals were investigated for use in the calculations of these compounds, with B3LYP, CAM-B3LYP, and ωB97Xd all used as possible functionals, 6-31++G(d,p) and 6-311G(d,p) both used as possible basis sets for carbon, nitrogen, oxygen, and hydrogen and SDD and LANL2DZ both used as possible basis sets for heavier atoms. The larger LANL2TZ basis set used for the heavier atoms by Champagne et al.,[163] was not accessible on UEA's high-performance computing set up so could not be used in this work.

Calculations performed on compound **8** were used to test potential functional and basis sets combinations, with results shown in table 3.3a. Here, the predicted bond angles and lengths resulting from geometry optimisation calculations as well the peak

wavelength of the IHCT transition as calculated by TD-DFT are compared with the experimental data. The bond angles and lengths were obtained from X-ray crystallography and the experimental absorbance spectrum was taken in acetonitrile. From the calculations, it was determined that using a combination of CAM-B3LYP, LANL2DZ and 6-31++G(d,p) produced the best results when compared to the experimental data. 6-311G(d,p), a larger basis set, also produced good geometry optimisation results, however since by the time this basis set was used, calculations had already been started on other compounds using 6-31++G(d,p) and there was not a considerable increase in accuracy, it was decided 6-31++G(d,p) would be used too for the remaining calculations.

Functional	Mo	Other atoms	Mo-N (Å)	O-Mo-N (°)	C-N-Mo (°)	LPCT λ_{max} / nm
Experimental			1.748	177.0	175.3	430
B3LYP	SDD	6-31++G(d,p)	1.758	180.0	180.0	500
ωB97Xd	SDD	6-31++G(d,p)	1.723	177.1	178.1	380
ωB97Xd	LANL2DZ	6-31++G(d,p)	1.728	176.3	178.1	400
B3LYP	LANL2DZ	6-31++G(d,p)	1.765	179.4	179.2	410
CAM-B3LYP	LANL2DZ	6-31++G(d,p)	1.738	177.3	178.5	415
CAM-B3LYP	SDD	6-31++G(d,p)	1.732	178.3	179.3	400
CAM-B3LYP	LANL2DZ	6-311G(d,p)	1.727	175.29	176.89	-

Table 3.3a Summary of functionals and basis sets used for DFT calculations of compound **8**.

After geometry optimisation calculations using CAM-B3LYP, LANL2DZ, 6-31++G(d,p) had been performed, TDDFT calculations were used to produce predicted spectra for compound **3**, **4**, **5**, **6**, **7**, **8**, **9**, and **10** in their natural states, along with

compound **4**, **5**, **6**, **8**, **9**, and **10** when reduced. The results of these calculations are shown in table 3.3b. In all cases, the TDDFT calculations of the compounds in their natural state produced spectra that were a relatively good fit when compared to the experimental data, with similar shapes and peaks to those observed in the experimental spectra, especially regarding compounds **2**, **3**, **7**, **8**, and **10**, compounds without the extended π system of the alkyne bridge. For all cases, calculations overestimated the intensity of the IHCT peaks compared to the experimental spectra. This was particularly apparent in calculations performed of the long diphenylethyne bridged compounds. Importantly, however, despite small differences in the lower energy peaks along with the intensity of some peaks, λ_{max} all calculated IHCT peaks showed relatively good agreement with the experimental values, with the calculated peak being within 15 nm of the experimental value in all cases.
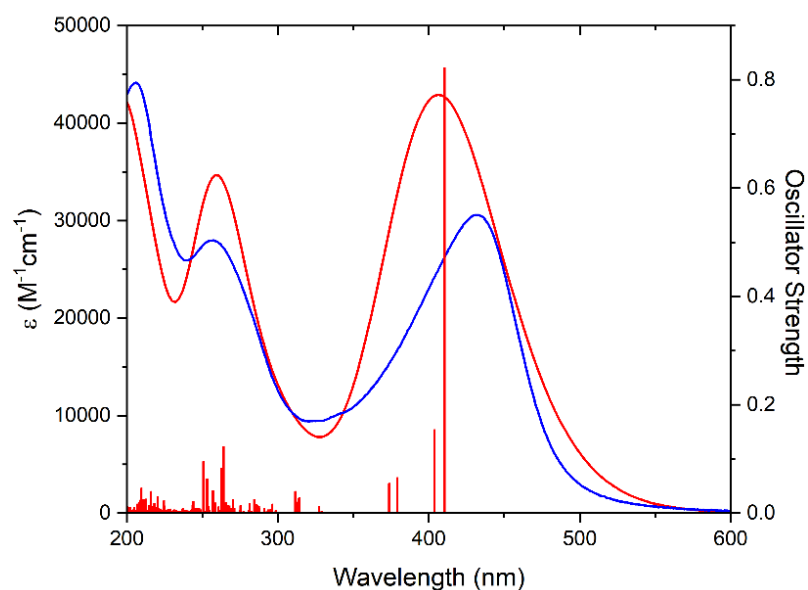
Figure 3.3a Electronic spectra of compound **8**, with the experimental spectrum shown in blue and the calculated spectrum shown in red. The Oscillator strength of the calculated spectrum is also included.

Calculations of the UV-Vis absorption spectra of the compounds allowed for useful investigation into the orbitals involved in the transitions. As had been expected, the higher energy transitions of the calculated spectra of compounds **3** to **10** could be

assigned as O to Mo transitions, with many small overlapping transitions forming what often presented as two larger peaks. The IHCT peaks of all compounds were calculated to be comprised of multiple transitions, and while the lowest energy transition was always calculated to be from a HOMO situated primarily on the ligand to an orbital situated primarily on the POM core, this was not necessarily the LUMO, but typically a LUMO+x instead.

In the cases of the compounds **4**, **5**, and **6**, the derivatives with extended alkyne bridges and amine donors, the most intense transitions were from the HOMO to the LUMO+3 orbital, and although these transitions were still primarily ligand to POM core, a considerable amount of the electron density remained on the aromatic ring proximal to the POM showing the electron density was not always fully transferred to the POM core. These calculations also showed the delocalisation of the electron density over the POM core in the excited state with electron density particularly dense on the electron negative oxygen anions, a visualisation of why these hexamolybdate cores function as strong electron acceptors despite their already negative charge.

6 HOMO
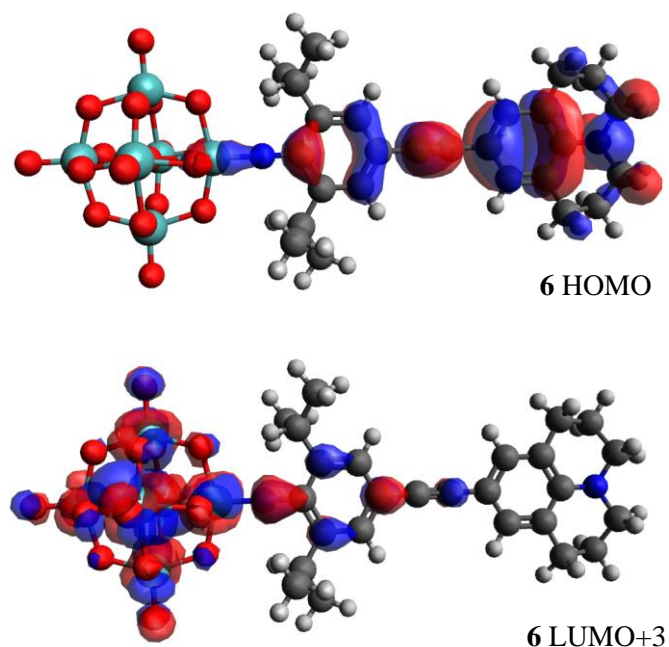
6 LUMO+3

Figure 3.3b Calculations predicted the IHCT peak of compound **6** primarily resulted from transitions from the HOMO (top), to the LUMO+3 (bottom).

In contrast to what was seen for the diphenylethyne bridged derivatives, the TD-DFT calculations performed on compounds **7** and **8** predicted the predominant transition of the IHCT peaks was to an orbital with very little organic character, suggesting the transition was a more complete ligand to POM charge transfer than what was seen for the diphenylethyne bridged compounds. This increased transfer of electron density in the transition suggests increased charge separation which, according to the two state model, should help to increase hyperpolarizability.

3 HOMO   **3** LUMO+4

8 HOMO   **8** LUMO+4

10 HOMO   **10** LUMO+1
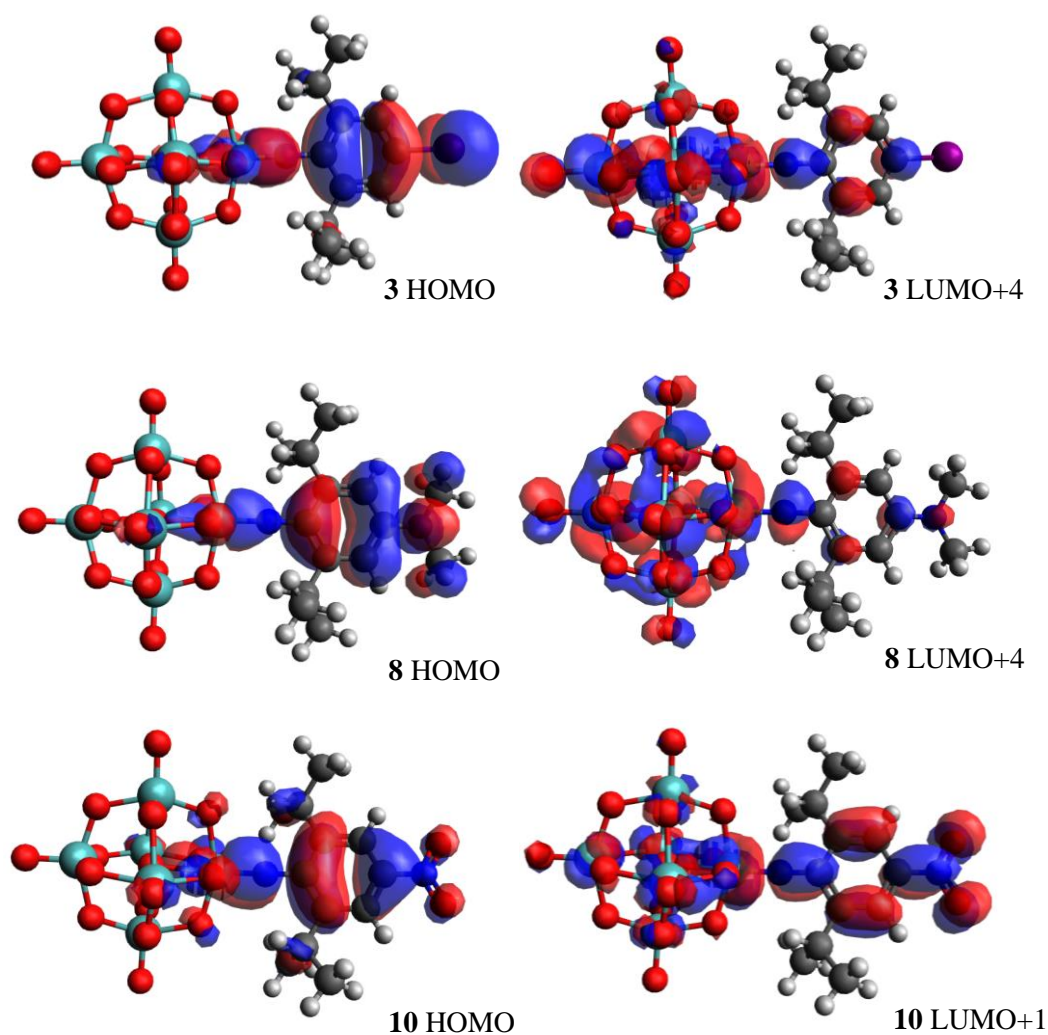
Figure 3.3c Calculations predicted the IHCT peak of compound **3** (top) resulted primarily from transitions from the HOMO (left), to the LUMO+4 (right), while the peak of compound **8** (middle) resulted primarily from transitions from the HOMO (left), to the LUMO+4 (right) and the IHCT peak of compound **10** (bottom) resulted primarily from transitions from the HOMO (left), to the LUMO+1 (right).

Comparison of compounds **3**, **8**, and **10**, the diisopropyl protected iodo derivative, the phenyl bridged, diisopropyl protected dimethylamino derivative, and the phenyl bridged, diisopropyl protected nitro derivative, showed relatively similar HOMOs and LUMOs, with the HOMO of all compounds primarily situated on the organic ligand and the LUMO of all three compounds focused on the POM core. However, as with the comparison between the diphenylethyne and phenyl bridged amine donor containing compounds, more differences were observed when the orbitals primarily involved in the IHCT peak were compared. In all three compounds, transitions occurred from the HOMO, which was predominantly situated on the organic ligand, to an orbital at an energy somewhat higher than the LUMO. This was the LUMO+4 for compounds **3** and **8** and the LUMO+1 for compound **10**. The LUMO+4 orbital of compound **8** was still primarily on the POM core, suggesting much of the electron density transferred from the ligand to the POM when excited, however, slightly less electron density was seen delocalised over the POM core in the LUMO+x of compound **3**, with slightly more electron density being left situated on the aromatic ring of the ligand. This is consistent with the higher energy charge transfer peak observed in the experimental electronic spectra.

In contrast to the IHCT transitions that occurred predominantly from the ligand to the POM core, for compound **10**, electron transfer occurred from the aromatic ring of the ligand to an orbital spread over the compound. More electron density was predicted to be present on the POM core in the LUMO+1 than in the HOMO suggesting some ligand to POM charge transfer character, but a considerable amount of electron density was also found on nitro group as well as on the aromatic ring, suggesting π to nitro and π to π^* transitions also contribute to the peak. It is likely this π to nitro transition that results in the experimental IHCT peak of **10** occurring at a lower energy than the IHCT peak of its iodo functionalised analogue. This would also result in a smaller overall change in net dipole moment than for the donor containing compounds, a factor that would decrease hyperpolarizability according to the two state model.

DT-DFT calculations on compound **9** showed this use of the nitro as an acceptor group to an even greater extent than for compound **10**, with the LUMO+1 orbital, the orbital involved in the transition giving the highest contribution to the peak, situating predominantly on the nitro group and the aromatic rings of the compound, suggesting the IHCT peak of compound **9** results primarily from π to nitro and π to π^* transitions

with only a small amount of ligand to POM character.

9 HOMO
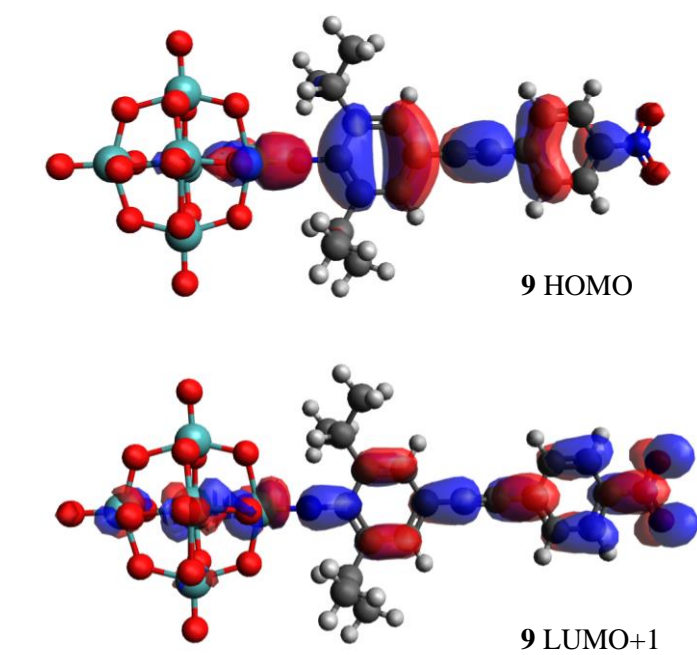
9 LUMO+1

Figure 3.3d Calculations predicted the IHCT peak of compound **9** primarily resulted from transitions from the HOMO (top), to the LUMO+1 (bottom).

TD-DFT calculations were also performed on a selection of compounds in their reduced states to better understand the changes observed during the spectroelectrochemistry. The calculations were performed using the same basis sets and functionals as those performed of the compounds in their natural states, with only the charge and multiplicity altered. Geometry optimisations were performed first, again using the structure obtained from X-ray crystallography as a starting point, before TD-DFT was used to predict the UV-vis absorption spectra for the compounds. Since the reduced state compounds have an unpaired electron and these are unrestricted calculation, orbitals with both α and β spin will be generated. Unfortunately, due to the method used to generate the images, the β orbitals could not be visualised.

Calculations performed on compound **8**, the phenyl bridged diisopropyl protected dimethylamine derivative, predicted shifting of the IHCT band to a shorter wavelength, a result also seen in the experimental spectroelectrochemistry. As was

seen for the predicted natural state absorption spectrum, the calculated peak was at a higher energy than the experimental value by about 15nm, however, overall a similar shift in the peak was seen upon reduction as in the experimental work. These calculations predicted that even when reduced, the most intense transitions contributing to the peaks were ligand to POM charge transfers, although these did appear weakened with some electron density still assigned to the ligand even in the excited state. This would result in a decrease in change in dipole moment in the transition, another indication that the hyperpolarizability should be weakened in the reduced state compared to the natural one.

8 HOMO

8 LUMO

Red **8** HOMO

Red **8** LUMO
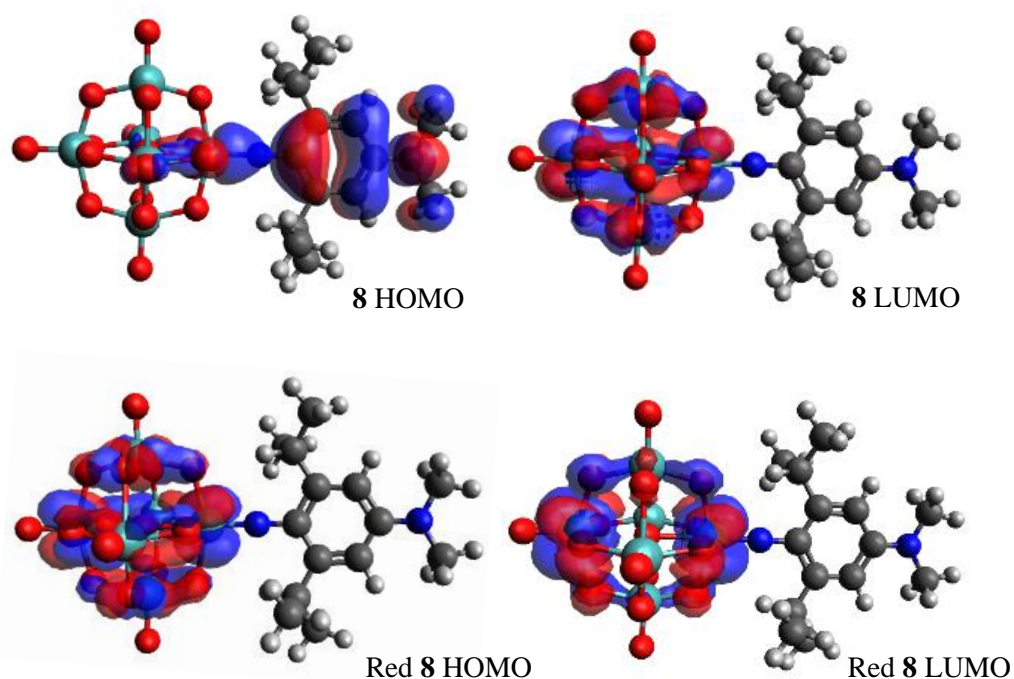
Figure 3.3e Calculations predicted the HOMO of compound **8** was localised on the ligand and the LUMO was delocalised over the POM core, while calculation performed on a reduced form of compound **8** predicted both the HOMO and LUMO were delocalised on the POM core.

A more significant change was seen with comparison of the HOMOs and LUMOs, as while in the natural state the HOMO was calculated to be situated entirely on the ligand with the LUMO delocalised over the POM core, in the reduced state, all electron density was delocalised over the POM core in both the HOMO and the LUMO. These

significant changes, along with the changes in the orbitals involved in the most intense charge transfer transitions and the similar increase in energy of the charge transfer peak in the reduced state to what was seen in the spectroelectrochemistry predict a weaker donor-acceptor relationship between the amine and the now reduced POM core, a factor that would likely result in the reduced non-linear optical activity hoped for from the reduced state amine functionalised hexamolybdate derivatives. A similar observation was made of the results of calculations made on the reduced states of compounds **4**, **5**, and **6**.

Red **10** HOMO   Red **10** LUMO

Red **9** HOMO

Red **9** LUMO
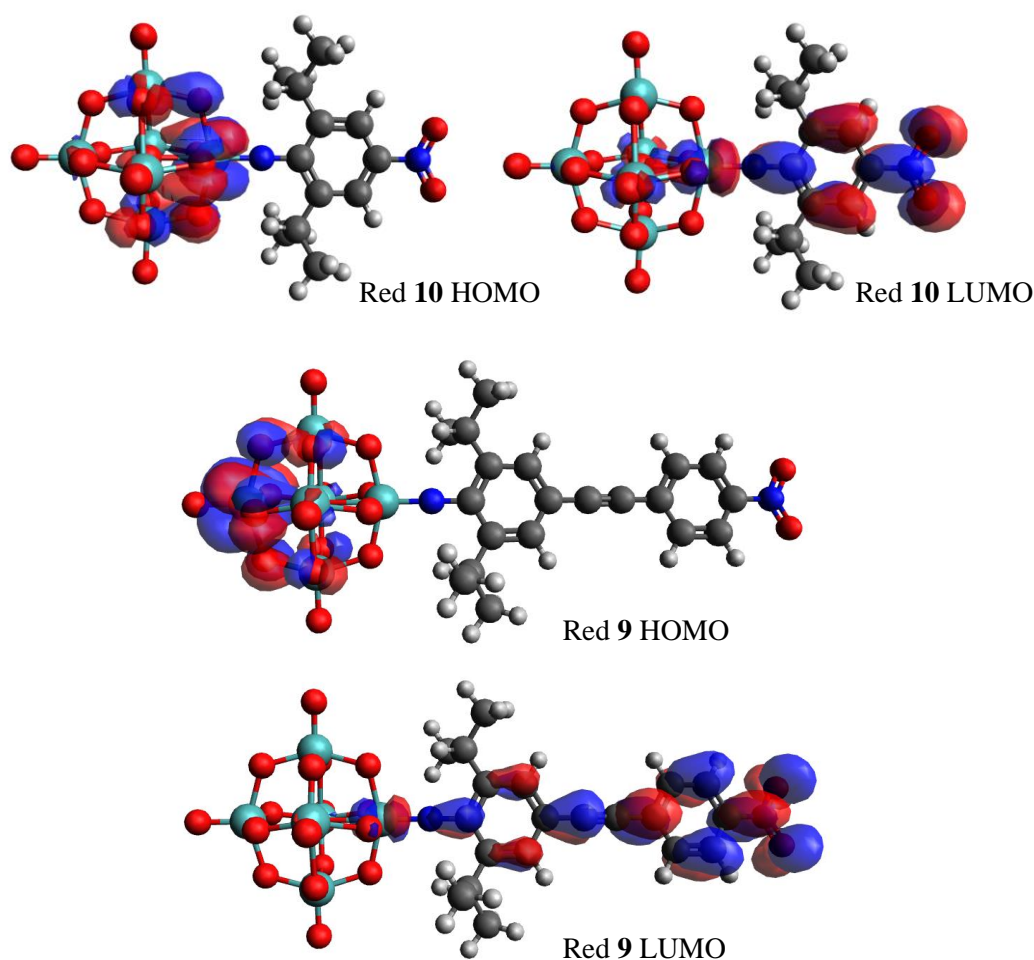
Figure 3.3f Calculations predicted the HOMO (left) of compound **10** when reduced was localised on the POM core and the LUMO (right) was primarily on the ligand. Similar results were seen for compound **9** when reduced, where the HOMO (middle) was localised on the POM core and the LUMO (bottom) was primarily on the ligand with significant electron density calculated to be on the nitro acceptor group.

Calculation performed on compound **10** predicted a considerably higher energy charge transfer peak than what was observed, with the maximum of the peak being at 359 nm, or 3.45 eV, compared to the 406 nm, or 3.05 eV, observed in the spectroelectrochemistry. As was observed for compound **8** only a small change was observed in the orbitals calculated to be involved in the most intense transition, however, a considerable change was observed of the HOMO and the LUMO. When oxidised, these appear very similar to those of the donor containing compounds, with the HOMO on the ligand and the LUMO on the POM core, however, when in the reduced state, these appear reversed, with the HOMO on the POM core and the LUMO primarily on the ligand. Significant electron density was calculated to be on the nitro group, suggesting, as had been predicted from the red-shifting of the IHCT peak when reduced, that upon reduction, the increased electron density of the POM allows for increased charge transfer from the POM to the ligand. A similar result was seen for compound **9**, with the HOMO being situated on the POM core and the LUMO being on the ligand. Significant electron density was again seen on the nitro group, suggesting the assignment of POM to ligand charge transfer transition to the red-shifted peak observed in the spectroelectrochemistry.

Gaussian calculations were also used to predict dynamic and static hyperpolarizability of compounds **3** to **10** in their natural state as well as of compounds **6**, **8**, **9**, and **10** in their reduced states. These calculations were performed using the same functionals, basis sets and solvent approximations as used previously in this work. For compounds **3**, **9**, and **10**, small but non-zero hyperpolarizabilities were predicted, with a $\beta_{zzz,1064}$ of 97×10^{-30} esu predicted for compound **3**, 57×10^{-30} esu predicted for compound **9** and 30×10^{-30} esu for compound **10**. Interestingly, the hyperpolarizabilities of compounds **9** and **10** were of the opposite sign to compound **3** and those of the compounds with amine donors, suggesting these small hyperpolarizabilities may be occurring due to ligand to nitro dipoles rather than the ligand to POM dipole normally responsible for the NLO activity of the hexamolybdate derivatives, a result compatible with the considerable π to nitro component of the IHCT peaks in the calculated spectra.

The calculations on compounds **4**, **5**, **6**, **7**, and **8**, compounds all featuring amine donor groups, predicted high dynamic hyperpolarizabilities roughly in line with what had been expected based on experimental results on previous compounds by Al-Yasari et al.[3,45,128] Compared to these previous experimental values, the calculations do result in

a considerable overestimation of the static hyperpolarizabilities, however, this can be explained by the calculations assuming the dynamic dielectric constant for the acetonitrile rather than the static even when the hyperpolarizability is extrapolated to the static limit.[164]

	Oxidised				Reduced			
	LPCT λ_{max} (nm)	Calc λ_{max} (nm)	$\beta_{zzz,1064}$ ($\times 10^{-30}$ esu)	$\beta_{zzz,0}$ ($\times 10^{-30}$ esu)	LPCT λ_{max} (nm)	Calc λ_{max} (nm)	$\beta_{zzz,1064}$ ($\times 10^{-30}$ esu)	$\beta_{zzz,0}$ ($\times 10^{-30}$ esu)
3	364	357	97	118	360	-	-	-
4	424	414	655	612	404	370	315	294
5	423	413	653	570	405	-	346	386
6	445	422	747	680	414	398	400	373
7	430	416	246	283	398	-	-	-
8	431	415	270	326	399	385	114	27
9	399	394	57	30	410	393	211	174
10	382	365	30	27	406	359	70	78

Table 3.3b Summary of experimental and computational β and UV-vis data in both the oxidised and reduced states.

The calculated dynamic hyperpolarizabilities of compounds **4**, **5**, and **6** were considerably higher than those of compounds **7** and **8**, a not unexpected result of the increased size of their extended conjugated π systems increasing charge transfer distances. For the three diphenylethyne bridged compounds, an increase in hyperpolarizability with increasing donor strength was seen, with compound **6**, the strongest donor, having the highest calculated hyperpolarizability and compound **5**, the weakest donor, having the lowest.

Calculations performed on compound **8** in the reduced state suggested a weakened NLO activity compared to the same compound in its natural state, with a 58% decrease in β_{1064} predicted compared to the oxidised form of compound **8**. Comparison of the calculated static hyperpolarizabilities predicted a larger decrease of 92%. Although neither calculation predicted an 100% turning off of the hyperpolarizability when

reduced, both still did predict that compound **8** would act as a redox activated switchable chromophore with a considerably higher hyperpolarizability in its natural state than its reduced. Calculations performed on compounds **4**, **5**, and **6** predicted similar results though with less efficient switching, with a static hyperpolarizability switching efficiency of 52% predicted for compound **4**, 32 % for compound **5**, and 45% for compound **6**.

Reduced state calculations on compounds **9** and **10** showed the opposite effect, with an increase in static hyperpolarizability of 580% and 280% respectively predicted upon reduction. As was seen for the calculations performed on the two nitro functionalised compounds in their natural states, these hyperpolarizabilities were of the opposite sign to those seen for the donor containing compounds, suggesting increased POM to ligand charge transfer was responsible for the increased NLO activity upon reduction rather than the ligand to POM charge transfer seen for compounds **4** through **8**. This increased hyperpolarizability when reduced suggested these nitro containing compounds may act as off/on NLO active chromophores, the opposite to their amine functionalised analogues, leading to the possibility of the polyoxometalate chromophores synthesised in this work showing both on/off and off/on redox activated NLO responses

3.4 Hyper-Rayleigh Scattering

There are three techniques to directly measuring hyperpolarizability: Second Harmonic Generation, EFISH, and Hyper-Rayleigh Scattering. While Second harmonic generation is only suitable for use with crystalline samples, both EFISH and Hyper-Rayleigh Scattering can be used for measuring the NLO activity of samples in solution. EFISH, however, uses an applied electric field to achieve alignment of the molecules in the solution, resulting in the overall dipole needed for second harmonic generation, and therefore it is an unsuitable technique for measuring charged chromophores such as the ionic polyoxometalate derivatives. To directly measure the nonlinear optical activity of charged compounds in solution state, Hyper-Rayleigh Scattering is used, which instead of requiring a permanent dipole, relies on a process that generates the frequency doubled light through the formation of temporary dipoles in the analyte solution.[53] This results in a relatively weak signal.

In this work, a system with a 1064 nm incident beam was used, generated from a femtosecond-pulsed laser, and focused onto a 4×10 mm cuvette. The scattered light produced by the sample was measured at an angle of 90° to the incident beam using a spectrograph coupled to a charge-coupled device enabling wavelength detection. In these measurements, the scattered light was measured without discriminating Z and X polarized light. The laser set up is shown in detail in figure 3.4a, where HWP, achromatic half-wave plate; Pol, Glan-Taylor polariser; PCL, plano-convex lens; AL, achromatic lens; DM, dichroic mirror; WP, Wollaston prism; Dprism, dove prism; BG39, absorptive filter; BBF, broad band filter, 720 nm blocking edge; EMCCD, electron multiplier charge coupled device. The nitrogen flow and potentiostat were used only for the redox switching experiments.
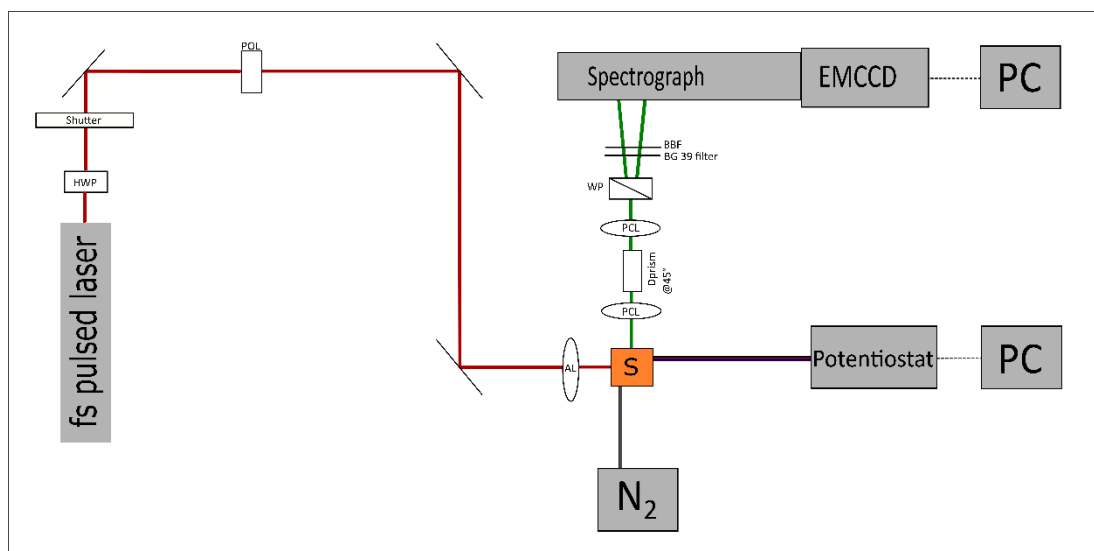
Figure 3.4a Scheme of the set up used for the femtosecond 1064 nm Hyper-Rayleigh scattering experiments performed on compounds **4** to **10** in acetonitrile solution.

Recording time for the measurements was between 2 and 5 seconds with 10 scans taken for each run which, when coupled with the high powered incident laser beam and sensitive detectors, allowed for the accurate measurement of the second harmonic scattered light, the signal of which is normally low under non-resonant conditions. Concentrations of around 5×10^{-5} M were used for the measurements, well within the 10^{-4}-10^{-6} range usually used. Concentrations lower than this can be difficult to detect, whereas concentrations higher can result in reabsorption of the scattered second

harmonic wavelength resulting in under estimations of the hyperpolarizability.

In older setups, instead of the spectrograph coupled to an intensified charge-coupled device, a photomultiplier detector was used to detect the scattered light, however, since this measured the intensity of all light emitted at the doubled frequency, it often led to an over estimation of Hyper-Rayleigh scattering due to overlap with bands resulting from two photon fluorescence. Choppers and signal generators were used to try to time gate out the fluorescence signal, however, using the more recent technique of recording a spectrum of the scattered light allows for deconvolution of these overlapped peaks and typically results in more accurate results. Figure 3.4b shows the recorded spectrum from a 1064 nm Hyper-Rayleigh Scattering experiment, with the sharp Hyper-Rayleigh Scattering peak observable at 532 nm and the broad two photon fluorescence peak overlapped at a slightly lower energy.
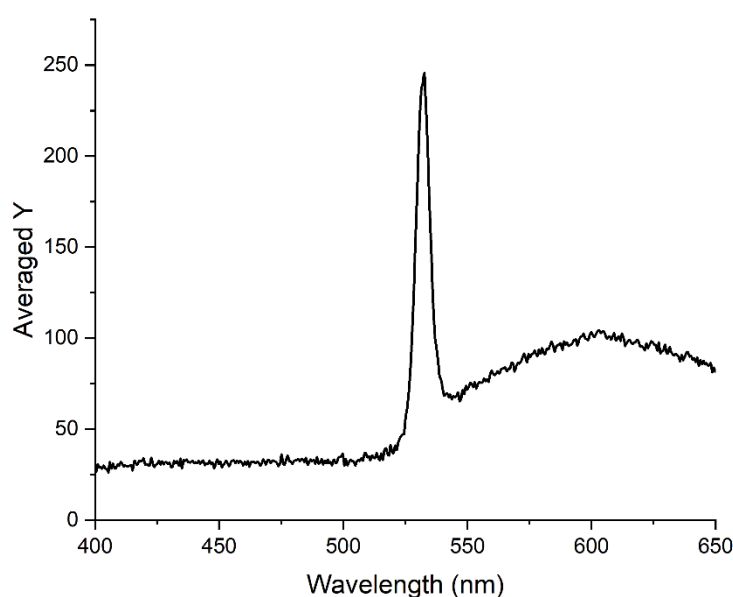
Figure 3.4b The recorded spectrum from a 1064 nm Hyper-Rayleigh Scattering experiment, with the sharp HRS peak at 532 nm and the broader two photon fluorescence peaks at a lower energy.

To determine the hyperpolarizability of the compounds measured, the internal reference method was used,[165] with the solvent, in this case acetonitrile, being used as the reference. The intensity with which a sample scatters light is given by equation

3.4.1, where $I_{2\omega}$ represents the intensity of the frequency doubled light, I_ω donates the intensity of the incident beam, G is a proportionally factor for the instrument, N_S and N_x donate the number density of the solvent and analyte respectively, and $\langle \beta_{HRS} \rangle$ denotes the hyperpolarizability of the solvent and analyte after orientational averaging.

$$I_{2\omega} = G(N_S\langle\beta^2_{HRS}\rangle_S + N_x\langle\beta^2_{HRS}\rangle_x)I^2_{2\omega}$$

By measuring $I_{2\omega}$ as a function of solute number density, achieved through taking measurements at a range of concentrations, a linear relationship can be obtained. From this the hyperpolarizability can be extracted. In these measurements, the intensity of the frequency doubled light is expressed as the area under the HRS peak after deconvolution and is plotted against the concentration of the sample, in this case a solution of compound **7**.
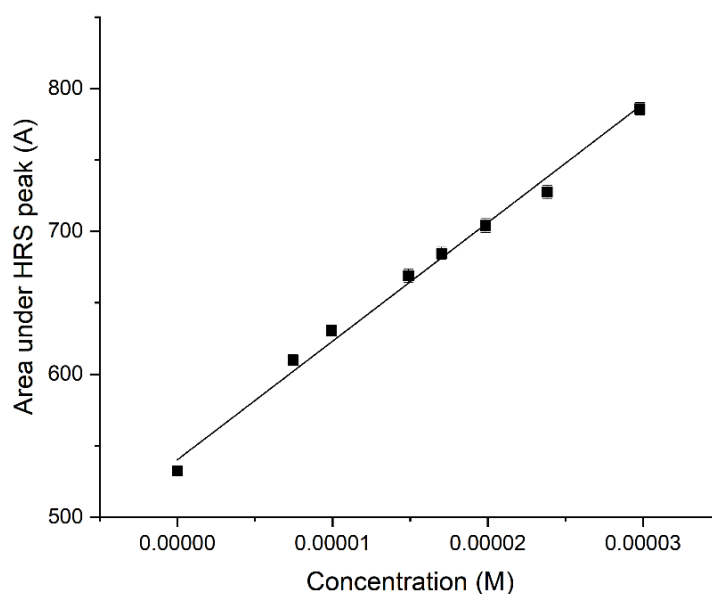
Figure 3.4c The plot of concentration against the area under the HRS peak after deconvolution from the two photon fluorescence peak for compound **7**. The gradient and Y axis intersect at a concentration of 0 are then used to calculate β_{1064} using equation 3.3.

Taking $I_{2\omega} = Ax + B$, where A is the slope and B is the HRS intensity at a concentration of 0 means equation 3.1 can be rewritten to give equation 3.4.2.

$$\frac{Slope}{intercept} = \frac{G\langle\beta_{HRS}^2\rangle_x}{GN_S\langle\beta_{HRS}^2\rangle_S} \tag{3.4.2}$$

Which can then be rearranged to give equation 3.4.3.

$$\langle\beta_{HRS}\rangle_x = \langle\beta_{HRS}\rangle_S \sqrt{\frac{slope}{intercept}N_S} \tag{3.4.3}$$

From equation 3.3, the first dynamic hyperpolarizability, in this case $\beta_{HRS,1064}$ can then be obtained assuming the solvent density and hyperpolarizability are already known. As the mono functionalised sterically protected polyoxometalate chromophores have only one dominant charge transfer axis, here assumed to be along the zzz axis, $\beta_{zzz,1064}$ for these compounds can be obtained by using equation 3.4.4.

$$\beta_{zzz} = \sqrt{\frac{35}{6}\langle\beta_{HRS}^2\rangle} \tag{3.4.4}$$

The static first hyperpolarizability can be calculated from the dynamic hyperpolarizability under non-resonant conditions and the maximum energy of the charge transfer peak responsible using the two-state model, shown in equation 3.4.5. This gives a measure of hyperpolarizability comparable to values obtained at other wavelengths or using other techniques, such as EFISH.

$$\beta_o = \beta\left[1 - \left(\frac{\lambda_{max}}{\lambda}\right)^2\right]\left[1 - \left(\frac{2\lambda_{max}}{\lambda}\right)^2\right] \tag{3.4.5}$$

Hyper-Rayleigh Scattering experiments were performed on compounds **4** through **10**, with both dynamic and static hyperpolarizabilities calculated for each. Measurements of compounds **2** and **3** were not performed due to unprotected analogue synthesised by Al-Yasari et al. having shown no measurable NLO activity. Al-Yasari's work had also shown that the nitro functionalised derivatives were inactive,[128] however, measurements were taken to acquire a baseline to which the switching could be compared. These baseline measurements, unexpectedly, showed that the nitro functionalised compounds were NLO active, with compound **9** in particular showing a much higher activity than expected. This unexpected NLO activity may be due to the electron donating diisopropyl groups on the aromatic ring increasing the electron density of the π system and resulting in lower energy π to POM or π to nitro transitions

than for the unprotected compounds. Analysis of the UV-vis absorption spectra confirmed compounds **9** and **10** both have lower energy IHCT transitions than their unprotected analogues, 399 nm vs 389 nm for the derivatives with diphenylethyne bridges and 382 nm vs 370 for the phenyl bridged derivatives.

Whether these NLO responses are a result of more prominent π to POM or π to nitro transitions cannot be determined from the Hyper-Rayleigh Scattering experiments, however the previously discussed DFT calculations did suggest the LUMO of the transition responsible featured more nitro than POM character, suggesting the overall dipole may be more towards the nitro end of the molecule than the POM. The calculations of β also suggested that the dipole presented in the opposite direction to that seen for the amine donor functionalised compounds, agreeing that the overall change in dipole moment goes towards the nitro group in the nitro functionalised compounds when excited.

	LPCT λ_{max} (nm)	Calc λ_{max} (nm)	$\beta_{zzz,1064}$ ($\times10^{-30}$ esu)	Calc $\beta_{zzz,1064}$ ($\times10^{-30}$ esu)	$\beta_{zzz,0}$ ($\times10^{-30}$ esu)	Calc $\beta_{zzz,0}$ ($\times10^{-30}$ esu)
4	424	414	531	655	162	219
5	423	413	717	653	222	220
6	445	422	1285	747	318	233
7	430	416	338	287	98	95
8	431	415	309	270	89	90
9	399	394	213	57	80	22
10	382	365	89	30	38	14

Table 3.4a Comparison of the experimental and DFT calculated absorption peaks, dynamic, and static polarizability for compounds **4** to **10**. Here, the calculated static polarizability was calculated from the DFT calculated dynamic hyperpolarizability and the calculated λ_{max} using the two-state model due to the inaccuracy of the DFT calculated value.

The Hyper-Rayleigh Scattering experiments of the amine donor functionalised compounds resulted in less unexpected results than those of the nitro compounds, with all five amino functionalised chromophores showing NLO activities similar to or

higher than activities given for the unprotected analogues previously synthesised by Al-Yasari. It was somewhat interesting that the sterically protected derivatives gave in most cases stronger NLO responses than their unprotected analogues, for example, 163 vs 139×10^{-10} esu for the diphenylethyne bridged dimethylamino derivatives, as there had been concerns that the increased electron density of the imido ring, a result of the electron donating alkyl groups, would diminish the strength of the charge transfer between the amine and the POM.

Comparison of the HOMO and LUMO+3 orbitals of compound **4**, the orbitals calculated to be involved in the most intense low energy transition, with those previously calculated for the unprotected analogue[128] showed in increased proportion of electron density on the polyoxometalate core in the LUMO+x of the compound. This increased electron density could be due to the isopropyl groups increasing electron density on the imido ring, decreasing its ability to form part of the electron acceptor resulting in increased electron donation onto the POM core. This would result in a larger change in dipole moment between the ground and excited states, increasing hyperpolarizability. The X-ray crystallography discussed in chapter 2 also showed the increased linearity of imido bond of the isopropyl protected compounds over their unprotected analogues, possibly increasing coupling between the donor and acceptor, another factor that could be contributing to the larger hyperpolarizabilities of the protected compounds.

As predicted by the calculations, compounds **4**, **5**, and **6**, the three chromophores with extended π bridges, gave higher dynamic and static hyperpolarizabilities than compounds **7** and **8**, the two phenyl bridged donor containing derivatives. This trend was also seen by Al-Yasari. Of the three diphenylethyne bridged compounds compound **6** gave the highest hyperpolarizability and compound **4** gave the lowest. Compound **6**, as the strongest donor, was expected to result in the highest NLO activity, and ultimately resulted in the higher activity seen so far for a functionalised hexamolybdate derivative, a group of compounds already having been shown to have higher hyperpolarizability for the size of their π systems than many organic chromophores.

Despite calculations predicting compound **4** would give a hyperpolarizability stronger than compound **5** and compound **4** having the marginally stronger donor, compound **5**

gave a stronger response. A similar result was also seen by Al-Yasari, with his diphenyl derivative giving a considerably higher NLO activity than his dimethyl functionalised chromophore. Overall, the Hyper-Rayleigh Scattering experiments of compounds **4** to **10** gave good results, with the measurements showing good NLO responses of the donor containing compounds with none of the feared loss of activity from the steric groups used to increase stability.

3.5 Redox Activated NLO Switching

The redox activated switching of compounds **2** to **10** was investigated initially using the linear absorption spectrum, as discussed in section **3.2**, with measurements and switching performed in a type of specially adapted Omni cell called an OTTLE cell. Since no commercially available cell could be found suitable for simultaneously performing redox activated switching and Hyper-Rayleigh Scattering experiments under the inert conditions needed to increase the stability of the reduced species, a Pyrex glass fluorescence cell was adapted to suit.

The completed adapted cell featured two chambers separated by a fritted glass disk, one cuvette quality with three perpendicular, unaltered faces suitable for hyper scattering measurements which was used to hold the sample, reference electrode, and working electrode, while the other was made of a Pyrex tube and used for counter oxidation of a solution of electrolyte. The two chambers, open above the solvent level to allow for pressure equalisation, were fitted with suba-seal tops to enable creation of the inert atmosphere through a purge tube.

Previous investigation had shown that three separate compartments was necessary for the full reduction and reoxidation of the sample, so the silver reference electrode in the working compartment was housed inside a small diameter glass tube fitted with a glass frit at the bottom. For quick reduction, space for a magnetic stirrer was also required in the bottom of the sample chamber. The mount inside the HRS set up was suitable for controlling the stirrer. The electrodes used were the same as were used during bulk electrolysis experiments, with platinum gauze used as the working electrode, a coil of platinum wire used as the counter, and a silver wire used as the reference.
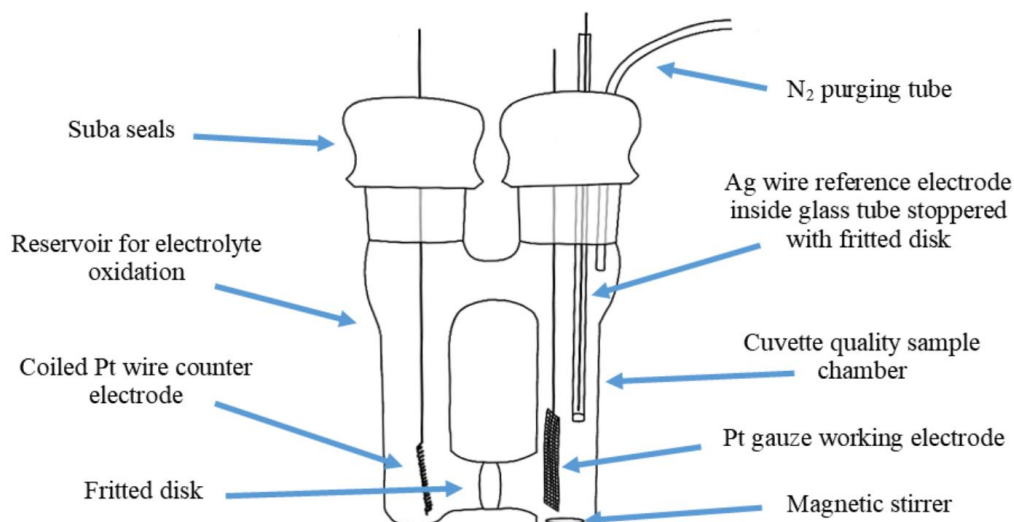
Figure 3.5a A schematic of the cell used during the Hyper-Rayleigh Scattering runs with simultaneous redox switching.

During the Hyper-Rayleigh Scattering runs performed with redox switching, the samples were typically reduced at a potential of -1.3 V for a total of 400 seconds before an oxidising potential of 0 V was applied for a further 400 seconds. HRS was recorded every five seconds, with ten measurements taken before the reduction potential was applied to achieve a baseline value for the compounds in their oxidised states. This would allow for conversion from intensity of the HRS peak to β_{1064}. From here, if a stable value of β_{1064} could be obtained for the compounds in the reduced state, the β_0 could then be calculated for the reduced state compounds using the two-state equation and the λ_{max} obtained in the spectroelectrochemistry.

The samples used in the redox switching experiments were of a concentration of around 0.1 mM in acetonitrile, a concentration higher than used during the measurements to determine the hyperpolarizability but still within the rage suitable for Hyper-Rayleigh scattering experiments. This higher concentration was used to give a more pronounced difference between the sample and the solvent and electrolyte baseline. It was also hoped having the sample at a concentration of the same order as was used in both the bulk electrolysis experiments and the spectroelectrochemistry would result in similarly good stability. Due to its superior stability over the diphenylethyne bridged derivatives, compound **8** was used initially in the investigations into the redox activated NLO switching responses of POM based chromophores before experiments were also carried out on compound **6**.

Before switching, the baseline of compound **8** was reasonably steady, allowing normalisation to the β_{1064} obtained in the earlier HRS experiments. After a series of 10 measurements had been recorded, a potential of -1.3 V was applied to the sample for 400 seconds. During this time, as the compounds reduced the NLO activity recorded decreased steadily until a plateau was eventually observed after around 350 seconds, suggesting full reduction of the compound had been achieved. Here, the apparent β_{1064} was around 20×10^{-30} esu, calculated to be a reduction of 94% compared to the activity of the compound in its oxidised form. Upon conversion to β_0, which gave a NLO activity of 7.6×10^{-30} esu, a reduction of 91% was revealed. After reoxidation, performed at a potential of 0 V, the NLO activity increased again, returning to an intensity near what had originally been measured in a similar timescale to which it took to reduce. The small decrease in intensity after re-oxidation is likely due to a small amount of decomposition having occurred, while an increase in fluorescence which was also observed after switching would result from the 2,6-diisopropyl-4-dimethylamino aniline formed during the decomposition.
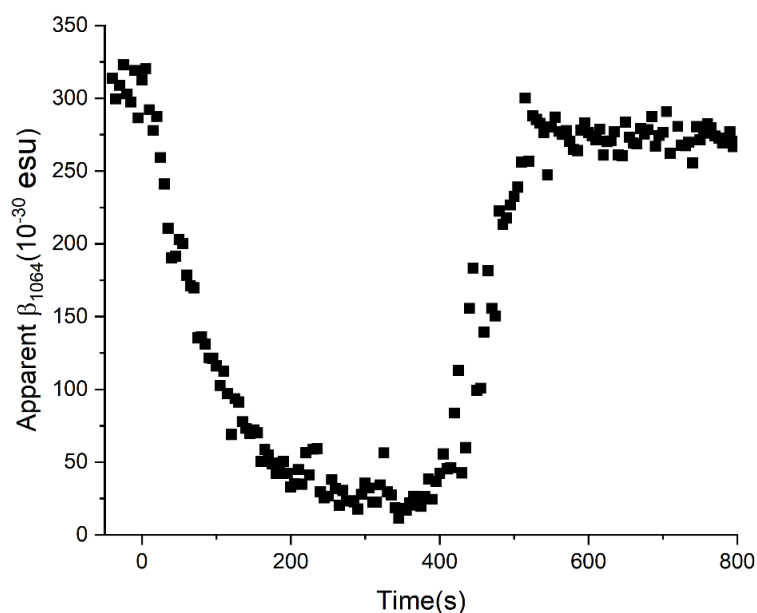
Figure 3.5b Apparent β_{1064} against time for compound **8**, with a weakening in the NLO activity occurring during reduction and an increase being observed upon reoxidation.

Similar switching was observed over three further runs performed on the sample, with a substantial decrease in β_{1064} being observed each time upon reduction followed by

an increase back to near the starting activity upon oxidation. After the initial decrease in oxidised NLO activity, no further decrease was seen, showing the reversibility and repeatability of the redox activated switching. The small increase of the apparent β_{1064} of the reduced compound observed in following runs was accounted for after investigation of the chronoamperometry data showed a decrease in the current passed during later runs, meaning a less thorough reduction of compound **8** had occurred.
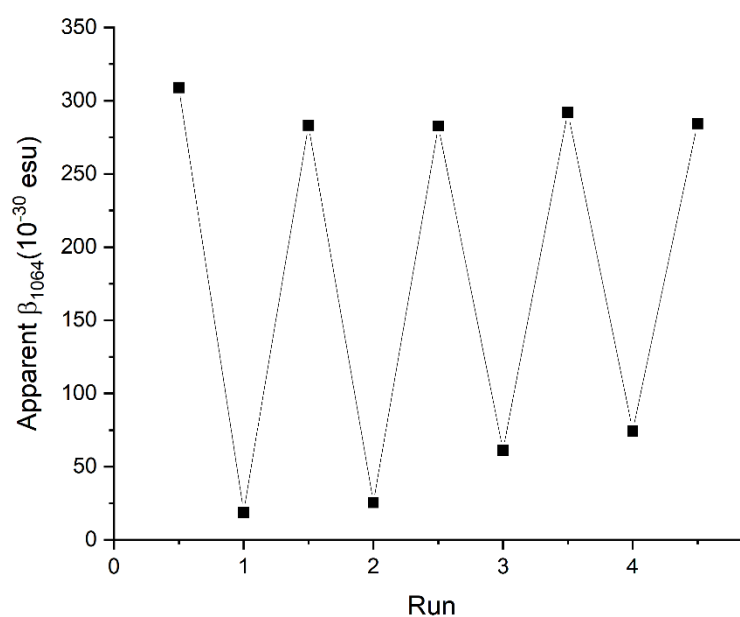
Figure 3.5c Apparent β_{1064} over the course of four runs performed on a sample of compound **8** demonstrating the repeatability of the redox activated NLO switching.

The oxidative switching of compound **8** was also investigated by simultaneous oxidation and HRS measurements. The conditions were as used for the reductive switching experiments, although an initial oxidative potential of 0.8 V was applied, followed by a reductive potential of 0 V. Initially results looked promising, with a considerable weakening of the HRS peak observed as the compound was oxidised before some was recovered upon re-reduction, however working up the data revealed issues with measuring the HRS of the oxidised compound due to reabsorption of the 532nm scattered light, a result of the oxidised compound's absorption peaks at 480 and 640 nm.

The reabsorption of the scattered light at the second harmonic reduced the intensity of the HRS peak to the extent that it fell below that of the reference peak, a key indication something was wrong with the data. Ultimately, what this meant was that any reduction of the peak would not necessarily have been caused by a decrease in the hyperpolarizability of the compound as the extent to which the reduction of the intensity of the scattered light was caused by reabsorption was unknown. More information on the oxidative switching of the compounds could be obtained by measuring the HRS of the oxidised compounds with a higher wavelength incident beam to result in Hyper-Rayleigh Scattering at a wavelength further away from the lower energy oxidised state absorption peaks.

After the successful switching experiments of compound **8**, investigation moved on to compound **6**, the chromophore which had given the best NLO responses during the HRS measurements. The bulk electrolysis experiments of compound **6** had previously demonstrated a decrease in the stability due to the newly observed POM core fragmentation, however, due to aggregation related scattering and three photon fluorescence causing difficulties during the HRS measurements of the more stable compound **5**, compound **6** was deemed the most suitable for the investigation of the switching of the derivatives with extended bridges given the limited timescale.
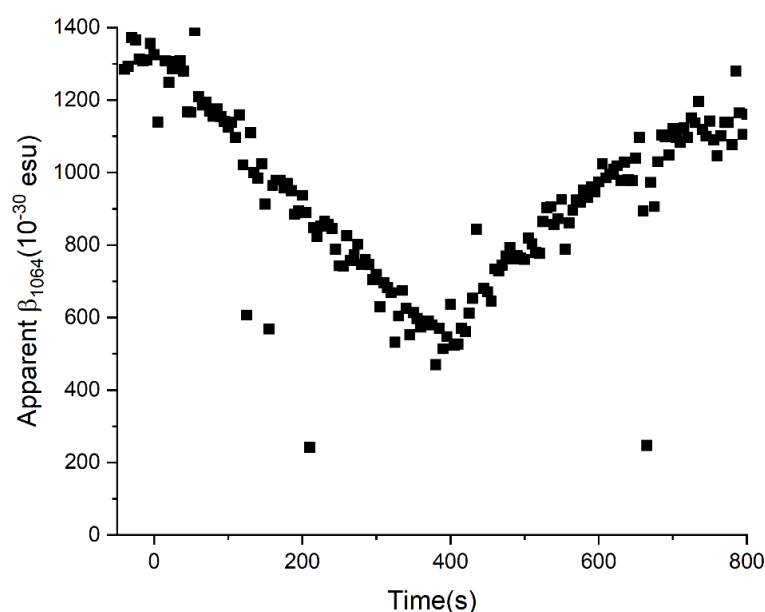
Figure 3.5d Apparent β_{1064} against time for compound **6**, with a weakening in the NLO activity occurring during reduction and an increase being observed upon reoxidation.

The HRS switching runs of compound **6** did proceed to show good redox switchable responses, with hyperpolarizability decreasing 65% during reduction before increasing again when the sample was re-oxidised. Although this weaking in the HRS intensity was not as strong as the 94% observed for compound **8**, it still shows the compound acts as a redox switchable chromophore. Also, the lack of plateauing of the HRS intensity as the 400 s of reduction mark approached suggested that sample was still being reduced when the potential was switched to oxidative, meaning the apparent β_{1064} of the sample could be lower than the 500×10^{-30} esu observed when fully reduced.

It is also possible that some of this continued decrease in intensity could be as a result of decomposition of the still somewhat HRS active reduced species, as, as had been expected from the results of the bulk electrolysis experiments, some decomposition did occur over the course of the experiment. This was still a considerably smaller amount than had been seen during the bulk electrolysis experiments, likely due to the shorter timescale, with approximately 20% of the original intensity of the HRS scattering being lost over the course of the experiment, suggesting a loss of 20% of the sample. Despite the decomposition of the sample, the switching HRS experiment performed on compound **6** still demonstrated the redox activated switching of the diphenylethyne bridged polyoxometalate chromophores for the first time, a property which could be further investigated if a method of increasing the stability of the compounds could be found.

Reductive switching of the two nitro derivatives was also investigated, and although the results of compound **10**, the phenyl bridged derivative, did not demonstrate any clear redox activated switching of the hyperpolarizability, the experiments performed on compound **9** did. Compound **9** in its oxidised state had a β_{1064} of 214×10^{-30} esu, and this, upon reduction, increased to around 3325×10^{-30} esu before decreasing again with re-oxidation, demonstrating clear redox activated off/on NLO switching responses for the first time. Using the two state model and the λ_{max} of the reduced state, the dynamic first hyperpolarizability can be converted to the static first hyperpolarizability to give a β_0 of 1125×10^{-30} esu. This is a 14 fold increase, a similar magnitude of change to what was observed for compound **8**, and results in an activity higher than seen for any of the donor containing compounds, possibly a result of the reduced POM core acting as a strong electron donor.
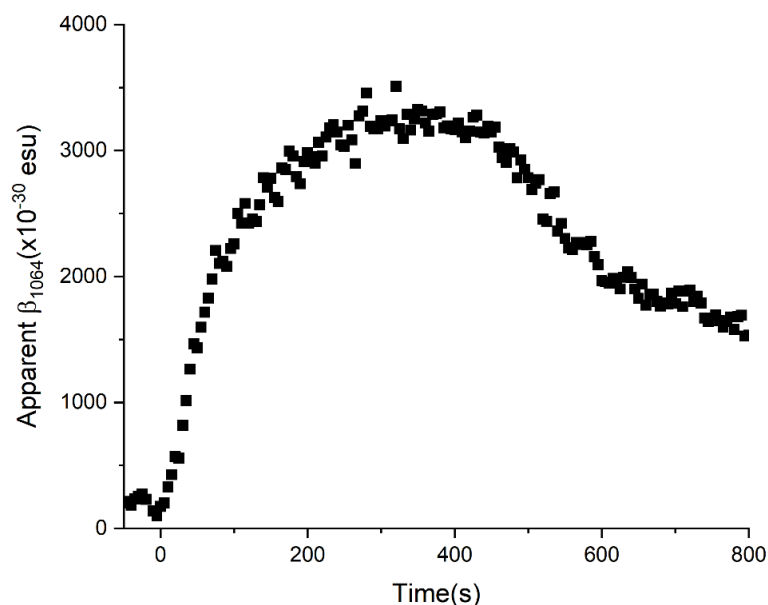
Figure 3.5e Apparent β_{1064} against time for compound **9**, with a weakening in the NLO activity occurring during reduction and an increase being observed upon reoxidation.

Investigation into the chronoamperometry data showed a significant decrease in the current passed during the re-oxidation runs, suggesting considerable reduced POM was still in the sample at the end of the run. This is likely to account for increased hyperpolarizability at the end of the run compared to the beginning. It is also possible some of this is due to decomposition of the compound into hexamolybdate and the nitro containing aniline, a compound that would also be NLO active. Despite this and the incomplete re-oxidation resulting of the sample, this HRS switching experiments did still demonstrate off/on switching of compound **9** to reveal a high reduced state hyperpolarizability, confirming the theory that these nitro functionalised hexamolybdate derivatives may act as NLO active chromophores in their reduced states.

3.6 Conclusion

In this chapter, the results of the UV-vis spectroelectrochemistry, DFT calculations, and Hyper-Rayleigh Scattering experiments performed on compounds **2** to **10** were discussed. Spectrochemical analysis revealed switchable redox activated responses of

all compounds, with compounds **2** and **3** showing small shifts of their IHCT peak to higher energies upon reduction, compounds **4** to **8** showing larger shifts also to higher energies, and reduction of compounds **9** and **10** resulting in shifts of the IHCT peak to lower energies. TD-DFT Gaussian calculations performed on compounds **3** through **10** were vital in helping to understand the origins of these switchable responses, particularly with regards to the nitro containing compounds.

Hyper-Rayleigh Scattering experiments were used to measure the dynamic and static hyperpolarizabilities of compounds **4** to **10**, revealing good NLO activity of the expected order for compounds **4** to **8**, with compounds **6** giving the highest static hyperpolarizability of any hexamolybdate derivative measured to date. Measurement of compounds **9** and **10** revealed small NLO responses despite previously synthesised non-protected analogues demonstrating no NLO activity at all, a result of the increased electron density in the aromatic π system due to the electron donating alky groups included for steric protection of the imido bond.

Redox activated switching of the NLO activity of compounds **6**, **8**, **9**, and **10** was then performed, with measurements recorded in a specially produced cell. These measurements revealed switchable responses for three of the four compounds, with a reversible and quasi-reversible decrease in β_{1064} recorded for compounds **6** and **8** respectively upon reduction, and a quasi-reversible increase in β_{1064} recorded for compound **9**. Compound **8** in particular showed good responses to switching, with a 94% reduction in hyperpolarizability recorded upon reduction. The compound was stable enough in its reduced state to allow for reversible and repeatable switching.

Overall, this work has demonstrated the high NLO activity of sterically stabilised hexamolybdate derivatives functionalised with strong donors such as julolidine as well as the redox activated reversibly switchable responses of these compounds, with both on/off and off/on type switching seen from the sterically protected, non-linear optically active Lindqvist polyoxometalate chromophores.

Chapter 4

Synthesis and Properties of Multidimensional

Polyoxometalate Chromophores

4.1 Introduction

Since the first discovery of linear molecular organometallic chromophores by Green et al.,[76] the advantages of multi-dimensional chromophores, such as increased stability and an improved efficiency/transparency trade off, have become apparent. In multi-dimensional chromophores, the inclusion of an additional donor or acceptor group allows for separation of the change in dipole moment of the transitions responsible for NLO activity from the overall molecular dipole, resulting in significant off-diagonal β components to the hyperpolarizability. Due to the polarization of the photons produced, these off diagonal β components cannot be reabsorbed, increasing the overall efficiency of the chromophore as well as improving stability by limiting thermal decomposition.
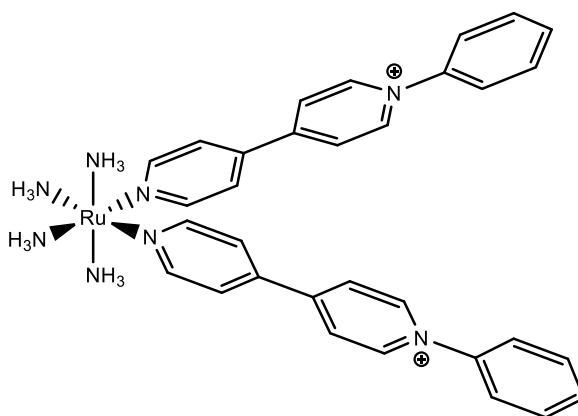
Figure 4.1a Two dimensional one-donor-two-acceptor complex synthesised by Coe et all, a chromophore which demonstrated increased β compared to its mono-substituted analogue.

Over the years, both one-donor-two-acceptor and two-acceptor-one-donor chromophores have been reported, with examples including the ruthenium(II) based one-donor-two-acceptor systems developed by Coe et al.,[99] and a two-donor-one-acceptor ferrocene donor based chromophore synthesised by Prabu et al.[100] These systems, amongst others, showed significant off-diagonal components to their hyperpolarizabilities, demonstrating the advantages of the two dimensional systems over their dipolar counterparts. Despite this and the high NLO activities seen of the dipolar compounds synthesised by Al-Yasari, no work into multidimensional POM NLO chromophores has so far been reported, however, calculations have predicted

good off-diagonal hyperpolarizabilities.[132]

In this work, two series of multidimensional hexamolybdate derivatives were synthesised with the aim of finding polyoxometalate chromophores with significant off-diagonal β components, potentially leading to compounds with higher NLO activities than had been seen for previously synthesised polyoxometalate chromophores. This chapter discusses the synthesis and properties of the two series of compounds as explored by ^{1}H-NMR, UV-vis spectroscopy, electrochemistry, and Hyper-Rayleigh Scattering.
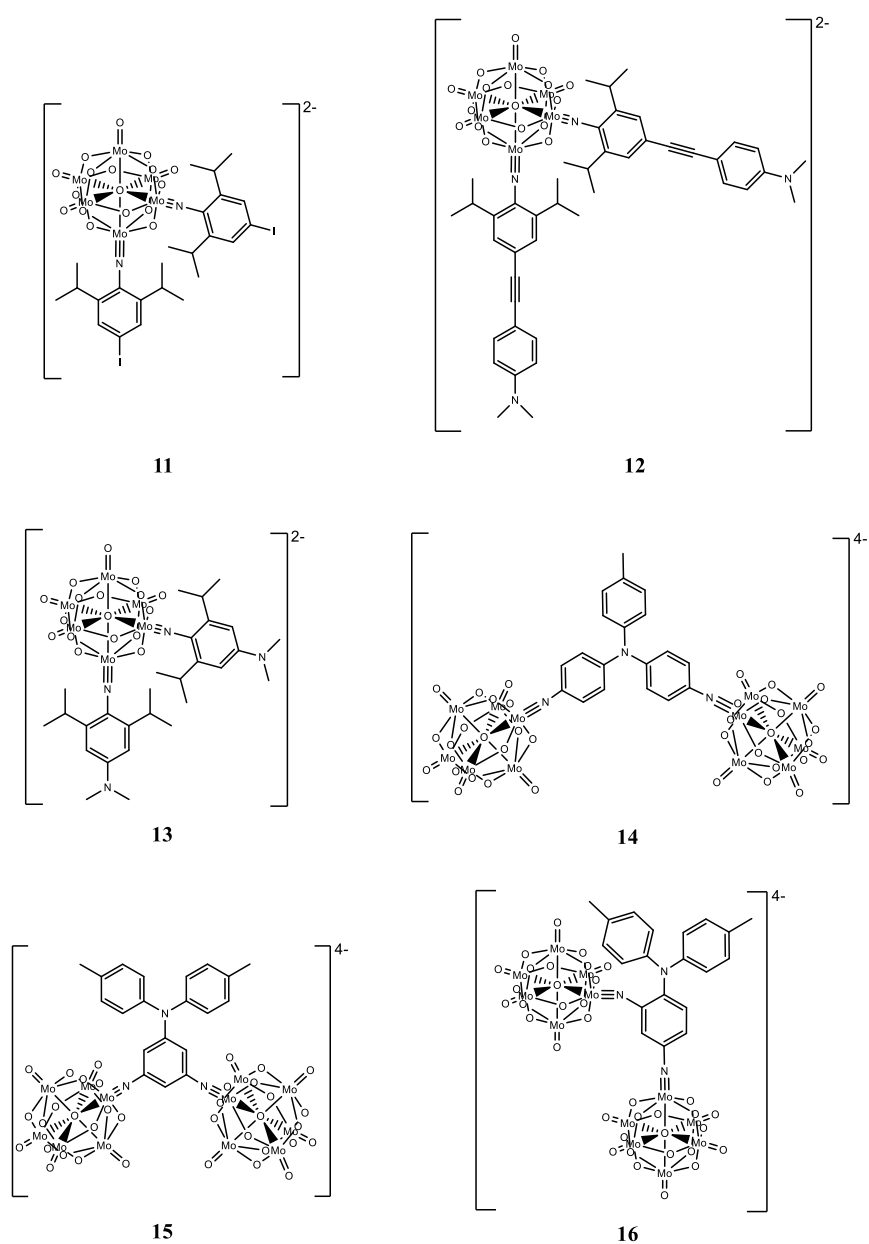
Figure 4.1b The two dimensional two-donor-one-acceptor polyoxometalate chromophores and one-donor-two-acceptor polyoxometalate chromophores synthesised in this chapter.

4.2 Synthesis of D-A-D Systems

Two sets of multidimensional POM chromophores were synthesised in this work, the two-donor-one-acceptor compounds, compounds **11** to **13**, and the one-donor-two-acceptor compounds, compounds **14** to **16**. The two-donor-one-acceptor chromophores were synthesised in much the same way as the monofunctionalised analogues, with compounds being synthesised using the same ligands as were used for compounds **3**, **4**, and **8**, while new ligands needed to be synthesised for the synthesis the one-donor-two-acceptor derivatives.

The first report of a *bis*-functionalised Lindqvist polyoxometalate was in 2000 by Strong et al.,[24] who synthesised a series of 2 to 5 multi-substituted Lindqvist derivatives from tetrabutylammonium hexamolybdate and 2,6-diisopropylphenyl isocyanate in pyridine. The DCC facilitated coupling reported by Wei et al.[33] improved the ease of synthesis, allowing for the synthesis of more multi-functionalised derivatives by increasing the number of equivalents of aniline and DCC to POM to encourage higher functionalisation. However, due to the hexamolybdate core's six equally reactive terminal oxygens, these reactions often produced a variety of multi-functionalised derivatives rather than just the intended species.[127] Examples of this were seen in chapter 2 of this work, where in some cases *bis*-functionalised hexamolybdate was seen in the crude product along with the desired monofunctionalised POM.

In 2002, Xu et al.[127] first reported the synthesis of a *bis*-functionalised derivative using octamolybdate as opposed to hexamolybdate as the molybdenum POM species. In the reaction the octamolybdate converted to hexamolybdate and functionalised to produce the desired *bis*-functionalised product in good yield and without contamination by other functionalised derivatives. Yield of the intended *bis*-functionalised derivative was further improved by the use of the hydrochloride salt in place of half of the aniline as this helped to convert the octamolybdate into hexamolybdate.

In this work, the octamolybdate based method was initially used for the synthesis of the *bis*-2,6-dimethyl-4-iodo derivative and although after multiple recrystallisations this did result in clean compound **11**, further work showed the time consumed in producing the hydrochloride salt and the limited improvement in yield and purity made the octamolybdate method unfavourable over the hexamolybdate method. Later

batches of compound **11** were made using hexamolybdate and the same DCC mediated coupling method as compound **3**, its monofunctionalised analogue, with the expected adjustments made to the molar ratios of DCC and 2,6-diisopropyly aniline along with increases to both the reaction temperature and time.
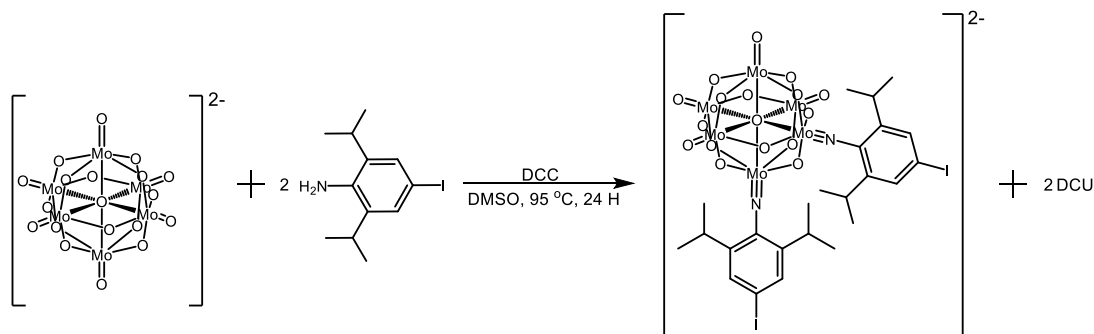
Figure 4.2a Method for the synthesis of compound **11** using tetrabutylammonium hexamolybdate as a starting material.

Reaction of hexamolybdate with 2.5 equivalents of DCC and 2 equivalents of 2,6-diisopropylaniline at 95°C for 24 hours resulted in a product consisting of 58% *bis*-functionalised derivative according to the NMR spectrum. A small amount of this, 12%, was thought to be due to the *trans* isomer rather than the *cis* due to a second, smaller peak appearing very slightly upfield of the aromatic peak of the expected *cis*-isomer. The rest of the sample was unfunctionalised hexamolybdate which, along with the *trans*-isomer, was removed through repeated recrystallisations to give compound **11** pure by ^{1}H-NMR, mass spectrometry, and elemental analysis in a 6% yield. This yield is considerably lower than had been reported in the literature, however the mass produced was still sufficient for this work.

^{1}H-NMR analysis of the pure compound showed one aromatic peak for the *bis*-substituted compound, just as had been seen for the monosubstituted, with the two peaks caused by the protons on the isopropyl groups also suggesting that both ligands were equivalent on the NMR timescale. Like its monosubstituted analogue, the ^{1}H-NMR of compound **11** showed a downfield shift of the aromatic protons compared to those of the aniline due to the proximity to the electron withdrawing POM core. This effect was mitigated compared to that seen for the monosubstituted compound, with a shift from 7.23 ppm to 7.51 ppm and 7.47 ppm for the *mono-* and *bis*-substituted

compounds respectively, a result of the multiple ligands weakening the effect felt by each individually.

	H-Ar	**H**(CH$_3$)$_2$	H(**CH**$_3$)$_2$
P2	7.23	2.58	1.18
3	7.51	3.78	1.28
11	7.47	3.82	1.26

Table 4.2a Comparison of ^{1}H-NMR shifts for compounds **P2**, **3**, and **11** shows weakened deshielding for the *bis*-substituted compound compared to the mono. All ^{1}H-NMR were taken in acetonitrile-d3 and referenced to TMS.

Compound **11** was also investigated by UV-vis absorption spectroscopy, with analysis showing very little change in the energy of the peaks when compared to compound **3**. There was, however, a considerable difference in the extinction coefficient of the peaks, with all peaks of compound **11** appearing with nearly double the intensity than those of compound **3**. For the LPCT peak, this is likely a result of having two rather than one ligand donating into the POM, while for the higher energy peaks, it is more likely simply a result of twice as many ligands with π to π* transitions.
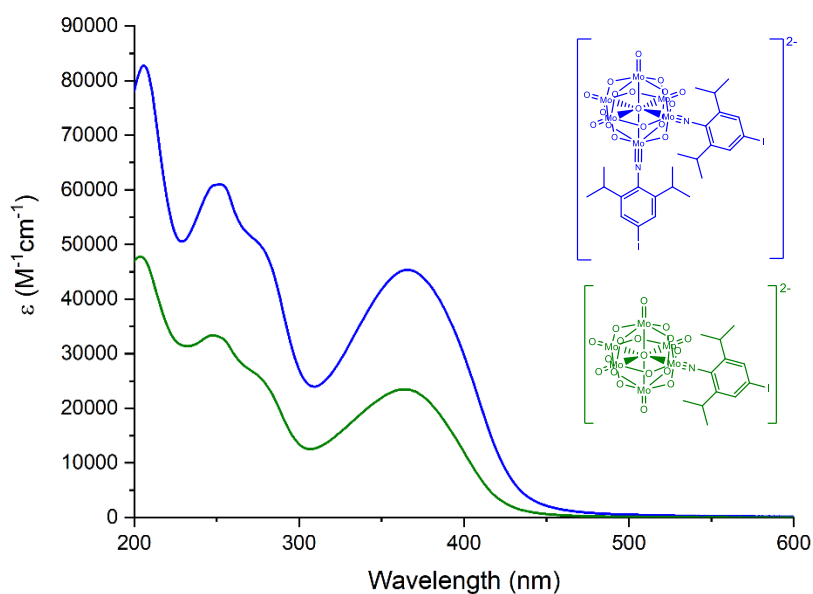
Figure 4.2b UV-vis absorption spectra of compounds **11** (blue) and **3** (green). Both spectra were taken in acetonitrile.

X-ray quality crystals of compound **11** were grown from hot acetonitrile, with the X-ray diffraction data of these confirming the cis-substitution of compound **11**. The unit cell and dimensions of the structure obtained matched data previously reported for the compound,[127] however ultimately it turned out the quality of the data was not sufficient for complete refinement. As the structure had already been reported, no further attempts at growing X-ray quality crystals were made. The imido bonds on the reported structure were slightly longer and less linear than seen on the monofunctionalised derivative, suggesting slightly weaker imido bonds in the *bis*-functionalised derivative than the mono. This was consistent with the weakened deshielding of the protons on the imido ring seen on the ^{1}H-NMR of compound **11** compared to compound **3**.
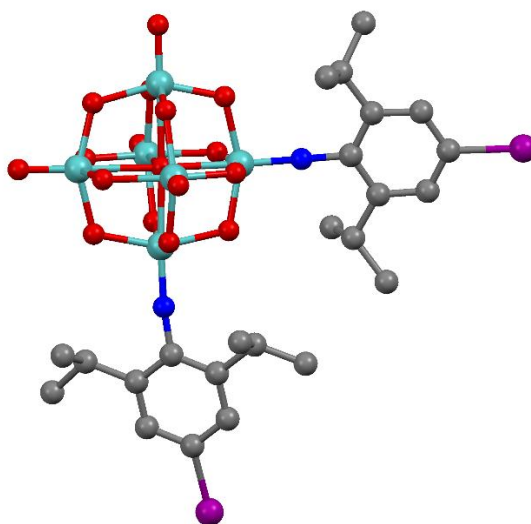
Figure 4.2c Crystal structure images of compound **11**. Atoms are shown as spheres 0.2 times their van der Waals radius. The colour scheme shows Mo in green, O in red, N in blue, C in grey, and I in purple. Tetrabutylammonium counter cations and hydrogen atoms are omitted for clarity.

The synthesis of compound **12**, the *bis*-substituted, diphenylethyne-bridged dimethylamino hexamolybdate derivative, was carried out using compound **11** and 1-ethynyl-N,N-dimethylbenzenamine in the same Sonogashira procedure as was used to synthesise compound **4** from compound **3** in chapter 2. Again, bis(triphenylphosphine) palladium(II) dichloride was used as a catalyst with copper iodide and triethylamine used as co-catalysts. Compound **12** was collected from the reaction in a 67% yield and

^{1}H-NMR analysis showed the reaction had gone to completion, with no signs of compound **11** present. Further purification was attempted through recrystallisation, however this was not successful. Elemental analysis of the crude product showed some inorganic impurity remained in the sample, but due to the small amount of product synthesised and the difficulties found when trying to achieve purity by recrystallisation, it was decided that no further attempts at purification would be attempted to ensure some sample remained for analysis. Mass spectrometry confirmed the identity of the compound, along with ^{1}H-NMR and ^{13}C-NMR.
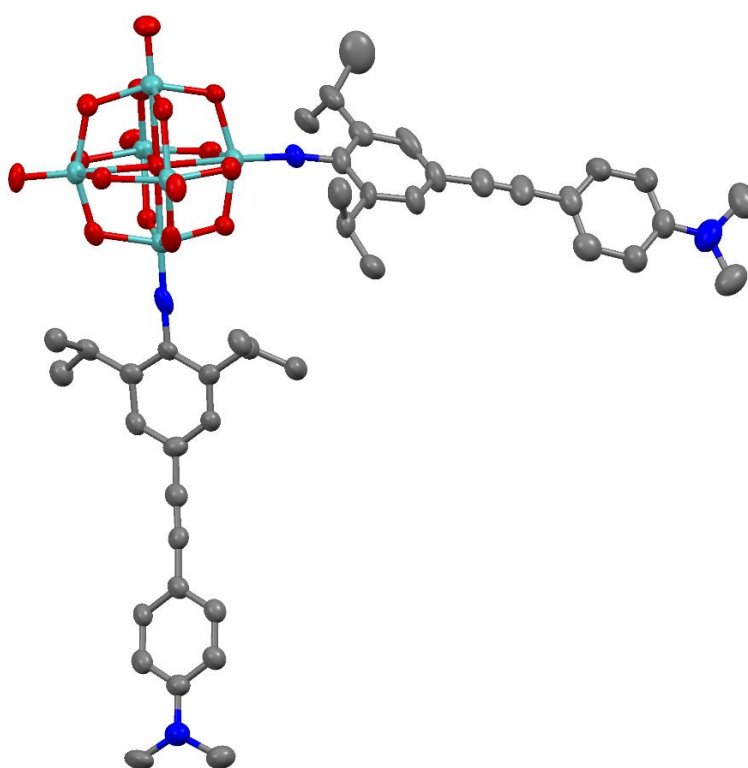
Figure 4.2d Crystal structure images of compound **12**. Thermal ellipsoids are at 30% probability level. The colour scheme shows Mo in green, O in red, N in blue, and C in grey. Tetrabutylammonium counter cations and hydrogen atoms are omitted for clarity.

X-ray quality crystals of compound **12** yielded a structure in the I-4 space group with an R_1 of 6.80%, however, due to the compounds not being identified as non-centrosymmetric prior to running, completeness for the data set was only 93%. Further attempts at growing suitable crystals were made, but these were not successful due to

the previously mentioned difficulties with crystallising compound **12**. Comparison of the Mo-N and N-C bond lengths and Mo-N-C bond angles with those of compound **4**, the monofunctionalised analogue, showed little difference, with significant variation only in the case of the Mo-N bond. The lengthening of this in the *bis*-functionalised derivative was similar to the previously observed difference between compounds **3** and **11**, again suggesting slight weakening of the imido bond in the *bis*-functionalised derivatives.

As was seen in the comparison of the ^{1}H-NMR of compounds **3** and **11**, an upfield shift of the *meta* protons on the imido ring of the *bis*-substituted compounds was observed compared to the mono. This shift was smaller than seen previously, at only 0.02 ppm compared to the 0.04 ppm seen for the iodo functionalised compounds, likely due to the already increased shielding of the donor groups negating the weakened deshielding from the POM core. No change was seen in the shift of the protons on the extended portion of the ligand.
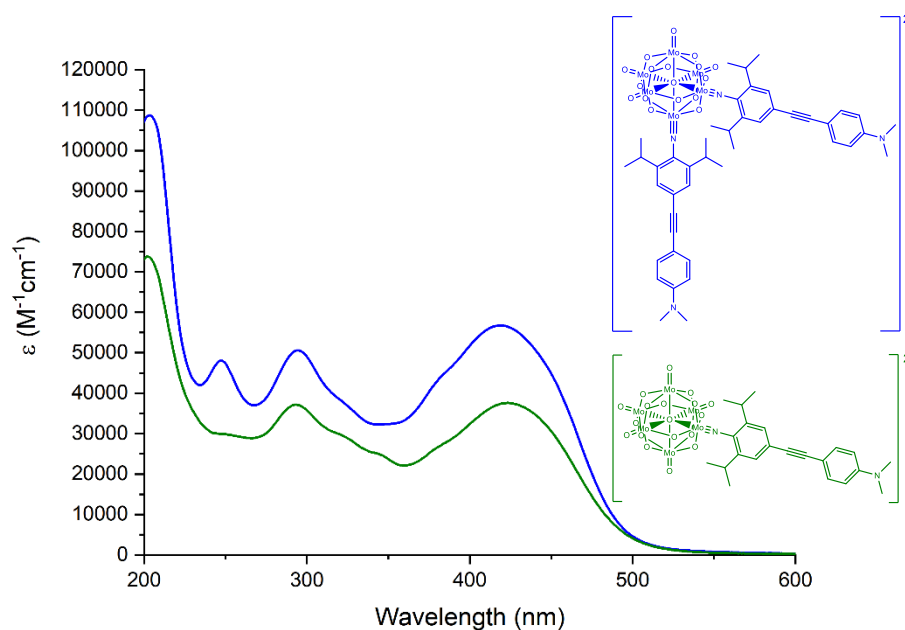
Figure 4.2e UV-vis of compound **12** (blue) and compound **4** (green), the monosubstituted analogue. Both spectra were taken in acetonitrile.

The UV-vis spectroscopy of compound **12** again showed the expected features of a donor functionalised hexamolybdate derivative, with the LPCT peak red-shifted

compared to that of the precursors. Like with compound **11**, the spectrum was very similar to that of the mono substituted analogue, with the LPCT peak at a similar wavelength of 419 nm compared to the 424 nm of compound **4**, however again there was significant increase in the intensity of the peaks, a result of the increased number of ligands and electron donors.

Compound **13**, the phenyl bridged *bis*-functionalised dimethylamino derivative, was synthesised from tetrabutylammonium hexamolybdate and 2,6-diisopropyl-4-dimethylamino aniline using the previously discussed DCC mediated coupling reaction. This was performed at 95°C for 24 hours, with 1.5 equivalents of aniline and 2.5 equivalents of DCC. A stoichiometric excess of hexamolybdate was used to decrease the amount of higher functionalised derivatives produced as hexamolybdate derivatives with both three and four ligands had been observed in earlier attempts.

The desired product, compound **13**, was the major product from the reaction, about 48% of the sample, although significant amounts of hexamolybdate, 12%, and the monofunctionalised derivative, 30%, were also present. Smaller amounts of the *tris* and *tetrakis* derivatives, 5% each, could also be seen in the ¹H⁻NMR. Although yield of the reaction was decent, with 83% of the POM mass recovered and nearly half of this being the desired product, purification of the sample proved difficult. Separation of the *mono-* and *bis*-functionalised derivatives could not be performed successfully through recrystallisation, with the ¹H-NMR spectra taken of the crystals always showing both the *mono-* and *bis*-derivatives were present. Originally, this was thought to be due to decomposition of the sample, however, X-ray crystallography repeatedly showed co-crystallisation had occurred, resulting in crystals made of what appeared to be a 1:1 ratio of the *mono-* and *bis*-substituted derivatives.

Slight differences in solubility allowed for some separation to be performed by precipitation from hot acetonitrile in the refrigerator. This resulted in the removal of most of the hexamolybdate and monofunctionalised derivative as shown by ¹H-NMR but left noticeable amounts of the *tris*-substituted derivative in the sample. Elemental analysis suggested approximately 10% of the sample was the *tris*-functionalised derivative, but due to issues with the stability and the *mono/bis* co-crystallisation mentioned previously, a sample with increased purity could not be produced.

^{1}H-NMR spectroscopy of impure compound **13** revealed the shift between the peaks of the *meta* protons on the imido rings of the four observed derivatives was small, with only 1 ppm between the peak of the most downfield *tetrakis* derivative and the most upfield mono-substituted derivative. The order of the peaks is reversed to what was seen for both the iodo *bis*-substituted derivative and the diphenylethyne-bridged dimethylamino derivative, with the more substituted derivatives showing less shielding of the *meta* protons on their imido rings. This is likely a result of these *meta* substituted protons being *ortho* to the electron donor, meaning that although increased substitution of the POM core decreases the electron withdrawing effect felt by each individual phenylimido group, this is more than compensated for by the corresponding decrease in donation from the more localised -NMe$_2$.

After re-precipitation, ^{1}H-NMR analysis of some samples showed two sets of defined ligand peaks resulting from what had been previously equivalent protons. This suggested two isomers were present. Although rearrangement of ligands has been seen on functionalised hexamolybdate derivatives, this has previously only been observed when DCC was present, suggesting the two different isomers were likely formed by rotation around the imido bond enabled by the heating during the recrystallisation process. At room temperature this rotation would be hindered by the isopropyl groups.
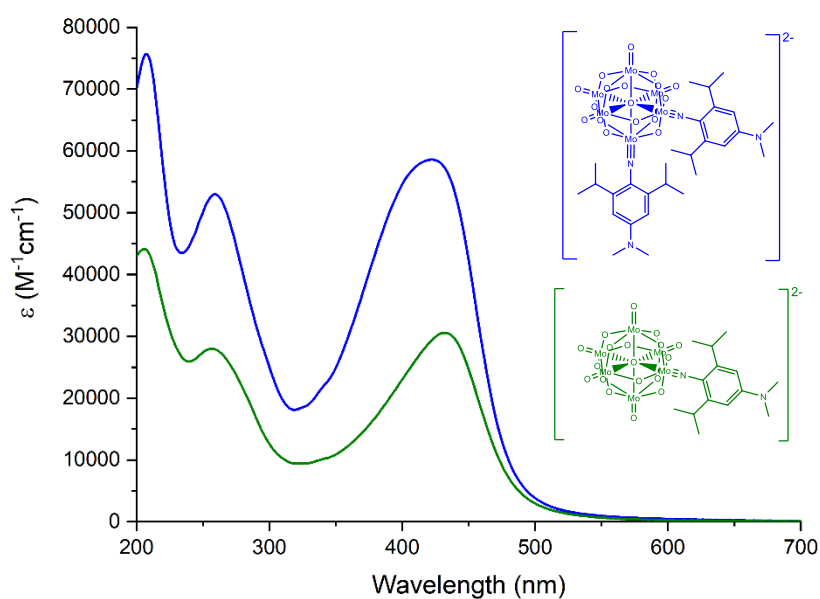
Figure 4.2f UV-vis of compound **13** (blue) and compound **8** (green), the monosubstituted analogue. Both spectra were taken in acetonitrile.

Analysis of compound **13** by UV-vis spectroscopy revealed a similar change compared to the mono-functionalised derivative as was seen for compounds **11** and **12**, with peaks appearing at similar wavelengths but with much higher intensities due to transitions involving the second ligand. The LPCT peak of compound **13** also appears to be made of two peaks instead of one, with a higher energy shoulder to the peak observed of the monofunctionalised derivative. This is likely a result of charge transfer involving the second ligand occurring at a slightly higher energy than the charge transfer from the first due to the already increased electron density of the POM.

Crystals of compound **13** were grown for X-ray crystallography, however, as mentioned earlier, these consistently consisted of co-crystallised *mono-* and *bis-*functionalised derivatives. Although only one anion could be found in the structure, the peaks caused by the second of the two ligands were much less intense, with the occupancy preferentially at 0.5. After splitting, one part of one of the two tetrabutyl ammonium cations was also much too close to the dimethylamino group on the ligand to allow for the ligand to be there in both parts. Attempts were made at solving the structure in a lower symmetry space group, and although this did result in two separate *mono-* and *bis-*substituted anions, doing so also significantly reduced the completeness of the data set and did not resolve the problem of the close proximity of the second ligand and the tetrabutylammonium cation. Although the structure was not sufficient for proper reporting or bond length analysis due to poor refinement of one ligand and overlap with the mono of the other, it was still useful in solving the mystery of why the crystallisations were not resulting in pure product, and also confirmed that the compound had been formed in the expected *cis* rather than the unexpected *trans* isomer.

4.3 Synthesis of A-D-A Systems.

Along with the three two-donor-one-acceptor chromophores, a series of one-donor-two-acceptor chromophores were also synthesised. Originally, a series of four of these had been planned, the two symmetrical compounds, compounds **14** and **15**, and then a compound synthesised from 3-bromo-5-amino aniline to which a diphenylethyne bridged electron donor could be added using a Sonogashira reaction after coupling to hexamolybdate. Although the bromo-functionalised compounds could be synthesised,

further reaction with the alkyne functionalised electron donor units proved unsuccessful. The reason for the will be discussed in more detail later in the chapter.

Of the two remaining one-donor-two-acceptor compounds, the first, compound **14**, was synthesised from a ligand previously reported by Hsiao,[166] with the nucleophilic aromatic fluoro-displacement of *p*-fluoronitrobenzene with *p*-toluidine being performed as reported. The reduction of the nitro groups to form the completed ligand, compound **P17**, was performed using tin chloride dihydrate in dry ethanol rather than the Pd/C and hydrazine hydrate used by Hsiao due to availability at the time.
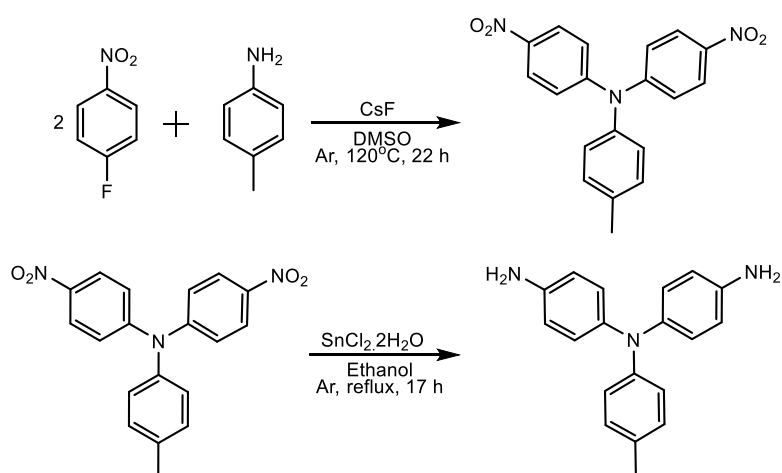
Figure 4.3a Method for the synthesis of compound **P16** and compound **P17**, the precursor for the synthesis of compound **14**.

Tetrabutylammonium hexamolybdate was coupled to the ligand using the standard DCC mediated coupling reaction, with 0.38 molar equivalents of **P17** and 1.1 equivalents of DCC heated with tetrabutylammonium hexamolybdate at 70°C for 10 hours. After filtering once cool to remove the DCU followed by precipitation in a mixture of ethanol and diethyl ether, the product was collected by filtration in an 83% crude yield. ^{1}H-NMR analysis suggested only the desired product had formed, with the compound being 70% pure and the only impurity being tetrabutylammonium hexamolybdate. Purification proved difficult due to the similarity in solubility of compound **14** to tetrabutylammonium hexamolybdate and the four oily tetrabutylammonium cations impeding purification by recrystallisation, however, pure

compound **14** was eventually achieved by washing with DCM before reprecipitating a concentrated acetone solution using diethyl ether. The identity and purity of the compound was proven by ^{1}H-NMR, ^{13}C-NMR, mass spectrometry, and elemental analysis. Attempts were also made to grow crystals suitable for X-ray crystallography, however, this was never achieved.

Analysis of compound **14** by UV-vis spectroscopy showed a LPCT peak at 473 nm, a considerably lower energy than seen for any hexamolybdate derivative so far. This lower energy transition is possibly a result of the second acceptor that lowering the energy of the excited state, although this would usually be accompanied by a similar lowering of the energy of the ground state too due to a weakening of the electron donor. Previous ruthenium based chromophore systems synthesised by Coe et al. have demonstrated this, where the MLCT peak of a one-donor-two-acceptor system occurred at a higher energy than the transition of the monosubstituted analogue.[99]
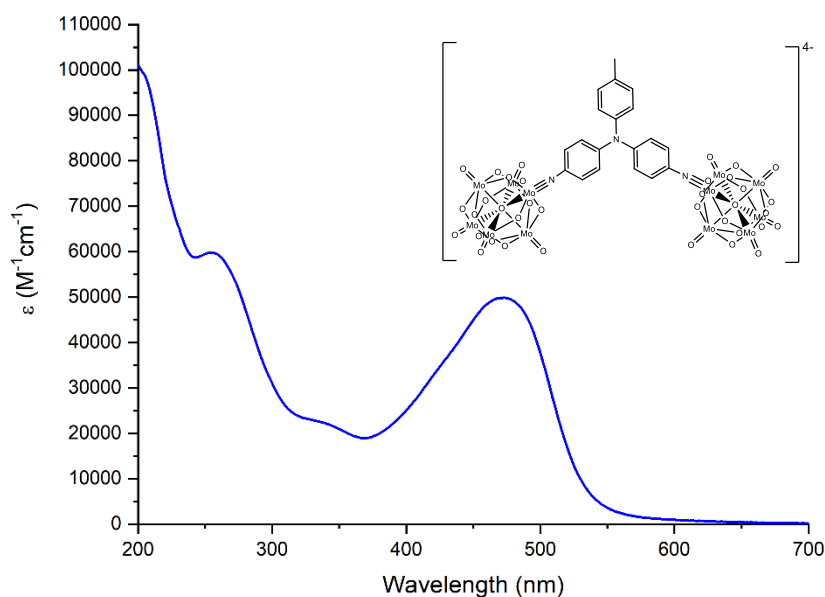
Figure 4.3b UV-vis spectrum of compound **14**, taken in acetonitrile.

Work by Thamaraiselvi involving similarly shaped *mono-* and *di-*cyanotriarylamines suggested that the red shift of the charge transfer peak observed upon addition of a second acceptor related to the influence of a spectating acceptor group on the donor/acceptor pair formed of the amine and the other electron acceptor.[167] It is

possible the redshift seen of compound **14** compared to typical dipolar POM chromophores occurs due to a similar process, where the influence of one POM lowers the energy of the LPCT to the other, although the red shift of compound **14** is much larger than was observed of the organic chromophores. It is also possible that the red-shifted peak comes from lower energy transitions that were symmetry forbidden in the dipolar compounds, however similar red-shifts do not occur for compounds **11** to **13** despite the similar changes in symmetry.

The synthesis of the second one-donor-two-acceptor hexamolybdate derivative, compound **15**, was also synthesised from an aniline ligand using the DCC mediated coupling reaction, with the ligand synthesised using a Buchwald reaction followed by a reduction using hydrazine hydrate and Pd/C. The Buchwald reaction to form compound **P18** was performed using 1-bromo-3,5-nitro benzene and di-*p*-tolyamine with bis(acetonitrile)dichloropalladium and x-phos forming the catalyst and potassium carbonate as the base. The reaction proceeded well to give the product in a 56% yield, however, the reduction proved less facile, with both tin chloride and activated zinc being used in attempts to form precursor **P19** before success was finally achieved using hydrazine hydrate and Pd/C.
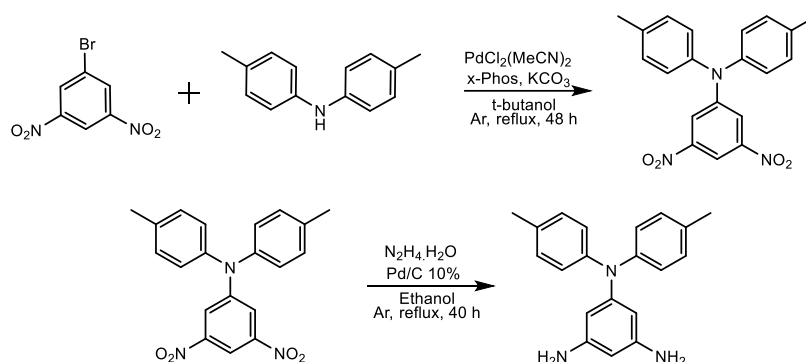
Figure 4.3c Method for the synthesis of compound **P18** and compound **P19**, the precursor for the synthesis of compound **15**.

Compound **15** was synthesised from compound **P19** and tetrabutylammonium hexamolybdate using the DCC mediated coupling reaction, with 0.47 molar equivalents of the aniline and 1.16 molar equivalents of DCC. The reaction was performed in DMSO heated to 70°C for ten hours. After filtration and precipitation

from ethanol and diethyl ether, compound **15** was collected in a 69% crude yield. Analysis by ^{1}H-NMR showed 46% of the crude sample was the desired product, with 48% of the sample being tetrabutylammonium hexamolybdate and 6% being the monofunctionalised ligand. The compound was purified by recrystallisation from a dilute acetone/diethyl ether mix.

The crystals grown were used for X-ray crystallography and yielded a structure with an R_1 of 9.87% in the P2$_1$/c space group**.** Two molecules of compound **15** were present in the asymmetric unit. The structure showed imido bonds with an average Mo-N-C angle of 168.8° and average Mo-N and N-C distances of 1.729 and 1.373 Å respectively. These are slightly shorter and more linear than seen for a previously synthesised compound featuring two *para* substituted POM cores on one aromatic ring,[129] possibly a result of steric repulsion of the *meta* substituted POM cores and the added bulky donor group limiting bending of the bonds. A similar effect was seen in chapter 2, where the imido bonds of the sterically protected derivatives were typically found to be shorter and straighter than those of previously synthesised unprotected analogues.
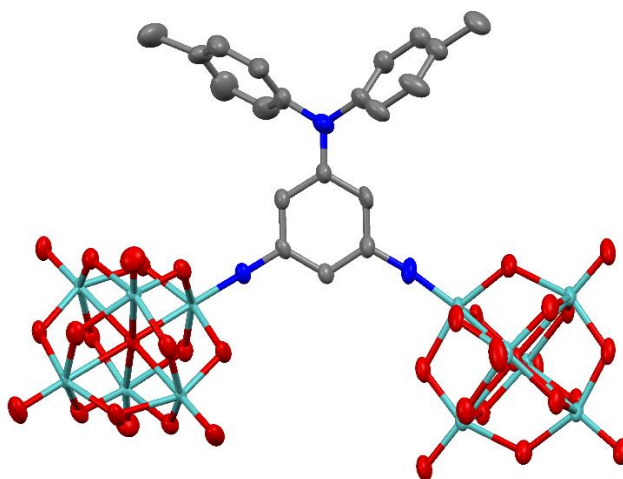
Figure 4.3d Crystal structure images of compound **15**. Thermal ellipsoids are at 30% probability level. The colour scheme shows Mo in green, O in red, N in blue, C in grey, and I in purple. Tetrabutylammonium counter cations and hydrogen atoms are omitted for clarity.

Compound **15** was also investigated by UV-vis spectroscopy, where significant

differences to the spectra of previously synthesised donor containing compounds was noticed. The LPCT peak was observed at 469 nm, a similar wavelength to that of compound **14**, however the extinction coefficient was far smaller, at 1.6×10^3 M^{-1}cm^{-1} compared to 49.4×10^3 M^{-1}cm^{-1}, showing incredibly weak charge transfer transitions between the electron donor and the POM cores.
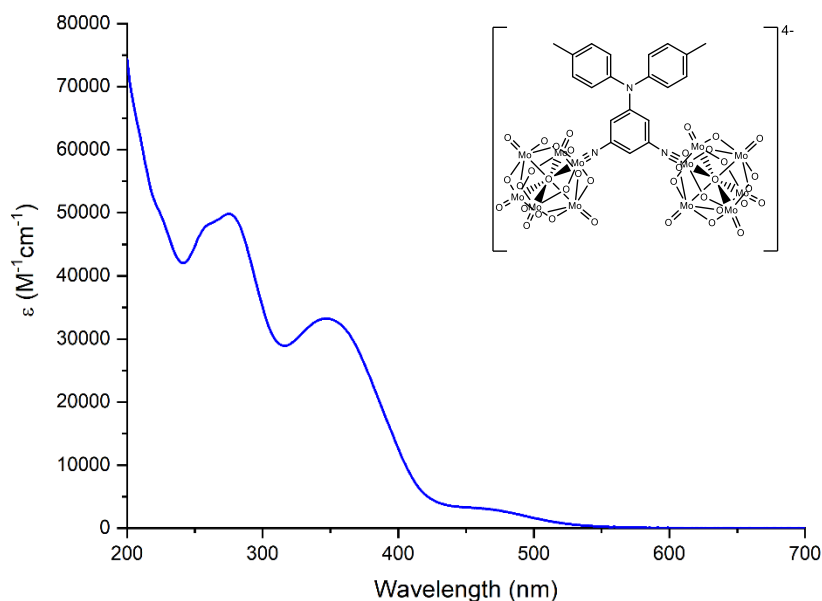
Figure 4.3e UV-vis spectrum of compound **15**, taken in acetonitrile.

A transition this weak had not been observed previously in any of the other derivatives in this work, but a similar phenomenon had been reported with a series of nitro functionalised compounds. In the work by Xue,[168] three nitro functionalised hexamolybdate derivatives were synthesised, with one featuring the nitro group in the *para* position and the other two *meta* to the imido bond. Although no weak peaks were observed in Xue's work, a considerable red-shifting of the IHCT peak of the *para* substituted derivative compared to the *meta* derivatives was, showing there is a stronger electronic interaction between the *para* substituted derivatives than the *meta*. Drawing out the resonance structures for the donation of electrons from the amino group to the POM core helps explain this, as when the electron donor is *para* to the imido bond, through conjugation allows for donation of the lone pair on the nitrogen into the POM core. Although not shown in figure 4.3f, this is also possible when the

electron donor and the POM are *ortho* substituted, however, when the amino group and the POM are *meta*, this donation of electrons into the POM core is not possible.
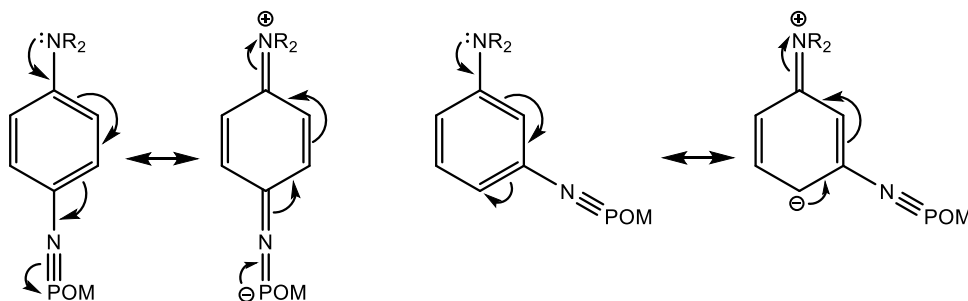
Figure 4.3f The resonance structures of the *para* and *meta* substituted hexamolybdate derivatives explained the small LPCT peak observed for compound **15**.

Earlier on in the chapter, the original intention of making a diphenylethyne bridged analogue of compound **15** from the *meta* bromo derivative was briefly mentioned, with the compound ultimately not having been made due to synthetic difficulties regarding the Sonogashira step. After the UV-vis demonstrated the weak communication between the POM cores and the electron donor at the *meta* position, the reason for this became clearer. In chapter 2, the quick, room temperature Sonogashira couplings as a result of activation of the C-I bond by the electron withdrawing POM cores were discussed, but this, as shown by the resonance structures, cannot happen when the POM cores are *meta* to the halogen due to the limited electronic communication. As a result, the inactivated coupling proved to be unsuccessful using the conditions tried, even when the bromo was replaced by the more reactive iodine, and ultimately synthesis of a diphenylethyne bridged analogue of compound **15** was abandoned.

Although the weak electronic coupling between the POMs and the *meta* position led to no diphenylethyne bridged analogue being successfully synthesised, it did still result in interesting properties of compound **15**. The very weak LPCT peak of compound **15** as a result of coupling in the *meta* position had not been previously seen before in a donor containing POM derivative and so the effect of this on the nonlinear optical activity had not been investigated. Despite the long wavelength of the λ_{max} showing a strong donor/acceptor pair, the low intensity suggests there must be considerably less

coupling between the donor and acceptor than usually observed for these derivatives, possibly increasing charge separation which has been shown by the two state model to increase NLO activity. Increased charge separation and long wave absorption could also suggest potential for other uses such as in solar cells.

The above findings spurred synthesis of another compound, compound **16**, which like compound **15**, featured two POM cores on the same aromatic ring of a triarylamine, however, instead of both being *meta* substituted to the amine, one is *ortho* and the other is *para*. The precursor ligand for compound **16**, compound **P21**, was synthesised using a method based of one reported for the synthesis of a similar compound by Hsiao.[169] This method involved reacting deprotonated diphenylamine with 4-fluoronitrobezene to form the triarylamine, before reducing the nitro group to an amine using hydrazine hydrate in ethanol. To synthesise compound **P20**, ditolylamine and 1-fluoro-2,4-dinitrobenzene were used in the places of the diphenylamine and 4-flurorontrobenzene, and as in the literature, sodium hydride was used to deprotonate the amine. Although yields were low, 20% for compound **P20** and 26% for compound **P21** both reactions proceeded successfully to give the desired products.
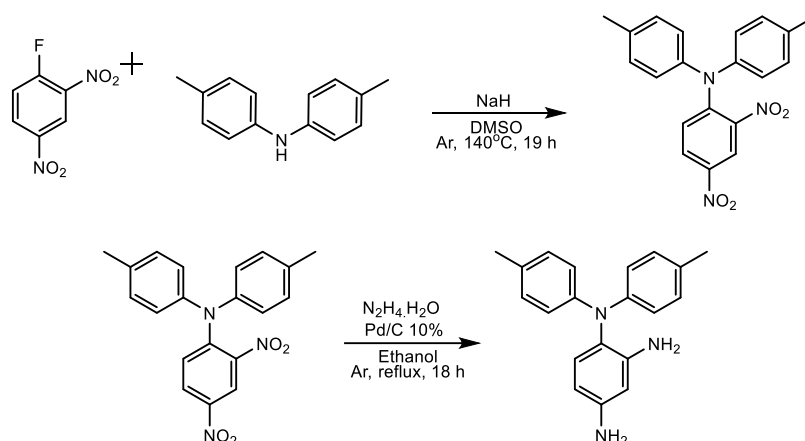
Figure 4.3g Method for the synthesis of compound **P20** and compound **P21**, the precursor for the synthesis of compound **16**.

Compound **16** was synthesised from ligand **P21** and tetrabutylammonium hexamolybdate using the DCC mediated coupling reaction, with 0.50 molar equivalents of aniline and 1.22 molar equivalents of DCC. The reaction proceeded

over 10 hours at 70°C to give, after filtering and precipitating using ethanol and diethyl ether, compound **16** in a 28 % crude yield. Unusually, the ^{1}H-NMR showed almost all the crude sample was the desired product, with only very small amounts of hexamolybdate and an impurity thought to be the mono-substituted ligand present. This was very different to what was observed for compound **15**, where the electronic isolation between the reacting amines and the activating electron donor meant that tetrabutylammonium hexamolybdate was by a few percent the major component of the crude product.

As with compounds **14** and **15**, crystallisation of compound **16** could not be easily achieved from hot acetonitrile due to the oily nature of the compound, however purification by recrystallisation from a dilute acetone solution with diethyl ether diffusion was eventually achieved to produce compound pure by ^{1}H-NMR, ^{13}C-NMR, mass spectrometry, and elemental analysis. The crystals formed were suitable for analysis by X-ray crystallography and yielded a high quality structure with an R_1 of 8.40% in the Pbca space group with one molecule of compound **16** in the asymmetric unit.
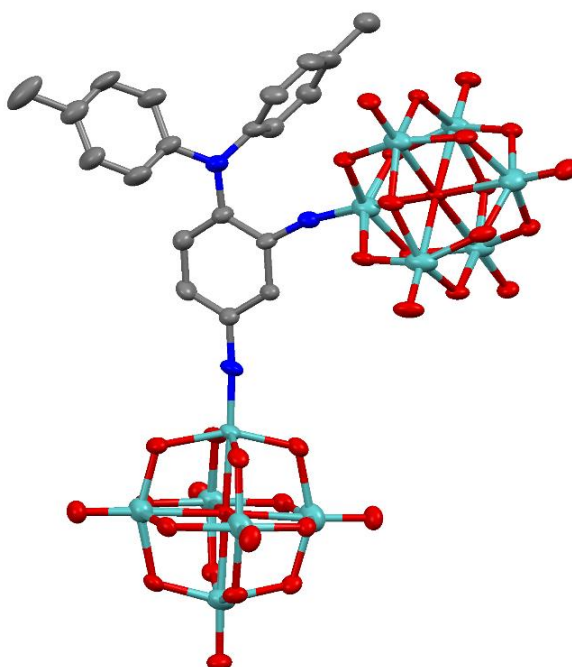
Figure 4.3h Crystal structure images of compound **16**. Thermal ellipsoids are at 30% probability level. The colour scheme shows Mo in green, O in red, N in blue, C in grey, and I in purple. Tetrabutylammonium counter cations and hydrogen atoms are omitted for clarity.

The structure of compound **16** revealed an imido bond of the *para* substituted POM with an Mo-N-C angle of 175.8° and Mo-N and N-C bond lengths of 1.726 and 1.396 Å respectively, suggesting a surprisingly linear imido bond for a compound without ortho positioned steric protecting groups, especially considering the steric effects of the second POM core. As a result of its proximity to the bulky ditolylamino donor, the imido bond of the second POM was longer and less linear, with an Mo-N-C angle of 167.0° and Mo-N and N-C bond lengths of 1.761 and 1.399 Å respectively. Despite the increased length and decreased bond angle, the imido bond was still more linear than seen for the previously synthesised C$_{2v}$ di-POM compound[129] as well as previously reported mono-substituted derivatives with high NLO activity,[128] suggesting the steric repulsion between POM core and the *ortho* ditolylamino donor was not resulting in substantial decrease in conjugation between the POM core and the ligand when compared to previous POM derivatives.
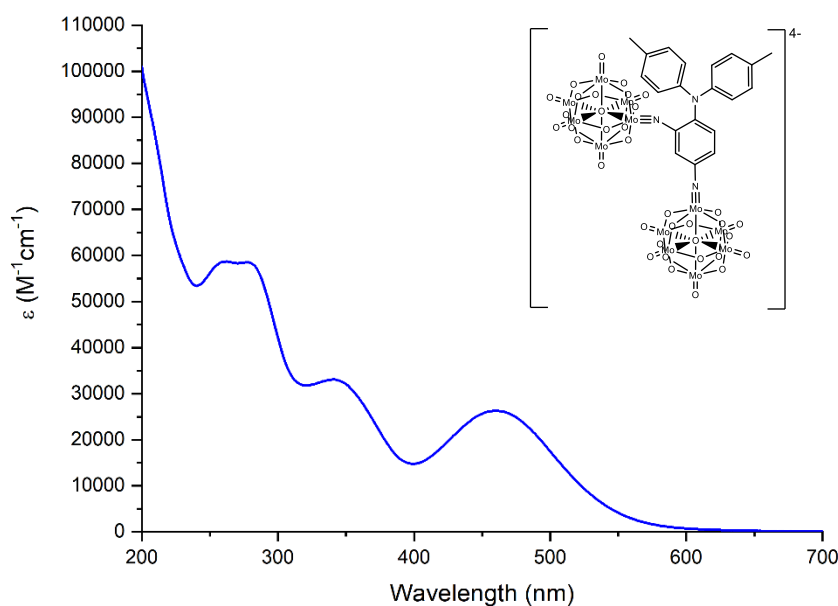
Figure 4.3i UV-vis spectrum of compound **16**, taken in acetonitrile.

As with the other compound, compound **16** was also investigated by UV-vis spectroscopy, with the LPCT peak appearing at 461 nm, again significantly lower in energy than typically observed for monofunctionalised POM derivatives. The LPCT

peak also showed a considerable increase in the intensity compared to that of compound **15**. This increase in the extinction coefficient, from 1.65×10^3 to 26.4×10^3 suggested an increase in coupling between the donor and the acceptors as expected due to the *ortho* and *para* substitutions of the POMs rather than the *meta* seen for compound **15**. The differences between the UV-vis spectra of compounds **15** and **16** show the strong electronic effect of changing the position of the POMs on the imido ring and suggest there could be significant difference in the NLO behaviour of the *ortho/para* and *meta* substituted compounds.

4.4 Electrochemical Studies

As with the mono-substituted chromophores discussed in chapters 2 and 3, the properties of the six multidimensional chromophores were investigated by electrochemical techniques. Cyclic voltammetry was used as outlined previously to investigate the reduction potentials of the POM cores of all six compounds before differential pulse voltammetry (DPV) was used to further investigate the one-donor-two-acceptor chromophores. Bulk electrolysis was not performed on either set of compounds as previous investigation had shown this would result in decomposition of any non-sterically protected derivative and although the two-donor-one-acceptor series were sterically protected, the CVs of these compounds also showed considerable instability in the case of compound **12** and impurity in compound **13**.

Of the three *bis*-substituted derivatives, only compound **11** gave a clean CV demonstrating what looked to be a reversible $[Ar_2Mo_6O_{17}]^{3-/2-}$ reduction peak. At -1.20 V vs Fc/Fc$^+$, the $[Ar_2Mo_6O_{17}]^{3-/2-}$ reduction peak was shifted by -0.2 V compared to the monosubstituted derivative, a result of increased electron density on the POM core from having two rather than one ligands. This is a similar shift to that observed between the first reduction peak of the monofunctionalised analogue and hexamolybdate. The small peak at around -0.8 is a result of hexamolybdate in the sample, either left over from the synthesis or present through a small amount of decomposition. As can be seen though, no other contaminants were present in the sample.
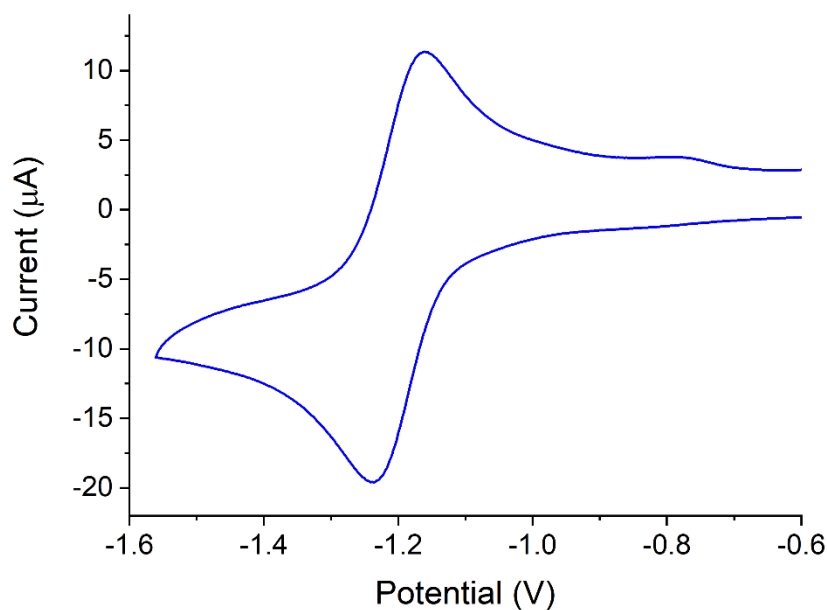
Figure 4.4a Cyclic voltammograms of 0.6 mM solutions of compound **11** in 0.1 M [Bu4N][BF4] in MeCN. Fc/Fc$^+$ was used as the internal reference. 0.1 mV/s scan rate.

The cyclic voltammogram of compound **12** showed a less reversible $[Ar_2Mo_6O_{17}]^{3-/2-}$ reduction peak than compound **11**, with considerable decomposition of the sample noticeable even on the CV timescale. This was not something that had been seen before, as even the unprotected compounds and the protected derivatives that also decomposed still showed good reversibility during their cyclic voltammograms. The decomposition also resulted in plating on the electrode along with a new peak at -0.75 V, possibly resulting from reoxidation of the decomposition product. While this is around the potential at which hexamolybdate would be re-oxidised, cycling did not show the corresponding reduction peak suggesting hexamolybdate was not the cause.

The CV of compound **12** also showed a quasi reversible reduction at -1.21 V, which was likely the result of the decomposition product as the NMR had suggested the sample was clean of any other functionalised hexamolybdate derivatives. Some decomposition of sterically protected derivatives with electron donors and extended π systems into a POM other than hexamolybdate had been previously observed during the bulk electrolysis experiments, as was discussed in chapter 2, and it is likely this decomposition results from a similar mechanism. The decomposition in both cases likely stems from the donation of electrons destabilising the POM core and therefore occurs more readily for compound **12** due to two ligands being present.
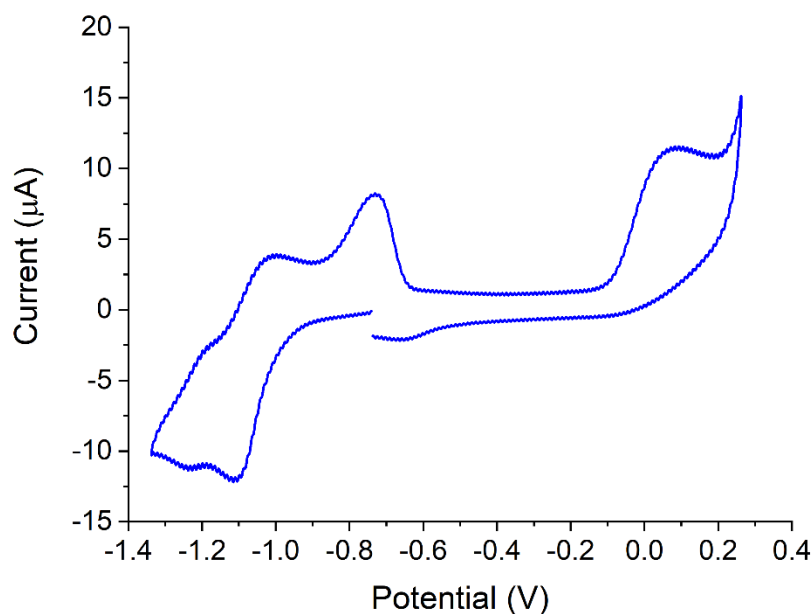
Figure 4.4b Cyclic voltammograms of 0.6 mM solutions of compound **12** in 0.1 M [Bu4N][BF4] in MeCN. Fc/Fc$^+$ was used as the internal reference. 0.1 mV/s scan rate.

Along with the interesting irreversibility of the $[Ar_2Mo_6O_{17}]^{3-/2-}$ reduction peak, the peak also sits at an unexpected potential of -1.056 V vs Fc/Fc$^+$. Typically, hexamolybdate derivatives with stronger electron donors reduce at more negative potentials due to the increased electron density on the POM core, but compound **12** appears to reduce at a less negative potential than compound **11**. This could suggest some kind of electronic isolation between the POM core and the electron donors and may be related to the decomposition observed of the compound upon reduction. It is also possible that the less negative peak is due to the sample that gets plated on the surface and the peak at -1.21 V is the $[Ar_2Mo_6O_{17}]^{3-/2-}$ reduction peak, however this would imply decomposition of the POM due to reduction was not the cause of the plating.

Compound **13** was also investigated by cyclic voltammetry which revealed a reversible $[Ar_2Mo_6O_{17}]^{3-/2-}$ peak despite the instability of compound **12**, but also showed the significant number of other hexamolybdate derivatives. The presence of these was not unexpected as they had been visible on the ^{1}H-NMR and had needed to be taken into account when fitting the elemental analysis results, but a higher percentage of the sample did look to be of these impurities than had been anticipated from the previous data. The CV containing all these peaks is interesting though, as it does allow

comparison of the shifts of the *mono-*, *bis-*, *tris-*, and *tetrakis*-functionalised derivatives, showing that with increasing substitution, increased donation of electron density results in an increasingly negative reduction potential of the POM core.
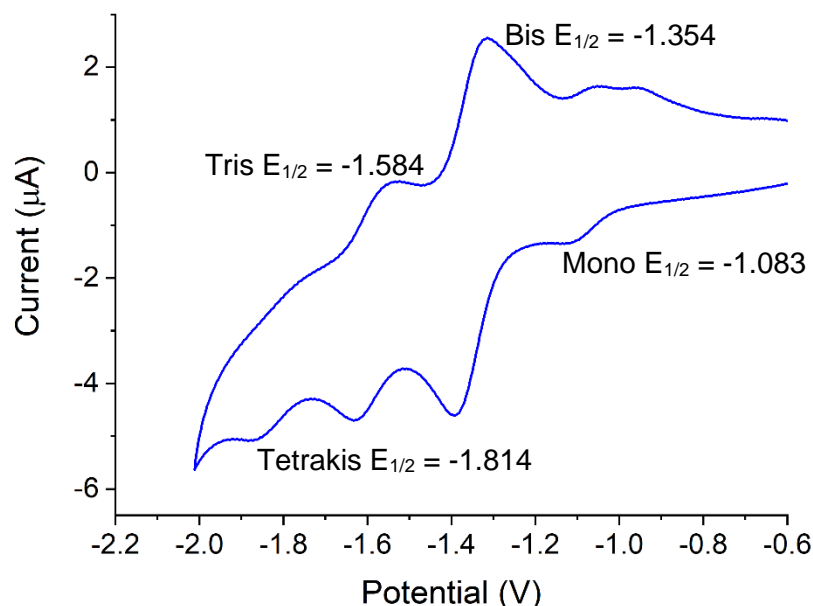
Figure 4.4c Cyclic voltammogram of 0.3 mM solutions of compound **13** in 0.1 M [Bu4N][BF4] in MeCN. Fc/Fc$^+$ was used as the internal reference. 0.1 mV/s scan rate.

Along with the multiple reduction peaks, the full scan of compound **13** also showed three reversible oxidation peaks, one with an $E_{1/2}$ of 0.272 V, one with an $E_{1/2}$ of 0.165 V, and a much smaller one with an $E_{1/2}$ of 0.04 V. The oxidation of the ligand of the monofunctionalised derivative was previously measured to be at 0.269 V, suggesting these peaks correspond to the *mono-*, *bis-*, and *tris*-substituted derivatives respectively, with oxidation becoming easier as the increased number of ligands decrease electron donation of each individually to the POM core. The oxidation of the ligand of the *tetrakis*-substituted derivative was likely too small to see due to the low concentration.

The CV taken of compound **13** also did show the stability of the *mono-*, *bis-*, and *tris*-substituted derivatives on the CV timescale, suggesting the compound could be candidates for redox switching and again demonstrating the increased stability of the phenyl bridged derivatives over the diphenylethyne bridged ones.

	E_{pc} $[Ar_xMo_6O_{19-x}]^{4-/3-}$	$E_{1/2}$ $[Ar_xMo_6O_{19-x}]^{3-/2-}$	ΔE_p (mV)	E_{pa} NR_2
11	-	-1.200	80	-
12	-	-1.056	107	
13	-2.131	-1.354	78	0.272 quas
3	-1.910	-1.002	85	-
4	-1.837	-1.013	73	0.338 irr
8	-1.885	-1.101	83	0.303 rev

Table 4.41 Table summarising the cyclic voltammetry peaks of compounds **11**, **12**, and **13** and their monosubstituted analogues, compounds **3**, **4** and **8** respectively. All peaks are reported in V. Cyclic voltammograms were taken at a 0.1 V/s scan rate using 0.3-0.8 mM solutions of analyte and 0.1 M [Bu4N][BF4] in MeCN. Fc/Fc$^+$ was used as the internal reference in all cases.

To investigate the three one-donor-two-acceptor chromophores, compounds **14**, **15**, and **16**, cyclic voltammetry was used along with differential pulse voltammetry (DPV). DPV is an electrochemical technique in which the potential of the system is varied through the application of a series of short pulses of around 10-100 ms long superimposed on the linearly increasing potential ramp seen in cyclic voltammetry. The current is measured both before and after the application of the potential pulse, with the current measured prior attributed to the potential ramp and the difference between the two reflects the response to the pulse. This separation of the ramp current from the current as a response of the sample can result in more sensitive measurements, while the small step size increases definition of the peaks and can allow for differentiation of peaks with similar enough reduction potentials that during cyclic voltammetry they appeared as one. It was hoped this would be useful in determining whether the equivalent POM cores on compounds **14** and **15** reduce simultaneously, or if electronic communication results in reduction of one increasing the potential of the reduction of the other.

The cyclic voltammetry experiments performed on compounds **14**, **15**, and **16** showed electrochemically reversible $[Ar(Mo_6O_{18})_2]^{6-/4-}$ reduction peaks based on their constant peak separations at varying current, with all three at a less negative potential than what was observed for compounds **7** and **8**, the only two other donor containing phenyl bridged derivatives. Irreversible $[Ar(Mo_6O_{18})_2]^{8-/6-}$ reduction peaks and quasi

reversible amine oxidation peaks were also seen for all three compounds.
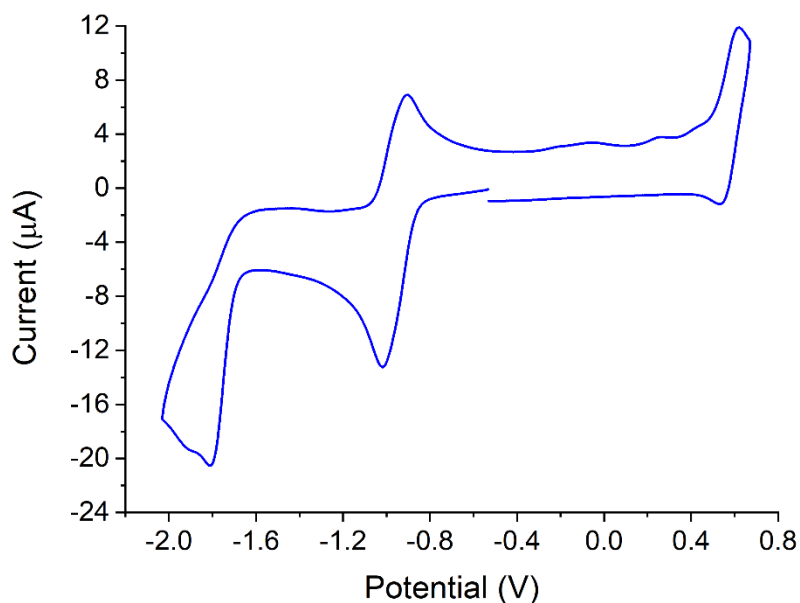
Figure 4.4d Cyclic voltammogram of 0.3 mM solutions of compound **15** in 0.1 M [Bu4N][BF4] in MeCN taken at a 0.1 V/s scan rate. Fc/Fc$^+$ was used as the internal reference.

	E_{pc} [Ar(Mo$_6$O$_{18}$)$_2$]$^{8-/6-}$	$E_{1/2}$ [Ar(Mo$_6$O$_{18}$)$_2$]$^{6-/4-}$	ΔE_c (mV)	E_{pa} NR$_2$
14	- 1.855	- 1.023	93	0.458
15	- 1.876	- 0.966	117	0.568
16	-1.803	-1.005	146	0.455

Table 4.4b Table summarising the cyclic voltammetry peaks of compounds **14**, **15**, and **16**. All peaks are reported in V. Cyclic voltammograms were taken at a 0.1 V/s scan rate using 0.3 to 0.4 mM solutions of analyte and 0.1 M [Bu4N][BF4] in MeCN. Fc/Fc$^+$ was used as the internal reference in all cases.

The most negative potential reduction peak of the three one-donor-two-acceptor chromophores was for compound **14**, at -1.02 V vs Fc/Fc$^+$. Although no monofunctionalised analogue of this exists for comparison, this is still less negative than the $E_{1/2}$ of other phenyl bridged derivatives such as compounds **7** and **8** which reduced at potentials of -1.10 V and -1.07 V respectively, a likely result of the

weakened electron donation from the amine into the two POM cores. It is also possible this difference is caused by the change in donor group, as the dimethylamino group should be a slightly stronger electron donor than the ditolylamino group. The peak separation is also a little larger than seen for the mono-substituted derivatives whereas a true two electron wave would have a smaller peak separation of around 30 mV, suggesting the $[Ar(Mo_6O_{18})_2]^{6-/4-}$ peak is not a true two electron wave caused by the POMs reducing simultaneously, but rather two one electron reductions at very similar potentials. This would occur due to electronic communication between the POMs resulting in the second reducing at a more negative potential because of the increased electron density of the system as a result of the first.
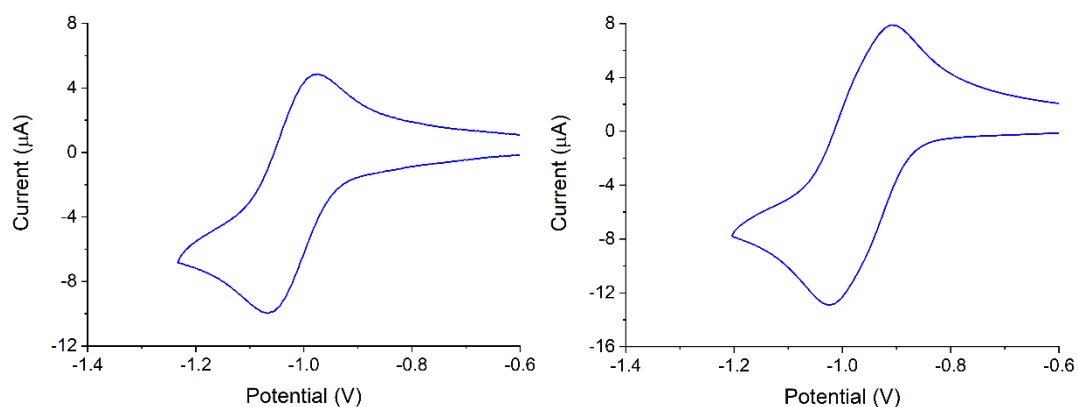
Figure 4.4e Cyclic voltammograms of compound **14** (left) and compound **15** (right). Both were taken as 0.4 mM solutions in 0.1M NBu_4BF_4 in acetonitrile. Referenced to Fc/Fc^+.

The $[Ar(Mo_6O_{18})_2]^{6-/4-}$ reduction peak of compound **15** was at -0.966 V, the least negative of any of the three compounds. This is very similar to the reduction peak of compound **2**, the dimethyl protected iodo compound, suggesting the increased potential needed to reduce compound **15** over hexamolybdate is more a result of the imido ring rather than the electron donor due to the isolation between the amine and the *meta* substituted POMs. The peak separation of compound **15** was again substantially larger than the ideal peak separation of 30 mV for a two electron wave, indicating electronic communication between the two POM cores was resulting in two different potential reduction processes rather than one simultaneous two electron reduction. The ΔE_c of compound **15** was larger than seen for compound **14**, a likely

result of the two POM cores being situated on the same aromatic ring of compound **15** and therefore being more electronically connected than the two in compound **14**. Differential pulse voltammetry performed on compound **15** confirmed the $[Ar(Mo_6O_{18})_2]^{6-/4-}$ reduction wave was formed of two separate but similar potential reductions, with fitting of the DPV wave revealing two reduction processes 71 mV apart. In contrast, the DPV of compound **14** revealed only one reduction process despite the larger than idea ΔE_c, showing the very close potential at which the two POM cores were reducing.
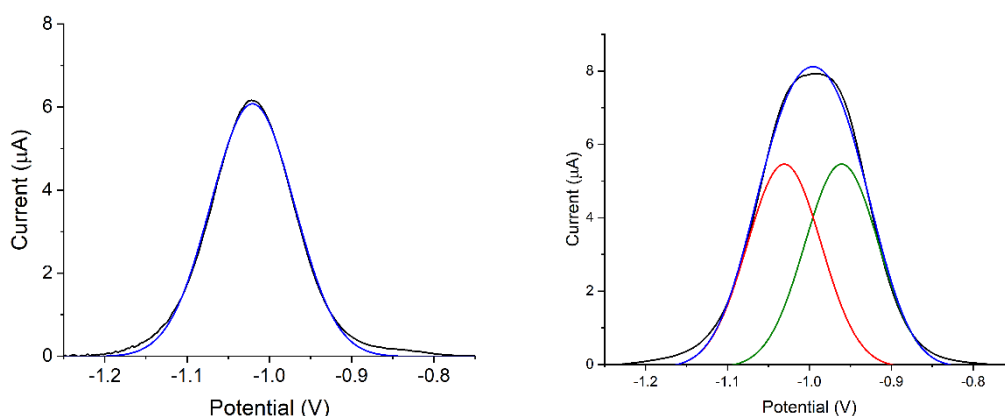
Figure 4.4f Differential pulse voltammograms of compound **14** (left) and compound **15** (right). Both were taken as 0.4 mM solutions in 0.1M NBu_4BF_4 in acetonitrile. Referenced to Fc/Fc^+.

The $[ArMo_6O_{18}]^{3-/2-}$ reduction wave of compound **16** was at a potential of -1.005 V, and even before the differential pulse voltammetry was performed on the compound, the shape of the CV made it evident this reduction wave was comprised of two processes with different reduction potentials. This was also suggested by the peak separation, which at 146 mV was the largest seen for any of the three compounds. Like compound **15**, both POMs on compound **16** are situated on the same aromatic ring which would result in increased electronic connection between them, however, unlike in compound **14** and **15** where the two POM cores are in identical positions on their imido rings, the two POM cores in compound **16** are also in different positions.

Fitting of the DPV curve confirmed the wave consisted of two peaks, with one at a potential 87 mV at a more negative than the other. This difference between the $E_{1/2}$

values of the two peaks is 16 mV larger than the difference between the two peaks of compound **15**. Of the two peaks, it is likely the less negative peak is a result of reduction of the *ortho* substituted POM, as although this is closer to the amine donor, X-ray diffraction shows the imido bond is also longer and less linear, suggesting less triple bond character and weaker coupling to the donor than the *para* substituted POM, making reduction easier.
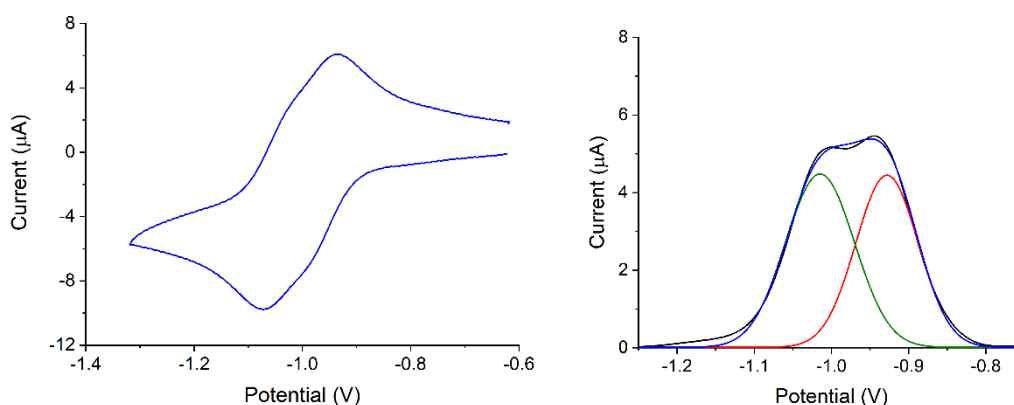
Figure 4.4g Cyclic voltammogram (left) and differential pulse voltammogram (right) of compound **16**. Both were taken as a 0.3 mM solution in 0.1M NBu$_4$BF$_4$ in acetonitrile. Referenced to Fc/Fc$^+$.

The peaks of compound **16**, when averaged, fell at -1.005 V, which was in between the reduction peak of compounds **14** and **15** in terms of potential, showing more influence of the electron donor on the POM core than compound **15** and suggesting more conjugation. This is consistent with the UV-vis absorption spectra, where the LPCT peak was much more intense for compound **16** than compound **15**.

4.5 Hyper-Rayleigh Scattering

Compounds **12** to **16** were investigated by Hyper-Rayleigh Scattering (HRS) to determine their non-linear optical properties. Compound **11** was not included in this analysis due to its lack of electron donor and the assumption that based on previous results, it would not be NLO active. HRS was performed as described in chapter 3, with the incident wavelength of 1064 nm again resulting in Hyper-Rayleigh Scattering

at 532 nm. The internal reference method was used to extract $\beta_{1064,HRS}$ from the raw data, and the two state model was used to calculate $\beta_{0,HRS}$ from there. In addition, the depolarization ratios of compounds **12** to **16** were calculated, with this being the ratio of the intensity of the light in scattered in the planes parallel and perpendicular to the incident laser beam. For dipolar compounds the depolarization ratio, ρ, should equal 5, while for perfectly octupolar molecules it should be 1.5. Multidimensional chromophores should be somewhere in between, with a higher depolarization ratio indicating a more dipolar compound.

Standard HRS analysis was carried out successfully on all compounds, allowing for comparison of the β_{HRS} between similar multidimensional chromophores and between the *mono-* and *bis*-substituted derivatives. As was seen for the monosubstituted analogues, the NLO activity of compound **12**, the diphenylethyne bridged analogue, was considerably higher than that of compound **13** due to the larger π system. Compound **12** also showed a higher β_{HRS} than its monosubstituted analogue compound **5**, 260 vs 220×10^{-30} esu while compound **13** showed a slightly lower β_{HRS} than its monofunctionalised analogue, 114 vs 127×10^{-30} esu, although the purity issues of compound **13** may have affected this.

Compound **15** gave a smaller β_{HRS} than seen for any other compound measured in this work, and one considerably smaller than the two other one-donor-two-acceptor chromophores, a likely result of the weakened donor-acceptor coupling due to the *meta* relationship between the donors and acceptors. Of compounds **14** and **16**, compound **14** gave a much higher β_{HRS}, possibly due to the POMs being on different rings of the triarylamine resulting in a larger change in dipole moment between the ground and excited states. After conversion to $\beta_{0,HRS}$ compound **12** appeared more active than both compounds **14** and **15** due to the large redshifting of their LPCT peaks, giving it the best NLO activity of any of the multidimensional POM derivatives tested.

Depolarization experiments performed on compounds **12** to **16** resulted in depolarization constants for compounds **13**, **14**, and **16**. No data could be obtained for compounds **12** or **15** due to the low activity of compound **15** and the background solvent background giving a more intense HRS peak than the sample for compound **12**. Of the three compounds successfully measured, all three had depolarization ratios of between 1.67 and 1.86 as seen in table 4.5a, showing HRS responses with significant

multidimensional character. Of the compounds, compound **13**, which has the smallest angle between the two donor branches at 90°, was the most dipolar, while compound **14**, which has a larger theoretical angle of 109.4° gave the smallest depolarisation ratio. Previous work has shown the importance of the angle between the branches on the diagonal and off-diagonal components of β, with the β_{zzz} typically decreasing as the angle between the branches increases, and the off-diagonal component increasing until an angle of 109.5 degrees was reached before decreasing too.

	LPCT λ_{max} (nm)	$\beta_{1064,\ HRS}$	$\beta_{0,\ HRS}$	ρ
12	419	259.7	83.3	
13	422	114.3	35.7	1.861
14	473	450.9	75.8	1.671
15	469	90.6	16.3	
16	461	295.1	59.7	1.801

Table 4.5a Comparison of the hyperpolarizabilities and depolarization ratios of compounds **12** to **16**. * β_{1064} and β_0 values for compound **12** are calculated using the depolarization constant for compound **13** due to their structural similarity.

The depolarization constant and β_{HRS} can also allow for calculation of $\beta_{0,zzz}$ and $\beta_{0,yyz}$ for some compounds with C_{2V} symmetry as described by Coe et al.[170] The depolarization ratios of compounds **13**, **14**, and **15** have high uncertainties, making them not ideally suited for such a treatment. Nonetheless, calculations have been performed for compounds **14** to acquire a rough estimate. This was the compound with the smallest uncertainty in the data and also the compound most suited to the analysis due to the previously discussed impurity of compound **13** and the lower symmetry of compound **16**.

The analysis of compound **14** suggested a $\beta_{0,zzz}$ of 162.4×10^{-30} esu and a high off diagonal $\beta_{0,yyz}$ of -101.7×10^{-30} esu. Since it has been suggested that the $\beta_{0,zzz}$ of a multidimensional chromophore should be lower than that of a dipolar analogue, it would be interesting to determine the $\beta_{0,zzz}$ of a dipolar analogue of compound **14**, as the $\beta_{0,zzz}$ of compound **14** is already much higher than would be expected for such an

analogue. For reference, compound **7**, which is the dimethyl protected dimethylamino compound and closest one dimensional comparison to **14**, had a $\beta_{0,zzz}$ of 98.1×10^{-30} esu, considerably weaker than the $\beta_{0,zzz}$ of 162.4×10^{-30} esu seen for compound **14**.[101]

4.6 Conclusion

In this chapter two families of multidimensional NLO active polyoxometalate chromophores were synthesised and investigated by UV-vis spectroscopy, electrochemistry, and Hyper-Rayleigh scattering, one set with two electron donor containing ligands coupled to one POM, and the other with one electron donor bonded to two POM cores. Synthesis of the two-donor-one-acceptor chromophores, compounds **11** to **13** was achieved through the same DCC mediated coupling used to synthesise their monofunctionalised analogues, while the one-donor-two-acceptor compounds were synthesised from a series of triarylamine based ligands. The three two-donor-one-acceptor chromophores showed very similar electronic spectra to their monofunctionalised analogues, albeit with higher extinction coefficients, while the one-donor-two-acceptor systems showed LPCT peaks with considerably higher λ_{max}. The LPCT peak of compound **15**, which featured the POMs *meta* to the electron donor, was unexpectedly weak compared to previously observed peaks, a result of the diminished electron conjugation explained by the resonance forms.

Hyper-Rayleigh scattering experiments were used to determine β_{HRS} for compounds **12** to **16**, showing high NLO activity in the cases of compound **12**, **13**, **15**, and **16**. The activity of compound **12** was higher than for its monofunctionalised analogue while the activity of compound **13** was marginally lower. Compounds **14** and **16** gave high $\beta_{1064,HRS}$ values with compound **14** giving the highest dynamic hyperpolarizability out of all five multidimensional POM chromophores, however, due to their very redshifted λ_{max} compound **12** gave a higher $\beta_{0,HRS}$. Depolarisation ratios were also obtained for compounds **13**, **14**, and **16**, showing the compounds had significant multidimensional character. The depolarization ratios allowed for estimations of $\beta_{0,zzz}$ and $\beta_{0,yyz}$ for compound **14**, with the $\beta_{0,zzz}$ of 162.4×10^{-30} esu of compound **14** being higher than any previously synthesised phenyl-bridged derivative and the $\beta_{0,yyz}$ of -101.7×10^{-30} esu showing a significant off diagonal response.

Chapter 5

Synthesis and analysis of an NLO active alkene bridged polyoxometalate derivative

5.1 Introduction

Molecular NLO active chromophores, whether organic such as DAST[74] or organometallic such as the early ferrocene-based compounds first synthesised by Green et al.[76], perturb laser light through its interaction with a changeable but permanent dipole, usually caused by a donor-π bridge-acceptor system. The two state model, shown in equation 5.1.1, models this and can be used to predict and explain the NLO activities of chromophores. Here, β_0 denotes the first hyperpolarizability, μ_{12} denotes the dipole moment of the ground state, $\Delta\mu_{12}$ denotes the difference in molecular dipole moment between the ground and excited state, and λ_{max} denotes the energy of the relevant charge transfer peak.[51]

$$\beta_0 = \frac{3\Delta\mu_{12}(\mu_{12})^2}{2(\lambda_{max})^2} \tag{5.1.1}$$

From this equation, it can be seen that increased NLO activity can be obtained by increasing the charge separation between the ground and excited states, which would increase the change in dipole moment, or by increasing coupling between the donor and acceptor, which would increase the dipole moment of the electronic transition. Decreasing the energy of the charge transfer peak by the use of stronger donor/acceptor pairs also increases the activity of the chromophore, however, it is difficult to simultaneously increase coupling and charge separation, meaning a reduction in λ_{max} can also result in a reduction in μ_{12}.

Over the years, NLO active chromophores with a range of donors, acceptors and π bridges have been synthesised with an aim towards increasing hyperpolarizability. Stronger donor/acceptor pairs typically result in higher NLO activity, as has been seen for both inorganic and organometallic compounds, while increased charge separation, such as in the TICTOID compounds synthesised by Shi et al.,[70] has also resulted in compounds with high hyperpolarizabilities. Compounds with alkene based π bridges have also shown increased NLO activity over alkyne analogues due to increased conjugation through their more planar π systems.[64]

Due to the well-developed post-functionalisation methods of synthesising alkyne bridged over alkene bridged POM chromophores as well as the increased complexity of synthesising alkene based systems, all hexamolybdate derivatives previously used in Hyper-Rayleigh scattering experiments to investigate their NLO activity have

featured alkynyl bridges. This leaves potentially more highly active hexamolybdate derivatives with alkene bridges as an area of research yet to be explored.

In this work, the first polyoxometalate chromophore with an alkene bridge was synthesised and investigated with the aim of determining if the increased conjugation this would result in would lead to higher NLO activity than seen for previously synthesised compounds with phenyl or diphenylethyne bridges.
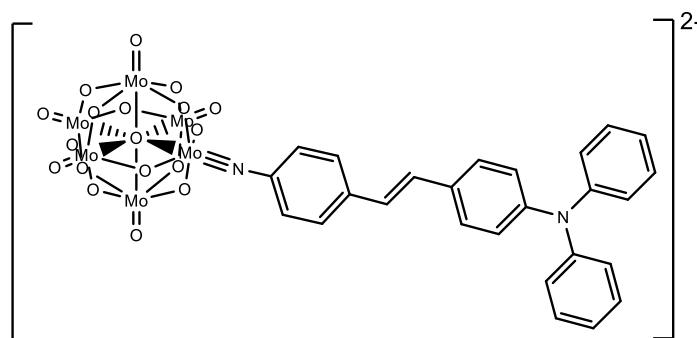
17

Figure 5.1a Compound 17, the main alkene bridged POM chromophore discussed in this chapter.

5.2 Synthesis

Synthesis of extended compounds **4**, **5**, and **6** was performed through the palladium catalysed Sonogashira coupling between an alkyne donor unit and compound **3**, a 4-iodo organoimido functionalised POM. These type of reactions are well reported, having been performed previously in the work of Xu,[38] Kang,[171] and Al-Yasari,[45] amongst others, and typically occur to give pure products in yields of 50 to 85%. The Sonogashira reactions performed on 4-iodoaryl hexamolybdate derivatives typically occur under mild conditions, with many examples going to completion at room temperature in under 30 minutes as a result of the electron withdrawing POM core increasing affinity of the aryl halide for oxidative addition to the catalyst. Heck carbon-carbon coupling reactions,[39] reactions that would be capable of forming an alkene bridge between compound **3** and an electron donor functionalised ligand, have also been reported, with Zhu et al publishing work on the successful synthesis of seven

different alkene containing compounds using heck reactions all with yields of over 72%.

Typically, Heck reactions, which are coupling reactions between aryl or vinyl halides and activated alkenes are performed using a palladium catalyst with a phosphine supporting ligand in dioxane or N-methyl-2-pyrrolidone (NMP). In contrast, Zhu performed the coupling reactions in a 2:3 mixture of THF and NMP due to solubility constraints and without the phosphine ligand typically included to stabilise the palladium catalyst since the POM anions and tetrabutylammonium cations reportedly played a similar role in the systems.[39] After much investigation regarding suitable bases to use in the reaction, bromomagnesium phenylamide was found to be the most suitable, resulting in the highest yield of the desired products.

After the improved stability of compounds **2** to **10** compared to unprotected derivatives was confirmed by bulk electrolysis, synthesis of a sterically protected, alkene bridged chromophore was attempted using the adapted Heck coupling conditions successfully used by Zhu et al. Compound **3**, the 2,6-diisopropyl-4-iodo derivative, was used as the starting material, along with N,N-dimethyl-4-vinylaniline. The bromomagnesium phenylamide was synthesised from ethylmagnesium bromide and aniline in THF as needed before being added to a solution of compound **3**, N,N-dimethyl-4-vinylaniline and Tris(dibenzylideneacetone)dipalladium(0) in NMP.
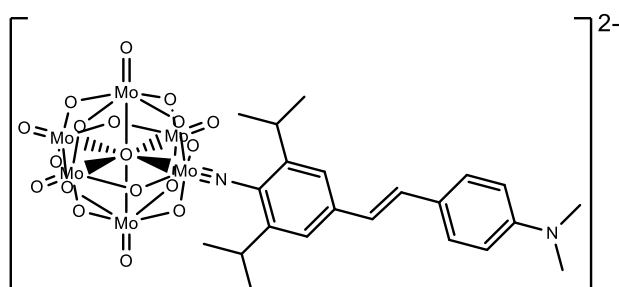
Figure 5.2a Synthesis of a sterically protected, alkene bridged hexamolybdate derivative was attempted with limited success.

After multiple attempts and despite the success of Zhu, the desired product could not be obtained pure or in good yield in this case, with problems resulting from incomplete

coupling as well as decomposition of both compound **3** and the desired product. The difference in reactivity observed between the reaction attempted in this work and the reactions performed by Zhu likely resulted from the amine on the donor unit as none of the alkenes used by Zhu featured electron donating functional groups. Heck couplings are also known to be enhanced by the inclusion of an electron withdrawing substituent on the alkene rather than the electron donating amines featured on the N,N-dimethyl-4-vinylaniline. Separation of the desired product, compound **3**, and the tetrabutylammonium hexamolybdate formed from the decomposition of the two functionalised POMs through recrystallisation would have been impossible due to the low proportion of the desired product in the sample and incredibly low crude yield.

Through an extended reaction time, on one occasion a small amount of product containing only tetrabutylammonium hexamolybdate and the desired alkene bridged derivative was obtained, and although purification of this was not successful, the lack of compound **3** in the sample did mean that UV-vis analysis of the crude product could be performed to determine the peak wavelength of the LPCT peak.
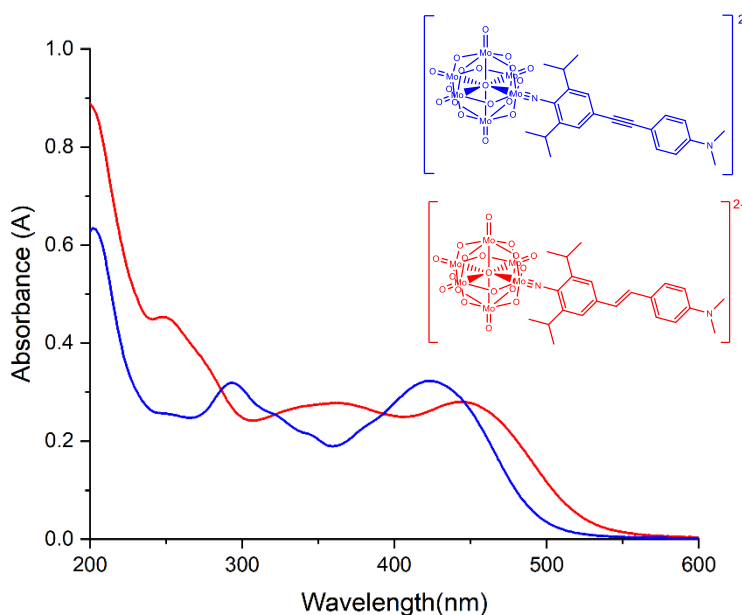
Figure 5.2b Electronic spectra for compound **4** (blue) and its alkene bridged analogue (red). Due to the hexamolybdate impurity present in the sample of the alkene bridged compound impeding determination of exact concentration and intensity of the peaks, data was left in absorbance units.

Comparison of the spectrum to that of compound **4**, the alkyne bridged analogue, showed the inclusion of the alkene bridge in the place of the alkyne one of compounds **4** had resulted in a red-shift of the LPCT peak, with the peak wavelength being 444 nm rather than the 431 nm observed for compound **4**. This increased λ_{max} of the LPCT peak suggests stronger coupling between the donor and the acceptor and is usually a good indication of improved NLO activity.

After UV-vis analysis suggested the alkene bridged hexamolybdate derivatives would be good candidates for improving the NLO activity of polyoxometalate chromophores, alternative methods of synthesising such compounds were investigated. Ultimately, it was decided that coupling a completed amine functionalised ligand to the hexamolybdate core using the DCC mediated coupling mechanism was likely to prove the most successful option.

17

III
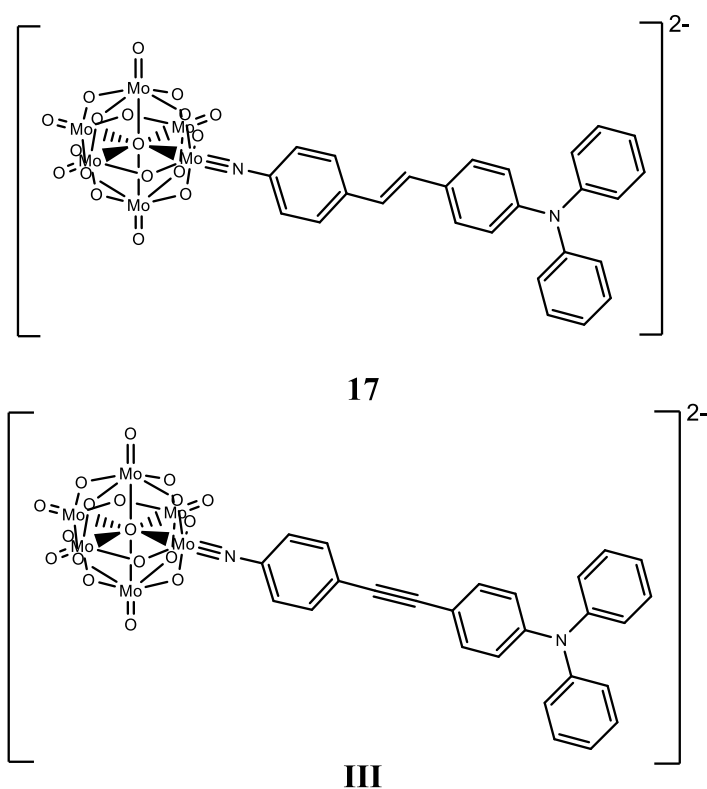
Figure 5.2c Compound **17** (top) and an alkyne bridged analogue synthesised by Al-Yasari et al. in 2018 (bottom).

Investigation into reported methods of synthesising a suitable alkene bridged donor

with alkyl groups at the 2 and 6 positions of the aniline ring brought up no suitable compounds, and in the end, the sterically bulky groups were sacrificed for ease of synthesis. The resulting compound was also very similar to one synthesised by Al-Yasari et al. in 2018[45] allowing for comparison of a compounds identical save for the alkene/alkyne bridge between the POM and the diphenylamino donor group.

A method based on one previously reported by Ding et al.[172] was followed to synthesise a suitable donor unit, with the first step being carried out as in the literature. The initial piperidine catalysed Doebner modification of the Knoevenagel condensation reaction between 4-nitrophenylacetic acid and diphenylaminobenzaldehyde was performed as described in the literature and progressed to form compound **P14** a with a 57% yield after purification, a slight improvement over the yield previously reported.

The reduction of compound **P14** to form the completed ligand, compound **P15**, was performed using hydrazine hydrate in dry ethanol rather than the acetic acid and iron powder method used in the literature due to the increased ease of work up. The reaction proceeded as expected to give pure compound **P15** in a 64% yield as confirmed by ^{1}H-NMR.
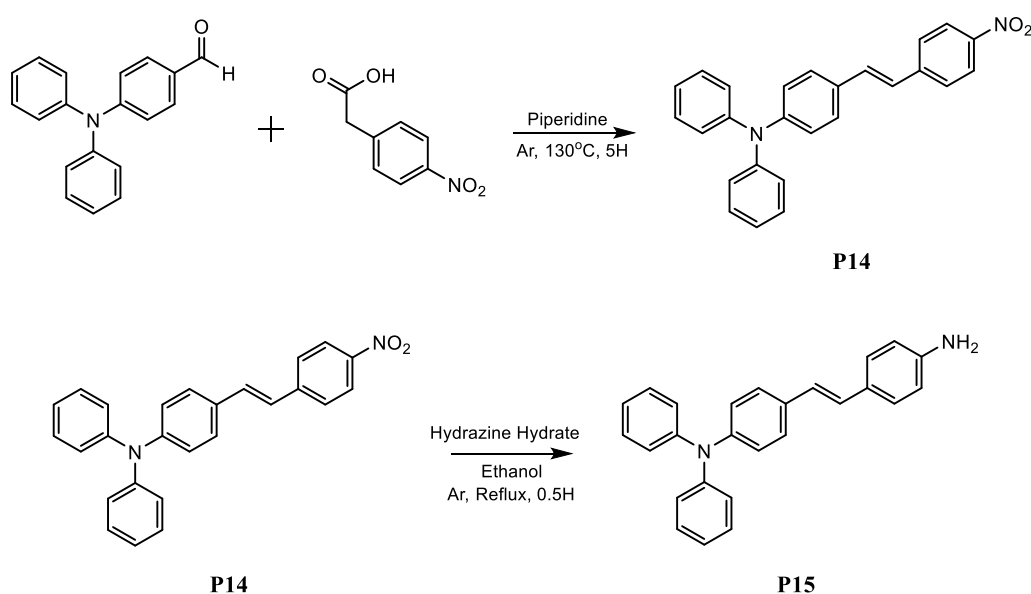
Figure 5.2d Scheme for the synthesis of precursor **P15**, the ligand used to synthesise compound **17**.

After the synthesis of precursor **P15**, compound **17** was synthesised using the DCC mediated coupling reaction as previously described, with the reaction proceeding over the standard 10 hours to produce the desired compound in a 70% crude yield. As usual, some hexamolybdate was present in the sample, with approximately 60% of the sample being compound **17** and the rest being unreacted tetrabutylammonium hexamolybdate. Purification was achieved through reprecipitation from acetonitrile and diethyl ether followed by a second reprecipitation by the slow diffusion of diethyl ether into an acetone solution of the product to give compound **17** 92% pure by ^{1}H-NMR. ^{13}C-NMR, mass spectrometry, and elemental analysis also confirmed the synthesis and purity of the compound. Attempts at growing crystals of compound **17** suitable for X-ray crystallography were performed using multiple conditions, however these were not successful due to the tendency of the compound to form an oil. Some decomposition of the compound was also noted while in solution, hindering attempts at slower recrystallisation.

5.3 Linear Optical and Electrochemical Analysis

Analysis of the UV-vis absorption spectra of compound **17** revealed many of the features expected for amine functionalised hexamolybdate derivatives, with the same intense high energy peak resulting from the O to Mo transitions within the POM core seen of hexamolybdate and the usual new intense low energy peak resulting from the LPCT transitions. For compound **17**, the λ_{max} of the LPCT peak came at 437 nm, the highest seen for any of the monofunctionalised derivatives synthesised in this work save for the julolidine donor containing compound **6**. This includes the ditolyl substituted compound, the closest alkyne bridged analogue synthesised in this work.

Comparison of the LPCT peak of compound **17** to that of the alkyne bridged analogue synthesised by Al-Yasari showed a strong red shift upon inclusion of the alkene bridge, with λ_{max} at a wavelength of 437 nm compared to 414 nm for Al-Yasari's compound. The extinction coefficients of the compounds were very similar, at 43.9×10^3 M^{-1}cm^{-1} for compound **17** and 45.3×10^3 M^{-1}cm^{-1} for the alkyne bridged analogue.
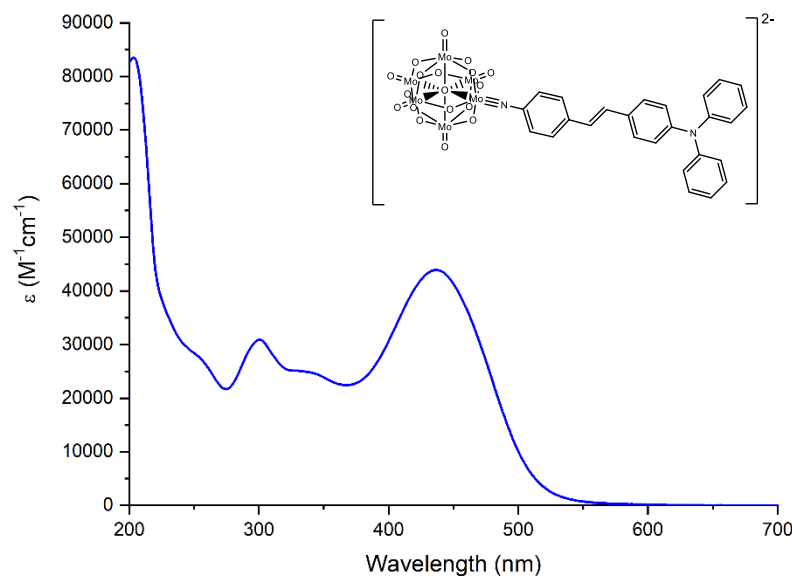
Figure 5.3a UV-vis absorbance spectrum for compound **17**, taken in acetonitrile. This showed a redshift of the LPCT peak when compared to compound **III**, an alkyne bridged analogue.

The literature reports a similar difference in λ_{max} between alkyne and alkene bridged organic chromophores, with the λ_{max} of trans-4-(N,N-dimethylamino)-4'-nitrostilbene appearing approximately 15nm higher than that of the alkyne bridged analogue, ~422 nm[173] vs 406 nm[174] respectively. Typically, this redshift is accompanied by an increase in NLO activity, with trans-4-(N,N-dimethylamino)-4'-nitrostilbene having a β_0 50% higher than its analogue,[64] an indication that compound **17** may have a higher hyperpolarizability than the alkyne bridged derivative.

Electrochemical analysis was also carried out on compound **17**, with the cyclic voltammetry being performed in a 10 mM solution of 0.1 M tetrabutylammonium tetrafluoroborate in acetonitrile. As in previous cyclic voltammetry experiments, glassy carbon was used as the working electrode, platinum wire as the counter, and silver as the internal reference. Unlike during the analysis of the other monofunctionalised derivatives, compounds **2** to **10**, bulk electrolysis was not performed as previous work by Al-Yasari had already demonstrated the susceptibility of the unprotected chromophores such as compound **17** to hydrolyse when reduced.

As was typically observed of these compounds, compound **17** demonstrated two reductive waves, one with an $E_{1/2}$ of -0.961 V vs Fc/Fc$^+$ which was fully reversible on

the CV timescale and resulted from the $[ArMo_6O_{18}]^{2/3-}$ reduction, and an irreversible second wave with an E_{pc} of -1.743 V vs Fc/Fc$^+$ caused by the $[ArMo_6O_{18}]^{3/4-}$ reduction. A third, smaller, reduction wave at a less negative potential than the $[ArMo_6O_{18}]^{2/3-}$ wave resulted from the reversible reduction of unfunctionalised tetrabutylammonium hexamolybdate either left in the sample from the synthesis or created through decomposition of the sample while in solution during the experiment.
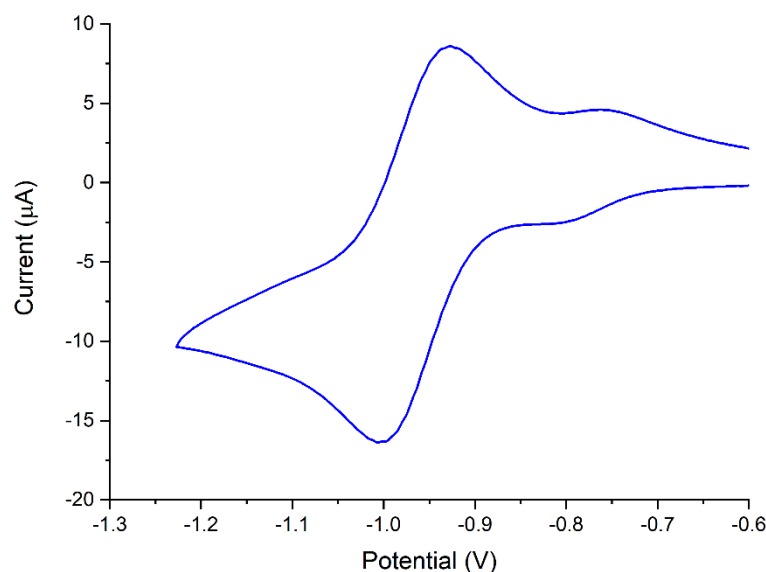
Figure 5.3b Cyclic voltammogram taken of compound **17** in 0.1 M [Bu$_4$N][BF$_4$] in MeCN. Fc/Fc$^+$ was used as the internal reference.

The $[ArMo_6O_{18}]^{2/3-}$ reductive wave of compound **17** appeared fully reversibly on the CV timescale and reversibility was confirmed by the linear peak current vs square root of scan rate relationship. The first reduction peak itself was at a less negative potential than seen for the corresponding peaks of both the monofunctionalised donor containing compounds synthesised in this work, compounds **4** to **8**, and the alkyne bridged analogue synthesised by Al-Yasari et al.. The less negative reduction of compound **17**, at -0.961 V vs -1.003 V for Al-Yasari's compound, suggested a less electron rich POM core, a result of weaker electron donation from the amine. This opposed the increased donor/acceptor coupling suggested by the electronic spectra and suggests more electronic isolation between the POM core and the electron donor in the alkene bridged compound.

162

5.4 DFT and TD-DFT Calculations

Like with compounds **3** to **10**, DFT calculations performed on compound **17** were used to assist with the analysis of the UV-vis absorption spectrum as well as predict the intensity of NLO responses. As in all previous calculations, CAM-B3LYP was used as the functional and 6-31++G(d,p) and LANL2DZ were used as the basis sets for the light and heavy atoms respectively. The solvent effects of acetonitrile were again modelled using SCRF and the W06 fitting set was used to produce UV-vis spectra from the calculated transitions. The geometry optimisation was performed prior to the TD-DFT and hyperpolarizability calculations, with the initial structure being produced in Avogadro due to no crystal structure data having been obtained. Calculations were also performed on compound **III** using the same functionals and basis sets for comparison.

Overall, the calculated spectrum for compound **17** was a good fit for the experimental data, with both the higher energy O to Mo peaks and the lower energy ligand to POM charge transfer peaks being present. As was seen for the calculations performed on compounds **3** to **10**, the calculations overestimated the intensity of the LPCT peak, and in this case underestimated the intensity of the O to Mo peaks. The considerable under estimation of the higher energy peak likely resulted from the limited number of transitions calculated, leaving more even higher energy transitions unaccounted for. Due to the large number of small high energy transitions, the number of states being calculated in these transitions is already high and although increasing this further could produce a predicted spectrum with more accurate high energy peaks, this would increase the time taken for each calculation to be performed and give little additional information. As with calculations performed on compounds **4**, **5**, **6**, and **9**, the calculations underestimated the intensity of the peaks at around 350 nm.

Interestingly, as can be seen from figure 5.4a, the calculations performed on compound **17** underestimated the energy of the charge transfer peak, observed experimentally at 436 nm and calculated to be 457 nm, and a similar result was seen for compound **III**. This was an unusual result as typically TD-DFT calculations performed on these monofunctionalised chromophores have resulted in higher energy transitions than seen in the experimental results. Examples of this include the work in chapter 3 as well as in literature published by Champagne et al..[163]
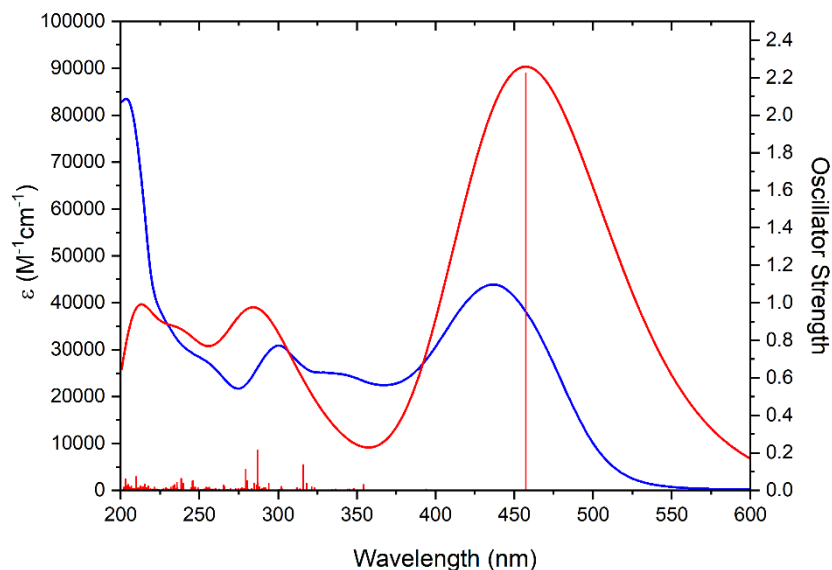
Figure 5.4a UV-vis absorption spectra of compound **17**, with the experimental spectrum shown in blue and the calculated spectrum shown in red. The Oscillator strength of the calculated spectrum is also included in red.

It is interesting that the use of the same basis sets, functionals, and solvent approximations had produced good results for compound **5** in chapter 3, a compound which has a similar donor and the same bridge between the donor and acceptor as compound **III**, and yet resulted in under estimations of the energy of the LPCT peak of compound **III**. It is possible this is a result of the methods used in this work better modelling compounds with the steric protecting groups in the 2 and 6 positions of the imido ring than those without. The X-ray crystallography data discussed in chapter 3 showed increased linearity of the imido bond with steric protection which should increase conjugation between the POM core and the imido ring. It is possible this enables the imido ring to act as part of the electron acceptor along with the POM core in contrast to the unprotected compounds where the entire ligand functions as the electron donor, resulting in increased electronic differences between the two systems.

The TD-DFT calculations performed were also used to identify which orbitals were involved in the predicted LPCT peaks. For both compounds **17** and **III**, the major contribution to the peak was a transition from the HOMO to the LUMO+3 orbital rather than the HOMO to the LUMO, a similar result to what was seen for the other monofunctionalised compounds. The HOMO of both compounds **17** and **III** was

situated primarily on the ligand with considerable electron density on the triarylamine. Like the LUMO, the LUMO+3 was situated almost entirely on the POM core for both compounds, suggesting the lowest energy peaks resulted primarily from ligand to POM charge transfer transitions. Surprisingly, very little difference between the orbitals of compound **17** and compound **III** could be seen despite the change in electron bridge.
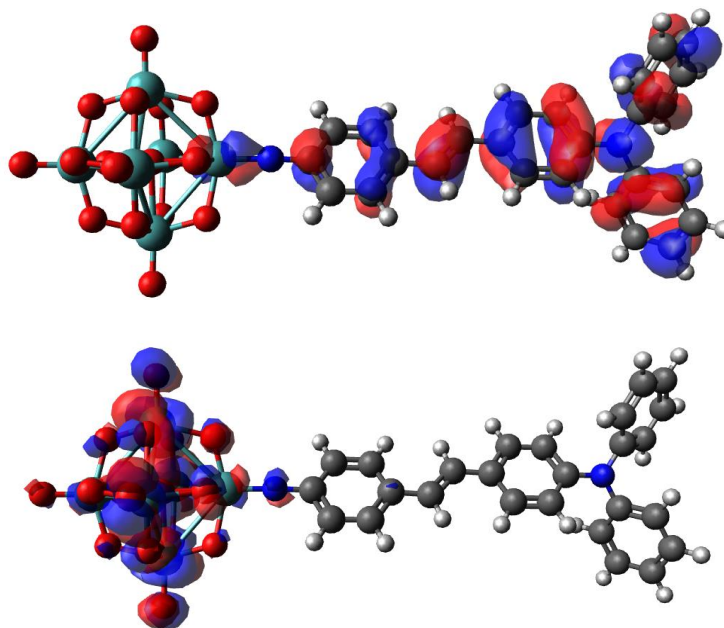
Figure 5.4b Calculations predicted the IHCT peak of compound **17** primarily resulted from transitions from the HOMO (top) to the LUMO+3 (bottom).

This very complete movement of electron density from the ligand to the POM was a slightly unexpected result in the case of compound **III** as the LUMO+4 orbital of compound **5**, the ditolyamino derivative, predicted some electron density remained on the imido ring even after excitation of the electron. This backs up the suggestion that the imido ring of the sterically protected derivatives may function more as part of the electron acceptor than in the unprotected derivatives due to their more conjugated imido bond. According to the two state model, this increased change in dipole moment would result in increased hyperpolarizability of the non-sterically protected compounds, although experimental comparison between diphenylethyne bridged dimethylamino derivatives **II** and **4** had already shown this was not always the case.

DFT calculations were also used to predict dynamic and static hyperpolarizabilities of compound **17**, with calculations also performed on compound **III** for comparison. These calculations predicted significantly higher $\beta_{zzz,1064}$ and $\beta_{zzz,0}$ values for compound **17** than compound **III**, 1092×10^{-30} esu compared to 886×10^{-30} esu for $\beta_{zzz,1064}$ and 891×10^{-30} esu compared to 743×10^{-30} esu for $\beta_{zzz,0}$, suggesting experimental hyperpolarizability could be improved through the inclusion of an alkene bridge in the place of the alkyne bridge previously used. This is likely a result of the increased strength of the donor/acceptor pair suggested by the decrease in the energy of both the LPCT peaks. A smaller difference was seen when $\beta_{zzz,0}$ was calculated from the calculated dynamic hyperpolarizability and λ_{max}, with values given of 233×10^{-30} esu for compound **17** and 249×10^{-30} esu for compound **III**. This, in contrast to the purely DFT calculated values of $\beta_{0,zzz}$, predicts a higher static hyperpolarizability of compound **III** than compound **17**, however the difference is only small.

	LPCT λ_{max} / (nm)	Calc λ_{max} (nm)	$\beta_{zzz,1064}$ ($\times10^{-30}$ esu)	$\beta_{zzz,0}{}^{a}$ ($\times10^{-30}$ esu)	$\beta_{zzz,0}{}^{b}$ ($\times10^{-30}$ esu)	$\beta_{zzz,0}{}^{c}$ ($\times10^{-30}$ esu)
17	437	457	1092	891	233	295
III	414	433	886	743	249	297

Table 3.3b Summary of experimental and computational β and UV-vis data for compounds **17** and **III**. Acetonitrile was used as the solvent in both the experimental and computational work. a was calculated purely using DFT. b was calculated using the DFT calculated values of λ_{max} and $\beta_{zzz,1064}$ by way of the two state model. c was calculated using the experimental value of λ_{max} and the DFT calculated $\beta_{zzz,1064}$ by way of the two state model.

5.5 Hyper-Rayleigh Scattering

Hyper-Rayleigh Scattering, previously used for the analysis of compounds **4** to **16**, was also used for the non-linear optical analysis of compound **17**. Analysis was performed using the same set up discussed in chapter two, with the incident beam again at 1064 nm and acetonitrile used as the solvent. As with the previous HRS runs discussed in this work, the internal reference method was used to analyse the data, and after calculation of $\beta_{zzz,1064}$, the static hyperpolarizability was calculated using the two-

state model. The HRS experiments gave compound **17** a $\beta_{zzz,1064}$ of 1040×10^{-30} esu and a $\beta_{zzz,0}$ of 281×10^{-30} esu, activities much higher than seen for any previously published POM based chromophore and only fractionally lower than that of compound **6**, a chromophore with a much stronger julolidine donor group.

	LPCT λ_{max} / (nm)	Calc λ_{max} (nm)	$\beta_{zzz,1064}$ ($\times10^{-30}$ esu)	Calc $\beta_{zzz,1064}$ ($\times10^{-30}$ esu)	$\beta_{zzz,0}$ ($\times10^{-30}$ esu)	Calc $\beta_{zzz,0}$ ($\times10^{-30}$ esu)
17	437	457	1040	1092	281	295
III	414	433	590	886	196	297

Table 5.5a Comparison of the experimental and DFT calculated absorption peaks, dynamic, and static polarizability for compounds **4** to **10**. Here, the calculated static polarizability was calculated from the DFT calculated dynamic hyperpolarizability and the experimental λ_{max} using the two-state model due to the inaccuracy of the purely DFT calculated value.

The hyperpolarizability of compound **17** was compared to that of compound **III** due to the similarity of the two compounds, with the hyperpolarizability activities of compound **III** used as published by Al-Yasari.[45] The $\beta_{zzz,1064}$ of compound **17**, 1040×10^{-30} esu, is almost double that of compound **III**, 590×10^{-30} esu, however once the difference in λ_{max} has been accounted for by converting to $\beta_{zzz,0}$, an increase of only 43% is seen, 281×10^{-30} esu compared to 196×10^{-30} esu for compound **III**. This increase is similar to what was seen for 4-(N,N-dimethylamino)-4'-nitrostilbene compared to its alkyne bridged analogue,[64] and confirms the hypothesis that hyperpolarizability of the hexamolybdate derivatives could be increased through the inclusion of an alkene bridge between the amine donor and the POM in place of the more commonly used alkyne. This is likely due to increased coupling between the donor acceptor pair, as can be seen from the longer wavelength LPCT peak in the UV-vis absorption spectra, as well as an increased change in dipole moment, as was suggested by the more complete transfer of electron density from the ligand into the POM core seen in the TD-DFT.

With the comparison of compounds **17** and **III** showing that inclusion of an alkene bond between the donor and acceptor in place of the alkyne often seen in these

compounds, it would be interesting to know what hyperpolarizability could be achieved through the inclusion of a stronger donor group such as julolidine too. It would also be interesting to know to what extent stability could be achieved by adding the diisopropyl protecting groups included in many of the compounds discussed in chapter 2, and whether these would also allow the alkene bridged derivatives to act as redox switchable NLO active chromophores.

5.6 Conclusion

In this chapter, the synthesis and analysis of an alkyne bridged polyoxometalate chromophore was discussed. Originally, synthesis of a compound with steric protection at the 2 and 6 positions of the imido ring was attempted, however the Heck couplings that had been successfully used by Zhu[39] to produce alkene containing POM derivatives proved fruitless in this work. In the end, the steric protecting groups were sacrificed to allow for ease of synthesis, and compound **17** was synthesised instead.

Investigation of compound **17** by UV-vis absorption spectroscopy showed a considerable redshift of the LPCT peak compared to compound **III**, an alkyne bridged analogue, which was hoped would equate to stronger NLO activity. Gaussian calculations also predicted an increase in hyperpolarizability compared to compound **III**. Hyper-Rayleigh Scattering confirmed this predicted increase, with the experiments giving compound **17** a $\beta_{zzz,0}$ of 281×10^{-30} esu, and increase of 43% over the 196×10^{-30} esu of compound **III**. This was also the second highest NLO activity recorded for such compounds and only fractionally lower than the activity shown by compound **6**, a chromophore with a much stronger julolidine donor group.

The increased NLO activity of alkene bridged chromophores over analogues with alkyne bridges has led to the possibility of hexamolybdate derivatives with even higher responses than previously seen. Inclusion of the diisopropyl groups used to stabilise the imido bond of a selection of the compounds discussed in chapter two would allow for the investigation into the stability of alkene bridged compounds when reduced with the hope of producing switchable chromophores with even higher NLO responses than has so far been seen so far for the alkyne bridged derivatives.

Chapter 6

Conclusions and Further Work

6.1 Conclusions

In this work, three series of novel polyoxometalate chromophores have been synthesised, characterised, and investigated by NMR, UV-vis and IR spectroscopy, electrochemistry, spectroelectrochemistry, and Hyper-Rayleigh Scattering. The first series of compounds consisted of five electron donor containing compounds, compounds **4** to **8**, two nitro acceptor containing compounds, compounds **9** and **10**, and two iodo functionalised compounds, compounds **2** and **3**, which were used predominantly for stability studies and as precursors for some donor and acceptor containing compounds. All nine of these compounds featured methyl or isopropyl groups at the 2 and 6 positions of the imido ring to provide steric protection for the imido bond. This in turn increased stability of the imido bond, and therefore the compounds, in the reduced state, a necessity to enable the redox activated switching for which these compounds were intended. Bulk electrolysis studies of the compounds showed significantly increased stability to hydrolysis compared to unprotected analogues, and this allowed for investigation of the optical properties of the reduced state to be probed by spectroelectrochemistry.

The spectroelectrochemistry experiments showed reversible changes in the LPCT peaks responsible for the NLO activity of the donor containing compounds, with the peaks shifting to a higher energy upon reduction. This suggested a weakening in charge transfer properties of compounds **4** to **8**, an achievement which would later prove to indeed result in a decrease in the hyperpolarizability of the NLO active compounds in their reduced states. The compounds featuring electron acceptors on their imido ring showed a shift of their IHCT peaks to a lower energy upon reduction, suggesting electron transfer from either the POM or the π system of the ligand to the nitro group. It was theorised that this could lead to off/on NLO switching of naturally NLO inactive compounds **9** and **10**, a theory which was later proven to be true in the case of compound **9**.

Hyper-Rayleigh Scattering experiments allowed for the determination of both the dynamic and static first hyperpolarizabilities of compounds **4** to **10**, with compounds showing equal or higher NLO activity than their non-protected analogues in all cases. Compound **6**, the julolidinyl functionalised chromophore, showed the highest hyperpolarizability of any POM derivative so far, and compounds **9** and **10** showed

surprising NLO activity considering their unprotected analogues had not shown activity when tested previously.

Redox activated NLO switching of compounds **6**, **8**, and **9** was performed, with switchable responses being observed for all three compounds. Compound **8**, the phenyl bridged, diisopropyl protected dimethylamino derivatives showed repeatable and reversable responses, with a 94% reduction of $\beta_{1064,zzz}$ being observed upon reduction. This could be fully reversed by re-oxidation of the sample. Compound **6** also showed switchable responses, with a reversible 65% weakening of $\beta_{1064,zzz}$ occurring upon reduction. Investigation of compound **9** by redox activated switching resulted in an impressive 14 fold increase in hyperpolarizability which was shown to be at least partially reversible upon re-oxidation. These compounds present the first experimental reports of both on/off and off/on switching of any type of polyoxometalate chromophore.

This work also explored the possibility of multidimensional POM based chromophores, with the intention of synthesising compounds with an increased efficiency over previously tested linear derivatives. Two different series of multidimensional chromophores were synthesised, one containing two-donor-one-acceptor derivatives and the other containing one-donor-two-acceptor derivatives. The family of two-donor-one-acceptor chromophores were made by coupling two ligands to one POM core, resulting in *bis*-substituted analogues of compounds **3**, **4**, and **8**. The UV-vis spectra of these revealed LPCT peaks of a similar energy but higher intensity to those seen for their monosubstituted analogues. Hyper-Rayleigh scattering experiments were used to determine $\beta_{0,HRS}$ for compounds **12** and **13** and the depolarization ratio for compound **13** which allowed both $\beta_{0,zzz}$ and $\beta_{0,yyz}$ to be calculated. These suggested significant off diagonal responses with only a small decrease of $\beta_{0,zzz}$ compared to that of the mono-substituted analogue and no decrease in transparency.

Three triarylamine based one-donor-two-accepter chromophores were also synthesised and analysed, with two POM cores being coupled to each ligand using the DCC mediated coupling reaction. UV-vis spectra of all three compounds showed significantly red-shifted LPCT peaks compared to the two-donor-one-acceptor and monofunctionalised derivatives, suggesting these compounds could have potentially

higher NLO responses. The spectrum of compound **15** also showed a considerably less intense LPCT peak than seen for any previous compound, a result of limited electronic connectivity between amine electron donor and the *meta* positioned POM cores. While Hyper-Rayleigh scattering experiments showed the hyperpolarizability of compound **15** was measurable but low, a result of the weakened conjugation between the amine and the POM cores, compounds **14** and **16** both showed strong responses, with the $\beta_{0,zzz}$ of 162.4×10^{-30} esu of compound **14** being higher than any previously synthesised short-bridged derivative and the $\beta_{0,yyz}$ of -101.7×10^{-30} esu showing a significant off diagonal response.

In order to investigate the effect of altering the bridge between the donor and acceptor in these compounds, a chromophore with an alkene bridge in the place of the alkyne bridges often seen in these compounds was synthesised. The UV-vis absorption spectroscopy of the compound showed a significantly red-shifted LPCT peak compared to a previously synthesised alkyne bridged analogue suggesting a stronger donor/acceptor communication. Hyper-Rayleigh scattering experiments later showed this resulted in increased hyperpolarizability of the alkene bridged chromophore over the previously synthesised alkyne bridged analogue, suggesting significant improvements in NLO activity could be brought about by the inclusion of the alkene bridge between the amine donor and the POM acceptor.

7.2 Further work

Possible paths for further work include the following:

- For possible use in future devices, solid phase NLO active materials would be needed, so it would be interesting and useful to investigate potential methods of achieving this. Alignment of the dipole of the chromophores would be necessary to achieve good responses and conductivity would be needed to allow for potential to be applied to initiate redox switching if required. Potential ideas would include oriented thin films or deposition on conductive glasses. The formation of crystalline materials of the chromophores would not allow for switching but could be used to form bulk NLO materials particularly of the multidimensional chromophores which showed good NLO responses but do not have the steric protection needed for switching.

172

- Of the NLO active compounds discussed in chapters 2 and 3, the phenylethyne bridged derivatives regularly showed higher NLO responses than their phenyl bridged analogues, and therefore improved switches could be discovered if a way to further prevent the decomposition of these compounds when reduced could be found. As this was caused by the fragmentation of the POM core itself, and observed more in coordinating solvents, this could be achieved by changing the solvent system or by the used of hexatungstate in the place of hexamolybdate as the POM core. Thus far very little success has been achieved with functionalised hexatungstate POMs, but work into the area is still ongoing so in the future synthesis of such systems may be possible.

- In order to increase stability of the highly NLO active materials discussed in chapters 4 and 5, work could be carried out to investigate possible methods of including steric protection of the imido bonds in the one-donor-two-acceptor multidimensional derivatives and the alkene bridged derivative. These compounds all demonstrated higher NLO activity than the monofunctionalised derivatives discussed in chapters 2 and 3, so increasing their stability to the point of enabling switching could result in compounds with higher contrast switching than demonstrated in this work.

- Polyoxometalate chromophores with possibly improved NLO activity could also be synthesised by combining successful elements of all the families of chromophores discussed in this work. For example, the synthesis of a sterically protected compound with a julolidinyl donor and an alkene bridge, or the synthesis of one-donor-two-acceptor systems with extended π bridges.

Chapter 7

Experimental

7.1 Materials

Dimethyl sulfoxide was purchased dry from Acros Organics in a sure seal bottle and used as supplied, acetonitrile and triethylamine were distilled over CaH_2 under a nitrogen atmosphere and stored over molecular sieves under argon/nitrogen. The acetonitrile used during HRS switching studies was purchased dry from Sigma Aldrich and used as received. All other reagents and solvents were obtained as ACS grade from Sigma Aldrich, Alfa Aesar, Fisher Scientific, Fluorochem, Acros Organics, or Apollo Scientific and used as supplied. Deuterated solvents were obtained from Eurisotop, Cambridge Isotope Laboratories, or Acros Organics and used as supplied.

7.2 General Methods

Synthesis of compounds **2** to **17** was carried out under an argon atmosphere using standard Schlenk techniques using a method based off one reported previously.[3] Organic synthesis was carried out under air unless otherwise stated. TLC plates were developed under UV light or using ninhydrin spray. Column chromatography was performed using silica as stationary phase. Precursors **P1** to **P17** were previously reported compounds. The methods used to synthesise them are described but full characterisation was not carried out where ^{1}H-NMR matched the literature.

7.3 Instrumentation

^{1}H-NMR and ^{13}C-NMR were performed using a Bruker Ascend 500 NMR spectrometer with shifts reported in ppm with respect to TMS using the solvent signals as a secondary standard. The quaternary carbon signals were not observed for compounds **2** to **17** using standard ^{13}C-NMR techniques. In some compounds, the shift of these peaks was identified using HSQC and HNBC techniques. FT-IR was performed using Bruker VERTEX 80 FTIR XSA spectrometer. UV-vis spectroscopy was performed using an Agilent Cary 60 UV-vis spectrophotometer. Mass spectrometry was performed by Lionel Hill at the John Innes Centre on a Shimadzu IT-ToF, using a Prominence/Nexera UPLC as a sample introduction system without chromatography. Elemental analysis was performed externally using services provided by London Metropolitan University and the University of Manchester.

7.4 X-ray Crystallography

Data was collected on a Rigaku XtalLab Synergy S diffractometer using a Photon-Jet Cu or Mo micro-focus source and a Hypix hybrid photon counting detector. Data reduction, cell refinement and absorption correction were carried out using Rigaku CrysAlisPro[175] and solved using SHELXT[176] in Olex2 V1.3.[177] Refinement was performed using the least squares method.

7.5 Electrochemistry

Cyclic voltammograms and differential pulse voltammograms were performed using an Autolab PGStat302N potentiostat in either a one compartment cell or a three compartment bulk electrolysis cell filled with 0.3-0.8 mM analyte solutions made up in 0.1 M NBu_4BF_4 in dry acetonitrile. The solutions were degassed prior to the experiments using acetonitrile saturated argon and blanketed with a continuous flow of acetonitrile saturated argon throughout the experiments. A glassy carbon working electrode, a platinum counter electrode, and a silver wire pseudo-reference electrode were used in all runs. For any samples also used for bulk electrolysis, the solutions of electrolyte were made up under an inert atmosphere and transferred to the dried and degassed bulk electrolysis cell by syringe. Bulk electrolysis runs were performed using a platinum gauze working electrode with vigorous stirring. The same counter and reference electrodes were used as for cyclic voltammetry. Spectroelectrochemistry was performed in an OTTLE cell[157] using 0.36 to 0.72 mM samples of analyte in 0.3 M NBu_4BF_4 solutions in dry acetonitrile. The potentials were applied using a μ-autolab III with the UV-vis absorbance traces recorded using an Agilent Cary 60 UV-vis spectrophotometer.

7.6 Hyper-Rayleigh Scattering

Hyper-Rayleigh Scattering was performed at KU Leven, Belgium, using a 1064 nm femtosecond pulsed source focused onto a 4mm cuvette for determination of β and the depolarization constant and a 10 mm cuvette for runs with electrochemical switching. The scattered light was measured at an angle of 90° to the incident beam using a spectrograph coupled to a charge-coupled device enabling wavelength detection.

During the β determination measurements and the electrochemical switching experiments, the scattered light was measured without discriminating Z and X polarized light. A schematic of the setup is shown in chapter 3.

During the runs with electrochemical switching, samples of analyte were made up in 0.3 M solutions of NBu_4BF_4 in dry acetonitrile under a nitrogen atmosphere. Potential was applied using a Princeton Applied Research Parstat 2273 Advanced Electrochemical System. The electrodes were the same as were used during bulk electrolysis with each housed in a separate compartment within the specially made cell. A detailed schematic of the cell is included in chapter 3. HRS scans were taken at five second intervals with a series of ten taken before application of the potential to create a baseline. In most cases, 400 seconds of reductive potential was applied before switching was reversed by application of a 0 V potential. Details on data work up are given in chapters 3 and 4. The measurements of the compounds discussed in chapter 4 were performed by Dr Yovan de Coene at KU Leuven in Belgium.

7.7 DFT and TD-DFT

Density Functional Theory calculations were performed using Gaussian 16 installed on the ADA cluster at the University of East Anglia. B3LYP, CAM-B3LYP, and ωB97Xd were tested for use as functionals. 6-31++G(d,p) and 6-311G(d,p) were tested for use as basis sets for the lighter atoms while LANL2DZ and SSD were tested for use as the basis sets for the heavier atoms. Ultimately, CAM-B3LYP, 6-31++G(d,p), and LANL2DZ were used for calculations of all compounds with SCRF used to model solvent effects. The W06 fitting set as used to produce electronic spectra from transitions calculated during TD-DFT.

7.8 Compound Numbering

Compounds **P1** to **P21** are precursors used in the synthesis of the hexamolybdate derivatives. Compounds **2** to **17** are the hexamolybdate derivatives studied in this work, with compounds **2** to **10** being the monofunctionalised derivatives discussed in chapters **2** and **3**, compounds **11** to **16** being the multidimensional chromophores

discussed in chapter **4** and compound **17** being the alkyne bridged derivative discussed in chapter **5**. Compound **1** is tetrabutylammonium hexamolybdate.

7.9 Compound Synthesis

Preparation of 4-iodo-2,6-dimethylaniline (P1)
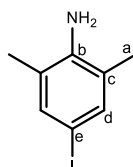
The preparation of compound **P1** was carried out under an argon atmosphere using standard Schlenk techniques. The procedure used was based on the method of B. R. D'Souza.[178]

To a mixture of 2,6-dimethylaniline (2.00 g. 16.5 mmol), and sodium bicarbonate (8.82g, 105 mmol) in 20 ml methanol, iodine monochloride solution in dichloromethane (1 M, 18.5 ml, 18.5 mmol) and 90 ml dichloromethane was added dropwise over the course of 1 hour. This reaction was stirred at room temperature for 48 hours. Solids were filtered from the mixture to give a red solution and the solvent was removed from the filtrate in vacuo to leave a dark red oil. To this, a 60 ml solution of saturated sodium thiosulfate was added, and this solution was stirred for 10 minutes before extracting with 3×200 ml portions of diethyl ether. The organic extracts were dried with magnesium sulfate, filtered, and then the filtrate was removed in vacuo to give 4-iodo-2,6-dimethylaniline (3.56 g, 14.4 mmol) as a black solid with an 87% yield.

^{1}H-NMR (500 MHz, CDCl$_3$) δ 7.24 (2H, s, H-d), 3.58 (2H, s, H-N), 2.13 (6H, s, H-a). FTIR: 3324 (br), 2967 (sh), 2906 (br), 2848 (sh), 1605 (s), 1574 (m), 1468 (s), 1377 (w), 1328 (m), 1310 (m), 1262 (m), 1224 (m), 1166 (m), 1089 (m), 1026 (m), 847 (s), 809 (m), 764 (s) cm^{-1}.

Preparation of 4-iodo-2,6-diisopropylaniline (P2)
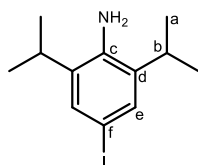
The preparation of compound **P2** was carried out under an argon atmosphere using standard Schlenk techniques. The procedure used was based on the method of B. R. D'Souza.[1]

To a mixture of 2,6-diisopropylaniline (5.3 ml, 4.98 g, 28.1 mmol) and sodium bicarbonate (7.106 g, 84.6 mmol) in 40 ml of dry methanol, a solution of iodine monochloride in dichloromethane (1 M, 30 ml, 30 mmol) was added dropwise over the course of five minutes. The mixture was stirred for 18 hours at room temperature to give a red solution over the pale solid. The solids were removed by filtration to give a red solution from which the solvent was removed to give a red oil. To this, 150 ml of saturated sodium thiosulfate solution was added and the mixture was stirred for 10 minutes before extracting with 3×100 ml of ethyl acetate. The organic extracts were dried over magnesium sulfate, filtered, and then the solvent was removed in vacuo to give 4-iodo-2,6-diisopropylaniline as a red oil (7.002 g, 23.1 mmol) with an 82% yield.

^{1}H-NMR (500 MHz, CDCl$_3$) δ 7.28 (2H, s, H-e), 3.78 (2H, s, H-N), 2.85 (2H, sept, J = 6.3 H-b), 1.25 (12H, d, J = 6.8 Hz, H-a). FTIR: 3486 (w), 3400 (w), 2960 (s), 2928 (sh), 2870 (m), 1739 (w), 1616 (s), 1571 (m), 1459 (s), 1437 (s), 1384 (m), 1363 (sh), 1348 (s), 1299 (w) 1249 (s) 1207 (s), 1124 (m), 1098 (sh), 1062 (m), 923 (w), 887 (w), 864 (s), 832 (m), 765 (m), 715 (m) cm^{-1}. UV-vis (MeCN) λ, nm (ε, M^{-1} cm^{-1}): 210 (28.3×10^{-3}); 252 (10.9×10^{-3}); 296 (2.60 ×10^{-3}).

Preparation of 4-bromophenyl-4,4'-ditolylamine (P3)
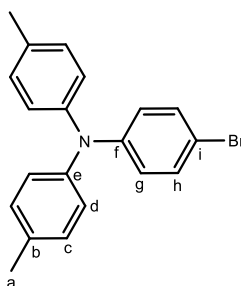
The preparation of compound **P3** was carried out under an argon atmosphere using standard Schlenk techniques. The procedure used was based on a method reported by W. Man.[140]

Di-p-tolylamine (4.761 g, 24.1 mmol), 1-bromo-4-iodobenzene (7.520 g, 26.6 mmol), tris(dibenzylideneacetone)dipalladium(0) (0.221 g, 0.241 mmol), 1,1'-bis(diphenylphosphino) ferrocene (0.405 g, 0.731 mmol), and sodium tert-butoxide (3.48 g, 36.2 mmol) dissolved in 15 ml of toluene. The resulting red solution was refluxed for 75 hours and then filtered once cool to produce a brown solution. The solvent was then removed to produce a brown oil which after purification by column chromatography in hexane:dichloromethane 97:3 gave compound **P3** as an off white solid (6.723 g, 19.1 mmol) with a 79% yield.

^{1}H-NMR (500 MHz, CDCl$_3$) δ 7.27 (2H, d, J = 8.9 Hz, H-h), 7.06 (4H, d, H-d), 6.97 (4H, d, J = 8.4 Hz, H-c), 6.89 (2H, d, J = 8.8 Hz, H-g), 2.31 (6H, s, H-a).

Preparation of 4-trimethylsilyethylphenyl-4,4'-ditolylamine (P4)
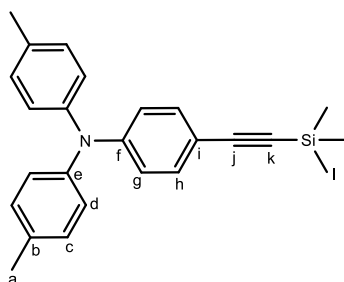
The preparation of compound **P4** was carried out under an argon atmosphere using standard Schlenk techniques. The procedure used was based on a method previously reported by S. Yamada.[179]

Compound **P3** (3.007 g, 8.54 mmol), copper iodide (0.157 g, 0.824 mmol), triphenylphosphine (0.232 g, 0.885 mmol), bis(triphenylphosphine) palladium(II) dichloride, (0.171 g, 0.244 mmol), and Trimethylsilylacetylene (1.8 ml, 1.242 g, 12.6 mmol) were dissolved in 30 ml triethylamine. The resulting yellow solution was refluxed for 20 hours then filtered to give a yellow solution. The solution was stirred with 40 ml of saturated ammonium chloride solution and then extracted with 2×40 ml ethyl acetate. The resulting solution was dried over magnesium sulfate and then the solvent was removed in vacuo to give the compound **P4** as a yellow oil (2.416 g, 6.54 mmol) with a 77% yield.

^{1}H-NMR (500 MHz, CDCl$_3$) δ 7.27 (2H, d, J = 8.8 Hz, H-g), 7.07 (4H, d, J = 8.2 Hz, H-d), 6.98 (4H, d, J = 8.4 Hz, H-c), 6.88 (2H, d, J = 8.8 Hz, H-h), 2.31 (6H, s, H-a), 0.23 (9H, s, H-l). ^{13}C-NMR (126 MHz, CDCl$_3$) δ 144.80, 133.41, 132.95, 130.14, 125.32, 121.06, 115.00, 20.99, 0.25.

Preparation of 4-ethylphenyl-4,4'-ditolylamine (P5)
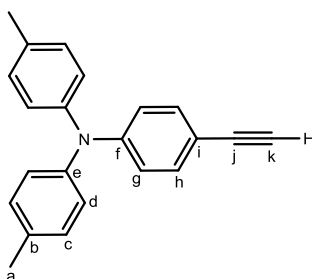
To compound **P4** (2.416 g, 6.54 mmol) in 6 ml of methanol and 6 ml tetrahydrofuran, potassium carbonate (1.826 g, 13.2 mmol) was added and resulting mixture was stirred for 3 hours under an argon atmosphere. After filtering, the resulting yellow solution was stirred with 40 ml of saturated ammonium chloride solution before extracting into 2×40 ml of ethyl acetate. The organic layer was washed with brine and dried over magnesium sulfate before the solvent was removed in vacuo to give compound **P5** (1.490 g, 5.01 mmol) as a yellow solid with a 77% yield.

^{1}H-NMR (500 MHz, CDCl$_3$) δ 7.30 – 7.27 (2H, m, H-g), 7.08 (4H, d, J = 8.1 Hz, H-d), 7.02 – 6.98 (4H, m, H-c), 6.92 – 6.88 (2H, m, H-h), 3.00 (1H, s, H-k), 2.32 (6H, s, J = 6.3 Hz, H-a). FTIR: 3262 (s), 3032 (w), 2919.21 (w), 2858 (m), 2102 (m), 2009 (m), 1643 (s), 1498 (s), 1317 (s), 1293 (s), 1270 (sh) 1174 (m), 1109 (m), 1019 (w) 833 (sh), 813 (s) cm^{-1}.

Preparation of N-tosyl-2,6-diisopropylaniline (P6)
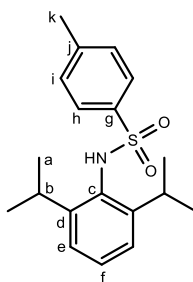
The preparation of compound **P6** was carried out under an argon atmosphere using standard Schlenk techniques in a method previously reported by F. Calver.[147]

Toluene sulfonyl chloride (10.124 g, 47.5 mmol) and 2,6-diisopropylaniline (9 ml, 8.46 g, 47.7 mmol) dissolved in 20 ml dry pyridine to give a yellow solution which was refluxed for 4 hours. The resulting orange solution was poured into 60 ml of 2M hydrochloric acid to give an orange solid which was collected by filtration and purified by recrystallisation in hot ethanol to give compound **P6** as colourless crystals (10.781 g, 32.5 mmol) in a 68% yield.

^{1}H-NMR (500 MHz, CDCl$_3$) δ 7.59 (2H, d, J = 8.3 Hz, H-ar), 7.25-7.20 (3H, m, 5.0 Hz, H-ar), 7.09 (2H, d, J = 7.7 Hz, H-ar), 6.13 (1H, s, H-N), 3.12 (2H, hept, J = 6.8 Hz, H-b), 2.39 (3H, s, H-k), 0.99 (12H, d, J = 6.9 Hz, H-a).

Preparation of N-tosyl-4-nitro-2,6-diisopropylaniline (P7)
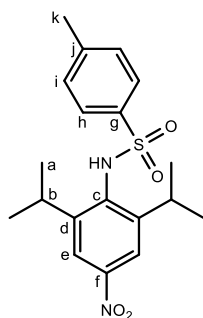
Compound **P7** was prepared as previously reported by F. Calver.[4]

To a mixture of compound **P6** (3.505 g, 10.6 mmol), 70 ml of water, and 15 ml nitric acid, 70 ml of glacial acetic acid was added followed by sodium nitrite (1.115 g, 16.2 mmol). The mixture was refluxed for 12 hours and then, once cooled, poured into 200 ml of water to give a pale yellow solution with a pale precipitate. Over the course of 2 days, pale yellow crystals formed which were then collected by filtration, washed with water, and dried in vacuo to give compound **P7** (2.242 g, 5.96 mmol) in a 56% yield.

^{1}H-NMR (500 MHz, CDCl$_3$) δ 7.97 (2H, s, H-e), 7.59 (2H, d, J = 7.7 Hz, H-h), 7.28 (2H, d, J = 7.7 Hz, H-i), 6.19 (1H, s, H-N), 3.23 – 3.14 (2H, hept, J = 6.8 Hz, H-b), 2.43 (3H, s, H-k), 1.06 (12H, d, J = 6.8 Hz, H-a).

Preparation of 4-nitro-2,6-diisopropylaniline (P8)
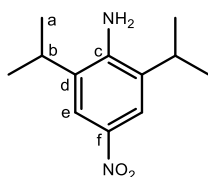
Compound **P8** was prepared as previously reported by F. Calver.[4]

Compound **7** (1.400 g, 3.72 mmol) was dissolved in 20 ml of 95% sulfuric acid and the resulting brown solution was left to stir at under argon overnight. The resulting dark brown solution was then poured over ice and made basic with sodium hydroxide before extracting into DCM. The orange organic layer was dried over magnesium sulfate before the solvent was removed in vacuo to give compound **P8** (0.546 g, 2.46 mmol) as a yellow solid in an 66% yield.

^{1}H-NMR (500 MHz, CDCl$_3$) δ 7.97 (2H, s, H-e), 4.48 (2H, s, H-N), 2.87 (2H, hept, J = 6.8 Hz, H-b), 1.31 (12H, d, J = 6.8 Hz, H-a).

Preparation of N-tosyl-4-amino-2,6-diisopropylaniline (P9)
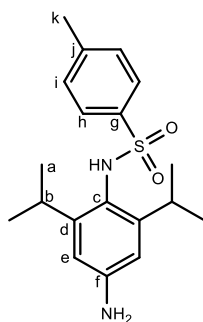
The preparation of compound **P9** was carried out under an argon atmosphere using standard Schlenk techniques using a method previously reported by F. Calver.[4]

Compound **P7** (0.101 g, 0.269 mmol) and tin(II) chloride dihydrate (0.200 g, 0.105 mmol) were dissolved in 6 ml degassed ethanol with heating. The resulting yellow solution was refluxed for 23 hours and then poured over ice to give a white precipitate. The resulting mixture was made basic with sodium bicarbonate and then extracted with ethyl acetate. The organic layer was dried over magnesium sulfate and then the solvent was removed in vacuo to give compound **P9** as a pale yellow solid (0.092 g, 0.266 mmol) in a 99% yield.

^{1}H-NMR (500 MHz, CDCl$_3$) δ 7.60 (2H, d, J = 8.3 Hz, H-h), 7.23 (2H, d, J = 7.2 Hz, H-i), 6.39 (2H, s, H-e), 5.83 (1H, d, J = 55.4 Hz, H-N), 3.65 (2H, s, H-N), 3.03 (2H, hept, J = 6.6 Hz, H-b), 2.40 (3H, s, H-k), 0.95 (12H, d, J = 6.8 Hz, H-a).

Preparation of N-tosyl-4-dimethylamino-2,6-diisopropylaniline (P10)
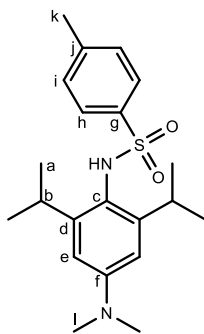
Compound **P10** was prepared as previously reported by F. Calver.[2]

A slurry of compound **P9** (0.970 g, 2.80 mmol) and sodium borohydride (0.817 g, 21.6 mmol) in 25 ml of tetrahydrofuran was slowly added to a solution of 40% aqueous formaldehyde (1.4 ml, 15.2 mmol) in 3 M hydrochloric acid (3 ml, 0.009 mmol) whilst keeping the temperature below 15ºC using an ice bath. When the addition was complete the mixture was made basic using sodium hydroxide and then the organic layer was decanted. The remaining slurry was extracted twice with ether and then the organic fractions were combined and dried over magnesium sulfate. The solvent was removed in vacuo to give compound **P10** as an off white solid (0.966 g, 2.58 mmol) in a 92% yield.

^{1}H-NMR (500 MHz, CDCl$_3$) δ 7.62 (2H, d, J = 8.3 Hz, H-h), 7.24 (2H, d, J = 8.0 Hz, H-i), 6.42 (2H, s, H-e), 5.79 (1H, s, H-N), 3.07 (2H, hept, J = 6.3 Hz, H-b), 2.95 (6H, s, H-l), 2.40 (3H, s, H-l), 0.99 (12H, d, J = 6.8 Hz, H-b).

Preparation of 4-dimethylamino-2,6-diisopropylaniline (P11)
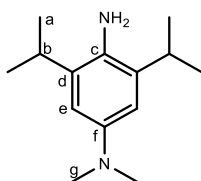
Compound 11 was prepared as previously reported by F. Calver.[2]

Compound **P10** (0.929 g, 2.48 mmol) was dissolved in 15 ml of 95% sulfuric acid and the resulting brown solution was left to stir at 40ºC overnight. The resulting dark brown solution was then poured over ice and made basic with sodium hydroxide before extracting into DCM. The orange organic layer was dried over magnesium sulfate before the solvent was removed in vacuo to give compound **P11** as a purple oil (0.451 g, 2.05 mmol) in an 83% yield.

^{1}H-NMR (500 MHz, CDCl$_3$) δ 6.53 (2H, s, H-e), 3.32 (2H, s, H-N), 2.90 (2H, hept, J = 6.7 Hz, H-b), 2.77 (6H, d, J = 7.1 Hz, H-g), 1.20 (12H, d, J = 6.8 Hz, H-a). FTIR: 2957 (s), 2868 (m), 2828 (w), 2782 (m), 1602 (s), 1481 (s), 1437 (sh), 1382 (w), 1353 (m), 1256 (m), 1216 (m), 1096 (m), 983 (s), 927 (w), 842 (m), 755 (m). UV-vis (MeCN) λ, nm (ε, M^{-1} cm^{-1}): 206 (26.7 ×10^3); 256 (11.7 ×10^3); 318 (3.04 ×10^3).

Preparation of 4-iodojulolidine (P12)
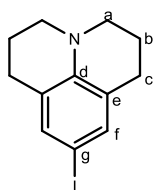
The preparation of compound **P12** was carried out under an argon atmosphere using dry solvents and standard Schlenk techniques.

To a solution of julolidine (2.500 g, 14.4 mmol) in 60 ml dioxane and 75 ml pyridine at 0°C, iodine (11 g, 43.3 mmol) was added. After stirring at room temperature for 2.5 hours, the reaction was quenched with saturated sodium thiosulfate. Extracting into dichloromethane, washing with water, then drying with magnesium sulfate and removing the solvent under vacuum gave compound **P12** (3.588 g, 12.0 mmol) as a dark orange oil in an 83% yield.

^{1}H-NMR (500 MHz, CDCl$_3$) δ 7.05 (t, J = 0.9 Hz, 2H, H-f), 3.19 – 3.04 (m, 4H, H-a), 2.69 (t, J = 6.5 Hz, 4H, H-b), 2.00 – 1.87 (m, 4H, H-c).

Preparation of 4-ethynyljulolidine (P13)
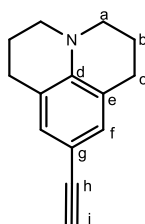
The preparation of compound **P13** was carried out under an argon atmosphere using degassed solvents and standard Schlenk techniques. The procedure was based on a method previously reported by B. Breiten.[142]

To a mixture of 4-iodojulolidine (3.203 g, 10.7 mmol), bis(triphenylphosphine) palladium(II) dichloride (0.209 g, 0.30 mmol), and copper iodide (0.099 g, 0.90 mmol) in 100 ml of diisopropylamine, ethynyltrimethylsilane (1.8 ml, g, 13.8 mmol) was added. The resulting mixture was stirred at room temperature for 3 days before being added to 125 ml of hexane and filtered through celite. The solvent was removed to give a dark oil which was dissolved in 25 ml of tetrahydrofuran and 25 ml of methanol. Potassium carbonate (4.503 g, 32.5 mmol) was added and the mixture stirred for 3 hours before filtering and removing the solvent under vacuum. Purification by column chromatography in DCM gave compound **P13** (1.186 g, 6.01 mmol) as a yellow oil with a 56% yield.

^{1}H-NMR (500 MHz, CDCl$_3$) δ 6.93 (t, J = 0.8 Hz, 2H, H-f), 3.17 (t, J = 5.6 Hz, 4H, H-a), 2.91 (s, 1H, H-i), 2.70 (t, J = 6.4 Hz, 4H, H-b), 1.96 – 1.91 (m, 4H, H-c).

Preparation of 4-(4-nitrophenylethenyl)-N,N-diphenylaniline (P14)
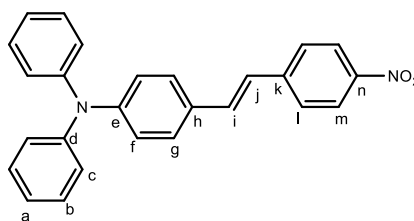
Compound **P14** was prepared using an adaption of a method previously reported by Ding.[172]

A mixture of 4-nitrophenylacetic acid (1.629 g, 8.99 mmol), 4-diphenylaminobenzaldehyde (0.820 g, 3.00 mmol), and piperidine (0.9 ml, 9.11 mmol) were stirred at 130°C for 5 hours before unreacted 4-diphenylaminobenzaldehyde was removed under vacuum. The red solid was then washed twice with ethanol before pure product was achieved by recrystallisation from hot ethanol. Compound **P14** (0.670 g, 1.71 mmol) was obtained as an orange solid in a 57% yield.

^{1}H-NMR (500 MHz, (CD$_3$)$_2$SO) δ 8.21 (d, J = 8.9 Hz, 2H, H-m), 7.82 (d, J = 8.9 Hz, 2H, H-l), 7.57 (d, J = 8.8 Hz, 2H, H-g), 7.48 (d, J = 16.4 Hz, 1H, H-i), 7.34 (dd, J = 8.5, 7.4 Hz, 4H, H-b), 7.26 (d, J = 16.4 Hz, 1H, H-j), 7.10 (tt, J = 7.5, 1.1 Hz, 2H, H-a) 7.07 (dd, J = 7.4, 1.1 Hz, 4H, H-c), 6.96 (d, J = 8.8 Hz, 2H, H-f).

Preparation of 4-(4-aminophenylethenyl)-N,N-diphenylaniline (P15)
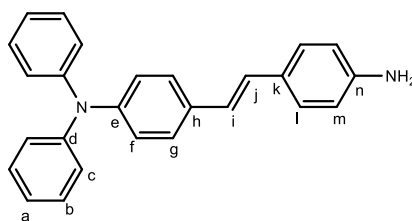
The preparation of compound **P14** was carried out under an argon atmosphere using dry solvents and standard Schlenk techniques.

To a mixture of compound **P14** (0.126 g, 0.321 mmol) and palladium on carbon 10% (0.014 g) in 4 ml ethanol, hydrazine hydrate (0.1 ml, 2.06 mmol) was added. The resulting mixture was refluxed for 30 minutes before filtering while hot. Upon cooling, yellow solid formed. This was collected by filtration to give compound **P15** (0.074 g, 0.204 mmol) as a yellow solid in a 64% yield.

^{1}H-NMR (500 MHz, (CD$_3$)$_2$SO) δ 7.41 (d, J = 8.6 Hz, 2H, H-g), 7.30 (dd, J = 8.5, 7.3 Hz, 4H, H-b), 7.24 (d, J = 8.6 Hz, 2H, H-f), 7.06 – 6.98 (m, 6H, H-a,c), 6.96 – 6.91 (m, 3H, H-i,l), 6.84 (d, J = 16.4 Hz, 1H, H-j), 6.55 (d, J = 8.5 Hz, 2H, H-m), 5.27 (s, 2H, H-NH).

Preparation of 4,4'-dinitro-4''-methyltriphenylamine (P16)
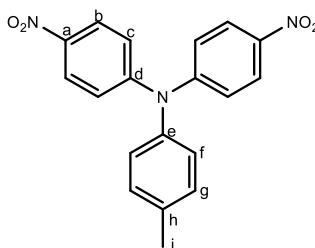
Compound **P16** was prepared using a method previously reported by Hsiao[166] under an argon atmosphere using dry solvents and standard Schlenk techniques.

1-fluoro-4-nitrobenzene (1.219 g, 8.64 mmol), p-toluidine (0.463, 4.32 mmol), and caesium fluoride (1.500 g, 9.9 mmol) were dissolved in 10 ml of dry dimethylsulfoxide. The resulting yellow solution was heated to 120ºC for 22 hours. The orange precipitate formed on cooling was collected by filtration, washed with water, methanol, then ethanol. The product was purified by purified by recrystallisation from hot DMF/methanol vapour diffusion, to give compound **P16** as an orange solid (0.512 g, 1.47 mmol) in a 34% yield.

^{1}H-NMR (500 MHz, CDCl$_3$) δ 8.16 – 8.10 (m, 4H, H-b), 7.25 – 7.22 (m, 2H, H-g), 7.16 – 7.11 (m, 4H, H-c), 7.06 (d, J = 8.4 Hz, 2H, H-f), 2.40 (s, 3H, H-i).

Preparation of 4,4'-diamino-4''-methyltriphenylamine (P17)
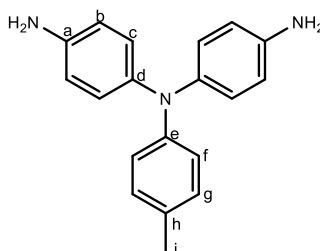
The preparation of compound **P17** was carried out under an argon atmosphere using dry solvents and standard Schlenk techniques.

Compound **P16** (0.294 g, 0.85 mmol) and tin chloride dihydrate (1.25 g, 6.59 mmol) were suspended in 20 ml of dry ethanol and set to reflux for 17 hours. The reaction was poured into ice, made basic with sodium bicarbonate, and then extracted with ethyl acetate. The organic layer was dried over magnesium sulfate, filtered, and then the solvent was removed under vacuum to give compound **P17** a dark orange solid (0.255g, 0.88 mmol) in an 100% yield. This was reacted on without further purification.

^{1}H-NMR (500 MHz, (CD$_3$)$_2$SO) δ 6.88 (dt, J = 7.3, 0.8 Hz, 2H, H-g), 6.73 (d, J = 8.6 Hz, 4H, H-c), 6.55 (d, J = 8.5 Hz, 2H, H-f), 6.53 – 6.48 (m, 4H, H-b), 4.90 (s, 4H, H-N), 2.16 (s, 3H, H-i).

Preparation of 3,5-dinitro-4',4''-dimethyltriphenylamine (P18)
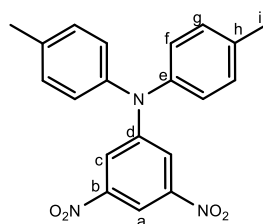
The preparation of compound **P18** was carried out under an argon atmosphere using dry solvents and standard Schlenk techniques.

1-bromo-3,5-dinitrobenzene (1.894 g, 11.2 mmol), di-p-tolylamine (1.556 g, 7.89 mmol), x-phos (0.329 g, 0.69 mmol), bis(acetonitrile)dichloropalladium(II) (0.060 g, 0.23 mmol) and potassium carbonate (1.483 g, 10.7 mmol) were suspended in 15 ml of dry tert-butanol and the resulting mixture refluxed for between 48 and 112 hours. When cool, the reaction mixture was poured into water, extracted with ethyl acetate, and the organic phase dried with magnesium sulfate, then filtered. The solvent was removed under vacuum to give a dark solid that was purified by washing with hexane and then recrystallising from hot hexane. Compound **P18** was obtained as orange crystals (1.604 g, 4.41 mmol) in a 56% yield.

^{1}H-NMR (500 MHz,CDCl$_3$) δ 8.35 (t, J = 2.0 Hz, 1H, H-a), 7.94 (d, J = 1.9 Hz, 2H, H-c), 7.23 – 7.17 (m, 4H, H-g), 7.09 – 7.04 (m, 4H, H-f), 2.37 (s, 6H, H-i). ^{13}C-NMR (126 MHz, CDCl$_3$) δ 150.73, 149.42, 142.49, 136.45, 131.16, 126.11, 117.16, 108.38, 21.17. Anal (Calcd) % for C$_{17}$H$_{17}$N$_3$O$_4$): C, 40.73 (66.11); H, 6.61 (4.72); N, 4.75 (11.56). FTIR: 3103 (vw), 3036 (vw), 2920 (vw), 2863 (vw), 1627 (w), 1609 (vw), 1540 (s), 1508 (s), 1457 (m), 1343 (s), 1327 (sh), 1303 (w), 1280 (m), 1231 (vw), 1213 (vw), 1196 (vw), 1177 (vw), 1112 (w), 1073 (w), 1021 (w), 933 (vw), 908 (w), 875 (w), 848 (w), 832 (w), 814 (m), 725 (s), 696 (sh), 653 (m), 588 (m). Anal (Calcd) % for C$_{58}$H$_{92}$N$_4$O$_{18}$Mo$_6$: C, 66.24 (66.11); H, 4.76 (4.72); N, 11.42 (11.36). MS (MALDI) = calcd for C$_{20}$H$_{17}$N$_3$O$_4$$^+$ 363.12, found 363.05. UV-vis (MeCN) λ, nm (ε, M^{-1} cm^{-1}): 281 (23.9×10^{-3}); 373 (2.97×10^{-3}).

Preparation of 3,5-diamino-4',4''-dimethyltriphenylamine (P19)

The preparation of compound **P19** was carried out under an argon atmosphere using dry solvents and standard Schlenk techniques.

Compound **P18** (1.137 g, 3.13 mmol), hydrazine monohydrate (0.6 ml, 12.0 mmol) and palladium on carbon 10% (0.140 g) were suspended in 40 ml of dry ethanol. The mixture was refluxed for 18 hours and then filtered while hot to give a colourless solution which cooled to give pure compound **P19** as colourless crystals (0.625 g, 2.06 mmol) in a 66% yield.

^{1}H-NMR (500 MHz, (CD$_3$)$_2$SO) δ 7.02 (d, J = 8.4 Hz, 4H, H-g), 6.83 (d, J = 8.4 Hz, 4H, H-f), 5.51 (t, J = 1.9 Hz, 1H, H-a), 5.46 (d, J = 1.8 Hz, 2H, H-c), 4.65 (s, 4H, H-NH), 2.22 (s, 6H, H-i). ^{13}C-NMR (126 MHz, (CD$_3$)$_2$SO) δ 149.79, 148.79, 145.53, 130.63, 129.50, 123.51, 99.34, 95.46, 20.32. Anal (Calcd) % for C$_{20}$H$_{21}$N$_3$: C, 79.08 (79.17); H, 7.04 (6.98); N, 13.63 (13.85). MS (MALDI) = calcd for C$_{20}$H$_{21}$N$_3{}^+$ 303.17, found 303.23. FTIR: 3392 (m), 3318 (m), 3204 (w), 3020 (vw), 2916 (vw), 2857 (vw), 1592 (s), 1504 (s), 1491 (s), 1474 (sh), 1364 (w), 1317 (w), 1271 (m), 1240 (s), 1182 (s), 1154 (m), 1112 (vw), 1020 (w), 836 (sh), 815 (s), 755 (m), 712 (w), 686 (s), 617 (m), 597 (m), 554 (w). UV-vis (MeCN) λ, nm (ε, M^{-1} cm^{-1}): 253 (18.2×10^{-3}); 300 (21.1×10^{-3}).

Preparation of 2,4-dinitro-4',4''-dimethyltriphenylamine (P20)

Compound **P20** was prepared under an argon atmosphere using dry solvents and standard Schlenk techniques.

To a solution of di-4-tolylamine (0.788g, 4.00 mmol) and sodium hydride 60% in oil (0.160) stirred in 4ml dimethylsulfoxide for 20 minutes at room temperature, dinitrofluorobenzene (0.51 ml, 4.03 mmol) was added. After heating to 140°C for 19 hours, the cooled solution was poured into 40 ml water and 40 ml methanol to produce an oily solid collected by filtration. Purified by column chromatography in dichloromethane followed by recrystallisation from hot ethanol gave compound **P20** (0.287 g, 0.790 mmol) as orange crystals in a 20% yield.

^{1}H-NMR (500 MHz, (CD$_3$)$_2$SO) δ 8.59 (d, J = 2.7 Hz, 1H, H-f), 8.30 (dd, J = 9.3, 2.7 Hz, 1H, H-b), 7.20 (d, J = 9.3 Hz, 1H, H-c), 7.17 (d J = 8.5 Hz, 4H, H-i), 6.92 (d, J = 8.5 Hz, 4H, H-k), 2.29 (s, 6H, H-k). ^{13}C-NMR (126 MHz, (CD$_3$)$_2$SO) δ 145.64, 142.80, 140.68, 139.80, 135.21, 130.46, 128.30, 126.31, 124.40, 123.04, 20.48. Anal (Calcd) % for C$_{17}$H$_{17}$N$_3$O$_4$): C, 65.83 (66.11); H, 4.42 (4.72); N, 11.39 (11.56). MS (MALDI) = calcd for C$_{20}$H$_{17}$N$_3$O$_4^+$ 363.12, found 363.11. FTIR: 3101 (vw), 3082 (vw), 2920 (vw), 2862 (vs), 1594 (s), 1533 (w), 1508 (s), 1478 (m), 1421 (vw), 1347 (sh), 1328 (s), 1298 (sh), 1280 (s), 1243 (sh), 1243 (sh), 1214 (m), 1152 (m), 1135 (w), 1113 (w), 1069 (vw), 1044 (vw), 1019 (vw), 978 (vw), 934 (vw), 914 (vw), 898 (m), 833 (vw), 815 (m), 801 (s), 757 (sh), 742 (m), 732 (m), 714 (m), 689 (sh), 652 (w), 623 (vw), 599 (w), 559 (m). UV-vis (MeCN) λ, nm (ε, M^{-1} cm^{-1}): 251 (19.5×10^{-3}); 410 (15.0×10^{-3}).

Preparation of 2,4-diamino-4,4'-dimethyltriphenylamine (P21)

The preparation of compound **P21** was carried out under an argon atmosphere using dry solvents and standard Schlenk techniques.

To compound **P20** (0.203 g, 0.559 mmol) and palladium on carbon 10% (0.0237 g) in 8 ml of ethanol, hydrazine hydrate (0.120 ml, g, 2.47 mmol) was added and the resulting mixture heated to reflux for 30 minutes. After the reaction appeared complete by TLC, the solid was removed by filtration and the volume reduced under vacuum to produce an off-white precipitate which was collected by filtration and washed with ethanol to give compound **P21** (0.045 g, 0.148 mmol) as an off-white solid with a 26% yield.

^{1}H-NMR (500 MHz, (CD$_3$)$_2$SO) δ 7.04 – 6.93 (m, 4H, H-i), 6.84 – 6.77 (m, 4H, H-h), 6.56 (d, J = 8.2 Hz, 1H, H-b), 5.98 (d, J = 2.5 Hz, 1H, H-c), 5.86 (dd, J = 8.3, 2.5 Hz, 1H, H-f), 4.81 (s, 2H, H-NH), 4.41 (s, 2H, H-NH), 2.20 (s, 6H, H-k). ^{13}C-NMR (126 MHz, (CD$_3$)$_2$SO) δ 147.95, 145.7, 144.96, 130.31, 129.37, 129.23, 120.63, 120.02, 104.47, 100.57, 20.22. MS (MALDI) = calcd for C$_{20}$H$_{21}$N$_3^+$ 303.17, found 303.28. FTIR: 3483 (w), 3429 (w), 3374 (w), 3338 (w), 3022 (vw), 2917 (vw), 2857 (vw), 1889 (vw), 1620 (m), 1607 (m), 1503 (s), 1460 (w), 1310 (m), 1289 (m), 1270 (sh), 1251 (s), 1206 (w), 1107 (w), 1036 (w), 1020 (vw), 965 (w), 833 (sh), 809 (s), 782 (sh), 755 (vw), 731 (w), 704 (w), 636 (w), 607 (sh), 564 (sh), 547 (m). UV-vis (MeCN) λ, nm (ε, M^{-1} cm^{-1}): 212 (55.0×10^{-3}); 302 (22.9×10^{-3}).

7.10 Polyoxometalate Synthesis

Preparation of C₃₂H₇₂N₂O₁₉Mo₆ (1)

Preparation of $C_{32}H_{72}N_2O_{19}Mo_6$ **(1)**

Sodium molybdate dihydrate (25.001 g, 121.4 mmol) dissolved in 100 ml of water before 6M hydrochloric acid (29 ml, 174 mmol) was added dropwise over 2-3 minutes to give a yellow solution. A solution of tetrabutylammonium bromide (12.104 g, 37.5 mmol) was added resulting in a white precipitate in a colourless solution that was then heated to 80ºC for forty five minutes. The resulting yellow precipitate was collected by filtration, washed with water, and then recrystallised from 700 ml of hot acetonitrile. Compound **1** was collected as yellow crystals (17.433 g, 12.8 mmol) in a 63% yield.

FTIR: 2962 (m), 2932 (sh), 2873 (m), 1469 (m), 1379 (m), 1175 (w), 1149 (w), 1106 (w), 1065 (w), 1030 (w), 951 (s), 880 (m), 787 (s), 739 (sh), 592 (m). UV-vis (MeCN) λ, nm (ε, M^{-1} cm^{-1}): 222 (25.0×10³); 255 (15.3×10³); 326 (7.8×10³).

Preparation of C$_{40}$H$_{80}$N$_3$O$_{18}$Mo$_6$I (2)

4-iodo-2,6-dimethylaniline (0.252 g, 1.02 mmol) tetrabutylammonium hexamolybdate (1.776 g, 1.30 mmol) and DCC (0.309 g, 1.49 mmol) dissolved in 15 ml of dry dimethylsulfoxide to form a brown solution. This was heated at 70°C for 10 hours which resulted in a red solution with a pale precipitate. The precipitate was removed by filtration and the solution precipitated by slow addition to a mixture of 200 ml of diethyl ether and 50 ml of ethanol. The resulting orange precipitate was collected from the orange solution by filtration and washed with ethanol and ether to give crude compound 1 (0.963 g, 0.615 mmol). Purification was achieved by recrystallisation from hot acetonitrile to give compound **2** (0.640 g, 0.41 mmol) as dark orange crystals with a 40% yield.

^{1}H-NMR (500 MHz, CD$_3$CN): δ 7.47 (2H, s, H-g), 3.12 – 3.05 (16H, m, H-a), 2.55 (6H, s, H-e), 1.65 – 1.54 (16H, m, H-b), 1.36 (16H, hex, J = 7.0 Hz, H-c), 0.97 (24H, t, J = 7.4 Hz, H-d). ^{13}C-NMR (126 MHz, CD$_3$CN): δ 153.68 (C-f), 140.59 (C-g), 136.73 (C-h), 93.85 (C-i) 59.28 (C-a), 24.32 (C-b), 20.30 (C-c), 18.05 (C-e) 13.80 (C-d). Anal (Calcd) % for C$_{40}$H$_{80}$N$_3$O$_{18}$Mo$_6$I C, 30.13 (30.22); H, 5.06 (5.17); N, 2.64 (2.70). HRMS (ESI, MeCN) = calcd for C$_8$H$_8$NO$_{18}$Mo$_6$I^{2-} 555.1573, found 555.1548. FTIR: 2959 (m), 2932 (sh), 2873 (m), 1564 (w), 1479 (m), 1456 (sh), 1378 (m), 1319 (m), 1248 (m), 1170 (w), 1151(w), 1107 (w), 1064 (w), 1026 (w), 974 (m), 945 (s), 881 (m), 858 (m), 772 br), 744 (s) cm^{-1}. UV-vis (MeCN) λ, nm (ε, M^{-1} cm^{-1}): 203 (53.4×10^3); 246 (36.9×10^3); 364 (27.5×10^3).

Preparation of C₄₄H₈₈N₃ O₁₈Mo₆I (3)

Tetrabutylammonium hexamolybdate (1.778 g, 1.32 mmol), DCC (0.310 g, 1.50 mmol), and 4-iodo-2,6-diisopropanylaniline (0.386 g, 1.27 mmol) were dissolved in 15 ml of dry dimethylsulfoxide to form a brown solution. This was heated at 70ºC for 10 hours which resulted in a red solution with a pale precipitate. The precipitate was removed by filtration and the solution precipitated by slow addition to a mixture of 200 ml of diethyl ether and 50 ml of ethanol. The resulting orange precipitate was collected from the orange solution by filtration and washed with ethanol and ether to give crude compound 3. Purification was achieved by recrystallisation from hot acetonitrile to give compound **3** (0.751 g, 0.455 mmol) as dark orange crystals with a 36% yield.

^{1}H-NMR (500 MHz, CD₃CN): δ 7.51 (2H, s, H-h), 3.78 (2H, hept, J = 6.8 Hz, H-f), 3.26 – 2.95 (16 H, m, H-a), 1.65 – 1.55 (16H, m, H-b), 1.36 (16H, m, J = 7.0 Hz, H-c), 1.27 (12H, d, J = 6.8 Hz, H-e), 0.97 (24H, t, J = 7.5 Hz H-d). ^{13}C-NMR (126 MHz, CD₃CN): δ 151.26 (C-g) 132.51 (C-h), 95.28 (C-j), 59.29 (C-a), 29.44 (C-f), 24.32 (C-b), 23.86 (C-e), 20.30 (C-c) 13.80 (C-d). Anal (Calcd) % for C₄₄H₈₈N₃O₁₈Mo₆I: C, 32.02 (32.18); H, 5.38 (5.48); N, 2.55 (2.60). HRMS (ESI, MeCN) = calcd for $C_{12}H_{16}NO_{18}Mo_6I^{2-}$ 581.6888, found 581.6875. FTIR: 2960 (m), 2933 (sh), 2873 (m), 1560 (w), 1479 (m), 1461 (w), 1418 (m), 1380 (m), 1363 (sh), 1337 (m), 1168 (w), 1148 (w), 1107 (w), 1068 (w), 1028 (w), 974 (m), 943 (s), 882 (w), 855 (sh), 769 (w). UV-vis (MeCN) λ, nm (ε, M^{-1} cm^{-1}): 204 (47.9×10³); 247 (33.3×10³); 364 (23.5×10³).

Preparation of C₅₄H₉₈N₄O₁₈Mo₆ (4)

Compound **3** (0.617 g, 0.374 mmol), 1-ethynyl-N,N-dimethylbenzenamine (0.0652 g, 0.449 mmol), copper iodide (0.0034 g), bis(triphenylphosphine) palladium(II) dichloride (0.0074 g) and potassium carbonate (0.375 g) were dissolved in dry acetonitrile (15 ml) before dry triethylamine (0.75 ml) was added. The resulting mixture was stirred at room temperature for 30 minutes before filtering. The filtrate was evaporated to 2 ml then poured into ethanol (50 ml) resulting in a dark red precipitate. This was collected by filtration, washed with ethanol and diethyl ether and then dried in vacuo to give compound **4** as a dark red solid (0.332 g, 0.201 mmol) with a 54 % yield.

^{1}H-NMR (500 MHz, CD$_3$CN): δ 7.37 (2H, d, J = 9.0 Hz, H-n), 7.25 (2H, s, H-h), 6.73 (2H, d, J = 9.0 Hz, H-o), 3.83 (2H, hept, J = 6.9 Hz, H-f), 3.13 – 3.06 (16H, m, H-a), 1.66 – 1.56 (16H, m, H-b), 1.36 (16H, dq, J = 14.8, 7.5 Hz, H-c), 1.31 (12H, d, J = 6.8 Hz, H-e), 0.97 (24H, t, J = 7.4 Hz, H-d). ^{13}C-NMR (500 MHz, CD$_3$CN): δ 132 (C-h), 59.40 (C-a), 29.55 (C-f), 24.41 (C-b), 23.96 (C-e), 20.42 (C-c) 13.89 (C-d). Anal (Calcd) % for C$_{54}$H$_{98}$N$_4$O$_{18}$Mo$_6$: C, 38.90 (38.90); H, 5.93 (5.89); N, 3.36 (3.35). (ESI, MeCN) = calcd for C$_{22}$H$_{26}$N$_2$Mo$_6$O$_{18}{}^{2-}$ 591.7767, found 591.7750. FTIR: 2960 (m), 2932 (sh), 2872 (m), 2187 (m), 1606 (m), 1585 (m), 1585 (s), 1521 (m), 1445 (m), 1350 (w), 1227 (w), 1191 (m), 1169 (m), 1150 (m), 1063 (w), 974 (s), 943 (m), 882 (w), 855 (sh), 769 (w), 740 (sh). UV-vis (MeCN) λ, nm (ε, M^{-1} cm^{-1}): 203 (73.6×10^3); 293 (37.1×10^3); 424 (37.6×10^3).

Preparation of C$_{66}$H$_{106}$N$_4$O$_{18}$Mo$_6$ (5)

To compound **3** (1.433 g, 0.941 mmol), **P5** (0.4163 g, 1.428 mmol), bis(triphenylphosphine) palladium(II) dichloride (12.6 mg, 0.018 mmol), copper iodide (8 mg, 0.04 mmol), and potassium carbonate (0.898 g, 6.50 mmol), 35 ml dry acetonitrile and triethylamine (1.8 ml, 1.306 g, 12.9 mmol) were added. The resulting red solution was stirred for 45 minutes to give a brown solution which was then filtered, evaporated to ~3 ml, and then poured into 200 ml of diethyl ether. The resulting dark red precipitate was collected by filtration, washed with ethanol and ether, and then dried in vacuo. NMR analysis showed the reaction had not gone to completion so the product was stirred with bis(triphenylphosphine) palladium(II) dichloride (3 mg, 0.004 mmol), copper iodide (3 mg, 0.02 mmol), and potassium carbonate (0.203 g, 1.47 mmol), 35 ml dry acetonitrile, trimethylamine (0.45 ml, 0.327 g, 3.23 mmol), and **P5** (0.058 g, 0.199 mmol) were added and the resulting solution was stirred for a further 35 minutes. The reaction was filtered, evaporated to ~3 ml, and then poured into 200 ml of diethyl ether. The resulting dark red precipitate was collected by filtration, washed with ethanol and ether, and then dried in vacuo to give compound **5** as a dark red solid (0.795 g, 0.438 mmol) with a 47 % yield.

^{1}H-NMR (500 MHz, CD$_3$CN) δ 7.33 (2H, d, J = 8.8 Hz, H-o), 7.28 (2H, s, H-h), 7.16 (4H, d, J = 8.1 Hz, H-r), 7.00 (4H, d, J = 8.4 Hz, H-n), 6.86 (2H, d, J = 8.8 Hz, H-n), 3.83 (2H, sept, J = 6.7 Hz, H-f), 3.15 – 3.06 (16H, m, H-a), 2.31 (6H, s, H-u), 1.66 – 1.56 (16H, m, H-b), 1.38 (16H, hex, J = 8 Hz, H-c), 1.31 (12H, d, J = 6.8 Hz, H-e), 0.97 (24H, t, J = 7.4 Hz, H-d). ^{13}C-NMR (126 MHz, CD$_3$CN): δ 149.80, 145.35, 134.99, 133.43, 131.11, 126.50, 126.00, 121.05, 59.28, 29.43, 24.31, 23.94, 20.84, 20.30, 13.78. Anal (Calcd) % for C$_{66}$H$_{106}$N$_4$O$_{18}$Mo$_6$: C, 43.57 (43.89); H, 5.87 (6.03);

N, 3.08 (3.02). HRMS (ESI, MeCN) = calcd for $C_{34}H_{34}N_2Mo_6O_{18}{}^{2-}$ 666.8079, found 666.8062. FTIR: 3485 (w), 2400 (w), 2960 (s), 2928 (sh), 2869 (m), 1739 (w), 1616 (s), 1571 (m), 1459 (s), 1437 (s), 1384 (sh), 1363 (w), 1348 (s), 1298 (w), 1249 (m), 1062 (m), 1207 (m), 1124 (w), 1098 (sh), 1062 (m), 923 (w), 887 (sh), 864 (s), 832 (m), 765 (m), 715 (m) cm^{-1}. UV-vis (MeCN) λ, nm (ε, M^{-1} cm^{-1}): 206 (90.4×10^3), 294 (33.1×10^3); 329 (19.0×10^3); 423 (39.4×10^3).

Preparation of C$_{58}$H$_{102}$N$_4$O$_{18}$Mo$_6$ (6)

To a mixture of compound **3** (0.618 g, 0.388 mmol), compound **P13** (0.106 g, 0.537 mmol), copper iodide (0.003 g, 0.027 mmol), bis(triphenylphosphine)palladium(II) chloride (0.009 g, 0.013 `mmol) and potassium carbonate (0.361 g, mmol) in 15 ml of dry acetonitrile, dry triethylamine (0.8 ml, 5.74 mmol) was added. The resulting mixture was stirred at room temperature for 30 minutes before filtering, evaporating to 2 ml, and pouring into 50 ml of diethyl ether. The resulting red oil was collected by decanting the solution then washing with ethyl acetate and diethyl ether. Drying in vacuo gave compound **6** as a dark red solid (0.372 g, 0.216 mmol) with a 56% yield. Further purification of 90 mg of sample was achieved by crystallisation from an acetone/diethyl ether diffusion to give pure compound **6** (0.041 g, 0.024 mmol) in an overall 26% yield.

^{1}H-NMR (500 MHz, (CD$_3$)$_2$CO) δ 7.18 (2H, s, H-h), 6.88 (2H, s, H-n), 3.98 (2H, sept, J = 6.8 Hz, H-f), 3.47 – 3.44 (16H, m, H-a), 3.21 (4H, t, J = 5.7 Hz, H-s), 2.70 (4H, t, J = 6.3, H-q), 1.92 (4H, m, H-r), 1.86 – 1.80 (16H, m, H-b), 1.45 (16H, hex, J = 6.8 Hz, H-c), 1.32 (12H, d, J = 6.9 Hz, H-e), 0.98 (24H, t, J = 7.3 Hz, H-d). ^{13}C-NMR (126 MHz, ((CD$_3$)$_2$CO) δ 131.09, 125.29, 121.85, 59.37, 50.42, 28.17, 24.54, 24.16, 22.44, 20.41, 15.61, 13.96. Anal (Calcd) % for C$_{58}$H$_{102}$N$_4$O$_{18}$Mo$_6$: C, 40.52 (40.86); H, 5.98 (5.95); N, 3.26 (3.24). HRMS (ESI, MeCN) = calcd for C$_{26}$H$_{30}$N$_2$Mo$_6$O$_{18}$$^{(2-)}$ 617.7933, found 617.7923. FTIR: 2960 (m), 2933 (sh), 2872 (m), 2187 (m), 1605 (sh), 1584 (m), 1511 (m), 1464 (m), 1380 (w), 1310 (m), 1249 (vw), 1208 (vw), 1185 (vw), 1145 (vw), 1170 (vw), 1052 (vw), 1030 (vw), 973 (m), 943 (s), 880 (m), 765 (s) 609 (w). UV-vis (MeCN) λ, nm (ε, M^{-1} cm^{-1}): 212 (65.3×10^3); 259 (30.3×10^3); 308 (30.0×10^3); 445 (37.8×10^3).

Preparation of C₄₂H₈₆N₄O₁₈Mo₆ (7)
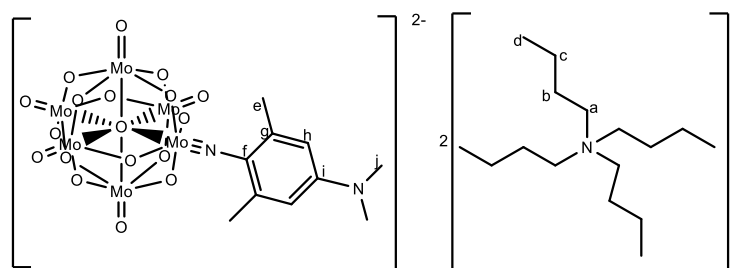
To a solution of tetrabutylammonium hexamolybdate (1.000 g, 0.733 mmol) and DCC (0.170 g, 0.824 mmol) dissolved in 10 ml of dry dimethylsulfoxide, 4-dimethyamino-2,6-dimethylaniline (0.118 g, 0.718 mmol) was added to form a brown solution which was then heated at 70ºC for 10 hours. After cooling, a pale precipitate was removed by filtration and the resulting red solution precipitated by slow addition to a mixture of 34 ml of diethyl ether and 135 ml of ethanol. After vigorous stirring to encourage flocculation, the precipitate was collected by filtration and washed with ethanol and ether to give compound **7** (0.832 g, 0.551 mmol) as a brown powder with a 77 % yield. Further purification of 0.685 g of sample was achieved by crystallisation from hot acetonitrile to give pure compound **7** (0.347 g, 0.223 mmol) in an overall 39% yield.

^{1}H-NMR (500 MHz, CD₃CN) δ 6.34 (s, 2H, H-h), 3.13 – 3.06 (m, 16H, H-a), 3.04 (s, 6H, H-j), 2.57 (d, $J = 0.7$ Hz, 6H, H-e), 1.65 – 1.56 (m, 16H, H-b), 1.36 (h, $J = 7.4$ Hz, 16H, H-c), 0.97 (t, $J = 7.4$ Hz, 24H, H-d). ^{13}C-NMR (126 MHz, CD₃CN): δ 141.25, 110.60, 94.09, 59.27, 40.18, 24.29, 20.29, 18.97, 13.76. Anal (Calcd) % for C₄₂H₈₆N₄O₁₈Mo₆: C, 33.39 (33.05); H, 5.74 (5.52); N, 3.71 (3.52). HRMS (ESI, MeCN) = calcd for C₁₀H₁₄N₂Mo₆O₁₈$^{2-}$ 512.7303, found 512.7293. FTIR: 2960 (s), 2932 (sh), 2872 (m), 1598 (m), 1501 (sh), 1479 (m), 1361 (m), 1233 (vw), 1155 (w), 1107 (vw), 1064 (vw), 1028 (vw), 970 (m), 924 (s), 880 (w), 771 (vs). UV-vis (MeCN) λ, nm (ε, M^{-1} cm^{-1}): 205 (46.1×10³); 257 (28.9×10³); 430 (33.3×10³).

Preparation of C₄₆H₉₄N₄O₁₈Mo₆ (8)
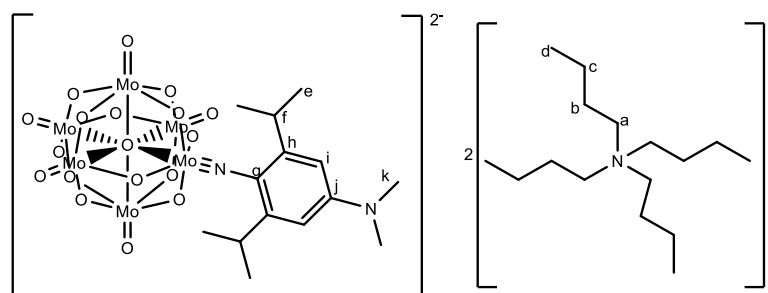
To compound **1** (0.999 g, 0.732 mmol) and DCC (0.170 g, 0.824 mmol), 10 ml of dry DMSO and **P11** (0.153 g, 0.694 mmol) were added. The resulting dark green solution was heated at 70ºC for 10 hours. When cool, the red solution was filtered to remove the pale precipitate and then poured into 40 ml of ethanol and 230 ml of diethyl ether. The resulting dark precipitate was collected by filtration, washed with ethanol and ether and then dried in vacuo to give crude compound **8** as a brown solid (0.911 g, 0.581 mmol) with a 79% yield. Further purification of 0.571 mg of sample was achieved by crystallisation from hot acetonitrile to give pure compound **8** (0.322 g, 0.206 mmol) in an overall 45% yield.

^{1}H-NMR (500 MHz, CD$_3$CN) δ 6.39 (s, 2H, H-i), 3.82 (hept, J = 6.8 Hz, 2H, H-f), 3.14 – 3.05 (m, 22H, H-k (3.09) and H-a), 1.66 – 1.55 (m, 16H, H-b), 1.36 (h, J = 7.4 Hz, 16H, H-c), 1.29 (d, J = 6.8 Hz, 12H, H-e), 0.97 (t, J = 7.4 Hz, 24H, H-d). ^{13}C-NMR (126 MHz, CD$_3$CN) δ 152.25, 106.08, 59.52, 40.51, 30.02, 24.54, 24.36, 20.53, 14.01. Anal (Calcd) % for C$_{46}$H$_{94}$N$_4$O$_{18}$Mo$_6$: C, 35.26 (35.11); H, 6.05 (5.98); N, 3.58 (3.58). HRMS (ESI, MeCN) = calcd for C$_{14}$H$_{22}$N$_2$Mo$_6$O$_{18}$$^{2-}$ 540.7617, found 540.7609. FTIR: 2959 (m), 2932 (sh), 2872 (m), 1590 (m), 1480 (m), 1462 (sh), 1372 (m), 1313 (m), 1233 (w), 1170 (m), 1125 (vw), 1108 (vw), 1065 (vw), 1029 (vw), 997 (w), 970 (m), 940 (s), 880 (w), 772 (s). UV-vis (MeCN) λ, nm (ε, M^{-1} cm^{-1}): 206 (44.3×10^3); 258 (28.1×10^3); 431 (30.7×10^3).

Preparation of C$_{52}$H$_{92}$N$_4$O$_{20}$Mo$_6$ (9)

Compound **3** (0.309 g, 0.19 mmol), 1-ethynyl-4-nitrobenzene (0.033 g, 0.22 mmol), CuI (0.002 g, 0.01 mmol), bis(triphenylphosphine)palladium(II) chloride (0.038 g, 0.05 mmol) and K$_2$CO$_3$ (0.180 g, 1.30 mmol) were degassed then dissolved in 7.5 ml of dry acetonitrile before dry triethylamine (0.4 ml, 2.87 mmol) was added. The resulting mixture was stirred at room temperature for 30 minutes before filtering, evaporating to 1 ml, and pouring into 50 ml of ethanol. The resulting orange precipitate was collected by filtration, washed with ethanol and diethyl ether and then dried in vacuo to give compound **4** as an orange solid (0.167 g, 0.10 mmol) with a 53% yield. Further purification of 145 mg of sample was achieved by crystallisation from hot acetonitrile to give pure compound **9** (47 mg, 0.028 mmol) in an overall 17% yield.

^{1}H-NMR (500 MHz, CD$_3$CN): δ 8.24 (2H, d, J = 9.0 Hz, H-o), 7.74 (2H, d, J = 9.0 Hz, H-m), 7.40 (2H, s, H-i), 3.86 (2H, hept, J = 6.9 Hz, H-f), 3.10 – 3.07 (16H, m, H-a), 1.63 – 1.57 (16H, m, H-b), 1.39-131 (28H, m, H-c,e), 0.97 (24H, t, J = 7.4 Hz, H-d). Anal (Calcd) % for C$_{52}$H$_{92}$N$_4$O$_{20}$Mo$_6$: C, 37.42 (37.67); H, 5.57 (5.62); N, 3.36 (3.29). HRMS (ESI, MeCN) = calcd for C$_{20}$H$_{20}$N$_2$Mo$_6$O$_{20}$$^{2-}$ 591.7489, found 591.7443. FTIR: 2961 (m), 2934 (sh), 2873(m), 2199 (m), 1594 (m), 1516 (m), 1461 (m), 1380 (m), 1363 (s), 1339 (m), 1245 (w), 1172 (w), 1153 (w), 1107 (w), 974 (m), 942 (vs) 882 (m), 854 (m) 767 (vs), UV-vis (MeCN) λ, nm (ε, M^{-1} cm^{-1}): 200 (67.7×10^3); 246 (37.3×10^3); 276 (30.4×10^3); 399 (53.7×10^3);.

Preparation of C$_{44}$H$_{88}$N$_4$O$_{20}$Mo$_6$ (10)
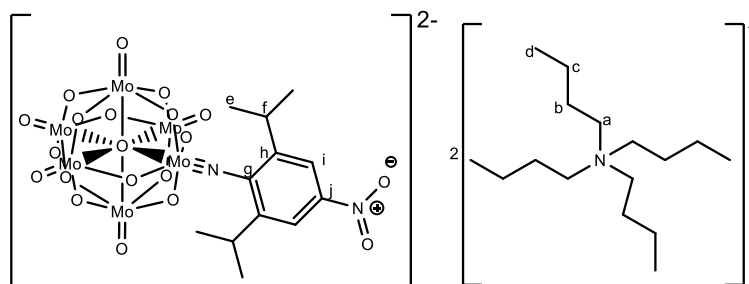
Compound **1** (0.500 g, 0.366 mmol), compound **P8** (0.077 g, 0.35 mmol) and DCC (0.079 g, 0.038 mmol), were dissolved in 5 ml of dry DMSO. The resulting yellow solution was heated at 70°C for 10 hours. When cool, the orange solution was filtered to remove the pale precipitate and then poured into a mixture of 100 ml diethyl ether and 20 ml of ethanol. A yellow solid was removed from the solution by filtration. Upon further addition of diethyl ether, an orange precipitate formed, which was then collected by filtration, washed with ethanol and diethyl ether and dried in vacuo to give crude compound **10** as an orange solid (0.157 g, 0.100 mmol) with a 29% yield. Further purification was achieved by recrystallisation from hot acetonitrile cooled to 4°C to give pure compound **10** (0.035 g, 0.022 mmol) in an overall 6% yield.

^{1}H-NMR (500 MHz, CD$_3$CN): δ 7.99 (2H, s, H-ar), 3.88 (2H, hept, J = 6.8 Hz, H-f), 3.11 – 3.08 (16H, m, H-a), 3.09 (6H, s, H-k), 1.64 – 1.58 (16H, m, H-b), 1.35c (16H, hep, J = 7.5 Hz, H-c), 1.34 (12H, d, J = 6.8 Hz, H-e), 0.97 (24H, t, J = 7.4 Hz, H-d). ^{13}C-NMR (126 MHz, CD$_3$CN) δ 155.59 (C-g), 150.43 (C-h), 146.87 (C-j), 118.30 (C-i), 59.34 (C-a), 29.86 (C-f), 24.40 (C-b), 23.70 (C-e), 20.37 (C-c), 13.87 (C-d). Anal (Calcd) % for C$_{44}$H$_{88}$N$_4$O$_{20}$Mo$_6$: C, 33.68 (33.80); H, 5.65 (5.68); N, 3.57 (3.55). HRMS (ESI, MeCN) = calcd for C$_{12}$H$_{16}$N$_2$Mo$_6$O$_{20}$$^{2-}$ 541.7331, found 541.7310. FTIR: 2962 (m), 2935 (sh), 2873(m), 1579 (m), 1515 (m), 1481 (sh), 1461 (m), 1422 (sh), 1380 (w), 1324 (s), 1259 (m), 1149 (w), 1108 (m), 1093 (m), 1073 (m), 1026 (m), 975 (m), 942 (vs), 883 (sh), 767 (vs) UV-vis (MeCN) λ, nm (ε, M^{-1} cm^{-1}): 201 (46.2×10^3); 382 (24.7×10^3).

Preparation of C$_{56}$H$_{104}$N$_4$O$_{17}$Mo$_6$ (11)

To tetrabutylammonium hexamolybdate (1.999 g, 1.46 mmol) and DCC (0.756 g, 3.68 mmol) dissolved in 15 ml of dry dimethylsulfoxide, 4-iodo-2,6-diisopropanylaniline (0.887 g, 2.93 mmol). The resulting brown solution was heated at 95°C for 24 hours. When cool, a pale yellow precipitate was removed by filtration and the solution precipitated by slow addition to a mixture of 400 ml of diethyl ether and 80 ml of ethanol. The yellow precipitate was removed, and more diethyl ether added until an orange precipitate formed. This was collected by filtration, washed with ethanol and diethyl ether, and then purified by recrystallisation from hot acetonitrile to give compound **11** (0.160 g, 0.083 mmol) as dark orange crystals with a 6% yield.

^{1}H-NMR (500 MHz, CD$_3$CN): δ 7.47 (2H, s, H-i), 3.82 (2H, hept, J = 6.8 Hz, H-f), 3.13 – 3.06 (16H, m, H-a), 1.60 (16H, tt, J = 8.2, 6.2 Hz, H-b), 1.36 (16H, hep, J = 7.4 Hz, H-c), 1.26 (12H, d, J = 6.9 Hz, H-e), 0.96 (24H, t, J = 7.4 Hz, H-d). ^{13}C-NMR (126 MHz, CD$_3$CN) δ 150.63, 132.38, 94.01, 59.28, 29.31, 24.29, 23.94, 20.31, 20.29, 13.77. Anal (Calcd) % for C$_{56}$H$_{104}$N$_4$O$_{17}$Mo$_6$: C, 34.76 (34.60); H, 5.42 (5.54); N, 2.90 (2.99). HRMS (ESI, MeCN) = calcd for C$_{24}$H$_{32}$N$_2$Mo$_6$O$_{17}$I^{2-} 725.7080, found 725.7063. FTIR: 2959 (m), 2931 (sh), 2872 (m), 1560 (m), 1476 (m), 1417 (sh), 1381 (m), 1361 (w), 1336 (m), 1309 (w), 1293 (s) 1229 (sh), 1169 (m), 1146 (sh), 1108 (w), 1069 (w), 1030 (w), 965 (s), 937 (vs), 882 (m), 863 (m), 759 (vs). UV-vis (MeCN) λ, nm (ε, M^{-1} cm^{-1}): 206 (82.8×10^3); 252 (61.0×10^3); 366 (45.3×10^3).

Preparation of C₇₆H₁₂₄N₆O₁₇Mo₆ (12)

To compound **11** (0.116 g, 0.060 mmol), 1-ethynyl-N,N-dimethylbenzenamine (0.029 g, 0.20 mmol), bis(triphenylphosphine) palladium(II) dichloride (8.5 mg, 0.012 mmol), copper iodide (5.2 mg, 0.027 mmol), and potassium carbonate (0.597 g, 4.31 mmol), 8 ml dry acetonitrile and triethylamine (0.8 ml, 5.74 mmol) were added. The resulting red solution was stirred for 40 minutes to give a brown solution which was filtered, evaporated to ~1 ml, and then precipitated with 15 ml of diethyl ether. The resulting dark red precipitate was collected by filtration, washed with ethyl acetate and diethyl ether, and then dried in vacuo to give compound **12** as a dark red solid (0.079 g, 0.040 mmol) with a 67% yield.

^{1}H-NMR (500 MHz, CD₃CN): δ 7.36 (4H, d, J = 9.0 Hz, H-n), 7.23 (4H, s, H-i), 6.73 (4H, d, J = 9.0 Hz, H-o), 3.88 (16H, hept, J = 6.8 Hz, H-f), 3.11 – 3.03 (16H, m, H-a), 3.09 (6H, s, H-k), 2.89 (12H, s, H-q), 1.65-1.55 (16H, m, H-b), 1.39-1-32 (16H, m, H-b), 1.30 (24H, d, J = 6.9 Hz, H-e), 0.96 (24H, t, J = 7.4 Hz, H-d). ^{13}C-NMR (126 MHz, CD₃CN) δ 149.12, 133.60, 125.74, 112.92, 59.36, 47.72, 40.38, 29.35, 24.34, 24.12, 20.35, 13.82. Anal Calcd % for C₇₆H₁₂₄N₆O₁₇Mo₆: C, 46.35 (43.33); H, 6.35 (5.92); N, 4.27 (4.12). HRMS (ESI, MeCN) = calcd for C₄₄H₅₂N₄Mo₆O₁₇$^{2-}$ 742.8852, found 742.8844. FTIR: 2960 (m), 2932 (sh), 2871 (m), 2810 (sh), 2188 (m), 1731 (w), 1606 (m), 1585 (s), 1521 (m), 1460 (m), 1444 (m), 1350 (m), 1242 (w), 1191 (m) 1150 (w), 1062 (w), 1043 (w), 965 (m), 942 (vs), 880 (m), 760 (vs). UV-vis (MeCN) λ, nm (ε, M^{-1} cm^{-1}): 204 (108.7×10³); 246 (48.1×10³); 295 (50.6×10³); 420 (56.7×10³).

Preparation of C$_{60}$H$_{116}$N$_6$O$_{17}$Mo$_6$ (13)

To tetrabutylammonium hexamolybdate (1.000 g, 0.733 mmol) and DCC (0.378 g, 1.83 mmol) dissolved in 10 ml of dry dimethylsulfoxide, 4-iodo-2,6-diisopropanylaniline (0.323 g, 1.47 mmol). The resulting brown solution was heated at 95°C for 24 hours. When cool, a pale yellow precipitate was removed by filtration and the solution precipitated by slow addition to a mixture of 260 ml of diethyl ether and 80 ml of ethyl acetate. The resulting precipitate was collected by filtration, washed with ethyl acetate and diethyl ether and then purified by reprecipitation from a concentrated solution of hot acetonitrile at 5°C to give compound **13** (51 mg, 0.029 mmol) in a 4% yield.

^{1}H-NMR (500 MHz, CD$_3$CN): δ 6.39 (2H, s, H-h), 3.17-3.07 (4H, m, H-f,f'), 3.12 – 3.09 (16H, m, H-a), 3.04 (6H, s, H-h), 3.00 (6H, s, H-h'), 1.64 – 1.57 (16H, m, H-b), 1.36, (16H, hep, J = 7.4 Hz, H-c), 1.29 (12H, d, J = 6.8 Hz, H-e), 1.28 (12H, d, J = 6.8 Hz, H-e'), 0.96 (24H, t, J = 7.4 Hz, H-d). ^{13}C-NMR (126 MHz, CD$_3$CN) δ 150.77, 149.77, 106.17, 105.97, 59.26, 40.54, 40.34, 24.41, 24.31, 24.28, 20.30, 13.78. Anal (Calcd) % for C$_{60}$H$_{116}$N$_6$O$_{17}$Mo$_6$: C, 40.73 (41.67); H, 6.61 (6.71); N, 4.75 (4.95). HRMS (ESI, MeCN) = C$_{28}$H$_{44}$N$_4$Mo$_6$O$_{17}$$^{(2-)}$ 641.8536, found 641.8519. FTIR: 2958 (m), 2931 (sh), 2871 (m), 1589 (s), 1481 (m), 1463 (m), 1435 (m), 1370 (m), 1309 (vw), 1293 (vw), 1257 (vw), 1232 (vw), 1169 (m), 1124 (vw), 1108 (vw), 1061 (vw), 1030 (vw), 995 (m), 936 (s), 888 (vw), 838 (w), 752 (vs). UV-vis (MeCN) λ, nm (ε, M^{-1} cm^{-1}): 208 (75.7×10^3); 259 (53.0×10^3); 422 (58.6×10^3).
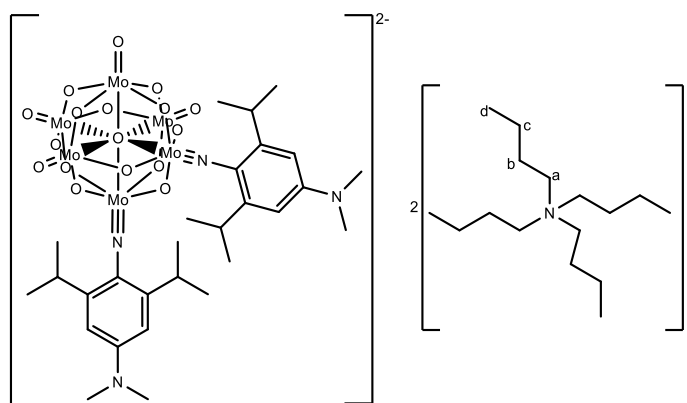
Preparation of C₈₃H₁₅₉N₇O₃₆Mo₁₂ (14)
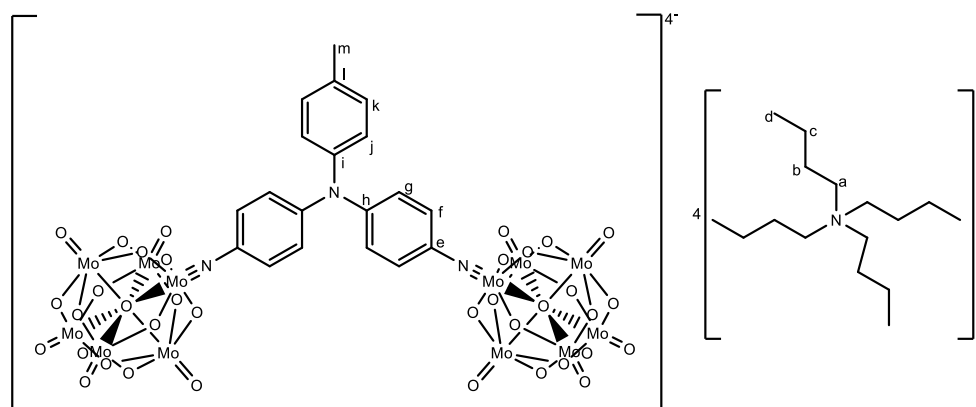
A solution of tetrabutylammonium hexamolybdate (1.305 g, 0.976 mmol), compound **P17** (0.118 g, 0.373 mmol), and DCC (0.230 g, 1.11 mmol) in 15 ml of dry dimethylsulfoxide was heated at 70°C for 10 hours. Once cool, the solution was filtered to remove the pale precipitate then poured into 40 ml of ethanol and 150 ml of diethyl ether to give a dark precipitate. The precipitate was washed with ethanol and ether before collecting by filtration to give crude compound **14** (1.225 g, 0.411 mmol) as a red solid with an 84% yield. Further purification was achieved by washing with DCM before reprecipitating a concentrated acetone solution using diethyl ether to give pure compound **14** (0.140 g, 0.050 mmol) in an overall 13 % yield.

^{1}H-NMR (500 MHz, CD$_3$CN) δ 7.20 (2H, d, J = 7.20 Hz, H-f), 7.12 (4H, d, J = 8.8 Hz, H-k), 7.01 (2H, d, J = 8.4 Hz, H-j), 6.95 (4H, d, J = 8.9 Hz, H-g), 3.18 – 3.04 (32H, m, H-a), 2.35 (3H, s, H-m), 1.64–1.58 (32H, m, H-b), 1.36 (32H, hept, J = 7.4 Hz, H-c), 0.97 (48H, t, J = 7.4 Hz, H-d). ^{13}C-NMR (126 MHz, CD$_3$CN) δ 151.0, 147.6, 136.4 (C-l), 131.7, 131.3 (C-k), 128.3, 127.5 (H-j), 123.3, 59.2 (C-a), 24.2 (C-b), 20.8 (C-m), 20.2 (C-c) 13.8 (C-d). Anal (Calcd) % for C$_{83}$H$_{159}$Mo$_{12}$O$_{36}$N$_7$: C, 33.42 (34.10); H 5.37 (5.32); N, 3.29 (3.45). HRMS (ESI, MeCN) = calcd for C$_{19}$H$_{15}$N$_3$Mo$_{12}$O$_{36}$$^{(4-)}$ 503.2044, found 503.2046. FTIR: 2960 (m), 2932 (sh), 2872 (m), 2163 (w), 2034 (w), 1576 (m), 1508 (m), 1482 (s), 1379 (m), 1315 (s), 1286 (m), 1167 (m), 1106 (w), 1065 (w), 1029 (w), 973 (m), 943 (vs), 882 (sh), 764 (vs). UV-vis (MeCN) λ, nm (ε, M^{-1} cm^{-1}): 200 (100.1×10^3); 255 (59.2×10^3); 337 (22.2×10^3); 473 (49.4×10^3).

Preparation of C₈₄H₁₆₁N₇O₃₆Mo₁₂ (15)

A solution of compound **P19** (0.094 g, 0.310 mmol), tetrabutylammonium hexamolybdate (0.859 g, 0.656 mmol) and DCC (0.157 g, 0.761 mmol) in 15 ml of dry dimethylsulfoxide was heated at 70°C for 10 hours. Once cool, the solution was filtered to remove the pale precipitate then poured into 40 ml of ethanol and 150 ml of diethyl ether to give a dark precipitate. The precipitate was washed with ethanol and ether before collecting by filtration to give compound **15** (0.648 g, 0.216 mmol) as a red solid in a 70% yield. Further purification of 204 mg was achieved by slow recrystallisation in acetone/diethyl ether to give pure compound **15** (66.5 mg, 0.022 mmol) in an overall 23% yield.

^{1}H-NMR (500 MHz, CD$_3$CN) δ 7.21 (4H, dt, J = 7.3, 0.8 Hz, H-k), 7.03 (4H, d, J = 8.3 Hz, H-j), 6.41 (1H, t, J = 1.7 Hz, H-e), 6.29 (2H, d, J = 1.7 Hz, H-g), 3.18 – 3.09 (32H, m, H-a), 2.34 (6H, s, H-m), 1.67 – 1.59 (32H, m, H-b), 1.38 (32H, h, J = 7.4 Hz, H-c), 0.97 (48H, t, J = 7.4 Hz, H-d). ^{13}C-NMR (126 MHz, CD$_3$CN) δ 155.0, 144.8, 135.9, 131.3, 126.8, 116.3 (C-g), 116.1 (C-e), 115.3, 59.2 (C-a), 24.2 (C-b), 20.9 (C-m), 20.2 (C-c), 13.7 (C-d). Anal Calcd % for C$_{84}$H$_{161}$Mo$_{12}$O$_{36}$N$_7$: C, 33.67 (34.15); H, 5.42 (5.45); N, 3.27 (3.26). HRMS (ESI, MeCN) = calcd for C$_{52}$H$_{89}$N$_5$Mo$_{12}$O$_{36}^{(2-)}$, 755.0391, found 755.0385. FTIR: 2961 (m), 2933 (sh), 2873 (m), 1708 (m), 1559 (m), 1507 (m), 1460 (m), 1425 (m), 1379 (m), 1362 (sh), 1309 (sh), 1293 (sh), 1258 (m), 1222 (sh), 1158 (w), 1108 (w), 1058 (w), 1033 (w), 975 (m), 944 (s), 764 (vs), 737 (vs). UV-vis (MeCN) λ, nm (ε, M^{-1} cm^{-1}): 257 (24.0×10^3); 275 (24.8×10^3); 345 (16.5 ×10^3); 469 (1.65×10^3).

Preparation of C$_{84}$H$_{161}$N$_7$O$_{36}$Mo$_{12}$ (16)

A solution of compound **P21** (0.046 g, 0.152 mmol), tetrabutylammonium hexamolybdate (0.418 g, 0.306 mmol) and DCC (0.077 g, 0.373 mmol) in 15 ml of dry dimethylsulfoxide was heated at 70°C for 10 hours. Once cool, the solution was filtered to remove the pale precipitate then poured into 40 ml of ethanol and 150 ml of diethyl ether to give a dark precipitate. The precipitate was washed with ethanol and ether before collecting by filtration to give compound **16** (0.393 g, 0.131 mmol) as a red solid with a 35% yield. Further purification of 201 mg was achieved by crystallisation in acetone/diethyl ether vapour diffusion to give compound **16** (65.2 mg, 0.022 mmol) in an overall 11% yield.

^{1}H-NMR (500 MHz, CD$_3$CN) δ 7.09 (4H, d, J = 8.0 Hz, H-m), 6.93 (1H, d, J = 0.6 Hz, H-f), 6.92 (1H, d, J = 2.1 Hz, H-j), 6.88 (1H, dd, J = 2.1, 0.6 Hz, H-i), 6.84 (4H, d, J = 8.4 Hz, H-l), 3.30 – 3.09 (32H, m, H-a), 2.34 (s, 6H), 1.73 – 1.58 (32H, m, H-b), 1.39 (32H, h, J = 7.3 Hz, H-c), 0.97 (48H, t, J = 7.3 Hz, H-d). ^{13}C-NMR (126 MHz, CD$_3$CN) δ 150.7, 145.4, 144.3, 134.6, 130.7, 128.0, 127.3, 127.1, 126.7, 124.5, 59.2, 24.3, 20.9, 20.2, 13.7. Anal Calcd % for C$_{84}$H$_{161}$Mo$_{12}$O$_{36}$N$_7$: C, 33.67 (33.98); H, 5.42 (5.50); N, 3.27 (3.30). HRMS (ESI, MeCN) = calcd for C$_{52}$H$_{89}$N$_5$Mo$_{12}$O$_{36}^{(2-)}$, 755.3725, found 755.3728. FTIR: 2961 (m), 2934 (sh), 2873 (m), 1731 (w), 1608 (w), 1567 (w), 1485 (m), 1469 (m), 1379 (m), 1348 (w), 1296 (m), 1259 (sh), 1152 (w), 1108 (w), 1065 (w), 1025 (w), 974 (m), 944 (s), 879 (w), 767 (vs). UV-vis (MeCN) λ, nm (ε, M^{-1} cm^{-1}): 257 (58.5×10^3); 262 (58.7×10^3); 340 (33.1×10^3); 461 (26.4×10^3).

Preparation of C$_{58}$H$_{92}$N$_4$O$_{18}$Mo$_6$ (17)

Tetrabutylammonium hexamolybdate (0.499 g, 0.366 mmol), compound **P15** (0.126g, 0.348 mmol), and DCC (0.086 g, 0.417 mmol) were dissolved in 5 ml of dry dimethylsulfoxide, and the resulting yellow solution heated at 70ºC for 10 hours. When cool, a pale yellow precipitate was removed by filtration and the solution precipitated by slow addition to a mixture of 75 ml of diethyl ether and 12 ml of ethyl acetate. The resulting solid was collected by filtration, washed with ethyl acetate and diethyl ether to give crude compound **17** (0.414 g, 0.242 mmol) as a dark red solid with a 70% crude yield. Purification was achieved by re-precipitation from acetonitrile using diethyl ether before the DCM soluble product was reprecipitated from an acetone/diethyl ether diffusion to give compound **17** (30mg, 0.018 mmol) in an overall 5% yield.

^{1}H-NMR (500 MHz, CD$_3$CN) 7.56 (2H, d, J = 8.7 Hz, H-f), 7.46 (2H, d, J = 8.7 Hz, H-g), 7.31 (4H, dd, J = 8.6, 7.4 Hz, H-q), 7.22 (2H, d, J = 8.6, H-r), 7.13-7.06 (8H, m, H-i,j,l,p), 6.99 (2H, d, J = 8.6, H-m), 3.10 – 3.04 (16H, m, H-a), 1.63 – 1.57 (16H, m, H-b), 1.35 (16H, hept, J = 7.3 Hz, H-c), 0.97 (24H, t, J = 7.4 Hz, H-d). ^{13}C-NMR (126 MHz, CD$_3$CN) δ 130.47, 128.80, 125.62, 123.85, 59.30, 24.34, 20.35, 13.81. Anal (Calcd) % for C$_{58}$H$_{92}$N$_4$O$_{18}$Mo$_6$: C, 40.76 (40.26); H, 5.43 (5.35); N, 3.28 (3.21). HRMS (ESI, MeCN) = calcd for C$_{26}$H$_{20}$N$_2$Mo$_6$O$_{18}$$^{(2-)}$ 611.7541, found 611.7550. FTIR: 2961 (m), 2933 (sh), 2873 (m), 1580 (m), 1507 (m), 1484 (m), 1379 (w), 1327 (m), 1315 (sh), 1276 (m), 1175 (vw), 1154 (vw), 1104 (vw), 1072 (vw), 1029 (vw), 974 (m), 945 (s), 879 (vw), 839 (vw), 773 (s), 695 (w). UV-vis (MeCN) λ, nm (ε, M^{-1} cm^{-1}): 203 (83.5×10^3); 300 (30.9×10^3); 437 (43.9×10^3).

References

[1] A. Bijelic, M. Aureliano, and A. Rompel, *Angew. Chem. Int. Ed.*, 2019, **58**,2980.

[2] R. Neumann, M. Dahan, *Nature*, 1997, **388**, 353.

[3] A. Al-Yasari, N. Van Steertegham, H. El Moll et al., *Dalton Trans.,* 2016, **45**, 2818.

[4] J. J. Berzelius, *Poggend. Ann. Phys. Chem.*, 1826, **6**, 369.

[5] J. Keggin, *Nature*, 1933, **132**, 351.

[6] S.S.Talismanov, *Zhurnal Neorganicheskoi Khimii*, 2002, **47**, 1446.

[7] B. Dawson, *Acta Cryst.,* 1953, **6**, 113.

[8] J. Keggin, *Royal Society*, 1934, **144**, 75.

[9] A. Müller, *Inorg. Chem.,* 2000, **39**, 3112.

[10] A. Muller, E, Beckmann, H. Bogge, at al., *Angew. Chem. Int. Ed.*, 2002, **41**, 1162.

[11] D. E. Katsoulis, *Chem. Rev.*, 1998, **98**, 359.

[12] T. Ruther, et al., *J. Am. Chem. Soc.*, 2003, **125**, 10133.

[13] A. Muller, et, al., *Agnew. Chem.*, 2003, **115**, 5193.

[14] D. A. Judd, J. H. Nettles, N. Nevins, at al., *J. Am. Chem. Soc.*, 2001, **123**, 886.

[15] S. She, S. Bian, R. Huo, et al., *Sci. Rep.*, 2016, **6**, 33529

[16] Pope, M. T. Heteropoly and Isopoly Oxometalates, Springer-Verlag: Berlin, 1983.

[17] M. Rosnes, C. Yvon, D. Long and L. Cronin, *Dalton Trans.,* 2012, **41**, 10071.

[18] D. Long and L. Cronin, *Chem. Eur. J.*, 2006, **12**, 3698.

[19] A. Wilson, W. Robinson, C. Wilkins, *Acta Crystallogr.*, 1983, **39**, 54.

[20] A. Muller, C. Serain, *Acc. Chem. Res.*, 2000, **33**, 2.

[21] A. Anyushin, A. Kondinski, and T. N. Prac-Vogt, *Chem. Soc. Rev.*, 2020, **49**, 382.

[22] A. Proust, R. Thouvenot, and P. Gouzerh, *Chem.Commun.*, 2008, 1837.

[23] S. K. Petrovskii, V. V. khistiaeva, A. A. Sizova, et al., *Inorg. Chem.*, 2020, **59**, 16122.

[24] J. B. Strong, G. Yap, R. Ostrander et al., *J. Am. Chem. Soc.,* 2000, **122**, 639.

[25] W. Clegg, R. Errington, K. Fraser, et al., *Chem. Commun.*, 1995, 455.

[26] A. Proust, R. Thouvenot, F. Robert, et al., *Inorg. Chem.,* 1993, **32**, 5299.

[27] C. Bustos, B. Hasenknopf, R. Thouvenot, *Eur. J. Inorg. Chem.*, 2003, 2757.

[28] Y. Huang, J. Zhang, J. Hao, and Y. *Wei, Sci. Rep.*, 2016, **6**, 24759.

[29] J. Hao, Y. Xia, L. Ruhlmann, et al., *Agnew. Chem. Int. Ed.*, 2008, **47**, 2626.

[30] W. Clegg, M. R. J. Elsegod, R. J. Errington and J. Havelock, *Dalton Trans.,* 1996, 681.

[31] Y. Du, A. L. Rheingold, A. J. Maatta, *J. Am. Chem. Soc.*, 1992, **114**, 346.

[32] J. B. Strong, R. Ostrander, A. L. Rheingold, E. A. Maatta, *J. Am. Chem. Soc*., 1994, **116**, 3601.

[33] Y. G. Wei, B. B. Xu, C. L. Barnes and Z. H. Peng, *J. Am. Chem. Soc*., 2001, **123**, 4083.

[34] C. Lv, R. Khan, J. Zhang, et. al., *Chem. Eur. J.*, 2013, **19**, 1174.

[35] J. B. Strong, B. S. Haggert, A. L. Rheingold et al., *Chem Commun.*, 1997, 1137.

[36] J. Stark, V. Young, A. Maatta, *Angew. Chem.,* 1995, **34**, 2547.

[37] M. Araghi, V. Mirkhani, M. Moghadam, et al., *Dalton Trans.*, 2012, **41**, 11745.

[38] B. Xu, Y. Wei, C. Barnes, and Z Peng, *Angew. Chem., Int. Ed*., 2001, **40**, 2290.

[39] Y. Zhu, L. Wang, J. Hao, *Chem. Eur. J.,* 2009, **15**, 3076.

[40] A. R. Moore, H. Kwen, A. Beatty, and E. A. Matta, Chem. Commun., 2000, 1793.

[41] M. Carraro and S. Gross, *Materials*, 2014, **7**, 3956.

[42] H. El Moll, F. Black, C. Wood, *Phys. Chem. Chem. Phys.*, 2017, **29**, 18831.

[43] S. A. Alshehri, A. Al-Yasari, F. Markden, and J. Fielden, *Macromolecules*, 2020, **53**, 11120.

[44] C. Lv, K. Chen, J. Hu, et al., *Sci. Rep.*, 2016, **6**, 27861.

[45] A. Al-Yasari, P. Spence, H. El Moll, et al., *Dalton Trans.*, 2018, **47**, 10415.

[46] S. Suresh, A. Ramanand, D. Jayaraman and P. Mani, *Rev. Adv. Mater. Sci.*, 2012, **30**, 175.

[47] L. R. Dalton, P. A. Sullivan, and D. H. Bale, *Chem. Rev.*, 2010, **110**, 25.

[48] L. R. Dalton, P. Günter, M. Jazbinsek, *Organic Electro-Optics and Photonics: Molecules, Polymers and Crystals*, Cambridge University Press, **2015**, Introduction.

[49] G. New, *Introduction to Nonlinear Optics*, Cambridge University Press, **2011**, Chapter 1.

[50] P. Franken, A. Hill, C. Peters and G. Weinreich, *Phys. Rev. Lett.*, 1961, **7**, 118.

[51] J. Oudar and D. Chemla, *Optic. Commun.*, 1975, **13**, 164.

[52] R. W. Terhune, P. D Maker, C. M. Savage, *Phys. Rev. Lett.*, 1962, **8**, 404.

[53] K. Clays and A. Persoons, *Phys. Rev. Lett.*, 1991, **66**, 2980.

[54] D. B. Hollis, *American Mineralogist*, 1988, **73**, 701.

[55] L. Karki, F. W. Vance, J. T. Hupp, et al., *J. Am. Chem. Soc.*, 1998, **120**, 2606.

[56] B. J. Coe, J. A. Harris, and B. S. Brunschwig, *J. Phys. Chem. A*, 2002, **106**, 897.

[57] K Tripathy, J. P. Moreno, M. G. Kuzyk, et al*., J. Chem. Phys.,* 2004, **121**, 7932.

[58] S. L. Shapiro, *Appl. Phys. Lett.,* 1968, **13**, 19.

[59] R.C. Miller, D.A. Kleinman, A. Savage, *Phys. Rev. Lett.,* 1963, **11**, 146.

[60] F. G. Parsons and R. K. Chang, *Opt. Commun*., 1971, **3**, 173.

[61] N. J. Long, *Angew. Chem. Int. Ed. Engl.,* 1995, **34**. 21.

[62] J. L. Oudar, *J. Chem. Phys*., 1977, **67**, 446.

[63] Y. Sheng and Y. Jiang, J. Chem. Soc., *Faraday T rans.*, 1998, **94**, 1829.

[64] T. Verbiest, S. Houbrechts, M. Kauranen et al., *J. Mater. Chem.,* 1997, **7**, 2175.

[65] L. Cheng and W. Tam, *J. Phys. Chem.,* 1991, **95**, 10643.

[66] A. E. Stiegman, E. Graham, K. J. Perry, L. R. Khundkar, et al., *J. Am. Chem. Soc*., 1991, **113**, 7658.

[67] V. Pushkara Rao, A. K-Y. Jen, K. Y. Wong and K. J. Drost, *Chem. Soc., Chem. Commun., 1993, 1118.*

[68] B. Xu and T. M. Swager, *J. Am. Chem. Soc.* 1993, **115**, 1160.

[69] L. Beverina, A. Sanguineti, G. Battagliarin, *Chem. Commun.,* 2011, **47**, 292.

[70] Y. Shi, A. Lou, G. He, et al., *J. Am. Chem. Soc*., 2015, **137**, 4622.

[71] V. Bruno, A. Castaldo, R. Centore et al., *J. Polym. Sci. A Polym. Chem., 2002, 40, 1468.*

[72] H. Umezawa, K. Tsuji, S. Okada et al., *Opt. Mater*., 2003, **21**, 75.

[73] X.-M. Duan, S. Okada, H. Oikawa, et al., *Jpn. J. Appl. Phys*., 1994, **33**, L1559.

[74] H. Nakanishi, H. Matsuda, S. Okada, and M. Kato*, Proc. MRS Int. Mtg. Adv. Mater.*, 1989, 97.

[75] T. Notake, K. Nawata, H. Kawamata, et al., *Opt. Express*, 2012, **20**, 25852.

[76] M. L. H. Green, S. R. Marder, M. E. Thompson, et al., *Nature*, 1987, **330**, 360.

[77] C. C. Frazier, M. A. Harvey, M. P. Cockerham, et al., *J. Phys. Chem.*, 1986, **90**, 5703.

[78] J. C. Calabrese, L.-T. Cheng, J. C. Green, *J. Am. Chem. Soc.*, 1991, **113**, 1221.

[79] C. E. Powell and M. G Humphrey, *Coord. Chem. Rev.*, 2004, **248,** 725.

[80] L. Pilia, M. Pizzotti, F. Tessore, and N. Robertson, *Inorg. Chem.*, 2014, **53**, 4517.

[81] I. R. Whittall, A. M. McDonagh, M. G. Humphrey and M. Samoc, *Adv. Organomet. Chem.*, 1998, **42**, 291.

[82] A. Valore, E. Cariati, C. Dragonetti, et al., *Chem. Eur. J.*, 2010, **16**, 4814.

[83] B. J. Coe, S. Houbrechts, I. Asselberghs, and A. Persoons, *Angew. Chem. Int. Ed.*, 1999, **38**, 366.

[84] B. J. Coe, M.C. Chamberlain, J.P. Essex-Lopresti, et al., *Inorg. Chem.*, 1997, **36**, 3284.

[85] W. M. Laidlaw, R. G. Denning, T. Verbiest, E. Chauchard and A. Persoons, *Nature*, 1993, **363**, 58.

[86] P.R. Kanis, P.G. Lacroix, A.A. Ratner, T.J. Marks, *J. Am. Chem. Soc.*, 1994, **116**, 10089.

[87] D. Roberto, R. Ugo, S. Bruni, et al., *Organometallics*, 2000, **19**, 1775.

[88] D. W. Bruce, and A Thornton, *A. Mol. Cryst. Liq. Cryst. Sci. Technol., Sect A*, 1993, **231**, 253.

[89] R. J. Durand, S. Gauthier, S. Achelle, et al., *Dalton Trans.*, 2017, **46**, 3059.

[90] J. P. Costes, J. F. Lamére, C. Lepetit, P. G. Lacroix, and F. Dahan, *Inorg. Chem.*, 2005, **44**, 1973.

[91] W. Chiang et al., *Spec. Publ. R. Soc. Chem.*, 1991, **91**, 210.

[92] C. Evans and D. Luneau, *J. Chem. Soc., Dalton Trans.,* 2002, 83.

[93] P. G. Lacroix, I. Malfant, and C. Lepetit, *Coord. Chem. Rev.*, 2016, **308**, 381.

[94] S. Houbrechts, K. Clays, A. Persoons, et al., *Organometallics*, 1996, **15** 5266.

[95] S. Di Bella, and I. Fragala, *Synthetic Metals*, 2000, **115**, 191.

[96] S. Di Bella, *Chem. Soc. Rev.*, 2001, **30**, 355.

[97] B. J. Coe, J. Fielden, S. Foxon et al., *J. Am. Chem. Soc.*, 2010, **132**, 10498.

[98] B. J. Coe, J. A. Harris, and B. S. Brunschwig, *Dalton Trans.*, 2003, 2384.

[99] B. J. Coe, J. A. Harris, L. A. Jones, et al., *J. Am. Chem. Soc.*, 2005, **127**, 4845.

[100] S. Prabu, E. David, T, Viswanathan, et al., *Dalton Trans.*, 2020, **49**, 1854.

[101] M. Yang and B. Champagne, *J. Phys. Chem. A*, 2003, **107**, 3942.

[102] S. Muhammad, H. Xu, Z, Su, et al., *Dalton Trans.*, 2013, **42**, 15053.

[103] Q. Song, C. Wan, C. K. Johnson, *J. Phys. Chem.*, 1994, **98**, 1999.

[104] Y. Han, C. Nickle, Z. Zhang, et al, *Nat. Mater.*, 2020, **19**, 843.

[105] S. van Bezouw, M.-J. Koo, S.-C. Lee, et al., *Chem. Commun.*, 2018, **54**, 7842.

[106] I. Whittall and J. Humphries, *Organometallics*, 1995, **14**, 5493.

[107] M. Malaun, Z. R. Reeves, R. L. Paul, et al., *Chem. Commun.*, 2001, 49.

[108] Physicsworld.com, https://physicsworld.com/a/powering-the-beast-why-we-shouldnt-worry-about-the-internets-rising-electricity-consumption (accessed March 2022)

[109] Newport.com, Practical Uses and Applications of Electro-Optic Modulators (accessed March 2022)

[110] B. J. Coe, *Chem. Eur. J.*, 1999, **5**, 2464.

[111] E. Hendrickx, K. Clays, A. Persoons, C. Dehu, J.-L. Bredas, *J. Am. Chem. Soc.*, 1995, **117**, 3547.

[112] S. L. Gilat, S. H. Kawai, J.-M. Lehn, *Chem. Eur. J.*, 1995, **1**, 275.

[113] M. Irie, O. Miyatake, K. Uchida, and T. Eriguchi, *J. Am. Chem. Soc.*, 1994, **116**, 9894.

[114] H. Zhao, E. Garoni, T. Roisnel, *Inorg. Chem.* 2018, **57**, 7051.

[115] J. Boixel, V. Guerchais, H. Le Bozec, *Chem. Commun.*, 2015, **51**, 7805.

[116] I. Asselberghs, K. Clays, A. Persoons, et al., *Chem. Phys. Lett.*, 2003, **368**, 408.

[117] T. Zhang, X-H. Wei, Y. Zuo, and T.-Y. Ma, *J. Mol. Struct.*, 2020, 1217, 128364.

[118] S. Di Bella, I. P. Oliveri, A. Colombo, et al., *Dalton Trans.*, 2012, **41**, 7013.

[119] S. Attar, D. Espa, F. ArtizzuInorg. Et al., *Inorg. Chem.*, 2017, **56**, 6763.

[120] C. Karthika, S. R. Sarath Kumar, L. Kathuria, P. K. Das and A. G. Samuelson, *Phys. Chem. Chem. Phys.,* 2019, **21**, 11079.

[121] L. Boubekeur-Lecaque, B. J. Coe, K. Clays, *J. Am. Chem. Soc.*, 2008, **130**, 3286.

[122] B. J. Coe, J. A. Harris, L. J. Harrington, et al., *A. Inorg. Chem.*, 1998, **37**, 3391.

[123] I. D. L. Albert, T. J. Marks and M. A. Ratner, *J. Am. Chem. Soc.*, 1998, **120**, 11174.

[124] L. Yan, G. Yang, W. Guan, et al., *J. Phys. Chem. B*, 2005, **109**, 22332.

[125] D. Attanasio, M. Bonamico, V. Fares and L. Suber, *J. Chem. Soc. Dalton Trans.,* 1992, 2523.

[126] E. Coronado and C. J. Gomez-Garcıa, *Chem. Rev.,* 1998, **98**, 273.

[127] L. Xu, M. Lu, B. Xu, Y. Wei et al., *Angew. Chem., Int. Ed.*, 2002, **41**, 4129.

[128] A. Al-Yasari, N. Van Steertegham, H. Kearns et al., *Inorg.. Chem.*, 2017, **56**, 10181.

[129] A. Al-Yasari, H. El Moll, R. Purdy et al., *Phys. Chem. Chem. Phys.*, 2021, **23** 11807.

[130] L. Sun, T. Zhang, B. Zho, *Dyes and Pigments*, 2017, **137**, 372.

[131] J. B. Strong, Glenn P. A. Yap, Robert Ostrander*, J. Am. Chem. Soc.*, 2000, **122**, 643.

[132] M. R. S. A. Janjua, M. Amin, M. Ali, et al., *Eur. J. Inorg. Chem.,* 2012, 705.

[133] A. Al-Yasari, PhD Thesis, University of East Anglia, 2016.

[134] T. R. Mohs et al., *Inorg. Chem.*, 1995, **32**, 9.

[135] Y. Wei, M. Lu, C. F. Cheung, C. Barnes, Z. Peng, *Inorg. Chem.*, 2001, **40**, 5489.

[136] C. Sanchez, J. Livage, J. P. Launay, M. Fournier, Y. Jeannin, *J. Am. Chem. Soc.*, 1982, **104**, 3194.

[137] M. Filowitz, R. K. C. Ho, W. G. Klemperer, W. Shum, *Inorg. Chem.*, 1979, **18**, 93.

[138] C. Falaise, M. A. Moussawi, S. Floquet, et al., *J. Am. Chem. Soc.*, 2012, **140**, 11198.

[139] D. E. Wigley, *Prog. Inorg. Chem.*, 1994, **42**, 239.

[140] W. Y. Man, K. B. Vincent, H. J. Spencer, *J. Clust. Sci.*, 2012, **23**, 853.

[141] A. Scarpaci, C. Monnereau, E. Blart, et. al, *Tetrahedron Lett.*, 2005, **46**, 5421.

[142] B. Breiten, Y. Wu, P. D. Jarowski, et al., *Chem. Sci.*, 2011, **2**, 88.

[143] X. Wang, Y. Song, J. Qu, and Y. Luo, *Organometallics*, 2017, **36**, 1042.

[144] T. Mino, S. Suzuki, K. Hirai, M. Sakamoto, T. Fujita, *Synlett*, 2011, 1277.

[145] M. Eckhardt, G. C. Fu, *J. Am. Chem. Soc.*, 2003, *125*, 13642.

[146] C. He, J. Ke, H. Xu, and A. Lei, *Angew. Chem., Int Ed.*, 2013, **52**, 1527.

[147] F.J. Carver, C. A. Hunter, D. J. Livingstone, et L., *Chem., Eur., J.*, 2002, *8*, 2847.

[148] S. A. Lahankar, R. West, O. Varnavski, et al., *J. Chem. Phys.*, 2004, **120**, 337.

[149] Y. Pocker and G. T. Spyridis*, J. Am. Chem. Soc.*, 2002, **124**, 739.

[150] J. J. Van Benschoten, J. Y. Lewis, W. R. Heineman, et al., *J. Chem. Educ.* 1983, **60**, 772.

[151] A. Babaei, P. A. Connor, A. J. McQuillan, S. Umapathy, *J. Chem. Educ.*, 1997, **74**, 1200.

[152] P. Canizares, J. Garcia-Gomez, I. Fernández de Marcos, et al., *J. Chem. Educ.*, 2006, **83**, 1204.

[153] S. Queiroz, M. P. de Araujo, A. A. Batista, et al., *J. Chem. Educ*. 2001, **78**, 89.

[154] N. Elgrishi, K. J. Rountree, B. D. McCarthy, *J. Chem. Educ.*, 2018, **95**, 197.

[155] M. Che, M. Fournier, J. P. Launay, *J. Chem. Phys.*, 1979, **79**, 1954.

[156] J. Cao, Q. Wang, C. Liu, S. An, *J. Am. Soc. Mass Spectrom*. 2018, **29**, 1331.

[157] M.Krejčik, M.Daněk, F.Hartl, *J. Electroanal. Chem.*, 1991, **317**, 179.

[158] Z. Li, J. Shen, J. Shao, and Y. Zhong, *ACS Omega,* 2018, *3*, 16744.

[159] A. Malinauskas and R. Holze, *Electrochim. Acta*, 1999, **44**, 2613.

[160] N. G. Connelly, and W. E. Geiger, *Chemical Reviews*, 1996, **96**, 877.

[161] M. M. MacInnes, S. Hlynchuk, S. Acharya, N. Lehnert, and S. Maldonado, *ACS Appl. Mater. Interfaces*, 2018, **10**, 2004

[162] É. Brémond, Á. J. Pérez-Jiménez, J. C. Sancho-García, and C. Adamo, *J. Chem. Phys.*, 2019, **150**, 201102.

[163] E. Rtibi, M. Adberrabba, S. Ayadi, and B. Champagne, *Inorg. Chem.*, 2019, **58**, 11210.

[164] C. Bouquiaux, C. Tonnele, F. Castet, and B. Champagne, *J. Phys. Chem. B*, 2020, **124**, 2101.

[165] H. Xu, F. Liu, D. L. Elder, et al., *Chem. Mater.*, 2020, **32** 1408.

[166] S-H Hsiao, K-H Lin, *J. Fluor. Chem.*, 2016, **188**, 33.

[167] P. Thamaraiselvi, A. Varathan, V. Subramanian, and S. Easwaramoorthi, *Dyes and Pigments*, 2020, **172**, 107838.

[168] S. Xue, A. Chai, Z. Cai, *Dalton Trans.*, 2008, **35**, 4770.

[169] S-H. Hsiao and Y-C. Liao, *Polymers*, 2017, **9**, 497.

[170] B. Coe, S. P. Foxon, E. C. Harper et al., *J. Am. Chem. Soc.*, 2010, **132**, 1706.

[171] J. Kang, B. Xu, Z. Peng, et al., *Angew. Chem. Int. Ed.*, 2005, **44**, 6902.

[172] G. Ding, Y. Lu, X. Quin, et al., *Dyes and Pigments*, **2017**, 139, 19.

[173] C. Singh, R. Ghosh, J. A. Mondal, and D. K. Palit, *J. Photochem. Photobiol. A: chem.*, 2013, **263**, 50.

[174] M. J. Gallagher and H. Noerdin, *Aust. J. Chem.*, 1985, **38**, 997.

[175] Rigaku Corporation, CrysAlisPro (Version 1.171.40.68a), Tokyo, Japan, 2019.

[176] G. M. Sheldrick, *Acta Crystallographica Section C Structural Chemistry*, 2015, **71**, 3.

[177] O. V. Dolomanov, L. J. Bourhis, R. J. Gildea, J. A. K. Howard and H. Puschmann, *J. Appl. Crystallogr.*, 2009, **42**, 339.

[178] B. R. D'Souza, T. K. Lane, and J. Louie, *Org. Lett.,* **2011**, *13*, 11, 2936.

[179] S. Yamada et al., *J. Fluor. Chem.*, **2017**, 202, 54.